SYSTEMS TECHNOLOGY, INC

13766 S. HAWTHORNE BOULEVARD • HAWTHORNE, CALIFORNIA 90250-7083 • PHONE (310) 679-2281
email: sti@systemstech.com FAX (310) 644-3887

Technical Report 1301-1

APPLYING VEHICLE DYNAMICS ANALYSIS AND VISUALIZATION TO ROADWAY AND ROADSIDE STUDIES

November 13, 1998

R. Wade Allen
Theodore J. Rosenthal
Systems Technology, Inc.

Jeffrey P. Chrstos
JPC & Associates

FHWA Contract No. DTFH61-93-C-00209

Publication No: FHWA-RD-98-030

TECHNICAL SUMMARY

INTRODUCTION

This report describes the application of vehicle dynamic modeling and visualization to highway safety design within the Interactive Highway Safety Design Model (IHSDM). This concept is intended to allow highway engineers to test roadway designs by computer simulation of vehicle encounters with roadway geometrics, and to assess roadway alignment and visibility features using three-dimensional (3D) graphical visualization. The procedures are intended to allow running a vehicle through design alternatives, to provide metrics of vehicle performance, and to permit visualization of the vehicle/roadway encounter.

BACKGROUND

IHSDM is intended to be compatible with State DOT design procedures, and include both new construction and reconstruction projects. Design assessment with a Vehicle Dynamics Module (VDM) is most important at the preliminary stage where alignment decisions are made. Visualization is more important at the detailed design stage.

Vehicle dynamics analysis within IHSDM can allow the designer to evaluate the demands a given design places on vehicle maneuvering and driver control. The modeling must include some form of driver control in order for the VDM to follow the horizontal geometry of the roadway design. Vehicle dynamics modeling is a fairly mature discipline, and driver control models are also reasonably well developed.

The objective of IHSDM visualization is to assist the highway designer in evaluating roadway safety by providing graphical animation of various vehicle configurations traveling along proposed/existing roadway designs. Design assessment through visualization can go beyond alignment analysis to include other issues that impact driver/vehicle safety such as Traffic Control Device (TCD) placement and visibility.

Previous work in vehicle dynamics analysis and visualization/animation has been carried out on fairly expensive engineering workstations. Intel compatible PCs (personal computers) running under Windows NT now are capable of carrying out all necessary processing requirements. Graphics accelerators are available that can provide 3D visualization rendering in real time. Software availability, including compilers and 3D modeling and rendering programs now permit carrying out engineering analysis and visualization/animation at adequate levels for roadway design applications.

VEHICLE DYNAMICS MODELING

A vehicle dynamics analysis program, VDANL (Vehicle Dynamics Analysis NonLinear), originally developed for the National Highway Traffic Safety Administration, has been successfully adapted to negotiate a roadway design file format produced by a commercial roadway design program (i.e. GEOPAC). The program was expanded to include both on and off road tire characteristics in order to accommodate shoulder and sideslope incursions. A fifth wheel trailer and other heavy truck features (e.g. brake heating) were added to accommodate several AASHTO design vehicles. Parameter sets were developed for 12 AASHTO design vehicles, and the vehicle model equations are described in detail in several appendices.

DRIVER CONTROL

The driver model for the VDANL software was expanded to include speed control dependent on lateral geometry. This expanded capability involved a review of speed selection data provided in recent

FHWA sponsored research. The data review indicated that drivers select speeds for horizontal curvature that keep cornering accelerations below 0.5 g. A simple driver speed control algorithm was developed that limits cornering acceleration according to horizontal curvature based on a look-ahead distance. A steering control algorithm was also set to regulate lateral lane position at a look-ahead distance down the road. Vehicle speed response is much slower than steering response, so the look-ahead distance for speed control is set to several times that for lateral control.

User Interface

A user interface has been set up that is convenient for Roadway designers. The VDANL software is run from detailed macro files, and an IHSDM interface has been added to VDANL that allows selection of predefined macro files that essentially list a desired set of run time options. The interface now allows the user to select vehicle type (i.e. AASHTO vehicle class), desired maneuvering (e.g. path following, speed profile), and terrain file input. When a run is complete screen output then includes plots of vehicle performance data and a table of roadway safety metrics.

VISUALIZATION

A procedure was developed for taking new roadway designs, running the vehicle dynamics model over the design, then animating the final vehicle trajectory. A number of software packages were reviewed for producing visualizations (i.e. color 3D models) of this animation process. This process is feasible and practical given the current capability of PC workstations and software packages.

HARDWARE AND SOFTWARE

It has been concluded that an Intel based PC workstation running Windows NT is more than adequate for running VDANL over new roadway designs, and rendering color 3D animations of this process. The Intel/Windows NT platform also will permit graphics to be displayed in real time. With the use of a VR (Virtual Reality) headset it would be possible for the highway designer to conduct a real-time drive-through of prospective designs. This would be especially relevant to review visibility issues, particularly if the roadway design 3D model includes TCDs. Such a review would allow the designer to visualize the visibility of upcoming curvature, intersecting roads or driveways, and the placement of warning signs and delineation. PC workstations can also be used for editing and producing videotapes that can be used in design review presentations.

CONCLUSION

The IHSDM concept including a vehicle dynamics drive-through of new designs is ready for implementation and application. Both software and hardware components are available that have more than adequate capability. The challenge is to integrate the process with common file formats and user-friendly interfaces that are convenient for the highway engineer/designer to use.

APPLYING VEHICLE DYNAMICS ANALYSIS AND VISUALIZATION TO ROADWAY AND ROADSIDE STUDIES

Report No. FHWA-RD-98-030

Prepared By

Systems Technology, Inc
13766 Hawthorne Blvd
Hawthorne, Ca 90250

Prepared For

Federal Highway Administration
Office of Contracts And Procurement
400 Seventh Street S.W.
Washington, Dc 20590

May 1998

FOREWORD

A George Ostensen
Director, Office of Safety
And Traffic Operations
Research and Development

NOTICE

Technical Report Documentation Page

1. Report No.	2. Government Accession No.	3. Recipient's Catalog No.
FHWA-RD-98-030		

4. Title and Subtitle	5. Report Date
Applying Vehicle Dynamics Analysis and Visualization to Roadway and Roadside Studies	May 1998
	6. Performing Organization Code
7. Author's R. Wade Allen, Theodore J. Rosenthal, Jeffrey P. Chrstos	8. Performing Organization Report No. STI TR-1301-1
9. Performing Organization Name and Address Systems Technology, Inc. 13766 Hawthorne Blvd. Hawthorne, CA 90250	10. Work Unit No. (TRAIS)
	11. Contract or Grant No. DTFH61-93-C-00209
12. Sponsoring Agency Name and Address Federal Highway Administration Office of Contracts and Procurement 400 Seventh STreet, S.W. Washington, D.C. 20590	13. Type of Report and Period Covered Final Report
	14. Sponsoring Agency Code

15. Supplementary Notes

16. Abstract

This report describes the application of vehicle dynamic modeling and visualization to highway safety design within the Interactive Highway Safety Design Model (IHSDM). This concept is intended to allow highway engineers to test roadway designs by computer simulation of vehicle encounters with roadway geometric and to assess roadway alignment and visibility features using three-dimensional (3D) graphical visualization. The procedures are intended to allow running a vehicle through design alternatives, to provide metrics of vehicle performance, and to permit visualization of the vehicle/roadway encounter.

This report reviews the overall design concept, the role of the Vehicle Dynamics Module (VDM) in providing performance metrics for a highway design, and the implementation of visualization procedures for viewing vehicle/roadway encounters including roadway features. An existing VDM (VDANL: Vehicle Dynamics Analysis, Nonlinear) was upgraded for this application to permit on- and off-road operation, articulated vehicles, and a generalized roadway design description. A simple interface and driver model was developed for running vehicles over highway designs. Several key performance measures were also developed for assessing the design, and were incorporated into the interface output.

Several appendices give detailed technical background on the VDM and vehicle parameter files. Software is provided with this report and an appendix includes a user's guide for the installation and operation of the VDM software. Some 3D graphics modeling and digital editing were carried out on a personal computer (PC) workstation. The emphasis in this project was in implementation of software on PC workstations. The applications were successful, and it is concluded that Intel/Windows NT PC workstations are quite capable of carrying out IHSDM/VDM analysis and visualization.

17. Key Words	18. Distribution Statement
Roadway Design, Vehicle Dynamics Model, 3D Graphics, IHSDM, VDANL	

19. Security Classif. (of this report)	20. Security Classif. (of this page)	21. No. of Pages	22. Price
		293	

METRIC (SI*) CONVERSION FACTORS

APPROXIMATE CONVERSIONS TO SI UNITS

Symbol	When You Know	Multiply By	To Find	Symbol
LENGTH				
in	inches	2.54	millimetres	mm
ft	feet	0.3048	metres	m
yd	yards	0.914	metres	m
mi	miles	1.61	kilometres	km
AREA				
in²	square inches	645.2	millimetres squared	mm²
ft²	square feet	0.0929	metres squared	m²
yd²	square yards	0.836	metres squared	m²
mi²	square miles	2.59	kilometres squared	km²
ac	acres	0.395	hectares	ha
MASS (weight)				
oz	ounces	28.35	grams	g
lb	pounds	0.454	kilograms	kg
T	short tons (2000 lb)	0.907	megagrams	Mg
VOLUME				
fl oz	fluid ounces	29.57	millilitres	mL
gal	gallons	3.785	litres	L
ft³	cubic feet	0.0328	metres cubed	m³
yd³	cubic yards	0.0765	metres cubed	m³

NOTE: Volumes greater than 1000 L shall be shown in m³.

TEMPERATURE (exact)

°F	Fahrenheit temperature	5/9 (after subtracting 32)	Celsius temperature	°C

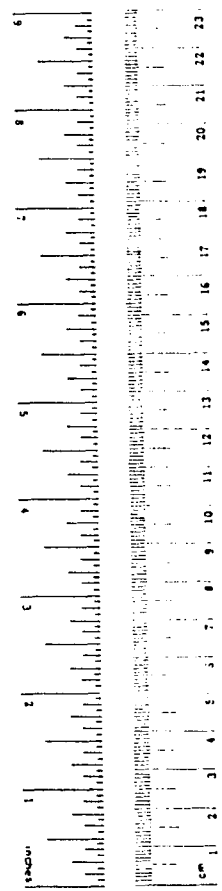

APPROXIMATE CONVERSIONS TO SI UNITS

Symbol	When You Know	Multiply By	To Find	Symbol
LENGTH				
mm	millimetres	0.039	inches	in
m	metres	3.28	feet	ft
m	metres	1.09	yards	yd
km	kilometres	0.621	miles	mi
AREA				
mm²	millimetres squared	0.0016	square inches	in²
m²	metres squared	10.764	square feet	ft²
km²	kilometres squared	0.39	square miles	mi²
ha	hectores (10 000 m²)	2.53	acres	ac
MASS (weight)				
g	grams	0.0353	ounces	oz
kg	kilograms	2.205	pounds	lb
Mg	megagrams (1 000 kg)	1.103	short tons	T
VOLUME				
mL	millilitres	0.034	fluid ounces	fl oz
L	litres	0.264	gallons	gal
m³	metres cubed	35.315	cubic feet	ft³
m³	metres cubed	1.308	cubic yards	yd³

TEMPERATURE (exact)

°C	Celsius temperature	9/5 (then add 32)	Fahrenheit temperature	°F

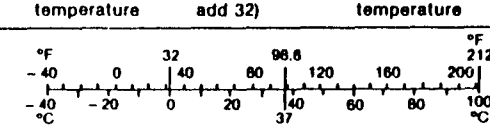

These factors conform to the requirement of FHWA Order 5190.1A.

* SI is the symbol for the International System of Measurements

TABLE OF CONTENTS

I. INTRODUCTION **1**

II. BACKGROUND **3**

A. IHSDM 3
B. VEHICLE DYNAMICS ANALYSIS 6
C. VISUALIZATION 7
D. COMPUTER HARDWARE AND SOFTWARE 8

III. VEHICLE DYNAMICS MODELING **9**

A. MODEL FORMULATION 9
B. VEHICLE MODEL PARAMETERS 11
C. ROADWAY DESCRIPTION 13

IV. DRIVER CONTROL **16**

A. STEERING CONTROL 16
B. SPEED CONTROL 17
1. Car Following 18
2. Speed Selection 19
C. DRIVER MODELS 24
1. Steering Control 24
2. Speed Control 24

V. USER INTERFACE **26**

VI. VISUALIZATION **29**

VII. HARDWARE AND SOFTWARE **33**

A. COMPUTER PLATFORMS 33
B. VISUALIZATION SOFTWARE 34
1. 3D Studio 35
2. Walkthru PC 36
3. ModelView PC 36
4. Spotlight Ray Tracer/Space-Time Animator 37
5. 3D Graphics Tools 37
6. High-End Workstation Packages 38
C. A PC-BASED COMPUTER/SOFTWARE PLATFORM 39

VIII. EXAMPLES OF APPLICATIONS **41**

A. TYPICAL RUN 41
B. VEHICLE ROLLOVER 45

IX. CONCLUSION **49**

X. REFERENCES **50**

TABLE OF CONTENTS (CONTINUED)

Appendix A. Computer Simulation 53
Appendix B. Vehicle Parameter File 130
Appendix C. Suspension Parameter File 148
Appendix D. Vehicle Parameter Measurement Test Methods 161
Appendix E. STIREMODE – The VDANL Tire Model 177
Appendix F. AASHTO Vehicle Data Sets for VDANL 204
Appendix G. IHSDM Roadway Design Database Format 260
Appendix H. User's Guide for IHSDM/VDANL Vehicle Dynamics Module 275

TABLE OF FIGURES

Figure 1. IHSDM Block Diagram ---- 3
Figure 2. VDM Incorporated Into Design Process ---- 5
Figure 3. VDANL Overall Block Diagram ---- 10
Figure 4. Roadway Description ---- 15
Figure 5. A Generic Steering Control Model Including Compensatory and Pursuit Control ---- 17
Figure 6. A Generic Speed Control Model ---- 18
Figure 7. A Compensatory Driver Speed Control Crossover Model ---- 18
Figure 8. Speed Distributions and Regression Analysis for Open Road Driving (Data from Ref. 39) ---- 20
Figure 9. VDANL Driver Steering Control Model ---- 25
Figure 10. VDANL Driver Speed Control Model ---- 25
Figure 11. VDANL/IHSDM Start-Up Screen ---- 27
Figure 12. Example of Vehicle Performance Plots vs. Station: Lateral Acceleration Profile of the Tractor of Vehicle 5 on a Winding Road ---- 27
Figure 13. Example of Roadway Safety Metric Screen ---- 28
Figure 14. VDANL Visualization Process Involving Data File Communication ---- 31
Figure 15. Horizontal and Vertical Alignment for the Typical Run Example ---- 43
Figure 16. Vehicle Performance Profile Plots for a Tractor/Trailer Driven on a Winding Road ---- 44
Figure 17. Vehicle Performance Profile Plots for a Roadside Intrusion without Rollover ---- 46
Figure 18. Vehicle Performance Profile Plots for a Roadside Intrusion with Rollover ---- 48

TABLES

1. VDANL Support for AASHTO Vehicles 12
2. Summary Of Site Characteristics and Speed Distributions for Open Road Driving (adapted from Refs. 35 and 39) 22

APPENDIX A
COMPUTER SIMULATION

TABLE OF CONTENTS

A. BACKGROUND AND OVERVIEW 53
B. AXIS SYSTEM AND DEGREES OF FREEDOM 53
C. VEHICLE INERTIAL DYNAMICS 59
D. FORCES AND MOMENTS ACTING ON INERTIAL DYNAMICS 60
E. UNSPRUNG MASS INERTIAL DYNAMICS 64
F. FORCES AND MOMENTS ACTING ON UNSPRUNG MASSES 65
G. SUSPENSION FORCE DEVELOPMENT 66
H. SUSPENSION AND STEERING GEOMETRY FUNCTIONS 69
1. Wheel Camber Angle Versus Suspension Deflection 71
2. Suspension Squat and Lift Forces 73
3. Individual Wheel Steer Angle 79
I. TIRE FORCES 87
1. Vertical (normal) Tire Loads 87
2. Tire Side Slip and Side Force Lag 88
3. Tire Longitudinal Slip and Wheel Spin Mode 90
J. COMPLIANT PIN JOINTS BETEEEN M_S AND M_U 92
K. INITIAL CONDITIONS 94
L. TRAILER HITCH MODELING 94
M. BRAKE SYSTEM MODEL 98
N. OTHER DYNAMIC VARIABLES 102
O. POWER AND DRIVE TRAIN MODELS 103
1. Overview 103
2. Engine Power Functions 105
3. Torque Converter Functions 107
4. Automatic Transmission 109
P. TABLES OF VARIABLES AND PARAMETERS, WHERE THEY ARE DEFINED, GIVEN A SIGN CONVENTION, AND AXIS SYSTEM 113
Q. APPENDIX A REFERENCES 129

APPENDIX A
COMPUTER SIMULATION (concluded)

TABLE OF FIGURES

Figure A-1. Vehicle Axis System 55
Figure A-2. Vehicle Dynamics Model Components and Their Interactions 57
Figure A-3. Major Variables Included in the Transient Dynamic Model 58
Figure A-4. Sprung Mass Free Body Diagram, End View 61
Figure A-5. Sprung Mass Free Body Diagram, Side View 61
Figure A-6. Unsprung Mass Free Body Diagram 64
Figure A-7. Tire Lateral Deflection Characteristics 65
Figure A-8. Suspension Spring and Damping Components 67
Figure A-9. Change in Suspension Spring Length 67
Figure A-10. VDANL Spring and Bump Stop Model Plot 68
Figure A-11. Static Test on Wheel Motions 70
Figure A-12. Chamber Change vs. Suspension Position 72
Figure A-13. Equivalent Single Swing Arm Approximation for a Multilink Suspension Showing Suspension Geometry Forces and Moments 73
Figure A-14. Squat/Lift Forces and Slope of Tire Patch Path 74
Figure A-15. McPherson Strut Suspension Steady State Forces 76
Figure A-16. Equivalent Tire Patch are Radius for a McPherson Strut Suspension 77
Figure A-17. Squat/Lift Function Slope Definitions 78
Figure A-18. Toe Change vs. Suspension Position 80
Figure A-19. Solid Axle or Beam Axle Suspensions with Ttrailing Links 81
Figure A-20. Ackermann Steer Relationship's 82
Figure A-21. Tire Lateral Deflection Due to Cornering (Side) Forces 84
Figure A-22. Simplified Steering System 85
Figure A-23. Tire Vertical Deflection Characteristics 88
Figure A-24. Wheel Spin Mode 91
Figure A-25. Compliant Pin Joints Connecting Unsprung and Sprung Masses 93
Figure A-26. Pitch Plane Diagram of Tractor/Semi-Trailer 96
Figure A-27. Yaw Plane Diagram of Tractor/Semi-Trailer 97
Figure A-28. Roll Plane Diagram of Tractor/Semi-Trailer 97
Figure A-29. Brake System Model 99
Figure A-30. Truck Brake Proportioning 100
Figure A-31. Power and Drive Train Model 104
Figure A-32. Engine/Transmission Model 104
Figure A-33. Forces, Torques and Angular Velocities in Drive Train 105
Figure A-34. Maximum Torque at Full and Closed Throttle 106
Figure A-35. Torque Converter Function 108
Figure A-36. A Typical Planetary Gear Set 109
Figure A-37. Torque and Angular Rate Over Time 109
Figure A-38. Gear Ratio Change Over Time 110
Figure A-39. Shift Sequence and Timing for Example Four Speed Transmission 111

TABLES

Table A-1. Basic Vehicle Model Degrees of Freedom 59
Table A-2 . Squat/Lift Slopes for Various Maneuvering Conditions 79

APPENDIX B
VEHICLE PARAMETER FILE

TABLE OF CONTENTS

A. BACKGROUND 130
B. LIST OF VEHICLE PARAMETERS AND ESTIMATION METHODS 133
C. APPENDIX B REFERENCES 147

TABLE OF FIGURES

Figure B-1. Sprung Mass Roll Inertia About cg, vs. Total Mass 135
Figure B-2. Sprung Mass Pitch Inertia About cg, vs. Total Mass 136
Figure B-3. Total Vehicle Yaw Inertia About cg, vs. Total Mass 138
Figure B-4. Steering Axis Lateral Offset 146

TABLE

Table B-1. Vehicle Parameters for a 1994 Ford Taurus 132

APPENDIX C
SUSPENSION PARAMETER FILE

TABLE OF CONTENTS

A. OVERVIEW 148
B. LIST OF SUSPENSION PARAMETERS AND ESTIMATION METHODS 149
1. SUSPENSIONF, set = 1 for independent, = 0 for solid axles 149
2. SUSPENSIONR, set = 1 for independent, = 0 for solid axles 149

TABLE OF FIGURES

Figure C-1. Suspension Side view Where Roll Steer Function is 149
Figure C-2. Static Tests on Wheel Motions 151
Figure C-3. Toe Change vs. Suspension Position 152
Figure C-4. Camber Change vs. Suspension Position 154
Figure C-5. Tread Change vs. Suspension Position 155
Figure C-6. Suspension Geometry Plot of Motion 157
Figure C-7. Suspension Geometry Plot of Motion 158
Figure C-8. VDANL Spring and Bump Stop Model Plot 160

TABLE

Table C-1. Suspension Parameter Input File for a 1995 Ford Taurus 148

APPENDIX D
VEHICLE PARAMETER MEASUREMENT TEST METHODS

TABLE OF CONTENTS

A. OVERVIEW 161
1. Center of Gravity Height Test 161
2. Roll Stiffness Test 164
3. Steering Compliance Test 164
4. Suspension Geometry Measurements 168
5. Steering Ratio Test 168
6. Suspension Spring Rate Test 174
7. Vehicle Weight and Longitudinal cg Location 174

TABLE OF FIGURES

Figure D-1. Center of Gravity Height Test 162
Figure D-2. Correction for Effects of Suspension Extension When One Axle is Raised Off the Ground 162
Figure D-3. Roll Stiffness Test 165
Figure D-4. Front Axle Roll Stiffness for Datsun 200SX 166
Figure D-5. Rear Axle Roll Stiffness for Datsun 200SX 166
Figure D-6. Steering Compliance Test for Drive 167
Figure D-7. Steering Compliance Test for Datsun 200SX 168
Figure D-8. Measurements to be Taken on the Vehicle's Suspension Components, From Front View .. 169
Figure D-9. Measurements to be Taken on Vehicle's Suspension From Side View 170
Figure D-10. Measurements to be Taken for Solid or Beam Axle Roll Steer Functions 171
Figure D-11. Special Case for Leaf Spring on Solid Axle Suspension 171
Figure D-12. Typical Examples of Suspension Geometry Layouts 172
Figure D-13. Typical Examples of Suspension Geometry Layouts 173
Figure D-14. Steering Ratio Test for Datsun 200SX 174
Figure D-15. Front Suspension Spring Rate for Datsun 200SX 175
Figure D-16. Rear Suspension Spring Rate for Datsun 200SX 175

APPENDIX E
STIREMODE — THE VDANL TIRE MODEL

TABLE OF CONTENTS

A. OVERVIEW 177
B. INTRODUCTION 177
C. BACKGROUND 178
D. BASIC MODEL 179
1. Adhesion Region 179
2. Transition and Saturation Regions 183
E. OFF-ROAD SHAPING FUNCTIONS 184
F. HIGH SLIP COEFFICIENT OF FRICTION 187
G. TIRE FORCE AND MOMENT MEASUREMENT 189
1. Paved Surface Characteristics 189
2. Off-Road Tire Characteristics 194
H. NOMENCLATURE 200
I. APPENDIX E REFERENCES 202

TABLE OF FIGURES

Figure E-1. Typical Tire Response Characteristics 179
Figure E-2. Later Force Response for Typical Off-Road Terrains 186
Figure E-3. Off-Road Tire Characteristics Related to Soil Mechanics 188
Figure E-4. Tire Parameter Identification Results for P205/65R15 Steel Belted Radial 195
Figure E-5. STIREMOD Validation Data for a General Tire Ameritech St P205/65R15: Normal Load 930 lb., Slip Angles of -4, -2, 2 and 4 deg in F_X, F_Y Plot 196
Figure E-6. Slip Conditions, Measurements and Interpretation for Christoffersen, et al. (1995) 197
Figure E-7. Tire/Terrain Friction Coefficients for Different Surfaces and Slip Angles as Derived from Christoffersen, et al. (1995) Data 197
Figure E-8. STIREMOD Response Under Off-Road Conditions: Metz (Ref. E.5} Plowed Field 199

TABLES

Table E-1. Typical Tire/Surface Coefficients of Friction (Ref. E.9) 178
Table E-2. Metz's Coefficients For Various Surfaces [Ref. E.8] 185

APPENDIX F
AASHTO VEHICLE DATA SETS FOR VDANL

TABLE OF CONTENTS

A. OVERVIEW 204
B. VEHICLE PARAMETER SETS 206
1. Passenger Car - P 206
a. Vehicle Parameter File "P.PAR" 206
b. Suspension Parameter File "P.SUS" 209
c. Tire Parameter File "P.TIR" 209
d. Driver Parameter File "DRIVER.PAR" 209
e. Other Parameters 209
f. Parameter Files 210
2. Single Unit Truck - SU 211
a. Vehicle Parameter File "SU.PAR" 211
b. Suspension Parameter File "SU.SUS" 213
c. Tire Parameter File "SU.TIR" 214
d. Driver Parameter File "DRIVER.PAR" 214
e. Other Parameters 214
f. Parameter Files 214
3. Single Unit Bus - BUS 215
a. Vehicle Parameter File "BUS.PAR" 215
b. Suspension Parameter File "BUS.SUS" 218
c. Tire Parameter File "BUS.TIR" 218
d. Driver Parameter File "DRIVER.PAR" 218
e. Other Parameters 218
f. Parameter Files 218
4. Articulated Bus - A-BUS 220
a. Vehicle Parameter File "A-BUS.PAR" 220
b. Suspension Parameter File "A-BUS.SUS" 220
c. Trailer Parameter File "A-BUS-TR.PAR" 220
d. Tire Parameter File "A-BUS.TIR" 222
e. Driver Parameter File "DRIVER.PAR" 223
f. Other Parameters 223
g. Parameter Files 223
5. Intermediate Semi-Trailer - WB-40 225
a. Vehicle Parameter File "WB-40.PAR" 225
b. Suspension Parameter File "WB-40.SUS" 227
c. Trailer Parameter File "WB-40-TR.PAR" 228
d. Tire Parameter File "WB-40.TIR" 230
e. Driver Parameter File "DRIVER.PAR" 230
f. Other Parameters 230
g. Parameter Files 231
6. Large Semi-Trailer - WB-50 232
a. Vehicle Parameter File "WB-50.PAR" 232
b. Suspension Parameter File "WB-50.SUS" 235
c. Trailer Parameter File "WB-50-TR.PAR" 235
d. Tire Parameter File "WB-50.TIR" 237
e. Driver Parameter File "DRIVER.PAR" 238
f. Other Parameters 238
g. Parameter Files 238
7. Interstate Semi-Trailer - WB-62 240
a. Trailer Parameter File "WB-62-TR.PAR" 240
b. Driver Parameter File "DRIVER.PAR" 240

APPENDIX F
AASHTO VEHICLE DATA SETS FOR VDANL

TABLE OF CONTENTS (concluded)

c. Other Parameters 240
d. Parameter Files 241
8. Interstate Semi-Trailer - WB-67 242
a. Trailer Parameter File "WB-67-TR.PAR" 242
b. Driver Parameter File "DRIVER.PAR" 243
c. Other Parameters 243
d. Parameter Files 243
9. Motor Home - MH 245
a. Vehicle Parameter File "MH.PAR" 245
b. Suspension Parameter File "MH.SUS" 247
c. Tire Parameter File "MH.TIR" 247
d. Driver Parameter File "DRIVER.PAR" 247
e. Other Parameters 247
f. Parameter Files 248
10. Car And Camper Trailer – PT 249
a. Trailer Parameter File "PT.PAR" 249
b. Driver Parameter File "DRIVER.PAR" 251
c. Other Parameters 251
d. Parameter Files 251
11. CAR and Boat Trailer – P/B 253
a. Trailer Parameter File "BT.PAR" 253
b. Driver Parameter File "DRIVER.PAR" 255
c. Other Parameters 255
d. Parameter Files 255
12. Motor HomE and Boat Trailer – MH/B 257
a. Driver Parameter File "DRIVER.PAR" 257
b. Other Parameters 257
c. Parameter Files 257
C. APPENDIX F REFERENCES 259

TABLE OF FIGURES

Figure F-1. Dimensions of AASHTO Passenger Car - P 206
Figure F-2. Dimensions of AASHTO Single Unit Truck - SU 211
Figure F-3. Dimensions of AASHTO Single Unit BUS - BUS 215
Figure F-4. Dimensions of AASHTO Articulated Bus - A-BUS 220
Figure F-5. Dimensions of AASHTO Intermediate Semi-Trailer - WB-40 225
Figure F-6. Dimensions of AASHTO Large Semi-Trailer - WB-50 232
Figure F-7. Dimensions of AASHTO Interstate Semi-Trailer - WB-62 240
Figure F-8. Dimensions of AASHTO Interstate Semi-Trailer - WB-67 242
Figure F-9. Dimensions of AASHTO Motor Home - MH 245
Figure F-10. Dimensions of AASHTO Car and Camper Trailer - PT 249
Figure F-11. Dimensions of AASHTO Car and Boat Trailer – P/B 253
Figure F-12. Dimensions of AASHTO Motor Home and Boat Trailer – MH/B 257

TABLE

Table F-1. AASHTO Vehicles Accommodated By VDANL 204

APPENDIX G
IHSDM ROADWAY DESIGN DATABASE FORMAT

TABLE OF CONTENTS

A. OVERVIEW 260
B. FILE FORMAT 260
Header File: 260
C. EXAMPLE OF DESIGN DATA BASE FILES 270

TABLES OF FIGURES

Figure G-1. Lane Designations 264
Figure G-2. Roadway Cross-section Including Side Slopes 268

APPENDIX H
USER'S GUIDE FOR IHSDM/VDANL VEHICLE DYNAMICS MODULE

TABLE OF CONTENTS

A. OVERVIEW 275
B. INSTALLATION 275
C. RUNNING A SIMULATION 275

I. INTRODUCTION

The Federal Highway Administration (FHWA) has defined an Interactive Highway Safety Design Model (IHSDM) that is envisioned as a tool for designers to interactively examine safety impacts of roadway geometric and roadside safety design decisions during the design process (e.g., Refs. 1 and 2). The IHSDM is intended to provide a tool for analyzing simple and compound horizontal curves, transitions between curves and tangents and adjacent features (shoulders and side slopes) that would influence vehicle roadside encroachments.

One of the objectives of IHSDM is to integrate vehicle dynamics module (VDMs) with roadway models and computer visualization techniques, so that roadway designs can be tested for safety over the entire vehicle operational range, and with a wide range of vehicle classes and configurations. The IHSDM and VDM should permit running a vehicle through the geometrics of any given design alternative and produce profiles of vehicle motions including speed, position, orientation, and maneuvering accelerations based on driver control laws (i.e., driver control actions based on vehicle motions and traffic control devices including delineation and advisory signing).

The overall IHSDM is intended to be used by both researchers and highway designers. The designer interface should allow the user to conveniently define/select roadway designs, vehicle characteristics, and driver control scenarios. The interface for researchers is somewhat more elaborate, allowing for the specification of shoulder and sideslope incursions. With minimum user interaction, the VDM should simulate all vehicle characteristics that are potentially related to steering and path following, tire/pavement friction, and rollover potential (Ref. 1).

This report is concerned with the development of a VDM that will appropriately interact with road design profiles to produce vehicle motion profiles and with the assessment of potential visualization methods for viewing roadway designs and vehicle/roadway encounters. These motion profiles can then be used to develop performance measures, and can also be visualized using commercial graphics programs. The approach taken in this project involved personal computer (PC) level hardware and software. At the beginning of this project (September 1993), a PC approach appeared to be quite ambitious, and most serious simulation and graphics applications were being carried out on Unix-level workstations with high-speed RISC (reduced instruction set) processors and storage media, and sophisticated graphics systems. The situation changed dramatically during the course of this project, and today reference is made to PC workstations. High-end PCs now appear to be more than adequate for three-dimensional (3D) graphics and simulation, as will be developed throughout the report.

Next we consider background for this effort, including the simulation and graphics software, and the hardware and operating system platform.

II. BACKGROUND

A. IHSDM

An overall block diagram for the IHSDM is given in Figure 1. This model grew out of FHWA efforts in the research and development (R&D) area of Highway Safety Design Practices and Criteria. The IHSDM is intended to be an integrated design process that systematically considers safety in developing and evaluating cost-effective highway design alternatives For efficiency, the IHSDM will evaluate alternative highway designs in a computer-aided design (CAD) environment. The evaluation is intended to include the roadway alignment, cross-section, and roadside hardware, including sideslopes, ditches, guardrails, utility poles, etc.

It is intended that the IHSDM be compatible with State department of transportation (DOT) design procedures, and include both new construction and reconstruction projects. IHSDM must also facilitate decision making, from planning through final design stages, including preliminary design (involving only limited information on the alignment, design speed, average daily traffic (ADT), traffic mix, cross-sections, and intersections) and detailed design (where final decisions are made on alignment; cross-section, intersection, and median layout; roadside hardware; signing and markings, etc.). Design assessment with a

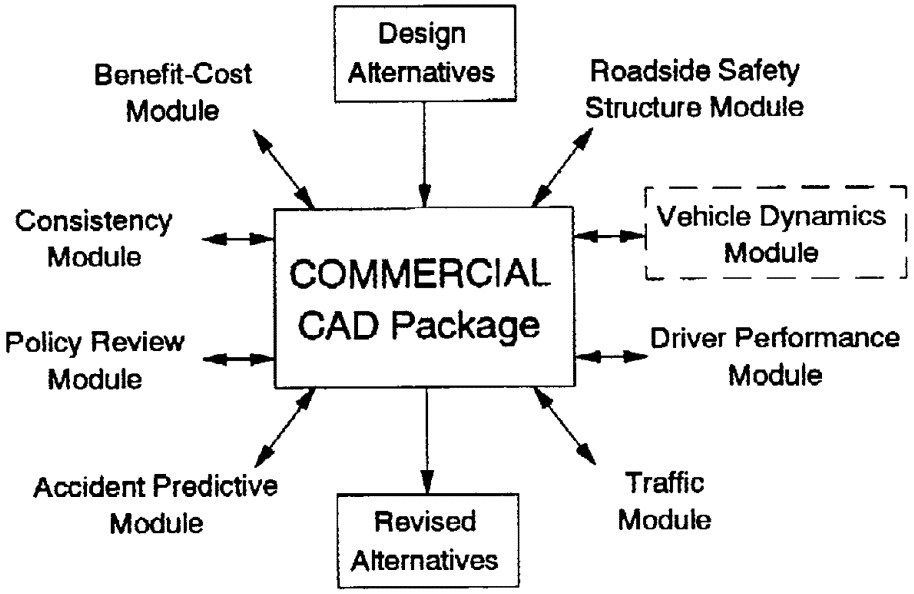

Figure 1. IHSDM Block Diagram

VDM is most important at the preliminary stage where alignment decisions are made. Visualization is more important at the detailed design stage where the placement of roadside hardware and traffic control devices is most critical.

One potential implementation of a VDM within the IHSDM is shown schematically in Figure 2. Geometric roadway design, vehicle dynamics modeling, and visualization techniques should be integrated together in order to produce the desired results. This integration implies roadway design file compatibility between several program components, and a convenient interface for the highway designer. This approach should be convenient and user friendly for the designer and should not require complicated procedures for vehicle dynamics analysis or esoteric photorealistic graphical rendering procedures.

The initial step for roadway specification is to use a design software package to create or modify the geometrics. In most instances, the roadway will be described from data that are collected during a survey, or will consist of a general geometric layout that the user is considering. In the case of a roadway modification, the roadway currently exists and the designer will only be making changes to portions of the roadway. Initial survey data will be put into a file format that can be read by the roadway design software. After survey data are assembled in a file, it can be read by the design software and manipulated to create roadways with different characteristics. Each time a new roadway has been created, it must then be saved to alignment and terrain description files for later use by both the VDM and the visualization software, as illustrated in Figure 2.

When the proposed roadway has been created and saved, it can be tested to see if certain vehicle configurations can safely traverse the roadway under various assumed operating conditions. This step is achieved using the VDM. The designer should be able to simply specify the vehicle/configuration and the operating conditions that will be used, and then direct the VDM to simulate the vehicle traveling over the roadway according to desired driver control laws. The VDM then creates a trajectory file that describes how the vehicle responds when traversing the roadway design. Next, the roadway design and vehicle trajectory files are passed to the visualization software to permit graphical portrayal of the vehicle motions over the roadway design.

The final step in the process is to create an animated graphical visualization of the vehicle's response with use of the vehicle dynamics trajectory file. To create the type of visual display that is required, the visualization package will require a terrain description file, a 3D vehicle model file for drawing the vehicle, and a vehicle motion trajectory file that will move the vehicle 3D model relative to the terrain. The terrain and trajectory files are created as described above. The vehicle 3D model file contains a graphical

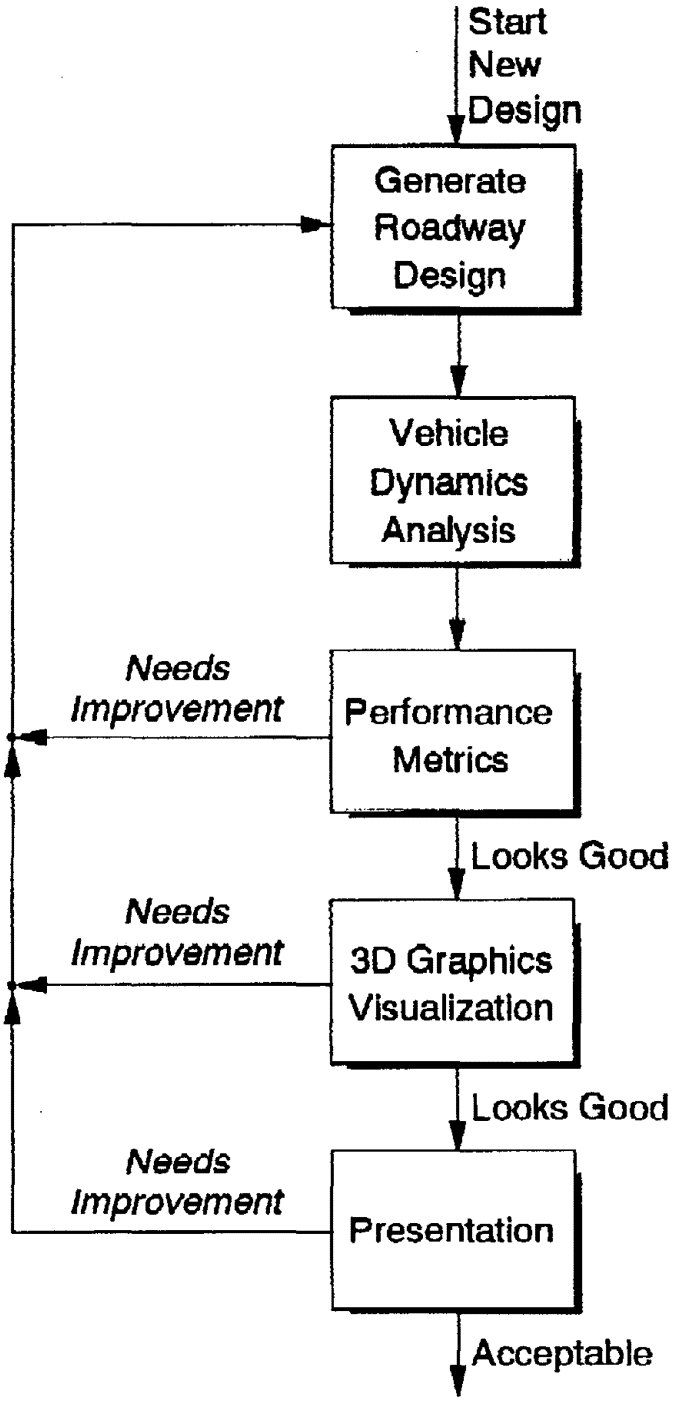

Figure 2. VDM Incorporated Into Design Process

representation of the vehicle/configuration that was used in the VDM and any roadway obstacles that are needed. Each of these files will be loaded into the visualization package and will be viewed together in an animated sequence. This allows the user to see a graphical representation of the vehicle traversing the proposed roadway design.

There are numerous roadway design software packages that are available (e.g., GEOPAK and INROADS). These packages allow roadway designers to create and modify geometric and roadway properties using CAD techniques. Since this software exists and is being used by roadway designers, the main problem to be resolved at this stage is reading the roadway terrain data files into the VDM and visualization software. The VDM must then be set up to respond to the terrain file, including the terrain profile and surface characteristics that influence tire/surface interaction.

The Figure 2 design process suggests iterative procedures that remain to be defined. The details of this process will only become clear when designers apply these procedures and some experience is gained from the system.

B. Vehicle Dynamics Analysis

Vehicle dynamics analysis should allow the designer to evaluate the demands a given design places on vehicle maneuvering and driver control. This analysis requires a VDM and some form of driver modeling for speed and steering control. Vehicle dynamics modeling is quite mature (e.g., Ref. 3), and driver control models are also reasonably well developed (e.g., Ref. 4). The analysis procedures should permit the designer to drive a selected vehicle (e.g. passenger car, tractor/trailer) over a given roadway design, and to obtain performance measures related to demands the design places on vehicle maneuvering and driver control.

The VDM is intended to provide realistic roadway tire/surface interaction over the full geometric layout of a roadway design. The VDM must be extensive enough to give accurate results over the entire range of operating points that will be encountered, including wheel lock-ups, plowout, spinout, and rollover, and over a broad class of highway vehicles and vehicle configurations of concern on public highways (i.e., passenger cars, light trucks and utility vehicles, buses, heavy articulated trucks, and vehicles towing trailers). For the VDM to operate at a desired condition, the designer must have a flexible array of inputs that can be used to control the vehicle. Therefore, the vehicle dynamics must be capable of accepting roadway design inputs and following simple control commands such as lane tracking, obstacle avoidance, speed, and steering.

Tire/terrain interaction will play a large part in determining tire forces and, ultimately, vehicle performance as the tire transition from one surface type to another. Tire forces generated at each wheel must incorporate characteristics from these varying roadway surfaces. Surfaces can range from hard pavement during normal driving to soft soil during roadside encroachment. Important properties include shear strength, surface coefficient of friction, and rolling drag. Coefficient of friction can decrease for hard but loose surfaces, while effective coefficient of friction can increase dramatically for soft shoulders and side slopes (i.e., low-shear-strength soils) under high-tire-sideslip conditions. Low coefficient of friction can also result from surfaces that are moist or icy/snowy.

The VDM also needs some means for speed selection and following the roadway design alignment. This essentially amounts to a driver model, which includes both steering and speed control. For steering control, the model must observe the relative orientation and position of the vehicle with respect to the roadway alignment and provide corrections to minimize lane following errors. For speed control, the model must observe cornering demands due to upcoming curvature, then select speeds that will maintain safe lateral acceleration. A simple model is developed here that involves look-ahead distances for judging upcoming curvature, lane position errors, and related cornering demands.

C. Visualization

The objective of IHSDM visualization is to assist the highway designer in evaluating roadway safety by providing graphical animation of various vehicle configurations traveling along proposed/existing roadway designs. A good review of the overall visualization approach in transportation studies is given in Ref. 5. Using a visualization package the designer can exert control over certain aspects of the visual display such as viewing orientation and position and speed of a drive over a roadway design. This is important because the designer can view the vehicle/roadway interaction both from within the vehicle (e.g., driver's eye view) and outside the vehicle (e.g., watching rollovers on sideslopes). Given a complete 3D model of the roadway design, including traffic control devices (TCDs) and roadway furniture, animation and visualization can permit the designer to review the complete environment that drivers will be subjected to if the design is built. Thus, design assessment can go beyond alignment analysis to other issues that impact driver/vehicle safety (e.g., TCD visibility).

It is important to keep in mind that the objective of the roadway designer is to design and retrofit roadways so that they are safe for all vehicle/configurations that will traverse them, not to do complex vehicle dynamic analysis or generate sophisticated photo realistic graphical displays. The tool that is created should provide the designer with an easy, efficient, user-friendly way to operate the analysis system

depicted in Figure 2. Capabilities much beyond this may add undesirable confusion and complexity to the designer's job.

D. Computer Hardware and Software

The IHSDM, VDM, and visualization process could be implemented on a variety of hardware platforms, which include the computer/processor, storage media, graphics accelerator(s), and display devices. Traditionally, relatively expensive workstations (e.g., Intergraph, Hewlett Packard, Digital Equipment Corporation, Sun MicroSystems, Silicon Graphics) with sophisticated graphics accelerators have been used for roadway design and visualization/animation. This situation has changed, however, over the relatively short period of this project (since September 1993). Low-cost PC technology has become quite powerful, including processors, sophisticated graphics accelerators and large, fast storage devices. Currently, the first three manufacturers mentioned above are producing sophisticated workstations based on PC technology, and it appears that this approach will become more powerful and prevalent as time goes on.

Software and available application programs have made similar advances as the hardware platforms discussed above. Throughout the 1980's sophisticated and expensive design and graphics/visualization applications were developed for the high-cost workstation market platforms. Furthermore, the C programming language and FORTRAN were the choice for scientific/engineering applications, which typically ran under the UNIX operating system and its variants. As PCs have become more prevalent and powerful, design and graphics/visualization application software has become available. Also, the Windows NT operating system is becoming the platform for scientific/engineering applications. A variety of higher level languages (e.g., C++, Visual Basic) can run under Windows NT, and can be mixed through the use of dynamic link libraries [dlls] e.g., Ref. 6.

With the availability of powerful, low-cost PCs running the Windows NT operating system and sophisticated software it would appear that this represents the future of affordable computing for design and graphics/visualization applications.

III. VEHICLE DYNAMICS MODELING

The VDM must follow a given roadway design in inertial or XYZ coordinates. The wheels must respond to elevation changes in the design, and the vehicle must follow the horizontal alignment geometry. Some driver speed and steering control functions will be required to follow the horizontal geometry, and the vehicle tires must respond to road surface friction to give longitudinal and lateral forces that will control the longitudinal and lateral/directional motions of the vehicle. The VDM that is considered here is Vehicle Dynamics/Analysis, Non-Linear (VDANL). VDANL is a comprehensive vehicle dynamics simulation program (Refs. 7 through 12) that currently runs on IBM-PC and compatible PCs, and was originally developed to run under the MS-DOS© operating system. VDANL has been under development for more than a decade and was firmly based on previous vehicle dynamics developments (e.g., Refs. 13 and 14). VDANL has also been evaluated and validated by a number of investigators (Refs. 15 through 18).

VDANL was initially intended for the analysis of passenger cars, light trucks, and multipurpose vehicles. The simulation model was designed to permit analysis of virtually all driver-induced maneuvering up through and including limit performance conditions defined by tire saturation characteristics (plowout, spinout) and rollover, and includes driver guidance and control features. One of the initial tasks on this project was to review VDANL and specify those features that needed to be updated to meet its intended application under IHSDM. As a result of this review, the following updates to VDANL were identified:

- Tire model expansion to accommodate off-road terrain interaction including low-shear--strength soils; ability to change parameters of each tire on the fly to accommodate shoulder and side slope incursions; independent lateral and longitudinal friction characteristics.
- Additions to accommodate tractor/trailer rigs; fifth-wheel hookup including hitch angle dependent roll stiffness; brake temperature fade effects.
- Road horizontal and vertical geometric alignment description consistent with the output from roadway design programs.

A. Model Formulation

Figure 3 gives a block diagram representation of the overall VDANL model, including driver control, and the interaction of the various individual VDANL components. The vehicle model equations cover the full range of lateral/directional and longitudinal motions up through large angles experienced in spinout and rollover. The vehicle model includes components for sprung and unsprung masses, suspension,

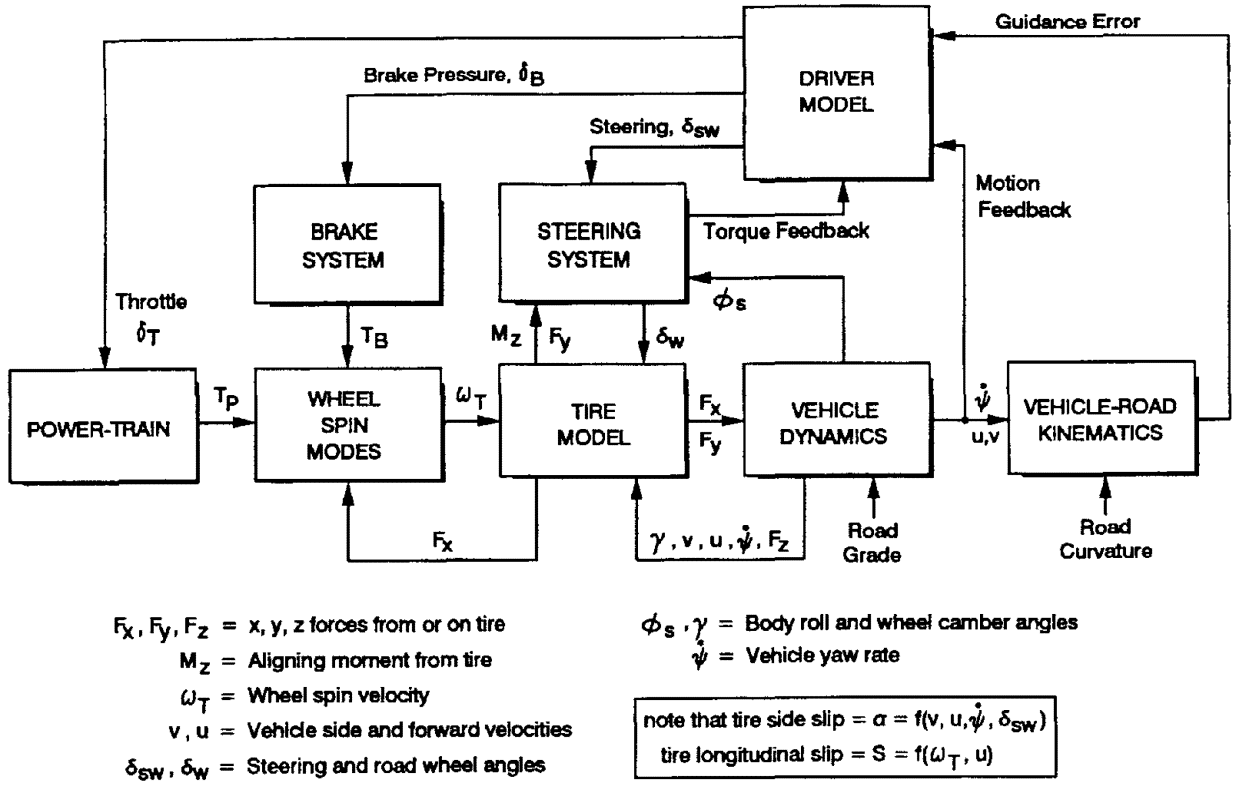

Figure 3. VDANL Overall Block Diagram

steering, braking, power train, drive train, and tires. The model accounts for all axles and tires and the effects of maneuver-induced load transfer. Additionally, the model allows for vehicles towing trailers, roadway terrain, and hazards. Both the vehicle dynamics and tire model are based on past research (Refs. 7.through 14) and have been extensively validated (Refs. 15-through 18). A complete description of the equations of motion describing the VDANL model is given in Appendix A.

Tire and wheel spin characteristics play a dramatic role in the vehicle dynamics response to vehicle maneuvering. The VDANL tire model is a nonlinear composite slip model that generates lateral and longitudinal forces and aligning moments as a function of normal load, lateral and longitudinal slip, and camber angle (Ref. 19). It correctly accounts for the interaction between the input variables including normal load, horizontal slip, camber angle, and tire/terrain friction. The wheel spin mode dynamics are important because angular velocity at each wheel is computed and used to determine the longitudinal slip ratio. This in turn defines the longitudinal force capability at each tire and should include effects such as locked wheels for skidding conditions. An antilock provision is also provided in the braking model.

Composite suspension characteristics are designed to represent wheel steer and camber motions relative to the sprung mass, and squat/lift forces resulting from tire ground plane forces acting on the suspension geometry. Wheel steer also arises from compliance in response to tire side force and aligning torque, and roll angle of the sprung mass relative to the unsprung mass.

VDANL allows for steering, throttle, and brake inputs. The steering model includes Ackermann steer effects, steer compliance, and a composite second order characteristic to simulate steering system dynamics in response to steering and aligning torque inputs. Throttle is used as an input to the power and drive trains that model engine, transmission, differentials, and torque splitting between the front and rear axles. Front, rear, and four-wheel-drive configurations can all be accommodated. The brake model includes simulation of vacuum boost run out and a nonlinear proportioning valve between the front and rear axles. There is also an option for using a generic antilock braking system and automatically setting front/rear brake proportioning.

VDANL can be used in a variety of ways to analyze vehicle maneuvering motions, handling, and stability. Input control commands (e.g., steering, braking, throttle, speed, aerodynamics) can be applied directly to the open-loop vehicle. Under driver model closed-loop control, the simulation can be excited with road curvature, lane position, speed commands, and obstacle avoidance inputs.

B. Vehicle Model Parameters

Given a vehicle dynamics model, specific vehicles are then simulated on the basis of parameter sets that describe the basic vehicle properties (e.g., configuration, size, inertial and suspension characteristics, tire properties). As with any complete vehicle dynamics simulation, VDANL has a rather detailed set of parameters required to describe a particular vehicle. Model parameters and measurement procedures are summarized in several Appendices to this report. Appendix B describes vehicle parameter measurement and estimation procedures. Appendix C describes suspension parameter measurement and estimation procedures. Appendix D reviews a variety of vehicle parameter measurement test methods. The detailed equations and parameter set for the VDANL tire mode__STIREMOD__are described in Appendix E.

Given the roadway design assessment application of VDANL within IHSDM, it was decided to use the American Association of State Highway Transportation Officers (AASHTO) design vehicles (Ref. 20). These vehicles provide a diverse range of characteristics of highway vehicles that are of interest for highway design. At the start of this project VDANL did not have the ability to model all 15 configurations found in the AASHTO Policy on Geometric Design of Highways and Streets. Specifically, it did not

provide for the modeling of multiple trailer towing. Furthermore, although VDANL includes parameters for a wide range of vehicles, not all of the vehicle configurations specified in AASHTO are included. Therefore, extensions were needed to accommodate large trucks and their trailers and tires.

Table 1 indicates each of the AASHTO vehicle configurations (Ref. 20), its classification symbol, and whether VDANL could originally support the configuration with or without parameter modifications. The table also shows what vehicles can be accommodated with the current upgraded version of VDANL, i.e., Version 6.0. The remaining vehicles are essentially multitrailer configurations, and it was deemed beyond the scope of this project to accommodate them. The modifications required to accommodate the vehicles with an upgraded VDANL included a fifth-wheel hitch with a hitch angle dependent roll compliance, and brake system upgrades including air pressure delays and thermodynamic effects that influence brake effectiveness.

Table 1. VDANL Support for AASHTO Vehicles

Vehicle Configuration	Symbol	VDANL originally supported	Upgraded VDANL (Version 6.0) supports with appropriate parameters	VDANL does not support
Passenger car	P	√		
Single-unit truck	SU	√		
Single-unit bus	BUS	√		
Articulated bus	A-BUS		√	
Intermediate semitrailer	WB-40		√	
Large semitrailer	WB-50		√	
"Double Bottom" semitrailer, full-trailer	WB-60			√
Interstate semitrailer	WB-62		√	
Interstate semitrailer	WB-67		√	
Triple semitrailer	WB-96			√
Turnpike double semitrailer	WB-114			√
Motor home	MH	√		
Car and camper trailer	P/T	√		
Car and boat trailer	P/B	√		
Motor home and boat trailer	MH/B	√		

The final requirement to simulate the AASHTO vehicles is to set up appropriate parameter sets. There are several sources for generic data on a range of vehicles (Refs. 7, and 21 through 25). The generic AASHTO vehicle parameter sets were configured from data given in these references, as summarized in Appendix F.

C. Roadway Description

The roadway design description must define the horizontal and vertical alignment of the road. The horizontal alignment will be used by the driver model to control steering and speed. Vertical terrain inputs affect the vehicle model through the tires. The altitude of the road surface must be specified at each tire on each axle continuously throughout a run corresponding to the vehicle's trajectory. The vehicle model must be able to convert the roadway terrain into a form so that the vehicle dynamics respond accordingly to tire normal load and lateral and longitudinal maneuvering forces. The roadway parameter description must also include attributes for each of the surfaces (i.e., pavement, shoulder, side slope) so that appropriate tire model parameters can be called for the generation of the maneuvering forces.

Several different issues had to be addressed in order to establish a useful roadway design parameter format for the VDM. First, the desired roadway description had to be consistent with current practice in roadway design software. Second, the design description should be relatively efficient, and not require excessively large amounts of data to obtain the necessary accuracy required for the alignment and cross-section description. Third, the roadway description must be consistent with vehicle dynamics simulation requirements.

Two main issues must be considered relative to vehicle dynamics simulation requirements. First, the roadway description should allow for direct computation of roadway height under each wheel. Second, the altitude computations from the design description must be continuous and relatively smooth from one calculation to the next so that the paved surfaces appear relatively smooth. This is the same issue road builders/repavers face in preparing a smooth paved surface that will not cause excessive excitation of vehicle suspensions. Variations must be down on the order of hundredths of a meter for acceptable smoothness.

The general problem of the roadway design description is essentially the finite element issue that is, getting a finite number of discrete elements to approximate a continuous entity. One model description that is commonly used in 3D graphics involves describing an entity (in this case the roadway and side slopes) as a triangular mesh. This essentially turns the roadway into a series of flat, triangular

plates. Depending on road geometry and the size of the plates, this description can lead to a very rough appearing road from the point of view of the vehicle dynamics. This description may give an adequate visual appearance, but be very rough in terms of vehicle suspension response. This is a common occurrence on roadways, where nonobvious undulations in the road bed cause a very rough ride.

The original version of VDANL used a rectangular grid approximation to roadway description. It was found that the roadway had to be defined in very small increments to avoid injecting unrealistic roughness. Some triangular mesh outputs from roadway design programs were studied at the outset of this project and were also found to be unnecessarily rough. One solution to this problem that is used in driving simulators is to use a smoothing function (typically, a polynomial such as a spline function) that is fitted to the points in the terrain description, which gives continuous derivatives at each of the altitude points in the polygon description. This allows one to use a terrain description intended for graphical visualization as an input to vehicle dynamics. This approach is still not very satisfactory, however, because the polynomial terrain files are usually large, and are difficult to search for determining tire locations and altitudes.

The FHWA has come up with a much more elegant solution to the above problem, using a roadway description that is common in highway design and surveying (e.g., Ref. 20). This approach is illustrated conceptually in Figure 4, which shows horizontal and vertical alignments and cross-sections defined at stations along the length of the road. Each station is defined in terms of an X,Y location and an altitude in the order in which they occur along the roadway. Stations are defined at points where the horizontal or vertical geometry changes. At each station the alignment is described in terms of curvature, and the cross-section is defined in terms of slopes of lanes, shoulders, and side slopes. There are also transitions defined for changes in horizontal and vertical geometry. Parabolic vertical curves are used to transition from one grade to another. Transition spirals are used to connect tangents to sections with horizontal curvature. The detailed roadway design definition for this approach is given in Appendix G. This approach gives smooth surfaces and, most importantly, a continuous derivative at transition points. It is also computationally convenient to locate and update wheel position relative to the roadway alignment as the vehicle moves along the road from station to station.

The above roadway description has now been defined as an output of the design program GEOPAK (Beiswenger, Hoch & Associates, Inc). This program is a civil engineering software package that runs within the MicroStation (Bentley Systems, Inc.) environments which is a CAD design program for civil and mechanical engineering. GEOPAK allows the user to model roadways as meshes of either triangular or rectangular elements. The GEOPAK roadway meshes that are composed of rectangles are

smoother and less coarse than roadway meshes composed of triangular elements but still not adequate for vehicle dynamics as discussed above. GEOPAK is highly "customizable" due to the fact that system features can be modified using routines written by the user in the C programming language. This approach has been taken to create the new roadway description format discussed above.

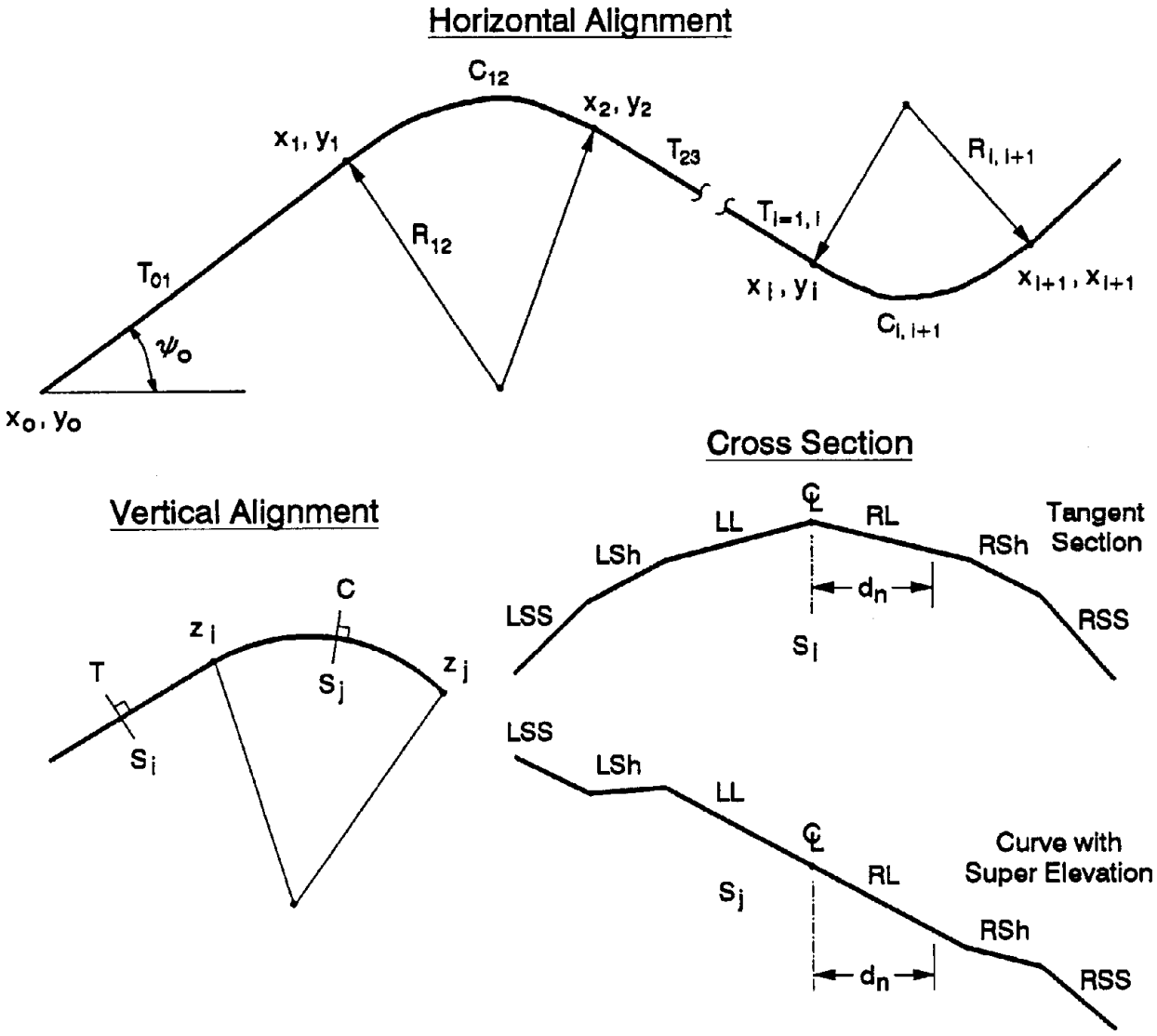

Figure 4. Roadway Description

IV. DRIVER CONTROL

There must be some sort of basic control features to guide the vehicle over the roadway horizontal alignment and control speed. This control must anticipate upcoming horizontal curvature in order to maintain lane position within a third of a meter or so, and to adjust speed to maintain safe lateral or cornering acceleration. These control features amount to a driver control model that is over and above the basic vehicle dynamics. VDANL has driver steering control functions. For this effort we have added some additional steering control features and a speed control model that anticipates upcoming horizontal curvature.

A. Steering Control

The driver exerts steering control to maintain lane position, and maneuver when following curving roadway alignments, changing lanes and avoiding obstacles. Unpredictable roadway and aerodynamic disturbances can randomly move the vehicle within the lane, and the driver must counteract these disturbances with compensatory behavior (i.e., reacting to perceived errors). When maneuvering to follow roadway alignments, change lanes, or avoid obstacles the driver has some preview of the required path, and in these cases steering inputs can be based on the perceived path information. In the manual tracking literature, this preview control has been referred to as "pursuit" control in as much as the driver is pursuing a perceived input (this terminology actually arose in the aviation psychology literature where pilots were said to be pursuing targets (e.g., Refs. 26, and 27).

A generic steering model for pursuit and compensatory control is shown Figure 5. While exerting steering control based on path preview, the driver must still control lane position errors in a compensatory fashion, so the driver's steering control process always includes compensatory behavior, and may include pursuit behavior depending on road alignment and traffic maneuvering demands. Compensatory control is carried out in a closed-loop fashion (e.g., the driver is continually reacting to perceived error, which results from a combination of input disturbances and the driver's control activity). This closed-loop compensatory control requires that the driver react in a stable manner, based on the amplitude and timing of the steering responses. We know that drivers behave in a stable manner most of the time, based on general experience and experimental measurements (e.g., Refs. 28 and 29). The stability requirements for driver closed-loop control have been analyzed in some detail (Ref. 30) and have been applied in previous versions of VDANL (Ref. 10).

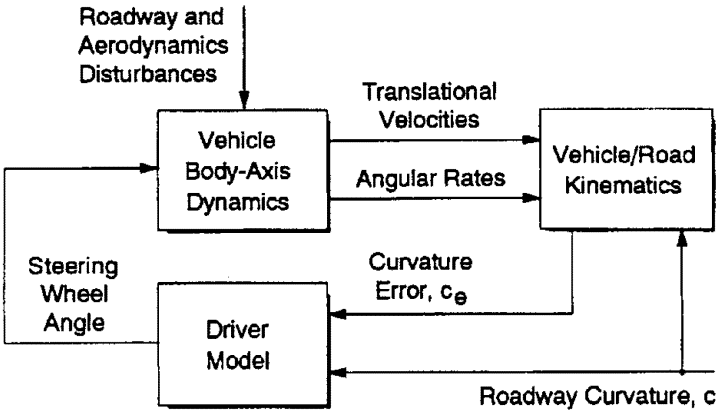

Figure 5. A Generic Steering Control Model Including Compensatory and Pursuit Control

For pursuit control, the driver must have some preview of the required path. This behavior has been studied in person-in-the-loop driving simulations (Refs. 31 and 32), and driver models have been developed from the experimental data that include steering actions directly proportional to roadway curvature. These models account for driver perception of road curvature some distance ahead of the vehicle, and have been characterized as incorporating a "look ahead" distance or headway time (distance divided by velocity).

B. Speed Control

Speed control is important in roadway design in that drivers must slow from high tangent approach speeds in order to safely negotiate curve sites with lower design speeds. This behavior involves two aspects, as suggested in the Figure 6 block diagram. First, drivers must decide on a speed profile (i.e., command speed) based on speed warning signs and perceived roadway curvature. The effect of signs on speed selection is not clear. Some research has tried to influence behavior at high-accident-site curves with innovative sign and delineation modifications to emphasize curvature perception (Ref. 33), but the signs were found not to be effective. Research in Scandinavia (Ref. 34) has shown a positive response to speed limit signs, and it is noted that enforcement and punishment of speed limit violations in Nordic countries may be a significant factor. Second, the driver must respond to the command speed in a stable manner similar to the above discussion for compensatory steering control. Data for driver compensatory speed control are available primarily from car following research, as discussed next. Little if any data have been available up to quite recently on command speed selection. A recent report with relevant results on driver speed selection in curve encounters is discussed subsequently (Ref. 35).

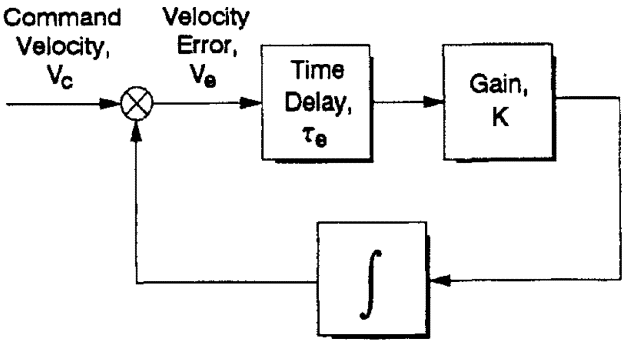

Figure 6. A Generic Speed Control Model

1. Car Following

Car following research can provide information on the compensatory dynamics defined in Figure 6. These dynamics are assumed to apply to all driver effort to control speed, and are reviewed here in the context of control to a desired or command speed. Past research has dealt with driver headway control models and measurements of driver behavior. Pipes (Ref. 36) carried out fundamental work in this area, and Bekey and his students at USC provided a useful summary of past work and further analysis on the general problem of driver lead car following (Ref. 37). The models assumed that, during car following, the driver attempts to minimize velocity differences with a lead vehicle (i.e., a well-defined stimulus), as illustrated in the Figure 7 compensatory structure where the command speed input is the lead car velocity.

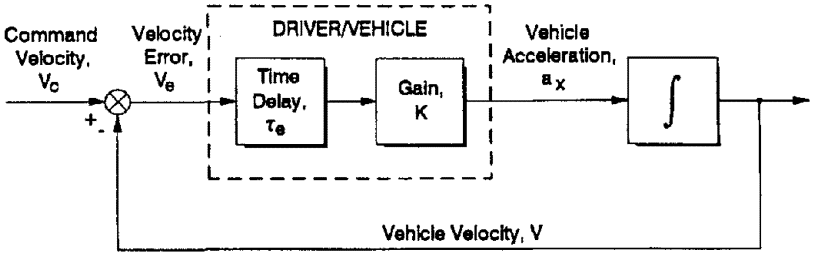

Figure 7. A Compensatory Driver Speed Control Crossover Model

Recent work has reported measured driver car following behavior under both test track and open highway driving conditions (Ref. 38). Driver behavior across a large number of subjects was consistent with earlier models. Driver speed control is carried out with a much lower bandwidth than steering control. Driver time delays are a factor of 10 times longer for speed control compared with steering control. Driver bandwidth in response to speed errors is therefore a factor of 10 times lower than for steering control.

Accelerations during speed control are typically less than 0.05 g (85 percentile levels are on the order of 0.03 g, (Ref. 38) while steering control can be on the order of 0.3 g. The speed maneuvering accelerations are consistent with the control authority the driver can command with the vehicle throttle. Higher decelerations can obviously be obtained by braking, but drivers do not routinely brake for geometry induced speed selection.

2. Speed Selection

An important aspect of our driver speed control model is the speeds exhibited by drivers during real world curve encounters. Recent work (Ref. 38) has reported on measured driver behavior at a range of locations involving a tangent approach to curves, and supplementary data described in Ref. 34 are available from this research. This database provides files of actual measures of driver speeds at specific tangent and curve sites in several states. Some supplementary data analysis was carried out on this data set to obtain additional insight into driver speed control over and above that provided in Ref. 39.

We looked at three sets of spot speed data: tangent, curve, and tangent-curve for speed pairs. The pair data were obtained by measuring tangent and curve speeds for a specific vehicle, then taking the differential between those two speeds for each observed vehicle. Distributions were calculated and plotted for the tangent, curve, and pair data, then a regression analysis was carried out to determine the relationship between tangent-curve differential speed and the initial tangent speed. The hypothesis was that drivers going faster on the tangent must slow down more in the curve.

We selected four sites from the Ref. 39 database for this preliminary analysis. Each site represented a different categorization according to the highest 85^{th} percentile velocity. The regression analysis indicates that there is a useful statistical relationship between driver tangent speed and the amount of slowing for the curve. This data analysis is summarized in Figure 8, and metrics from this analysis are summarized in Table 2. Not surprisingly, the faster a driver's tangent speed, the more he or she generally slows in the curve. A significant linear regression relationship for this slowing was found at three of the four sites. Faster drivers do not slow as much as might be expected, however, because the slope of speed change versus tangent speed was only about 40 to70 percent depending on the degree of curvature. Once the regression relationship is accounted for, the speed variability (standard deviation) about the regression line is on the order of 4.0 to 5.6 km/h.

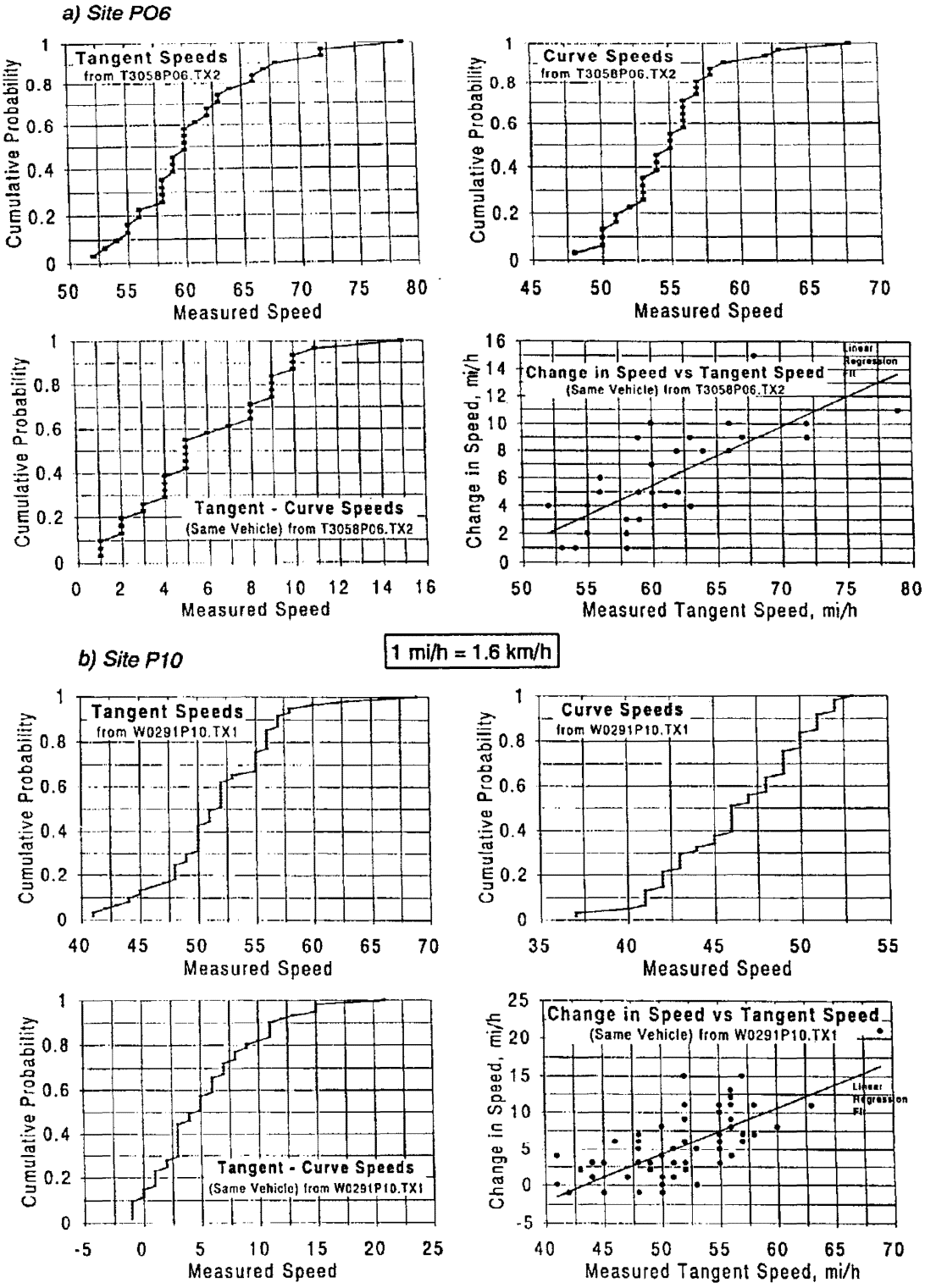

Figure 8. Speed Distributions and Regression Analysis for Open Road Driving (Data from Ref. 39)

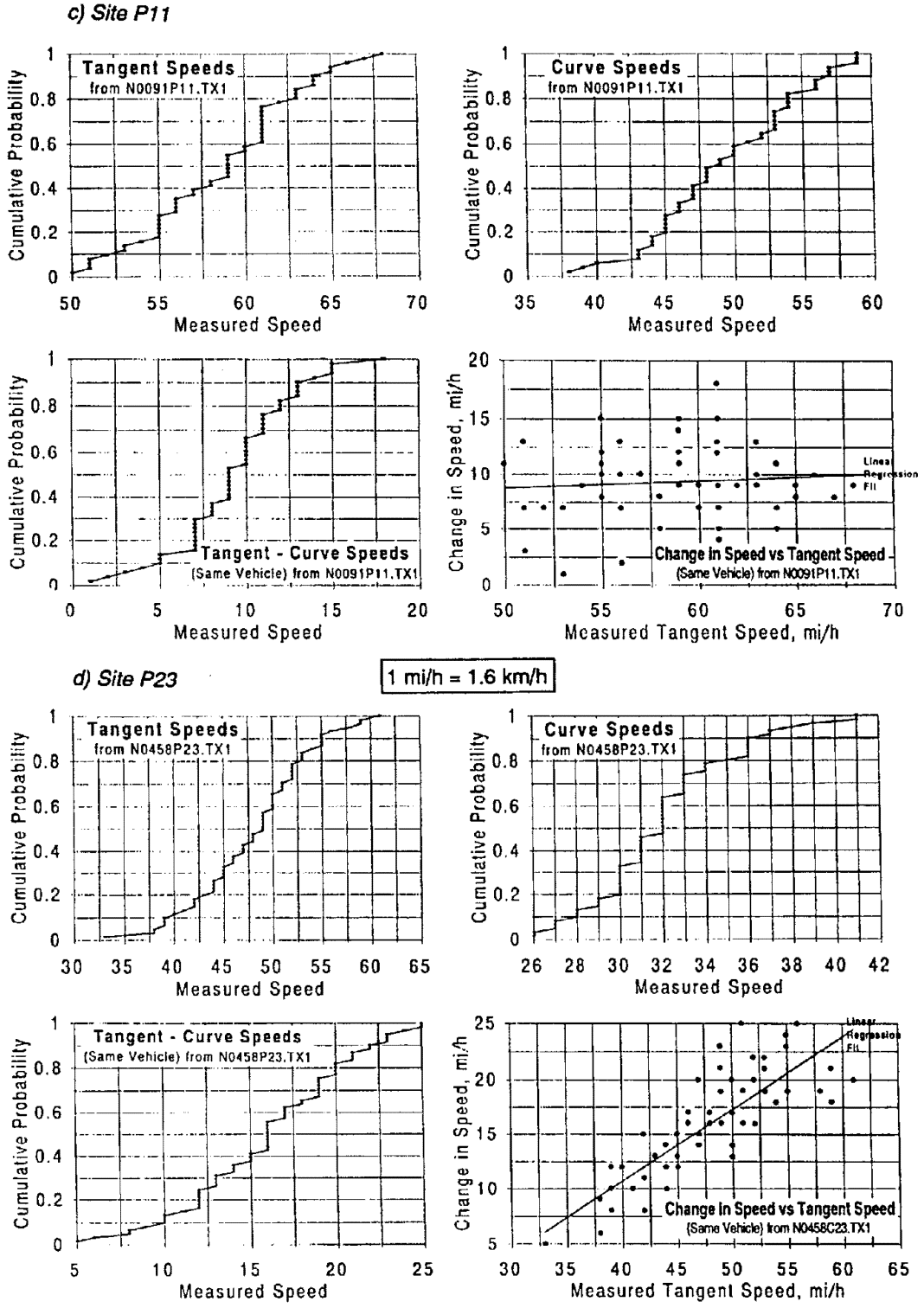

Figure 8. Speed Distributions and Regression Analysis for Open Road Driving (Data from Ref. 39) (concluded)

Table 2. Summary Of Site Characteristics and Speed Distributions for Open Road Driving (adapted from Refs. 35 and 39)

Tangent/Curve Fair Site		P06	P10	P11	P23
Curve Characteristics	Degree Curv. (Radius)	6° (955′)	10° (530′)	11° (521′)	23° (249′)
	Length	1015′	NR	190′	438′
	Super Elev.	0.08	0.06	0.07	0.10
	Design Speed (mi/h)†	55	44*	40	30
85th Percentile Speeds (mi/h)	Tangent	68	56	63	54
	Curve	58	51	56	36
	Tangent-Curve	9	11	13	21
Maximum Observed Speed (mi/h)†		68	53	59	41
Calculated Speed for 0.75 g Cornering		103.3	77.0	76.3	52.8
Computed Cornering Acceleration (g)	@85th Percentile Speed	0.237	0.329	0.404	0.349
	@ Maximum Speed	0.325	0.356	0.440	0.453
Regression Analysis	R^2	0.55	0.48	.01	0.66
	DOF	29	59	49	59
	X Intercept (mi/h)	57	43	NA	24
	Slope	0.43	0.64	0.07	0.66
	Stand. Error σ_y/x (mi/h)†	2.37	3.49	3.44	2.75

*Calculated from radius and superelevation
† 1 mi/h = 1.61 km/h

The data are notable in that driver speed change was independent of tangent speed according to the regression analysis. This site consequently had a wider distribution of curve speeds and may be a problem location in terms of design consistency. The data show that drivers on the average slowed down about 14.5 km/hr (9 mi/h) in the curve. Also note that the curve speed distribution shows several drivers at speeds of about 93.6 km/hr (58 mi/h) on a curve with a design speed of 64.5 km/hr (40 mi/h). In the Ref. 35 analysis, the data were classified as a curve with one of the highest differentials between the 85th percentile speed and design speed.

In Table 2, lateral accelerations are computed for the 85th percentile and maximum curve speeds assuming drivers faithfully follow the curve. This data summary shows that, even at the maximum speeds observed, drivers keep their lateral acceleration below 0.5 g. At the 85th percentile speeds, driver lateral accelerations range from 0.24 to 0.40 g. However, given the number of observations (e.g., note the degrees of freedom (DOF) for the regression analysis), we only have the ability to see at most the 97th to 98th percentile point. Accidents are rare events, and true extreme speeds are probably much higher than shown in Table 2 (e.g., the 99.9th percentile data). In Table 1 we have computed speeds required to give 0.75 g lateral acceleration (a typical level for maximum vehicle cornering capacity). Here we see for the sharpest curve (site P23), the speed for limit performance cornering is only a little over 16.1 km/hr (10 mi/h) above the maximum observed speed. Also, note that this site had the highest calculated lateral acceleration.

This preliminary analysis of the raw data from Refs. 35 and 39 data suggests that there is considerable additional information to be learned about the statistical nature of driver speed reduction in approaching curves. Further analysis was outside the scope of this project, but adequate data have been obtained on which to base preliminary driver model requirements for speed selection. The basic characteristics of interest here include speed reduction as some percentage of the curvature requirement (nominally the design speed), and speed variability beyond this nominal requirement. For sharper curves, the preliminary analysis suggests that extreme speeds could approach typical vehicle limit cornering performance limits.

It should be noted here that there are higher level models of driver behavior, including cognitive and stochastic factors, which could be considered (e.g., Ref. 40). It was felt that deterministic modeling was appropriate in order not to introduce variability into the analysis process. Cognitive issues were not felt to be important because of the general design problem at hand namely two-lane rural roads without traffic.

C. Driver Models

1. Steering Control

VDANL has had a fairly well-developed driver steering control model for responding to curvature errors, and this model is based on measurement of driver steering behavior and stability analysis (Refs. 10, 29, and 30). On the basis of previous research on driver response to perceived curvature (Refs. 31 and 32), the VDANL driver model was updated with a steering "feed forward" command so that the driver model now responds to curvature error commands as well as directly to perceived curvature, as illustrated in Figure 9. The compensatory steering loop that responds to curvature error has also been compensated for basic vehicle understeer, so that steering stability will be maintained over the full speed range.

The driver model look-ahead distance for steering control is on the order of 1 s, which is consistent with previous research. At a speed of 105 km/h (65 mi/h or about 96 ft/s), the driver would be looking ahead on the order of 30 m (100 ft). Other driver parameters are set to nominal values based on past research (e.g., Refs. 10 and 29 through 32).

2. Speed Control

Driver speed control is based on a combination of a prevailing speed limit for tangent speeds, and maintenance of safe cornering acceleration during curve encounters, as summarized in Figure 10. The speed command is determined by either the speed limit or a lower speed based on maintaining a safe/comfortable cornering acceleration. On straight sections the driver will continue at a specified tangent speed (i.e., the speed limit). When the driver detects curvature at the specified look-ahead time, speed is then reduced accordingly to maintain desired cornering acceleration.

Look-ahead time for speed control is set to a much larger value than for steering because of the much slower speed response of the driver/vehicle longitudinal control discussed above. Look-ahead time for speed control is set on the order of a few seconds. Thus at 105 km/h (65 mi/h) or about 96 ft/s), the driver would be looking for curvature cues on the order of several 30 m (100 ft) ahead of the vehicle. A deceleration of 0.05 g at a look-ahead distance of several seconds would allow the driver to decelerate on the order of a few kilometers per hour.

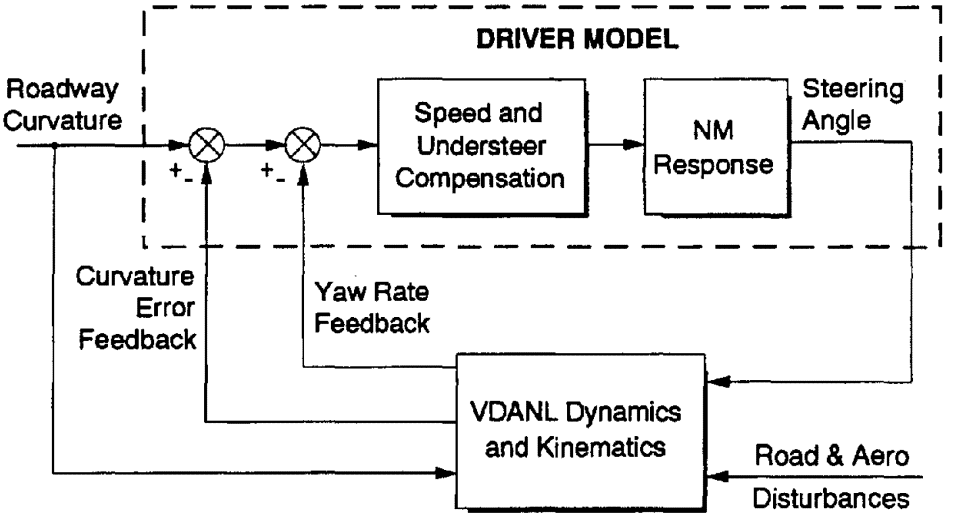

Figure 9. VDANL Driver Steering Control Model

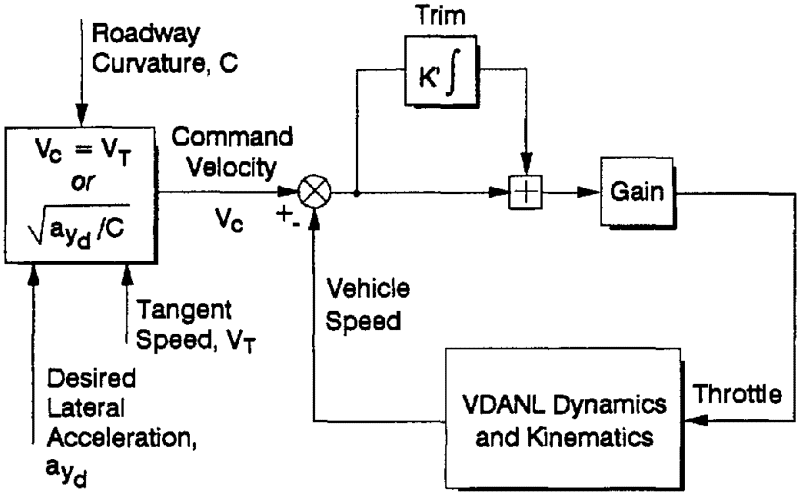

Figure 10. VDANL Driver Speed Control Model

V. USER INTERFACE

It is critical for the VDM user interface to be convenient for roadway designers. While the detailed VDANL user interface is designed for vehicle dynamics analysts, the interface options can be specified and run automatically through the use of macro files that essentially list a desired set of run time options. The roadway designers interface for VDANL allows specification and selection of predefined macro files.

These macro files allow for the selection of a vehicle type (i.e., AASHTO vehicle class), desired maneuvering (e.g., path following, speed profile), and terrain file input. Vehicle and driver characteristics are predefined in parameter files that the roadway designer need not be concerned with. However, options allow for the driver to be more or less aggressive given specification of a speed limit and maximum maneuvering acceleration.

The VDANL/IHSDM start-up screen is shown in Figure 11. On the left side we see the first option for selecting 1 of 12 AASHTO vehicles to be used in the roadway design evaluation. The second option allows for selecting the desired roadway design for analysis. The third option permits the designer to select a predetermined speed profile for running the analysis. If a speed profile is not selected, then the driver model will control speed during the run according to its speed control algorithms. The third and fourth options allow the user to select a speed limit and maximum desired maneuvering acceleration. The speed limit will constrain tangent speeds to the value stated. The maximum desired maneuvering acceleration limits speed on curves to give the stated cornering acceleration. The fifth option allows the user to specify the distance over which the analysis will be carried out. The sixth option allows the user to place the vehicle at a desired lateral position.

From the roadway designer's point of view, the VDM interface allows for selection of options relevant to roadway design. Data collection and presentation are predefined so that the designer has access to meaningful performance plots similar to
Figure 12 and data files that can be used for visualization, as discussed next. Performance metrics have also been defined that summarize vehicle maneuvering on a given run. The so-called Roadway Safety Metric screen is illustrated
Figure 13 for a given run. This screen gives the peak value of several different metrics of vehicle performance and the station (distance down the road) at which they occurred.

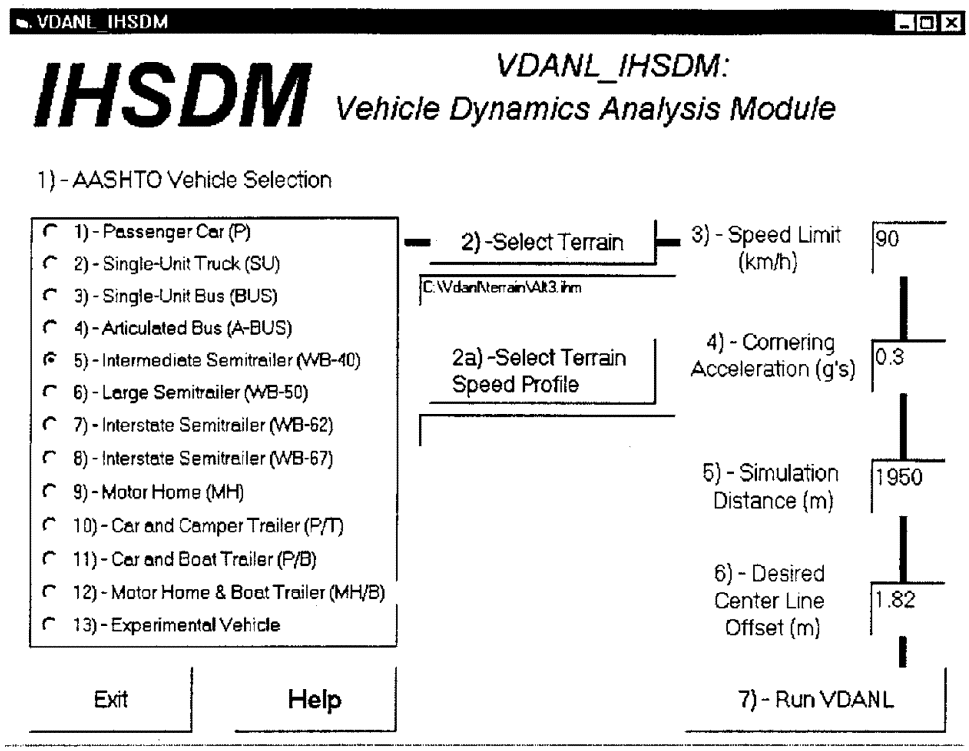

Figure 11. VDANL/IHSDM Start-Up Screen

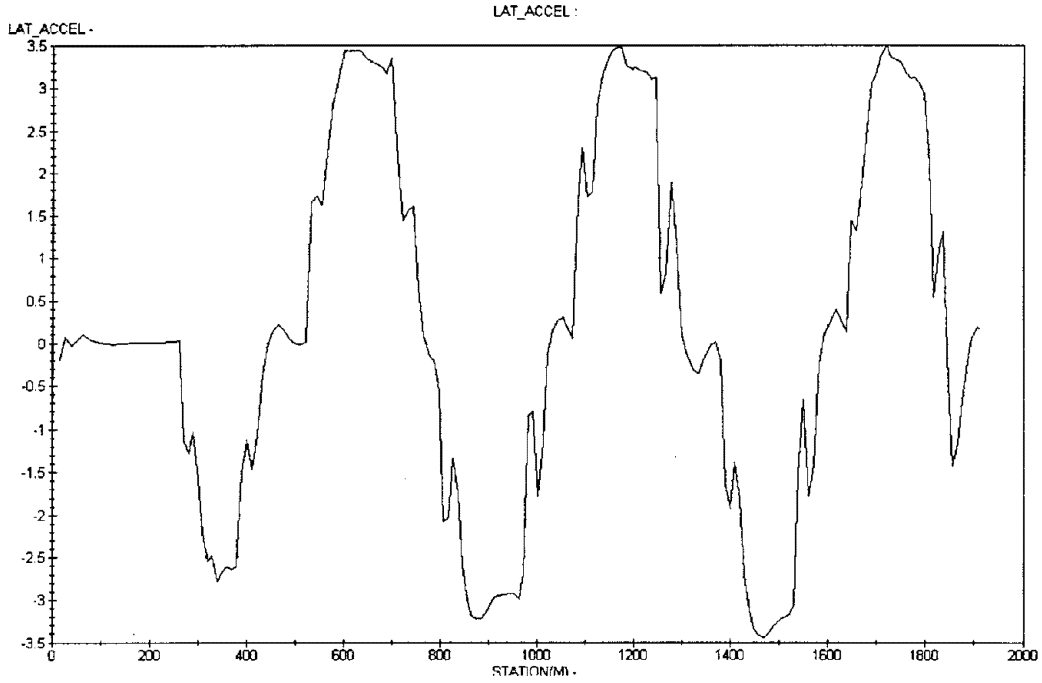

Figure 12. Example of Vehicle Performance Plots vs. Station: Lateral Acceleration Profile of the Tractor of Vehicle 5 on a Winding Road

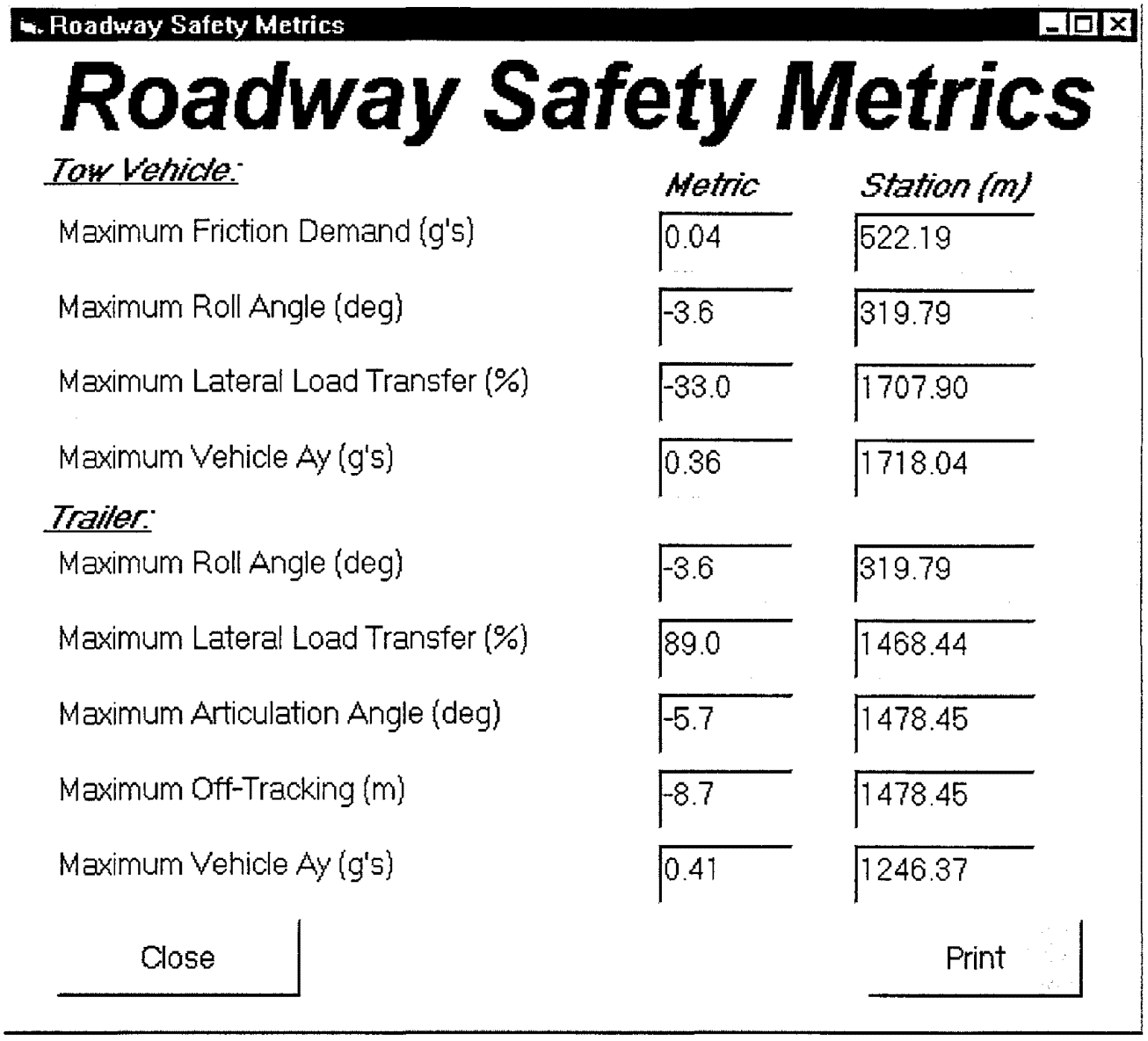

Figure 13. Example of Roadway Safety Metric Screen

VI. VISUALIZATION

CAD has become a major driving force in the expansion of the computer industry. Currently there is a wide range of CAD software packages that allow users to both design and visualize complex 3D images on various computer platforms. Additionally, there are support packages that can be used in conjunction with CAD systems to provide an even greater range of flexibility (e.g., Ref. 5). Some examples of these support packages include surveying, photo-realistic graphical displays, animation, roadway design, and mapping. One must determine exactly what is of interest for a particular project and then choose the tools that will best achieve specified goals.

For this portion of IHSDM, the first two steps of the design and analysis process shown in Figure 2 are to generate the roadway that the vehicle will be traversing, and then, using a comprehensive validated VDM, generate the vehicle responses as the vehicle traverses the roadway. The final step allows the user to visually see what happens when the vehicle travels over the specified roadway. To be able to do this, a visualization software package must be included in the system. The requirements and application of the visualization software and how it relates to IHSDM will be discussed next.

In general, the graphic scenes that are created will take images comprised of polygon meshes and perform the transformations required to convert the images from physical to viewing space, a process which is usually referred to as rendering. Rendering encompasses a wide range of activities, including transforming the objects into the viewing axis system, perspective transformations, hidden surface removal, lighting effects, object shading, and texture mapping. To accomplish the 3D animation required by IHSDM, the visualization software must be able to perform various degrees of rendering. For detailed information on computer graphics rendering techniques, see Refs. 41 and 42.

The quality of the rendering will ultimately determine the quality of the image displayed to the user and, at a minimum, the rendering capabilities must include transformations from 3D physical space to the 2D viewing screen, perspective transformations, hidden surface removal, and shading. Initially, for this application, advanced features such as texture mapping and ray tracing (this allows for effects such as shadows and reflections) are not necessary, but could be used later on to produce photorealism when designs are to be submitted for review. In the end, the sophistication of the rendering techniques used will be decided on the basis of performance tradeoffs. These tradeoffs deal with the computational time and complexity that is involved in generating the visualization scenes. Different rendering techniques require more computation time in order to create the image, but may not greatly enhance the overall quality of the image displayed.

The performance tradeoff becomes increasingly more important depending on how many polygons the total display scene contains. Since each polygon must be rendered independently, the more complex the display scene the longer it will take the software to compute the display. Therefore, although ray tracing may be acceptable for simple displays, too much computation time may be required to render complex display scenes. Another method should then be used instead. Since rendering encompasses everything that is required for displaying an image, by default, it becomes the limiting factor in how fast the computer system can generate images. This is why, when possible, rendering is generally done with hardware graphics accelerators.

In addition to the rendering capabilities, the IHSDM system also requires that the visualization software communicate with the other software components via data files as indicated in Figure 14. This software-to-software interface is important because there will be different file types that the visualization software will need in order to create an animated display for the roadway designer. These file types consist of a terrain description, a vehicle dynamic trajectory output description, and a vehicle 3D model description. The terrain description will include the roadway, shoulders, side slopes, surrounding terrain as desired, and can include TCDs and highway furniture. Together, the two 3D model files and vehicle dynamic trajectory description along with observer specification will determine what is displayed to the user.

Given new computer hardware capability that will be discussed in the next section, it is also possible to give the design a more dynamic view of the VDM. Current visualization approaches specify the animation and observer's position and orientation. For example, the observer might view the vehicle traversing the roadway design from some point over the road and possibly moving along the road with the vehicle. Alternatively, the viewer might be placed in the vehicle with a forward view. Given new low-cost hardware, including fast graphics accelerators and head-mounted virtual reality displays, it is also possible to allow the designer to drive through a new design and look wherever is desired. This drive-through could even amount to a simple, low-cost driving simulator, with the designer controlling his or her movement with a steering wheel, and accelerator and brake pedals.

The design analysis and review process was shown earlier in Figure 2, and in more detail in Figure 14. Basically, the entire process will work as follows. The user will use CAD roadway design software (e.g., GEOPAK) to design and create a test roadway. This roadway will then be saved to a file that the visualization and VDM software can use. The VDM will then use this roadway, a specific vehicle configuration, and a set of operating conditions to create a vehicle dynamics trajectory file that the visualization software can use. The user can then use these two files and a predefined vehicle 3D model description file to create the desired animation.

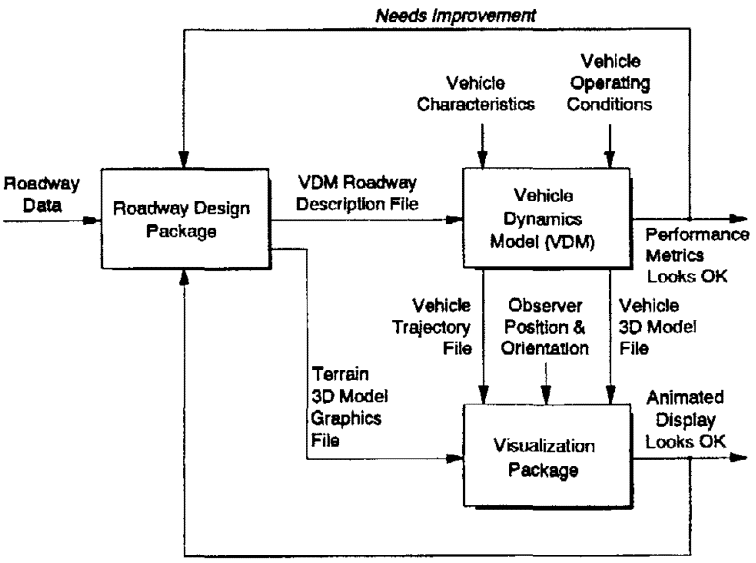

Figure 14. VDANL Visualization Process Involving Data File Communication

The dynamic vehicle trajectory file will control how the vehicle configuration will be moving with respect to the roadway. Depending on the complexity of the vehicle configuration and final animation that will be displayed, the trajectory file will contain various data. Basically, the trajectory file will contain the body axis angles and inertial vehicle positions for each mass that is being displayed. The body axis angles will be used to rotate the vehicle and the inertial positions will be used to translate the vehicle in 3D space.

The final information that is required by the visualization program consists of object configuration 3D model files. These files contain the 3D shape of the object that will be shown to the designer during the animation process. These description files will be predefined and simply loaded into the visualization program when they are needed. By saying that the descriptions are predefined we mean that the user or someone else has already created the 3D model and it is currently available for use. Several sources offer a wide range of ground vehicles that have already been created and saved in various file formats. In general, object files can include the vehicle that is being used in the VDM, roadway signs, guard rails, curbs, etc.

When all the required visualization files have been loaded, the next step is to animate the objects so that the software shows the vehicle actually traversing the specified roadway. This will require the software to display the objects and allow them to move relative to one another each time a new display frame is shown. First the roadway terrain and all fixed obstacles in the display scene are generated. These will not be moving so they will be used as a reference for all remaining dynamic objects. The software must then allow the vehicle and any other moving masses (axles, trailers, etc.) to be displayed on top of the roadway. This is

done for a specified number of time steps, thus creating an animated display. Additionally, if the observer's position is changing, the software must be capable of creating the display such that each object is displayed in its correct position relative to one another.

Part of the rendering process deals with the position of the observer. This will ultimately determine how the final animation will be displayed. The best analogy for understanding the observer position is to think of the observer as a camera. In the simplest example for photographing the vehicle traversing the roadway, the camera would be placed at a single location and that would be the view seen by the user. By placing the camera at strategic positions, the user can see how the vehicle traversed certain portions of the proposed design. In most cases this single camera angle approach is probably sufficient, and it is also the easiest viewing system to implement.

Some more advanced viewing systems allow the camera to move, both rotating and translating. In some cases, it may be desired to have the ability to move the camera or change the camera angle during the animation run. For example, the camera can be placed in the middle of a curve and will be pointing at the vehicle at all times. Therefore, as the vehicle approaches and passes the camera, the camera rotates with the vehicle and the vehicle is always in the camera's view. Additionally, there may be other applications where the camera itself will be moving (helicopter view), and the user will need to specify the path of the camera. One final camera position that is of particular interest for IHSDM is the driver's eye view. By placing the observer's position at the driver's eye, the designer can obtain views of the proposed roadway from a driver's perspective. This allows the designer to make judgments about sight lines and other visual cues that are important to the driver.

Although there are some very sophisticated visualization software packages that include many advanced features for creating photorealistic graphical displays, most of these features are not necessary for the IHSDM project. The visualization portion of the IHSDM project simply requires an animated graphical display that shows the vehicle traversing the proposed roadway design. The final result does not have to be motion picture quality; it only needs to give the user a realistic representation of what happened when the vehicle traveled over the proposed roadway design. More photorealism may be important, however, for cases where designs are to be reviewed by planning groups and/or the public. Hardware and software considerations are discussed in the next section.

VII. HARDWARE AND SOFTWARE

Clearly, hardware and software are significant issues in carrying out vehicle dynamics analysis and visualization. As stated earlier in the background section, hardware and software capabilities have changed rather dramatically during the course of this project, and there is every indication that dramatic improvements will continue in the near future. At the beginning of this project, serious graphics capability was the domain of UNIX-based workstations. At the time of this writing, sophisticated graphics processing can now be carried out on low-cost Intel-based PCs running Windows NT. For example, bench marks were recently published for a range of graphics systems (Ref. 43) and several Intel-based systems with graphics accelerators were shown to be as powerful as mid-level UNIX-based systems from Silicon Graphics, Inc. With-low cost PCs and graphics accelerators, it is now even possible to run VDANL in real time in response to steering, throttle, and brake commands, and to produce real-time photorealistic graphics that can be driven in the sense of an interactive driving simulator (Ref. 44). Head mounted virtual reality displays can also be used, which frees the highway designer to be able to look around, in real time, in whatever direction is of interest (Ref. 45).

A. Computer Platforms

Because of rapid hardware/software developments, evaluations performed on this project are seriously out of date. We will report on these project evaluations, but will also attempt to update them to cover trends that should be taken into account for future IHSDM investments. For example, MS-DOS and UNIX software were the focus of evaluations at the beginning of this project, while the VDANL software developed here currently runs under Windows NT along with several sophisticated graphical visualization programs. PC processing and storage speed and capacity have probably increased on the order of five times during the course of this project, and very powerful, low-cost graphics accelerators have been introduced that can carry out sophisticated photorealistic rendering in real time. These developments were not contemplated at the beginning of this project, but will clearly dictate CAD decision making in the future.

The IHSDM is intended to be used as a tool for various tasks dealing with roadway and roadside safety applications. Therefore, the primary users will be Federal and State highway departments and their consultants. These two separate groups tend to work on different computer platforms. In general, many highway departments have invested in UNIX-based workstations for their CAD requirements, whereas many consultants and contractors tend to use PCs. This difference in platforms has been primarily based on the cost and performance of each system. Until recently the price/performance ratios for workstations have far exceeded those for PCs and therefore highway departments have used them for their computational

needs. Unfortunately, the price of a workstation has prevented most consultants from purchasing them and they have been relegated to using less powerful but cheaper PC. These distinctions are becoming outmoded, however, with rapidly advancing PC technology. Today's PCs are beginning to match the performance of low-end workstations, and several manufacturers are now producing Intel/Windows NT-based PC workstations at costs significantly lower than those of traditional RISC/UNIX-based systems. With the PCs price/performance ratio becoming equivalent to mid-level workstations (e.g., Ref. 43), PCs are becoming more and more prevalent in engineering analysis.

B. Visualization Software

A key consideration in visualization software is the ability to take a vehicle trajectory file from the VDM and move a model vehicle through the terrain graphics database. The vehicle trajectory file consists of time histories of the three orientation angles (pitch, roll, and yaw) and three inertial positions (X, Y, and Z) of the vehicle's trajectory. An initial survey found that many otherwise very capable modeling and visualization programs were limited in that vehicle graphics models could not be manipulated with outside files. The attributes of several commercially available, animation software packages were reviewed to identify those animation software packages that are best suited for incorporation into the IHSDM environment. The animation packages that were considered include:

- 3D Studio (Autodesk)
- Walkthru PC (Bechtel Software, Inc.)
- ModelView PC (Intergraph)
- Spotlight Ray Tracer (Spotlight Graphics)
- 3D Graphics Tools, Ref. e.g.
- High-End Workstation Packages

The vendors of the aforementioned products were asked to respond to the following issues about their respective animation software packages:

1. Product cost.
2. Minimum hardware requirements.
3. Recommended hardware.
4. Cost of recommended hardware.
5. Allowable input file formats for key-framing (e.g., Animating sub-models).
6. Animation control.
7. Animation type(s) supported (i.e., playback or double buffering).

8. Time required to render a 10,000 polygon CAD image for a given hardware configuration.
9. Availability of product technical support.
10. Most significant product features currently available.
11. Significant features anticipated for incorporation into next software release/version.

Then the suitability of the animation package for incorporation into the IHSDM environment was determined.

In general each of the packages discussed will meet the CAD visualization software requirements specified earlier. Each of the software packages will support high resolution on PC- and UNIX-based systems, have sufficient rendering capabilities, allow the user to specify the viewing position and angles, allow for the loading and animation of multiple objects, and will use data created by the VDM. The data that are created by the VDM will most likely be manipulated into a script file that the visualization program can then read and act upon. In general-script files are ASCII text files that contain programming instructions in a language that is familiar to the visualization software, and the VDM data will be converted into commands that tell the visualization program how to move the vehicle.

1. 3D Studio

3D Studio is a photorealistic rendering real-time animation, CAD design software package originally developed for MS-DOS-based computers that now runs under Windows NT. The user may build CAD models within 3D Studio or may import objects that are in the DXF file format. The time required to render animation frames can be minimized by accessing the available collective resources of several PCs that are interconnected by a Local Area Network (LAN) (i.e., 3D Studio rendering speeds are increased by adding more PCs to the LAN). Even though 3D Studio rendering speeds can be increased through the addition of more PCs to the LAN system, it has been shown that the law of "diminishing returns" applies (i.e., doubling the number of processors used to render an image will not double the rendering speed).

Depending on the complexity of a model, including texturing, lighting, and polygon count, 3D Studio might take hours to render a few minutes of visualization. 3D Studio does not require any additional hardware; however, the rendering process can be sped up to near real-time performance with the use of graphics accelerators that provide 3D support. The cost of the software package is just under $3,000.

2. Walkthru PC

Walkthru PC is high-resolution, real-time 3D animation software that has versions that run on both PCs and workstation platforms. Keyframes are developed by rendering files imported from MicroStation, DXF, or IGES formats. It does not allow the user to design objects. Animation may be controlled interactively or through an ASCII script file. The animation that is created may be recorded on videotape or to a hard disk (other options are also available).

To accomplish real-time animation, Walkthru PC relies on a special piece of hardware called the IRISVision graphics card (essentially a disembodied Silicon Graphics video board made by Pellucid). Although the software is designed for real time, it is unlikely that this set-up will realize true real-time visualization of IHSDM simulations if complete CAD vehicles are used. Using Walkthru PC and IRISVision to render a single animation frame having 10,000 polygons will require a couple of seconds. However, if the number of polygons is reduced, seamless higher quality animation can be produced.

Walkthru PC will run on today's standard PC but requires 16 Mb of random access memory (RAM). The cost of Walkthru PC is between $3,500 and $8,500 depending on if the IRISVision board is used and if different interface modules are purchased.

3. ModelView PC

ModelView PC is a photorealistic, rendering, and real-time animation software package that has versions for both the PC and workstations. ModelView PC is not a design package and therefore cannot create CAD models. 3D models complete with surfaces, material types, and colors are imported for rendering as animation keyframes from DXF or MicroStation file formats. The animation that is created may be controlled either interactively or from ASCII script files, and the frames can be stored to videotape as they are developed.

ModelView PC enables the user to render animation at three levels of resolution. Ray tracing (i.e., accounting for the multiple reflections and partial absorption of each light ray) is the highest resolution rendering level and is capable of generating photorealistic frames. Quick tracing, ModelView's mid-level rendering resolution, produces high-quality images but neglects shadows and multiple reflections. The low-level rendering resolution option would not be useful to the IHSDM user. Additionally, frames that smooth the animation between key frames ("tweens") may be automatically generated from fourth-order B-spline interpolations.

Model View PC does not require any additional hardware but the more RAM memory the better. The speed for ray tracing a 10,000-polygon image requires 3 to 4 h. To quick trace the same image requires several minutes. The cost for ModelView PC is $2,500.

4. Spotlight Ray Tracer/Space-Time Animator

Together, Spotlight Ray Tracer and Space-Time Animator provide photorealistic, real-time playbacks. Keyframes may be imported in DXF or IGDS file formats and animation may be controlled interactively or through script files. Playbacks may be recorded to hard disk, videotape, digital tape, or optical disks. Later versions of this software will provide for distributed/parallel rendering. This package has an added attraction if GEOPAK is chosen as the roadway design software because the creators of GEOPAK and Spotlight Ray Tracer are working together on a number of different programs. Furthermore the developers of Spotlight Ray Tracer are currently under contract with NASA to explore cutting edge visualization technologies.

The recommended minimum hardware requires a 50-MHz 486 PC with 16 Mb of RAM. On an 80-MHz 486 with 32 Mb of RAM, a 10,000-polygon image can be rendered in 10 to 40 s. The cost of the ray tracing and animation software together is $2,075.

5. 3D Graphics Tools

Another approach that merits consideration deals with creating a visualization package using a set of existing graphics programming tools. Computer visualization and animation is becoming more and more prevalent, and several software companies have recently begun distributing graphics tools that allow programmers to create their own custom visualization and animation software.

As with every option, there are advantages and disadvantages to this approach. The main advantage is that it allows a customized visualization program to be written specifically with roadway designers and researchers in mind. Generic full-blown visualization software packages come with a lot of excess options that the user probably does not need or will never use. Furthermore, several of these options may be required in order for the user to produce the desired animation, adding additional steps and complexity and ultimately making the animation process inefficient. A customized visualization program can be created that includes only requirements for the IHSDM project, and therefore should increase user efficiency. This approach ensures that each and every requirement that the IHSDM project requires will be accounted for, including the user interface. Yet another advantage deals with future modifications. Since the program would be written specifically for this project, future needs and

modifications can easily be taken care of by simply modifying the existing source code and creating a new version of the software. This would allow hooks to be added to the program that would allow the software to interface with more elaborate visualization packages, and 3D Graphic Tools has support for DXF files.

The biggest disadvantage to this approach is that the actual software has not yet been written; therefore, the initial cost will be higher than it would be if an existing software package were used. Over time, as more designers and researchers use the software, the overall cost benefit should be better. Additionally, a custom piece of software would not contain all of the features of some of the current visualization software packages, and therefore will be strictly limited to helping designers and researchers and would not be able to do presentations and other special tasks. One final drawback with this type of approach may be the speed. Although the IHSDM project may not require true real time animation, the visualization software will be more effective the faster it runs. This will also improve the designer's efficiency. The 3D Graphic Tools examples did not run in real time.

We had the chance to review one particular set of tools from Micro System Options® called 3D Graphic Tools®. This is a comprehensive set of tools that can be used to create visualization and animation on PCs running under Windows. This package contains a wide range of graphics capabilities that meet and exceed all of the requirements specified in the section entitled CAD Visualization Software Requirements. The tools mentioned include color capabilities and use the default Windows graphics mode. This means if the graphics system has a driver that will support high-resolution graphics modes, and Windows is set up to run in this mode, then 3D Graphic Tools will also run in this mode. Rendering is supported using two basic algorithms, and can include lighting effects and texturing. Observer positioning is handled exactly like a camera. One simply specifies the location of the camera, where it is pointing, and a viewing angle and the software takes care of the rest. The other two requirements (multiple objects animated and displayed relative to one another and external data support) will both be supported because the program would be written to account for them.

6. High-End Workstation Packages

At the high end of the workstation environment, visualization packages promise features such as expert systems, object-oriented databases, photorealistic real-time double buffering animation, intelligent texture/geometry control ("smart-skins"), and simultaneous plotting of vehicle dynamics variables.

A few of examples would be the IGRIP software package from Deneb Robotics, Jspace, and Visualized from Wavefront. The IGRIP program is a $60,000 package that presents excellent rendering

and animation capabilities. Jspace can be found on both personal computers and workstations and cost between $6,000 and $26,000 depending on what is purchased and it offers object oriented code and is partially preset as an expert system. Finally, Visualizer offers excellent postprocessing for physics based simulation results, and is convenient for plotting system variables in a multitude of formats. There are several modules that would be attractive to the IHSDM designer but the cost would be about $40,000.

C. A PC-BASED COMPUTER/SOFTWARE PLATFORM

About the time of the initiation of this project Intergraph announced that they were going to put their main efforts into an Intel based workstation platform that would run under the Windows NT platform. At that time VDANL ran on MS-DOS based PCs, and it was decided that our team would focus on PC platforms. Subsequently, VDANL has been modified and upgraded to run under Windows NT, and visualization software such as 3D Studio has also been upgraded to also run under Windows NT. As a result of the above visualization software review, we selected 3D Studio for further detailed assessment on a PC platform. The detailed assessment for IHSDM so far has been restricted to the MS-DOS version.

VDANL seems to run quite efficiently under Windows NT. VDANL now runs in a 32 bit mode with relatively unlimited memory space, compared to the 16 bit MS-DOS with its 640K memory limitation. With an update frame time of 5 msec VDANL can run in real time on a 200 MHz Pentium, and in fact is now used for real-time driving simulation applications (Ref. 44). Thus, Intel based platforms seem to be adequate for vehicle dynamics analysis.

Using the 3D Studio scripting language, we are able to manipulate vehicle models within a terrain graphics data base using VDANL trajectory output files. Our experience with 3D Studio indicates that has a reasonably intuitive user interface that permits vehicle trajectory modeling to be carried out quite efficiently. 3D Studio seems to have all of the modeling and animation capability that would be desirable for the roadway designer, and indeed has capability for rendering polished visualizations that might be required for subsequent design reviews.

3D Studio capabilities include a range of geometric modeling options, a variety of texturing, lighting and shading options, and a full range of camera positioning and dynamic motions that permit complete freedom in specifying the observer's point of view. The are also a range of third party software `plugins' that allow for a wide variety of special effects. 3D Studio works with common graphics file formats (e.g. DFX) and their own native format 3DS. 3D graphics models of vehicles, signs and other elements common to highway environments are also readily available

As discussed previously, the Intel/Windows NT platform also will permit graphics to be displayed in real time (Ref. 43). With the use of a VR (Virtual Reality) head-set (Ref. 45) it would be possible for the highway designer to conduct a real-time drive-through of a prospective design. This would be especially relevant to review visibility issues, particularly if the roadway design 3D model includes TCDs. Such a review would allow the designer to visualize the visibility of upcoming curvature, intersecting roads or driveways, and the placement of warning signs and delineation.

One final visualization capability deserves comment that was not originally within the scope of this project. That is the capability of preparing, editing, and recording videotapes and CDs for presentation and review. There are a number of video editing systems that will run on an Intel platform and allow a range of editing capability, including titling, multiple screen splits, real video clips, sound editing, etc. These systems require fast, large-capacity drives (SCSI AV hard drives), and also some means for large capacity backup in order to archive work (e.g. DAT tape backup drive).

VIII. EXAMPLES OF APPLICATIONS

One of the goals of the IHSDM program is to allow researchers to simulate single-vehicle accident scenarios and study roadway design features that may help eliminate or reduce the severity of the accident. This section demonstrates the use of the IHSDM vehicle dynamics model to study a run-off-the-road rollover accident. A user's guide for installing the IHSDM/VDANL software and running cases is given in Appendix H.

A. TYPICAL RUN

The vehicle chosen for this run was number 65 the AASHTO large semitrailer (WB-50). A description of this vehicle can be found in Appendix F. The roadway design chosen for this example was supplied by FHWA and the database file name is Alt3.ihm. This database describes a two-lane rural road with a serpentine alignment that goes left and right for three oscillations. The curve radii vary between 125 and 155, and the grade is relatively flat. Figure 15 shows plots of the roadway design horizontal and vertical alignment.

This run was set to be fairly aggressive, as indicated in Figure 11, with the speed limit set at 90 km/h for tangents, and the maximum maneuvering acceleration set at 0.3 g. The total length of the run was set at the length of the data file (1950 meters). The Roadway Safety Metric screen for this run is given in

Figure 13. Here we see that the tractor reached a lateral acceleration of 0.47 g while the trailer reached 0.47 g. The roll angles of the tractor and trailer are not particularly large (-3.6 and 3.8°, respectively), but the maximum load transfer gives a rather dramatic insight into the risk in this run. While the tractor load transfer is only 33 percent, the trailer has reached 97 percent load transfer. In other words, at one point in the run, at station 1240.25, the inside wheels of the trailer were completely unloaded so that the trailer was on the verge of rollover!

Figure 16 shows vehicle performance plots for the tractor/trailer winding road analysis discussed above. Here we see that the roll angles of both vehicle are about the same during the curve encounters. This suggests that the roll gradient of each vehicle is about the same [i.e., roll gradient is the roll angle per g and is determined by the roll stiffness, center of gravity (cg) height and suspension design]. However, the load transfer or percentage of weight transferred from the inside to outside wheels during cornering, tells a much more dramatic story. Here we see, as indicated in the Roadway Safety Metric screen (

Figure 13), that the tractor load transfer peaks during cornering are only about one-third as large

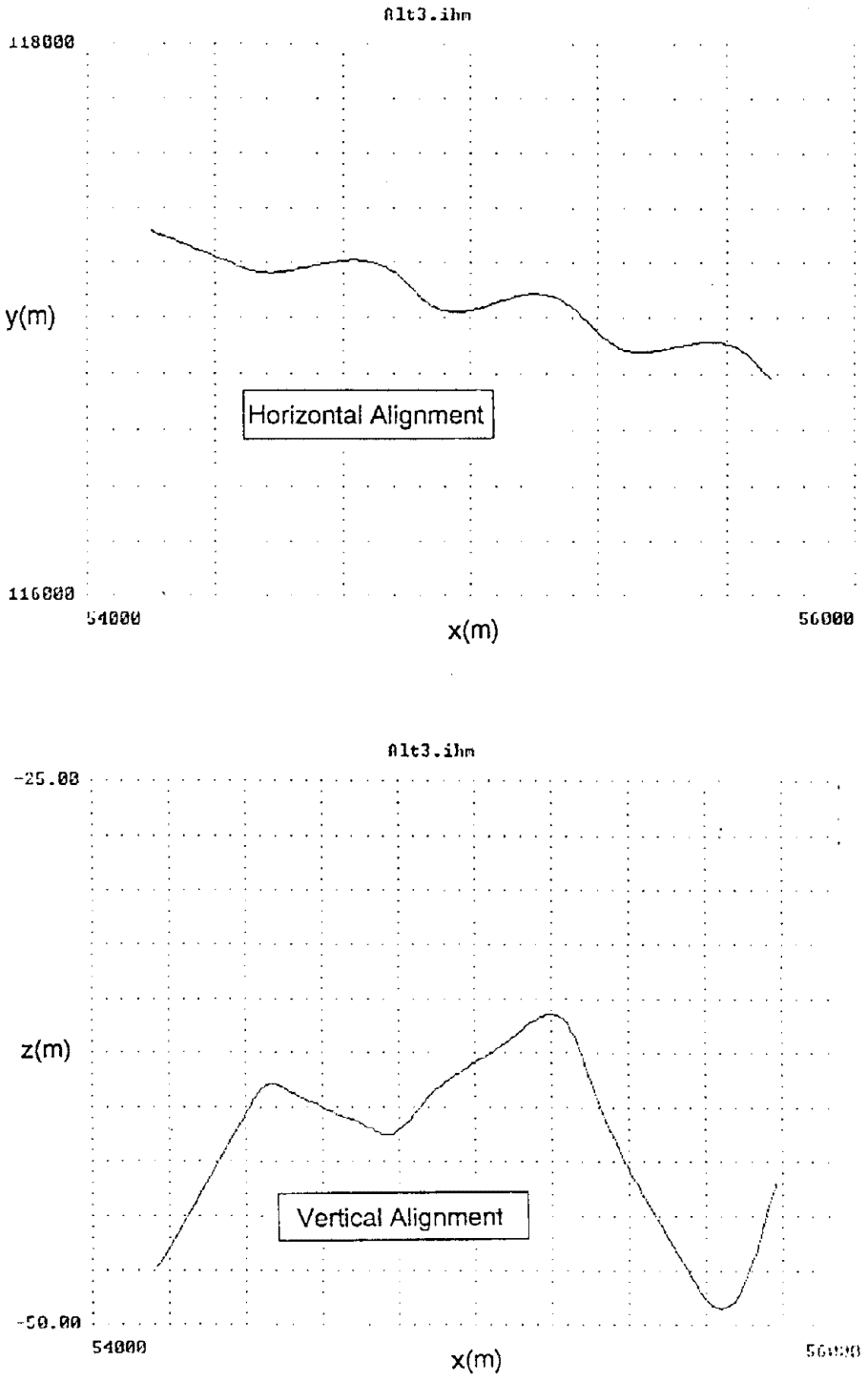

Figure 15. Horizontal and Vertical Alignment for the Typical Run Example

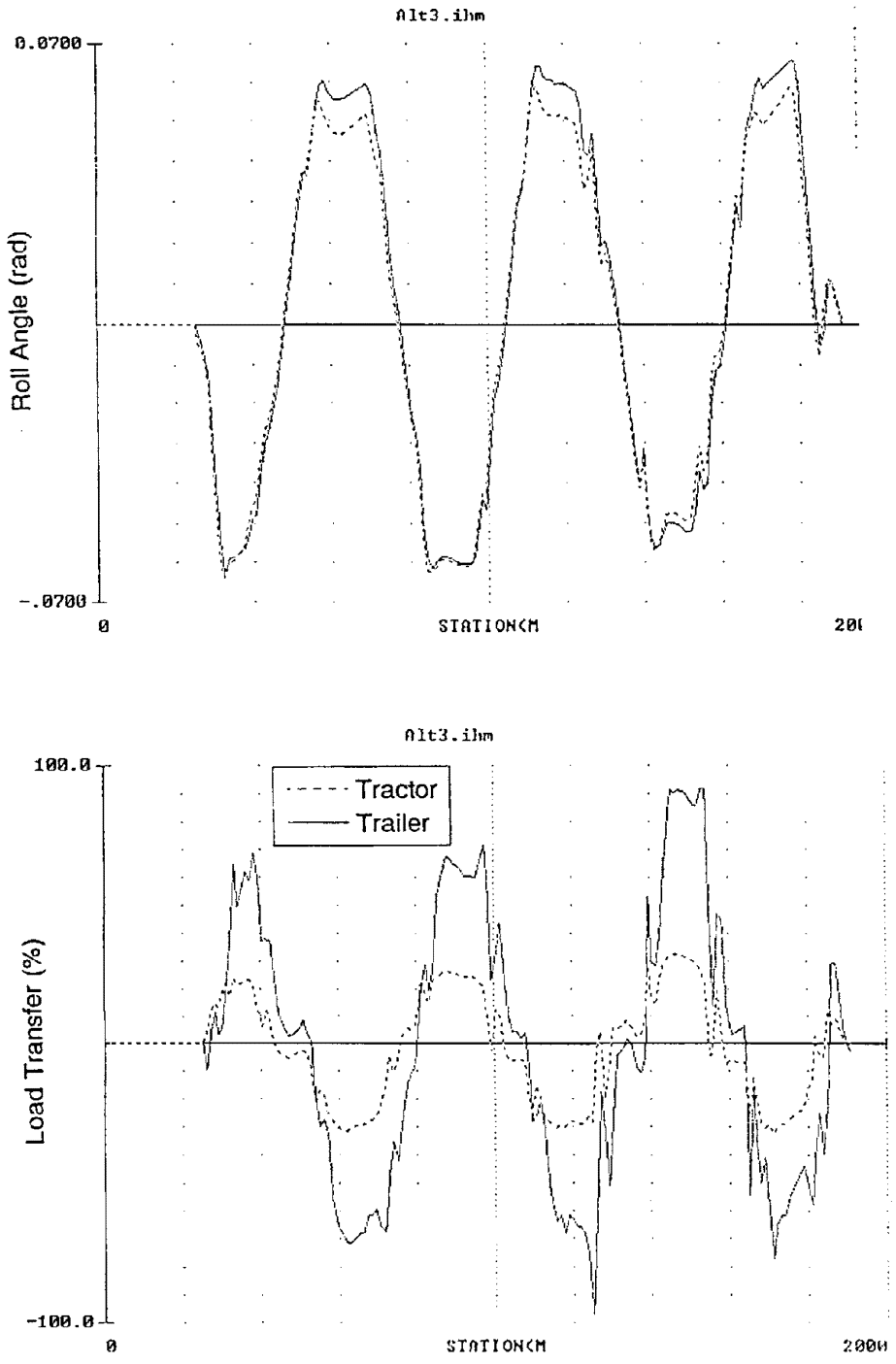

Figure 16. Vehicle Performance Profile Plots for a Tractor/Trailer Driven on a Winding Road

as the trailer load transfer. This is because the trailer has a much higher cg than the tractor, which gives a larger moment are for the lateral acceleration to work on. The load transfer performance plot indicates that the trailer is getting near rollover conditions.

B. VEHICLE ROLLOVER

The vehicle chosen for the demonstration is the AASHTO passenger vehicle (P), which is a passenger car (see Appendix F for a description of the vehicle). A terrain database supplied by FHWA was used for the demonstration (the name of the terrain database file is ALT2.IHM). The database is a two-lane rural road (3.3-m-wide lanes), starting with a 2 percent downgrade for the first 400-m. At station 244.916, a 125-m radius left-hand corner begins, with a deflection angle of -39.66659 degrees.

The accident scenario is for the driver to approach the corner too fast for conditions and skid off the outside of the turn onto the shoulder. This situation is set up as follows: the passenger vehicle is driving on the tangent leading to the first corner at 105 km/h. The friction of the paved road surface is assumed to be low (*MUNON* parameters in the tire parameter files set to 0.4 for the front tires and 0.3 for the rear tires). To prevent the driver model from slowing the vehicle as it approaches the corner, the brake gain parameter (*KFBP*) in the driver parameter file (DRIVER.TMP) is set to zero. The driver model will anticipate the corner and lift off the throttle, but no brakes will be applied. The driver model will attempt to steer the vehicle through the turn, but there is not enough available road friction and the vehicle leaves the road at station 282 at a speed of 80 km/h, and a sideslip angle of 26 degrees. The high sideslip angle shows that the vehicle is in an out-of-control oversteering condition and beginning to spin out. The right-rear tire contacts the right shoulder first, followed by the right-front tire. At the point of road departure, the super elevation was 8 percent.

Two scenarios are simulated, with the differences being in the side slope and soil conditions of the right shoulder. (Note: Terrain database ALT2.IHM initially contained only the two travel lanes. A 30-m wide right shoulder was manually added for this demonstration.) In the first scenario, the shoulder is assumed to be grass-covered firm soil, with a side slope of 7 percent. This allows the vehicle to leave the road onto approximately the unchanged geometry. The grass is assumed to have a peak coefficient of friction of 0.4. The firm soil condition is simulated by setting the *Kmu* parameters in the right shoulder tire parameter file to positive 0.6 (see Appendix E on the VDANL tire model). Figure 17 shows the vehicle sideslip angle (beta), roll angle and lateral load transfer plotted against roadway station. The sideslip angle plot shows that the vehicle continued to spin and reached a 90-degree sideslip angle (sliding sideways) at roadway station 315. At this point, maximum roll angle of 5.3 deg and maximum

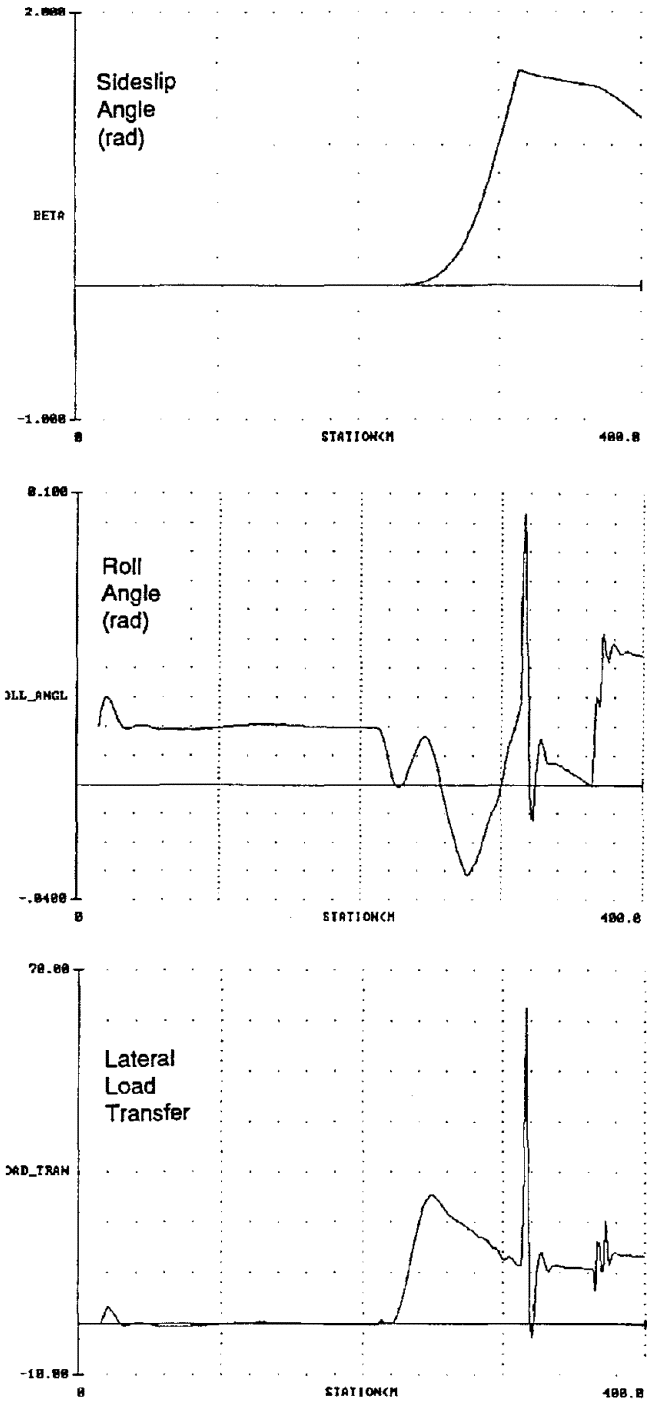

Figure 17. Vehicle Performance Profile Plots for a Roadside Intrusion without Rollover

lateral load transfer of 62.3 percent occur. While the vehicle is out of control, it does not roll over and would eventually skid to a stop.

In the second scenario, the shoulder side slope is changed from 7 percent to –25 percent to simulate a roadside ditch. In addition to the change in slope, soil plowing effects are simulated by changing the *Kmu* parameters in the right shoulder tire file from 0.6 to –0.6. This has the effect of increasing the tire lateral force at high slip angles. Identical road departure conditions as in the first scenario are used. With these roadside features, the vehicle skids down the ditch and eventually rolls over. Figure 18 shows the vehicle sideslip angle (beta), roll angle, and lateral load transfer plotted against roadway station. The plot of sideslip angle shows that, after leaving the road, the sideslip angle actually decreases for a time, before starting to spin again, and reaches a 90-degree sideslip angle at station 372. The vehicle roll angle is also more complex than the first scenario, with the roll angle actually going back near zero just before rolling over. The lateral load transfer fluctuates rapidly, reaching 100 percent (both left-side tires off the ground) momentarily 20 m before the vehicle rolled over.

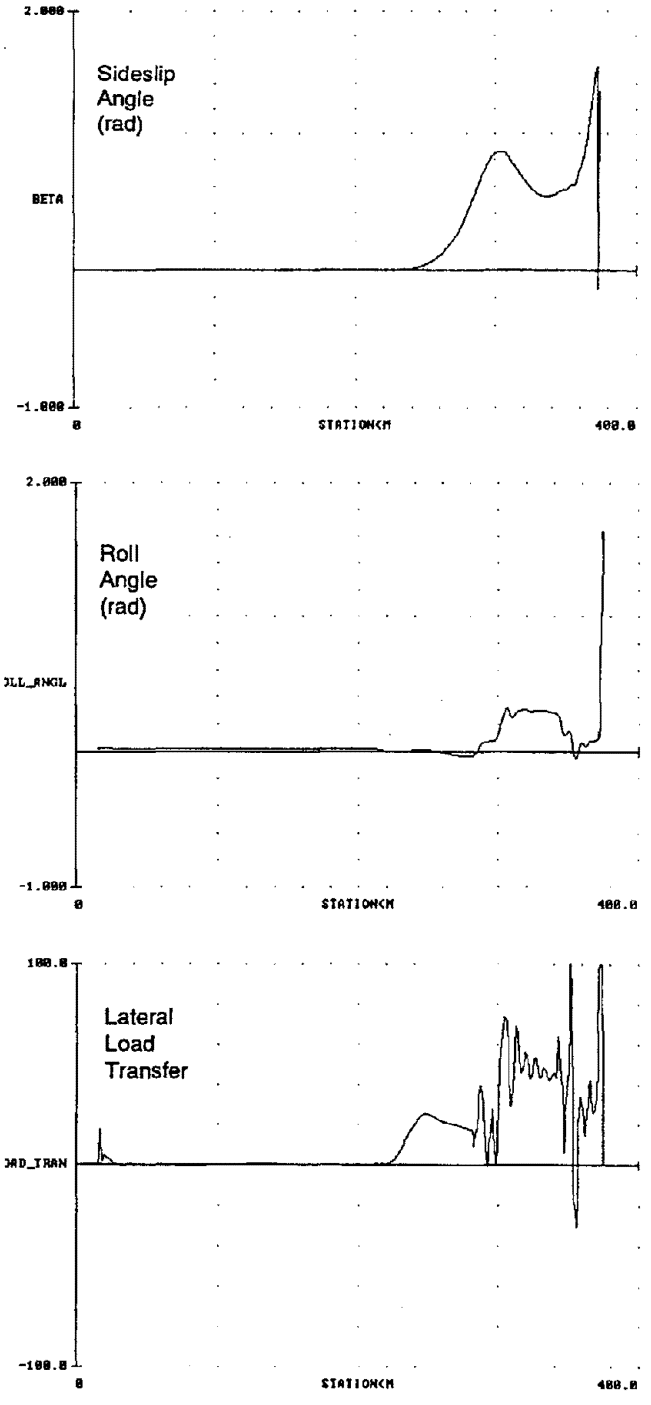

Figure 18. Vehicle Performance Profile Plots for a Roadside Intrusion with Rollover

IX. CONCLUSION

The IHSDM (Refs. 1 and 2) is a concept that is ready for implementation and application. Both software and hardware components are available that have more than adequate capability. The current challenge is to integrate the process illustrated in Figure 2 and Figure 14, with common file formats and user-friendly interfaces that are convenient for the highway engineer/designer to use. The interfaces must allow the designer to conveniently select road profiles, vehicles and driver maneuvering conditions that will provide comprehensive safety assessment of highway designs, and quantify the evaluation in terms of meaningful highway engineering metrics and visualizations.

X. REFERENCES

1. Harwood, D.W., Mason, J.M. and Graham, J.L., *Conceptual Plan for an Interactive Highway Safety Design Model*, Report No. FHWA-RD-93-122, Federal Highway Administration, Washington, DC, Feb. 1994.

2. Paniati, J.F. and True, J., *Interactive Highway Safety Design Model (IHSDM): Designing Highways with Safety in Mind*, Transportation Research Circular No. 453, Feb. 1996.

3. Allen, R.W. and Rosenthal, T.J., " Requirements for Vehicle Dynamics Simulation Models," SAE Paper 940175, Society of Automotive Engineers, Warrendale, PA, Feb. 1994.

4. Allen, R.W., Rosenthal, T.J. and Hogue, J.R., "Modeling and Simulation of Driver/Vehicle Interaction," SAE Paper 960177, Society of Automotive Engineers, Warrendale, PA, 1996.

5. Landphair, H.C. and Larsen, T.R., *Applications of 3-D and 4-D Visualization Technology in Transportation*, Synthesis of Highway Practice 229, National Cooperative Highway Research Program; National Academy Press, Washington, DC, 1996.

6. Appleman, D, Dan Appleman's *Visual Basic 5.0 Programmer's Guide to the WIN32 API*, McMillan Computer Publishing USA, Emeryville, CA, ©1997.

7. Allen, R.W., Szostak, H.T., et al., *Analytical Modeling of Driver Response in Crash Avoidance Maneuvering, Vol. I: Technical Background*, National Highway Traffic Safety Administration, DOT HS 807 270, April 1988.

8. Allen, R.W., et al., *Vehicle Stability and Rollover*, National Highway Traffic Safety Administration, DOT HS 807 956, June 1992.

9. Allen, R.W., Rosenthal, T.J., and Szostak, H.T., "Steady State and Transient Analysis of Ground Vehicle Handling," SAE Paper 870495, Society of Automotive Engineers, Warrendale, PA, Feb. 1987.

10. Allen, R.W., Szostak, H.T. and Rosenthal, T.J., "Analysis and Computer Simulation of Driver/Vehicle Interaction," SAE Paper 871086, Society of Automotive Engineers, Warrendale, PA, May 1987.

11. Allen, R.W., Szostak, H.T., Rosenthal, T.J. and Klyde, D.H., "Field Testing and Computer Simulation Analysis of Ground Vehicle Dynamic Stability," SAE Paper 900127, Society of Automotive Engineers, Warrendale, PA, Feb. 1990.

12. Allen, R.W., Szostak, H.T., Rosenthal, T.J., Klyde, D.H., and Owens, K.J., "Characteristics Influencing Ground Vehicle Lateral/Directional Dynamic Stability," SAE Paper 910234, Society of Automotive Engineers, Warrendale, PA, Feb. 1991.

13. Segal, L., "Theoretical Prediction and Experimental Substantiation of the Response of the Automobile to Steering Control," *Proceedings of the Automobile Division*, The Institution of Mechanical Engineers, No. 7, 1956-7, pg. 26-46.

14. Weir, D.H., Shortwell, C.P., and Johnson, W.A., "Dynamics of the Automobile Related to Driver Control," SAE Paper No. 680194, February 1997.

15. Allen, R.W., Rosenthal, T.J., Klyde, D.H., Owens, K.J., and Szostak, H.T., "Validation of Ground Vehicle Computer Simulations Developed for Dynamics Stability Analysis," SAE Paper 920054, Society of Automotive Engineers, Warrendale, PA, Feb. 1992.

16. Chrstos, J.P. and Heydinger, G.J., *Evaluation of NHTSA Light Vehicle Handling Simulations*, Report No. DOT HS 807 868, US DOT/National Highway Traffic Safety Administration, Washington, DC, Aug. 1992.

17. Bernard, J.E., Bhatnagar, A., Clover, C.L., *Evaluation of Select Vehicle Dynamics*, Report No. IOWA 9114-C11302, Iowa State University, College of Engineering, June 1992.

18. Chrstos, J.R. and Heydinger, G.J., "Evaluation of VDANL and VDM RoAD for Predicting the Vehicle Dynamics of a 1994 Ford Taurus," SAE Paper 970566, Society of Automotive Engineers, Warrendale, PA, 1997.

19. Allen, R.W., Rosenthal, T.J. and Chrstos, J.P., "A Vehicle Dynamic Tire Model for Both Pavement and Off-Road Conditions," SAE Paper 970559, Society of Automotive Engineers, Warrendale, PA, 1997.

20. American Association of State Highway and Transportation Officials, *A Policy on Geometric Design of Highways and Streets*, Washington, DC, 1990.

21. Reide, P.M., Leffert, R.L. and Cobb, W.A., "Typical Vehicle Parameters for Dynamic Studies Revised for the 1980's," SAE Paper 840561, 1984.

22. Chrstos, J.P., "Parameter Measurement and Computation Procedures for 1994 Ford Taurus GL", NHTSA Final Report (draft) 1996.

23. Fancher, P.S., Ervin, R.D., Winkler, C.B. and Gillespie, T.D., *A Factbook of the Mechanical Properties of the Components for Single-Unit and Articulated Heavy Trucks*, University of Michigan Transportation Institute Final Report No. UMTRI-86-12, 1986.

24. *Mechanics of Heavy-Duty Trucks and Truck Combinations*, The University of Michigan, College of Engineering, Course Notes, July 1998.

25. Winkler, C.B., Bogard, S.E. and Karamihas, S.M., *Parameter Measurements of a Highway Tractor and Semitrailer*, University of Michigan Transportation Institute Final Technical Report UMTRI-95-47, Dec. 1995.

26. McRuer, D.T. and Krendel, E.S., "Mathematical Models of Human Pilot Behavior," AGARDogaph AGARD-AG-188, 1974.

27. Allen, R.W. and McRuer, D.T., "The Man/Machine Control Interface - Pursuit Control," *Automatica*, vol. 15, pp. 683-686, 1979.

28. Hoffmann, E.R., "Human Control of Road Vehicles," *Vehicle System Dynamics*, 5(1-2), pp. 105-126, 1975.

29. McRuer, D.T., Allen, R.W., et al., "New Results in Driver Steering Control Models," *Human Factors*, 19(4), pp. 381-397, 1977.

30. Allen, R.W., "Stability and Performance Analysis of Automobile Driver Steering Control," SAE Paper 820303, International Congress & Exposition, Detroit, MI, 1982.

31. Donges, E., "A Two-Level Model of Driver Steering Behavior," *Human Factors*, vol. 20, no. 67, pp. 691-707, 1978.

32. Allen, R.W., O'Hanlon, J.F., et al., *Driver's Visibility Requirements for Roadway Delineation*, FHWA-RD-77-165, Federal Highway Administration, Washington, DC, 1977.

33. Shinar, D., Rockwell, T.H. and Malecki, J.A., "The Effects of Changes in Driver Perception on Rural Curve Negotiation," *Ergonomics*, vol. 23, no. 3, pp. 263-275.

34. Lajunen, T., Hakkarainen, P. and Summala, H., "The Ergonomics of Road Signs: Explicit and Embedded Speed Limits," *Ergonomics*, vol. 39, no. 8, pp. 1069-1083, 1996.

35. Krammes, R.A. and Collins, K.M., *State-of-the-Practice Geometric Design Consistency: Data Base User's Guide*, Research Report 7193-2, Texas Transportation Institute, March. 1994.

36. Pipes, L.A., "An Operational Analysis of Traffic Dynamics," *Journal of Applied Physics*, vol. 24, pp. 271-281, 1953.

37. Bekey, G.A., Burnham, G.O. and Seo, J., "Control Theoretic Models of Human Drivers in Car Following," *Human Factors* vol. 19, no. 4, pp. 399-413, 1977.

38. Allen, R.W., Serafin, C., et al., "Driver Car Following Behavior Under Test Track and Open Road Driving Conditions," SAE Paper 970170, Society of Automotive Engineers, Warrendale, PA, 1997.

39. Krammes, K.A., Brackett, R.Q., et al., *Horizontal Alignment Design Consistency for Rural Two-Lane Highways*, FHWA-RD-94-034, Jan. 1995.

40. Ranney, T.A., "Models of Driving Behavior: A Review of Their Evolution," *Accident Analysis and Prevention*, vol. 26, no. 6, pp. 733-750, Elsevier Science Ltd., 1994.

41. Watt, A., *3D Computer Graphics*, Addison-Wesley, 1993.

42. Oliver, D., et. al., *Tricks of the Graphics Gurus*, Sams, 1993.

43. Latham Roy, "Gemini Benchmarks for Real Time Simulation," *Real Time Graphics* , vol. 5 no. 5, Dec. 1996, pp1&3

44. Allen, R.W., Klyde, D.H., et al., "A Vehicle Dynamics Model for Low Cost, PC Based Driving Simulations," *Proceedings of the Third Driving Simulation Congress – DSC'97*, Lyon, France, ETNA, Paris, France, 1997.

45. "The Outlook for Head-Mounted Displays," *Real Time Graphics*, vol. 6 no. 2, Aug. 1997 p. 11.

APPENDIX A
COMPUTER SIMULATION

A. BACKGROUND AND OVERVIEW

The *Vehicle Dynamics Analysis, Non-Linear* (VDANL) computer simulation has been adapted from earlier STI automobile simulation's (Refs. A.1. and A.2). The earliest versions of this vehicle simulation used a fixed roll axis assumption for derivation of the equations of motion. The fixed roll axis concept has been abandoned, and instead a composite description of wheel/suspension motion is used, which in effect determines the instantaneous location of the roll axis at the front and rear axles. This approach is taken to adequately account for the response of independent suspension to vertical terrain profiles.

The equations of motion explicitly account for all motions in the longitudinal and lateral directional dynamics. Earlier versions of this simulation did not completely account for the longitudinal pitch and heave modes, which are now specifically addressed. All wheels have separate spin modes. Tire horizontal forces are computed using a nonlinear composite force tire model (Refs. A.1 and A.3). Load transfer between tires and axles occurs due to both lateral and longitudinal acceleration.

The inertial dynamics are modeled by a variety of force and moment equations that describe the motions of the vehicle sprung mass (body, frame, and power train) and wheel and suspension unsprung masses. Sprung and unsprung mass motions are modeled separately in the pitch, heave, lateral, and roll modes. Longitudinal motions are for the total vehicle mass. In yaw rotations, the unsprung masses (axles) rotate with the sprung mass. However, they have a lateral degree-of-freedom relative to the sprung mass, so they do not translate laterally with the sprung mass. This approach is taken to provide the "simplest" set of equations that adequately account for all longitudinal and lateral/directional motions. Finally, pitch and roll equations account for large angle effects, so that rollover and pitch-over are adequately accounted for.

VDANL also contains a model of a single or dual axle trailer. The equations of motion used for the trailer are identical to the tow vehicle equations. The trailer can be connected to the vehicle through a ball hitch or a fifth-wheel.

B. AXIS SYSTEM AND DEGREES OF FREEDOM

The model development divides the vehicle into three mass components: the vehicle sprung mass and the front and rear axle unsprung masses. Tire forces developed at the roadway surface drive the motions of the basic vehicle sprung mass. These tire forces result from slip motions relative to the roadway surface. The slip motions in turn require specification of the motions of the tires, wheels, and other unsprung mass (suspension) components in the roadway axis system. Therefore, the unsprung mass

motion variables are all set up to act in the roadway plane. The roadway is defined based on a 3D-terrain model that allows the terrain altitude, grade, and slope to be determined for each tire. The roadway axis system used by the unsprung masses uses the average terrain altitude at the front axle and the rear axle along with wheelbase to compute the roadway pitch angle. The roadway roll angle is computed separately at the front and rear axles based on the tire altitudes and the axle track width. The vehicle sprung mass motions then only need be modeled in the way forces react back to the unsprung masses, and to define suspension and steering affects that result from motions between the masses.

The above distinction is important, and is shown in Figure A-1, where a "sleeve" carries and defines the unsprung masses in the roadway plane axis system. The sprung mass, and even the unsprung mass in rollover motions, can rotate in the roll direction relative to this sleeve. This approach focuses on motions at the road surface, rather than at the sprung mass cg, because of the way in which tire force development is tested and modeled. All tire test data are defined as forces and moments acting in the road plane, in response to side slip angle, longitudinal slip, camber angle, and normal load relative to the roadway plane.

Pitch angles are assumed to be very small, with a maximum of 0.05 to 0.07 radians reached even on very bumpy road surfaces. On smooth roads, the only pitch disturbance is from longitudinal acceleration (A_x) transients, or suspension squat/lift reactions, which result in only very small pitch angles. The primary purpose for the pitch degree-of-freedom is to define suspension deflections, that produce changes in suspension forces and steering geometry. Therefore, we are defining pitch motions to take place in the body axis system. This means that during tip-over (large ϕ_s angles), the pitch motion directions will follow the suspension as the entire vehicle rolls over. The fact that the pitch motions are extremely small allows us to assume that most classical motion-variable cross-product terms can be ignored as an insignificant effect.

The basic vehicle model degrees of freedom (DOF's) are summarized in Table A-1. In this document, degrees of freedom are defined as motion variables. In addition to explicit motion DOF's, there are several differential equations used to model other "dynamics" of the vehicle system. The variables of these differential equations will be referred to as state variables (separate from the states of the DOF's). Wherever possible, composite parameter characteristics have been employed in the modeling to minimize the total number of parameters and give parameters (i.e., composite characteristics) that are easy to measure and/or estimate. The following features are included in the vehicle model:

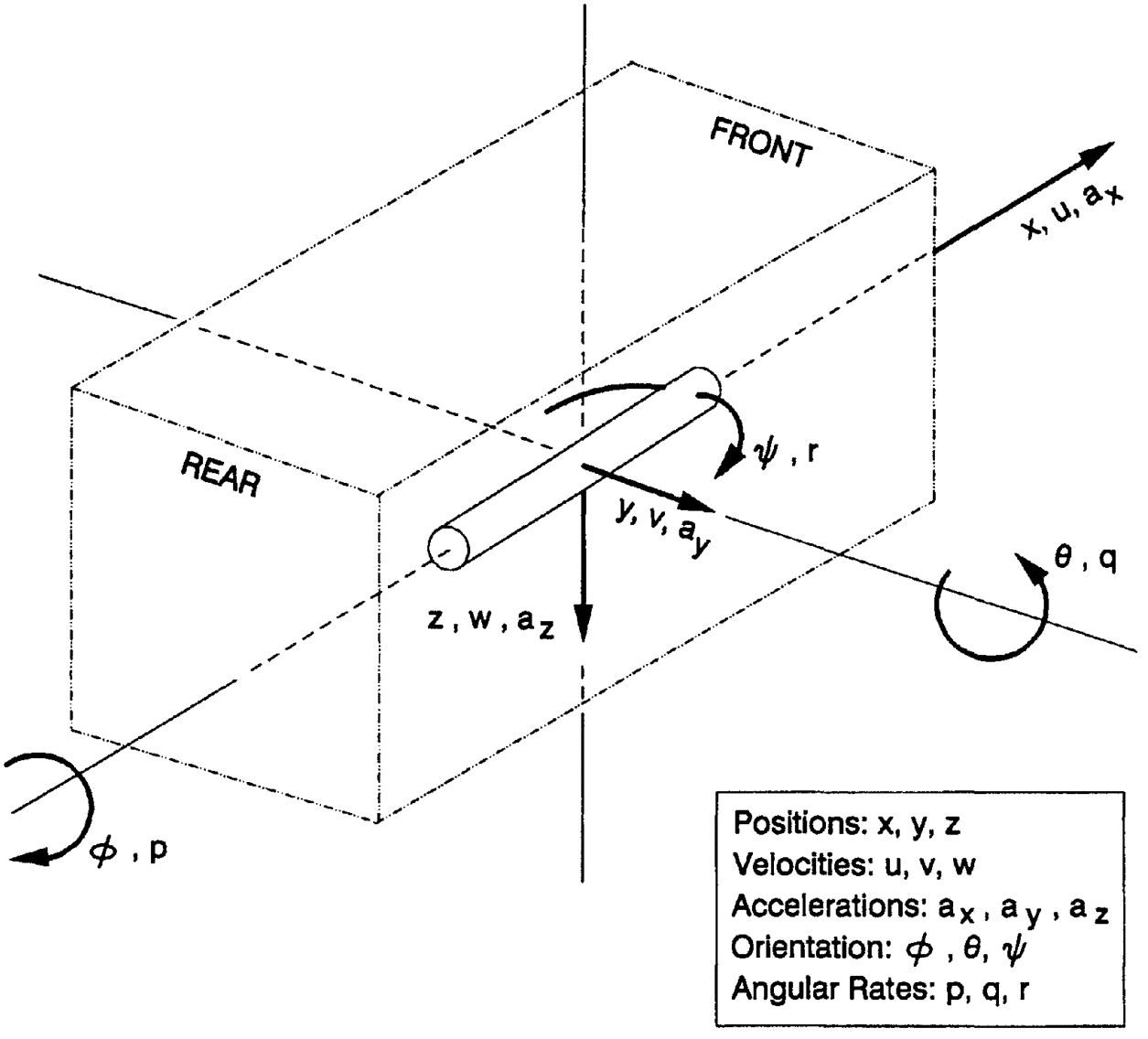

ψ ,y, v, a_y, z are fixed to a sleeve over the longitudinal body axis, which allows ψ,y, v, a_y to stay level with the road plane (do not rotate with ϕ), and z to remain perpendicular to road plane.

Figure A-1. Vehicle Axis System

1. Suspension force mechanisms acting at each wheel, including
   - Spring
   - Damping (shock absorbers)
   - Bump stops
   - Auxiliary roll stiffness (antiroll bars)
   - Squat/lift forces (due to suspension geometry)
2. Steering and suspension geometry effects
   - Wheel camber angle vs. deflection
   - Suspension squat/lift forces due to lateral and longitudinal tire force
   - Wheel steer as a function of:
     - Suspension deflections
     - Lateral force applied to suspension compliance
     - Tire aligning torque applied to steering system compliance
     - Ackerman steer geometry
3. Compliant pin joints at the roll axis between the sprung and unsprung masses to simulate real rubber bushing effects and to avoid computational instabilities.
4. First order differential equations for lateral and longitudinal tire slip that simulate tire relaxation length and minimize computational instabilities in the wheel spin mode.
5. Lateral force deflection of tire, wheel, and suspension, which results in a significant loss in track width under vehicle rollover conditions
6. Full resolution of all forces to accommodate vehicle rollover conditions.

Table A-1 lists 17 DOF's for the vehicle model. Associated with each tire, there are two first order differential equations for its lateral and longitudinal slip variables. This adds eight additional state variables to the model. The drivetrain model has two DOF's for the engine and transmission rotational velocities. The trailer model has identical DOF's and states as the vehicle model with the exception of the steering system DOF, and the drivetrain DOF's.

A guide to the subsequent vehicle motion equation development is given in Figure A-2, which shows the various VDANL model components and their interactions. The dynamic variables are defined in Tables at the end of this appendix. The major VDANL transient dynamic variables are portrayed schematically in Figure A-3. The following sections will detail the development of these variables.

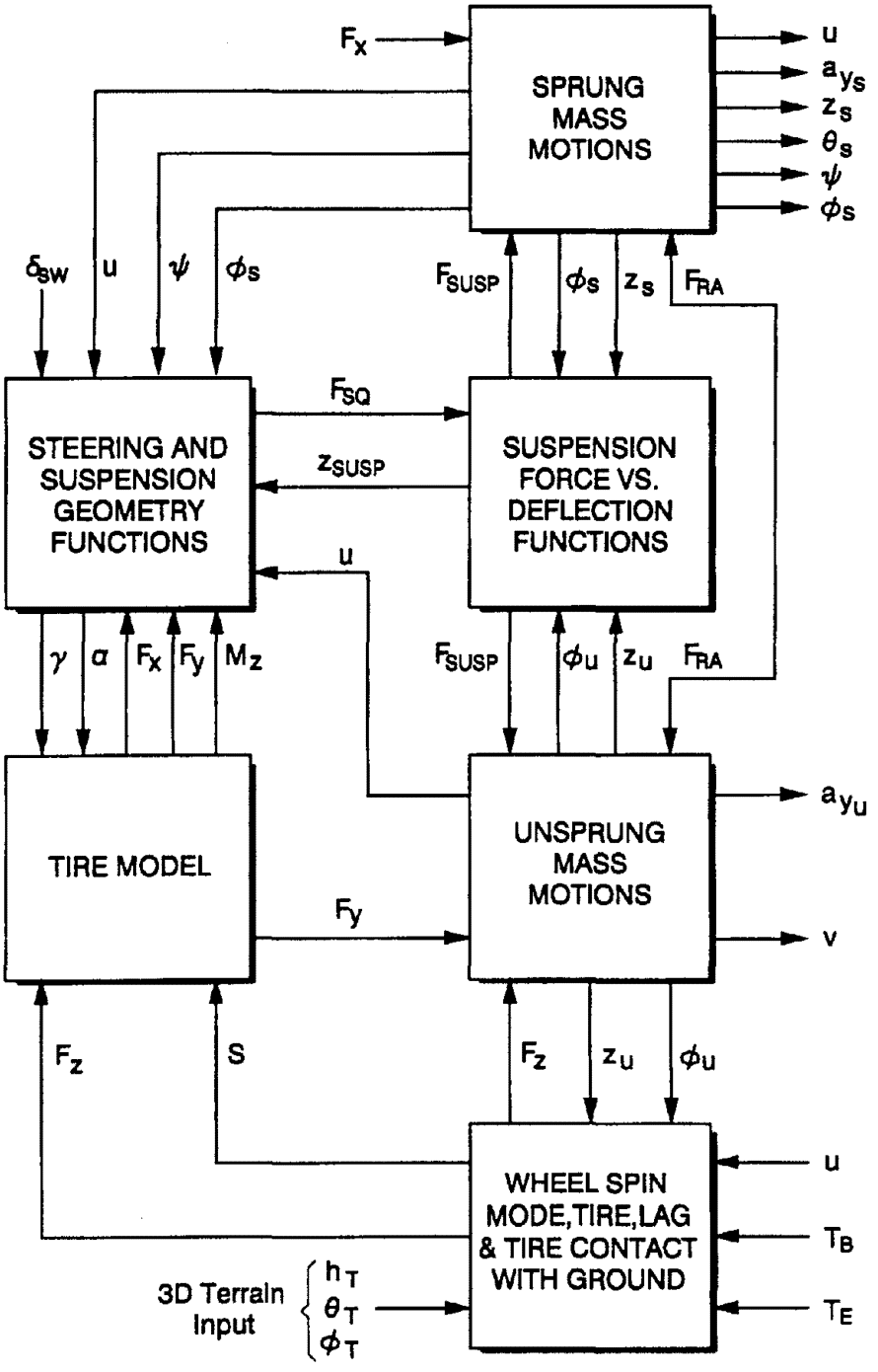

Figure A-2. Vehicle Dynamics Model Components and Their Interactions
(Variables defined in tables at the end of this appendix)

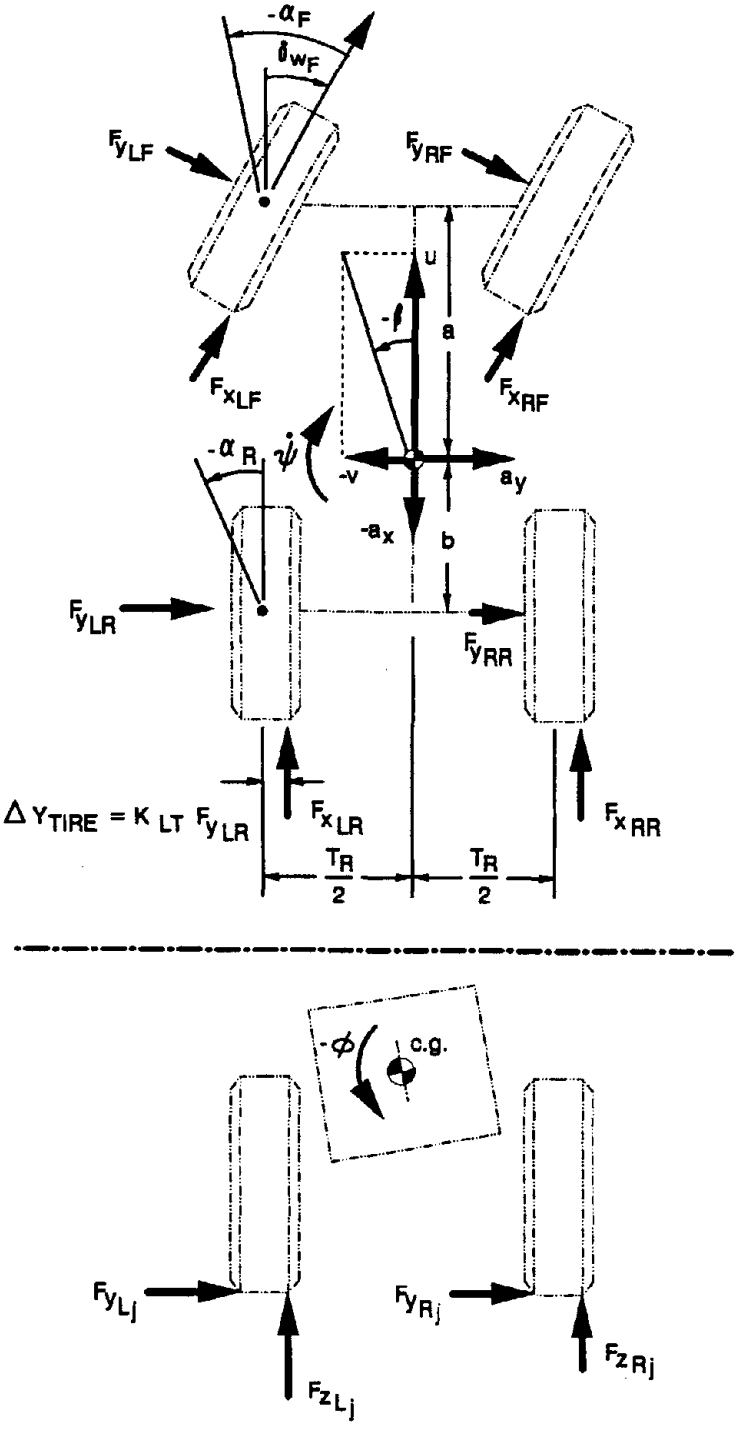

Figure A-3. Major Variables Included in the Transient Dynamic Model

Table A-1. Basic Vehicle Model Degrees of Freedom

MASS		MOTION VARIABLES	D.O.F.
Sprung Mass	(m_s)	$\theta_s, \phi_s, z_s, a_{y_s}$	4
Total Mass	(m)	ψ, v	2
Front Unsprung	(m_{UF})	$z_{UF}, \phi_{UF}, a_{y_{UR}}$	3
Rear Unsprung	(m_{UR})	$z_{UR}, \phi_{UR}, a_{y_{UR}}$	3
Wheel rotational inertia	(I_W)	ω_{ij}(spin mode, 4 wheels)	4
Wheel inertia about steer axis	(I_{FW})	δ_{WF}	1
TOTAL DEGREES OF FREEDOM			17

C. VEHICLE INERTIAL DYNAMICS

Longitudinal Force (forward velocity) — The longitudinal force equation accounts for the entire vehicle mass (see Figure A-3):

$$m(\dot{u} - \dot{\psi}v) = \Sigma X \tag{A-1}$$

Yawing Moment (yaw rate) — This equation is assumed to compute the angular rate of the entire vehicle mass in the horizontal plane independent of roll angle. The relationship accounts for roll acceleration cross coupling (see Figure A-2):

$$I_z \ddot{\psi} - I_{xz_S} \ddot{\phi}_S = \Sigma N \tag{A-2}$$

Sprung Mass Side Force (lateral acceleration) — Forces acting at the roll axis and at the suspension produce sprung mass lateral acceleration (see Figure A-4):

$$m_s a_{y_s} = \Sigma Y_s \tag{A-3}$$

Sprung Mass Rolling Moment (roll rate) —Taking moments about the sprung mass cg, in Figure A-4, produces sprung mass roll motions.

$$I_{\phi_s} \ddot{\phi}_s - I_{xz_s} \ddot{\psi} = \Sigma L_s \tag{A-4}$$

Sprung Mass Vertical Force (vertical acceleration) — The sprung mass vertical motions result from the action of vertical forces (see Figure A-4):

$$m_s \ddot{z}_s = m_s g_{z_S} - \Sigma Z_s \tag{A-5}$$

Sprung Mass Pitch Moment (pitch rate) — Sprung mass pitch motions result from moments about the sprung mass cg, in Figure A-5:

$$I_{y_s} \ddot{\theta}_s = \Sigma M_s \tag{A-6}$$

D. FORCES AND MOMENTS ACTING ON INERTIAL DYNAMICS

These are the sums of forces and moments acting in each direction upon the sprung or total mass, as defined in Section C, as shown in Figure A-3, through Figure A-5.

Longitudinal Force

$$\begin{aligned}\Sigma X \;=\; & F_{xN_{LF}} \cos\delta_{LF} + F_{xN_{RF}} \cos\delta_{RF} + F_{xN_{LR}} \cos\delta_{LR} + F_{xN_{RR}} \cos\delta_{RR} \\ & - F_{y_{LF}} \sin\delta_{LF} - F_{y_{RF}} \sin\delta_{RF} - F_{y_{LR}} \sin\delta_{LR} - F_{y_{RR}} \sin\delta_{RR} \\ & - X_A + mg_x + F_{x_{HITCH}} + F_{x_{COLLISION}}\end{aligned} \tag{A-7}$$

Yawing Moment

$$\begin{aligned}\Sigma N \;=\; & \frac{T_F}{2}\left(F_{xN_{LF}} \cos\delta_{LF} - F_{y_{LF}} \sin\delta_{LF}\right) - \frac{T_F}{2}\left(F_{xN_{RF}} \cos\delta_{RF} - F_{y_{RF}} \sin\delta_{RF}\right) \\ & + \frac{T_R}{2}\left(F_{xN_{LR}} \cos\delta_{LR} - F_{y_{LR}} \sin\delta_{LR}\right) - \frac{T_R}{2}\left(F_{xN_{RR}} \cos\delta_{RR} - F_{y_{RR}} \sin\delta_{RR}\right) \\ & + a_{CG}\left(F_{y_{LF}} \cos\delta_{LF} + F_{y_{RF}} \cos\delta_{RF} + F_{xN_{LF}} \sin\delta_{LF} + F_{xN_{RF}} \sin\delta_{RF} + F_{y_{LF_{CURB}}} + F_{y_{RF_{CURB}}}\right) \\ & + b_{CG}\left(F_{y_{LR}} + F_{y_{RR}} + F_{y_{LR_{CURB}}} + F_{y_{RR_{CURB}}}\right) \\ & + M_{z_{LF}} + M_{z_{RF}} + M_{z_{LR}} + M_{z_{RR}} + N_A - d\,F_{y_{HITCH}} + M_{z_{COLLISION}}\end{aligned} \tag{A-8}$$

Sprung Mass Side Force

$$\begin{aligned}\Sigma Y_S \;=\; & \left(F_{RAF} + F_{RAR}\right)\cos\phi_s \\ & + \left(F_{SLF} + F_{SRF} + F_{SLR} + F_{SRR}\right)\sin\phi_s \\ & + F_{y_{HITCH}} + Y_A + F_{y_{COLLISION}} + m_s g_{y_S}\end{aligned} \tag{A-9}$$

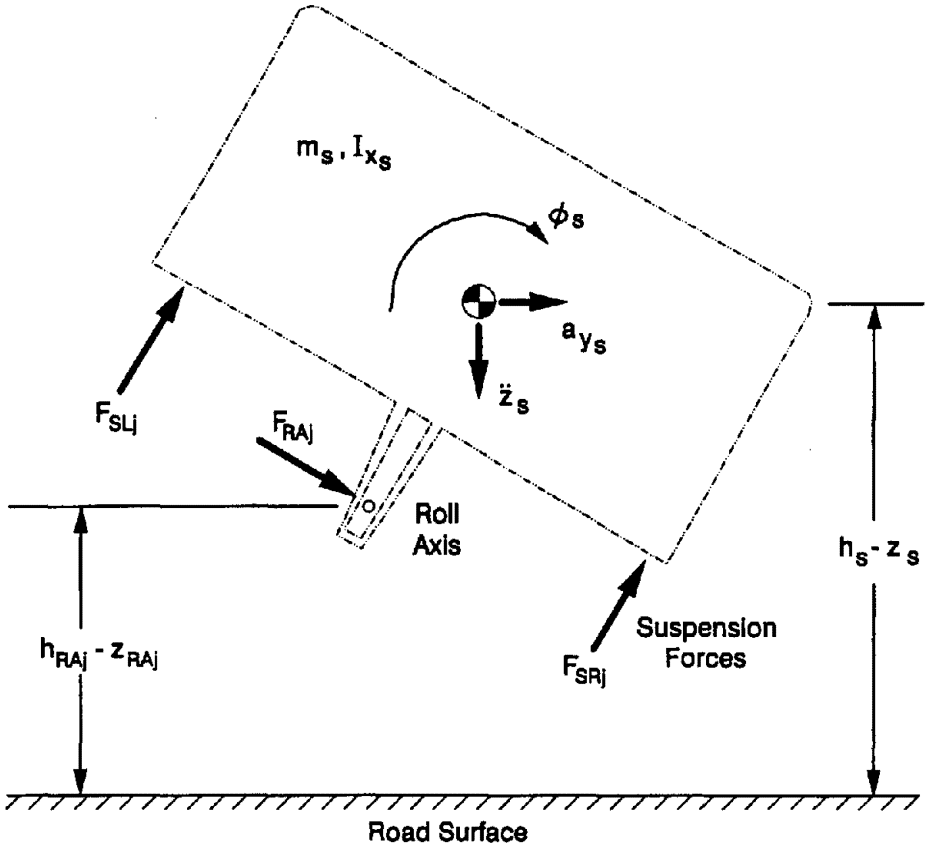

Figure A-4. Sprung Mass Free Body Diagram, End View

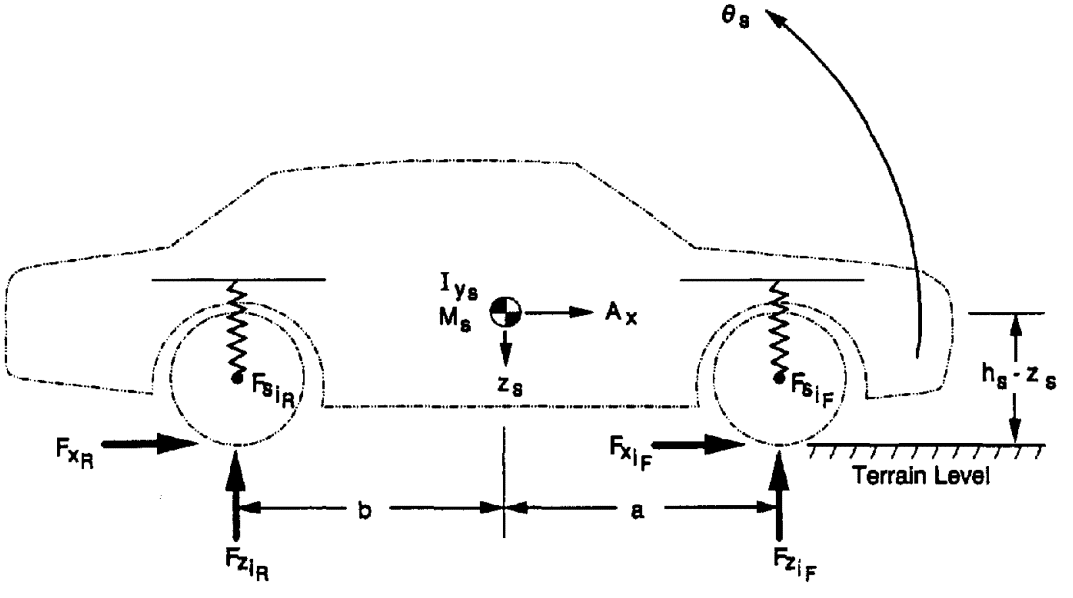

Figure A-5. Sprung Mass Free Body Diagram, Side View

Sprung Mass Rolling Moment

$$\begin{aligned}\Sigma L_S &= F_{SLF}\frac{T_F}{2} - F_{SRF}\frac{T_F}{2} + F_{SLR}\frac{T_R}{2} - F_{SRR}\frac{T_R}{2} \\ &- \frac{F_{RAF}}{\cos\phi_s}\left[h_s - z_s - RR_F + z_{UF} - \left(h_{RAF} - RR_F\right)\cos\phi_{UF}\right] \\ &- \frac{F_{RAR}}{\cos\phi_s}\left[h_s - z_s - RR_R + z_{UR} - \left(h_{RAR} - RR_R\right)\cos\phi_{UR}\right] \\ &+ L_A - H_H F_{y_{HITCH}} + M_{x_{HITCH}} + M_{x_{COLLISION}}\end{aligned} \tag{A-10}$$

Sprung Mass Vertical Force

$$\begin{aligned}\Sigma Z_S &= \left(F_{SLF} + F_{SRF} + F_{SLR} + F_{SRR}\right)\cos\phi_s \\ &- \left(F_{RAF} + F_{RAR}\right)\sin\phi_s + F_{z_{HITCH}} + F_{z_{COLLISION}}\end{aligned} \tag{A-11}$$

Sprung Mass Pitch Moment

$$\begin{aligned}\Sigma M_S &= \mathrm{a}\ \left(F_{SLF} + F_{SRF}\right) - \mathrm{b}\left(F_{SLR} + F_{SRR}\right) \\ &+ \left(F_{xN_{LF}}\cos\delta_{LF} - F_{y_{LF}}\sin\delta_{LF}\right)\left(h_s - z_s + h_{T_{LF}}\right) \\ &+ \left(F_{xN_{RF}}\cos\delta_{RF} - F_{y_{RF}}\sin\delta_{RF}\right)\left(h_s - z_s + h_{T_{RF}}\right) \\ &+ F_{xN_{LR}}\cos\delta_{LR}\left(h_s - z_s + h_{T_{LR}}\right) + F_{xN_{RR}}\cos\delta_{RR}\left(h_s - z_s + h_{T_{RR}}\right) \\ &+ H_H F_{x_{HITCH}} - d\,F_{y_{HITCH}} + M_{y_{COLLISION}}\end{aligned} \tag{A-12}$$

Aerodynamic Effects

Aerodynamic forces and moments are defined according to standard conditions:

$$\begin{aligned}Y_A &= \frac{\partial Y_A}{\partial v}\left(v - v_g\right)\frac{u}{U_{AERO}} \\ N_A &= \frac{\partial N_A}{\partial v}\left(v - v_g\right)\frac{u}{U_{AERO}} \\ L_A &= \frac{\partial L_A}{\partial v}\left(v - v_g\right)\frac{u}{U_{AERO}} \\ X_A &= \tfrac{1}{2}\rho A\, C_D u^2 sign(u)\end{aligned} \tag{A-13}$$

Roadway Pitch and Roll Angles

The yaw plane is always parallel with the road surface. As the road plane rotates in pitch and roll, the orientation of the gravity force vector changes relative to the yaw plane. The following equations resolve the gravity force into the vehicle body x, y and z axes.

$$\theta_T = 0.5\left[\tan^{-1}\left(\frac{\left(h_{T_{LR}} - h_{T_{LF}}\right)}{\left(\left(a+b\right)^2 - \left(h_{T_{LF}} - h_{T_{LR}}\right)^2\right)^{0.5}}\right) + \tan^{-1}\left(\frac{\left(h_{T_{RR}} - h_{T_{RF}}\right)}{\left(\left(a+b\right)^2 - \left(h_{T_{RF}} - h_{T_{RR}}\right)^2\right)^{0.5}}\right)\right]$$

$$\phi_{T_F} = \tan^{-1}\left(\frac{\left(h_{T_{RF}} - h_{T_{LF}}\right)}{\left(T_F{}^2 - \left(h_{T_{RF}} - h_{T_{LF}}\right)^2\right)^{0.5}}\right) \qquad \text{(A-14)}$$

$$\phi_{T_R} = \tan^{-1}\left(\frac{\left(h_{T_{RR}} - h_{T_{LR}}\right)}{\left(T_R{}^2 - \left(h_{T_{RR}} - h_{T_{LR}}\right)^2\right)^{0.5}}\right)$$

$$\phi_{T_S} = 0.5\left(\phi_{T_F} + \phi_{T_R}\right)$$

Gravity terms to account for non-horizontal roads:

$$\begin{aligned} g_x &= -g\sin\left(\theta_T\right) \\ g_{y_S} &= g\cos\left(\theta_T\right)\sin\left(\phi_{T_S}\right) \\ g_{y_F} &= g\cos\left(\theta_T\right)\sin\left(\phi_{T_F}\right) \\ g_{y_R} &= g\cos\left(\theta_T\right)\sin\left(\phi_{T_R}\right) \\ g_{z_S} &= g\cos\left(\theta_T\right)\cos\left(\phi_{T_S}\right) \\ g_{z_F} &= g\cos\left(\theta_T\right)\cos\left(\phi_{T_F}\right) \\ g_{z_R} &= g\cos\left(\theta_T\right)\cos\left(\phi_{T_R}\right) \end{aligned} \qquad \text{(A-15)}$$

Location of total vehicle center of gravity for yaw moment equation:

$$\begin{aligned} a_{CG} &= \frac{m_{uF} + \left(\frac{a}{a+b}\right)m_S}{m}\left(a+b\right) \\ b_{CG} &= \frac{m_{uR} + \left(\frac{b}{a+b}\right)m_S}{m}\left(a+b\right) \end{aligned} \qquad \text{(A-16)}$$

E. UNSPRUNG MASS INERTIAL DYNAMICS

Unsprung Mass Rolling Moment — The unsprung masses are acted upon by inertial and tire forces, and reaction forces at the roll axis pin and suspension, as illustrated in Figure A-6, for each axle. Following from the axle free body diagram in Figure A-6 the roll moment equation is the same at the front and rear:

$$I_{uj}\ddot{\phi}_{uj} = \Sigma L_{uj} \tag{A-17}$$

Unsprung Mass Vertical Acceleration — The tires are permitted vertical compliance, and large roll angles are a consequence of cg elevation, so vertical acceleration equations for each axle are required. Following from the Figure A-6 axle free body diagram,

$$m_{uj}\ddot{z}_{uj} = m_{uj}g_{z_j} - \Sigma Z_{uj} \tag{A-18}$$

Unsprung Mass Lateral Acceleration — From Figure A-6, the net sum of all lateral forces act on the unsprung mass to produce lateral acceleration.

$$m_{uj}a_{y_{uj}} = \Sigma Y_{uj} \tag{A-19}$$

where $i = F$ for front, or R for rear

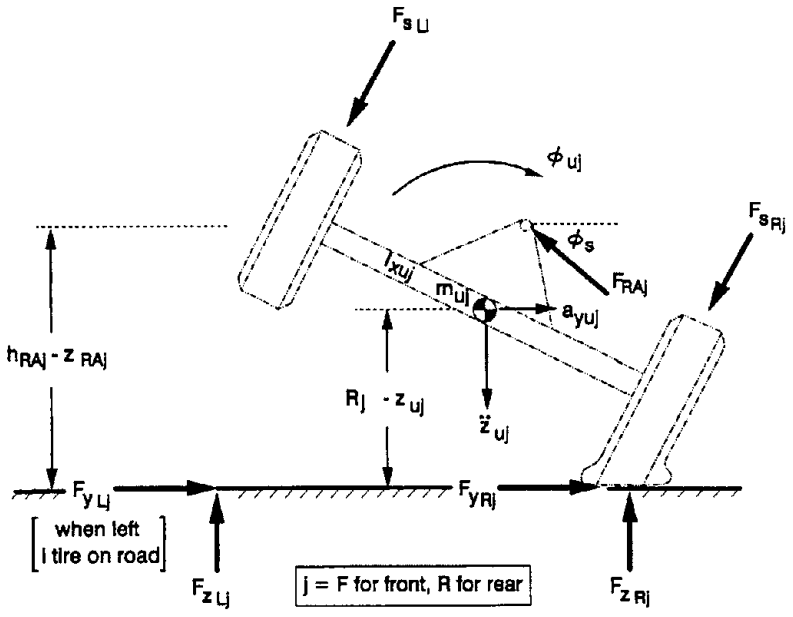

Figure A-6. Unsprung Mass Free Body Diagram

F. FORCES AND MOMENTS ACTING ON UNSPRUNG MASSES

Note that K_{LT} relates to lateral tire compliance, as illustrated in Figure A-7. This can be an important effect in rollover situations since it reduces the effective axle track width at the outside wheel.

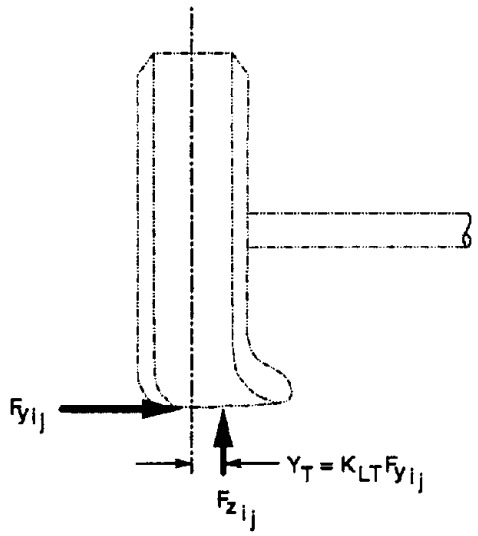

Figure A-7. Tire Lateral Deflection Characteristics

$$
\begin{aligned}
\Sigma L_{ui} \;=\;& F_{SRi}\frac{T_j}{2} - F_{SLi}\frac{T_j}{2} - F_{RAj}\left(h_{RAj} - RR_j\right) \\
&+ F_{Z_{Lj}}\left[RR_F \sin\phi_{uj} + \frac{T_j}{2}\cos\phi_{uj} - K_{LT}F_{y_{Lj}}\right] \\
&- F_{Z_{Rj}}\left[-RR_F \sin\phi_{uj} + \frac{T_j}{2}\cos\phi_{uj} + K_{LT}F_{y_{Rj}}\right] \\
&- \left(RR_F - z_{uj} + h_{T_{Lj}}\right)\left[F_{y_{Lj}}\cos\delta_{w_{Lj}} + F_{xN_{Lj}}\sin\delta_{w_{Lj}}\right] \\
&- \left(RR_F - z_{uj} + h_{T_{Rj}}\right)\left[F_{y_{Rj}}\cos\delta_{w_{Rj}} + F_{xN_{Rj}}\sin\delta_{w_{Rj}}\right] \\
&- \left(RR_F - z_{uj} + h_{T_{Lj}} - h_{CURB}\right)F_{y_{LjCURB}} \\
&- \left(RR_F - z_{uj} + h_{T_{Rj}} - h_{CURB}\right)F_{y_{RjCURB}}
\end{aligned}
\tag{A-20}
$$

$$
\Sigma Z_{uj} \;=\; F_{Z_{Lj}} + F_{Z_{Rj}} + F_{RA_j}\sin\phi_s - \left(F_{SL_j} + F_{SR_j}\right)\cos\phi_s \tag{A-21}
$$

$$
\begin{aligned}
\Sigma Y_{uj} \;=\;& F_{y_{Lj}}\cos\delta_{w_{Lj}} + F_{y_{Rj}}\cos\delta_{w_{Rj}} + F_{xN_{Lj}}\sin\delta_{w_{Lj}} + F_{xN_{Rj}}\sin\delta_{w_{Rj}} \\
&- F_{RA_j}\cos\phi_s - \left[F_{SL_j} + F_{SR_j}\right]\sin\phi_s + F_{y_{LjCURB}} + F_{y_{RjCURB}} + m_{uj}g_{y_j}
\end{aligned}
\tag{A-22}
$$

G. SUSPENSION FORCE DEVELOPMENT

The suspension forces acting on the sprung and unsprung masses depend on the suspension compression, relative roll angle, and squat/lift reactions. In an effort to maintain generalized applicability to any type of suspension, all of the force reactions are modified to have their equivalent force acting at the track width, (i.e., at each wheel). This includes effects from suspension spring load, shock absorber damping, auxiliary roll stiffness, bump stop forces, and squat/lift forces from suspension geometry reactions (see Figure A-8 and Figure A-9).

$$F_{SLj} = F_{SLj_0} - z_{SLj}K_{Sj} - \dot{z}_{SLj}K_{SDj} + \frac{(\phi_s - \phi_{Uj})K_{TSj}}{T_j} + F_{BSLj} + F_{SQLj} \quad \text{(A-23)}$$

$$F_{SRj} = F_{SRj_0} - z_{SRj}K_{Sj} - \dot{z}_{SRj}K_{SDj} - \frac{(\phi_s - \phi_{Uj})K_{TSj}}{T_j} + F_{BSRj} + F_{SQRj} \quad \text{(A-24)}$$

In the preceding suspension force equations, the values z_{Sij} and $\dot{z}_{Sij}$ need to be computed. These equations define the change in spring length, starting from what the spring length is at curb load, F_{Sij_o} (See Figure A-9).

$$\begin{aligned}
z_{SLF} &= \frac{h_S - RR_F + z_{UF} - z_S}{\cos\phi_S} - h_S + RR_F + a\theta + (\phi_S - \phi_{UF})\frac{T_F}{2} \\
z_{SRF} &= \frac{h_S - RR_F + z_{UF} - z_S}{\cos\phi_S} - h_S + RR_F + a\theta - (\phi_S - \phi_{UF})\frac{T_F}{2} \\
z_{SLR} &= \frac{h_S - RR_R + z_{UR} - z_S}{\cos\phi_S} - h_S + RR_R - b\theta + (\phi_S - \phi_{UR})\frac{T_R}{2} \\
z_{SRR} &= \frac{h_S - RR_R + z_{UR} - z_S}{\cos\phi_S} - h_S + RR_R - b\theta - (\phi_S - \phi_{UR})\frac{T_R}{2}
\end{aligned} \quad \text{(A-25)}$$

$$\begin{aligned}
\dot{z}_{SLF} &= (h_S - RR_F + z_{UF} - z_S)\frac{\tan(\phi_s)}{\cos(\phi_s)}\dot{\phi}_S + \frac{\dot{z}_{UF} - \dot{z}_S}{\cos(\phi_s)} + a\dot{\theta} + (\dot{\phi}_S - \dot{\phi}_{UF})\frac{T_F}{2} \\
\dot{z}_{SRF} &= (h_S - RR_F + z_{UF} - z_S)\frac{\tan(\phi_s)}{\cos(\phi_s)}\dot{\phi}_S + \frac{\dot{z}_{UF} - \dot{z}_S}{\cos(\phi_s)} + a\dot{\theta} - (\dot{\phi}_S - \dot{\phi}_{UF})\frac{T_F}{2} \\
\dot{z}_{SLR} &= (h_S - RR_R + z_{UR} - z_S)\frac{\tan(\phi_s)}{\cos(\phi_s)}\dot{\phi}_S + \frac{\dot{z}_{UR} - \dot{z}_S}{\cos(\phi_s)} - b\dot{\theta} + (\dot{\phi}_S - \dot{\phi}_{UF})\frac{T_R}{2} \\
\dot{z}_{SRR} &= (h_S - RR_R + z_{UR} - z_S)\frac{\tan(\phi_s)}{\cos(\phi_s)}\dot{\phi}_S + \frac{\dot{z}_{UR} - \dot{z}_S}{\cos(\phi_s)} - b\dot{\theta} - (\dot{\phi}_S - \dot{\phi}_{UF})\frac{T_R}{2}
\end{aligned} \quad \text{(A-26)}$$

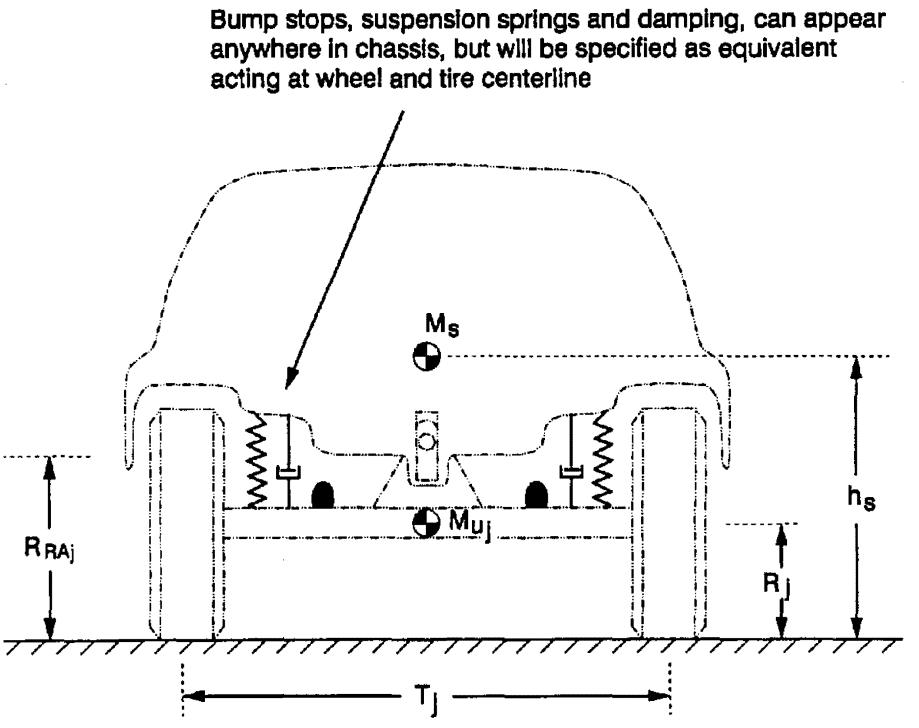

Figure A-8. Suspension Spring and Damping Components

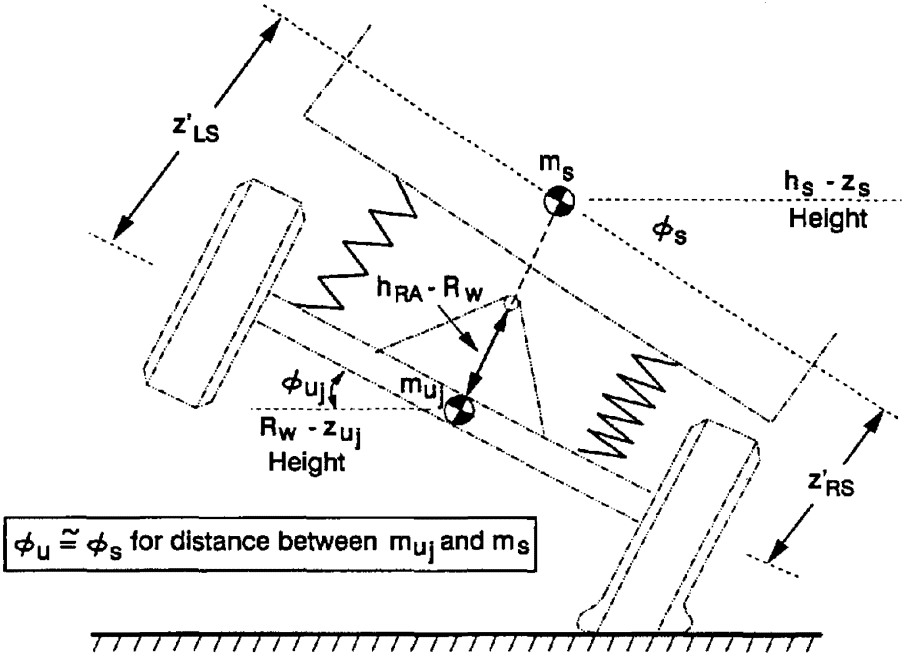

Figure A-9. Change in Suspension Spring Length

The bump stop model has been upgraded to address three areas: 1) non-symmetry, 2) separate front and rear models, and 3) a smooth transition as the bump stop is contacted. Figure A-10 shows a representative graph of the spring and bump stop models. The spring is still modeled as a linear spring, K_{Si}, acting on the suspension deflection, z_{Sij}. The bump stop contact points in compression and extension are specified by parameters H_{BSCi} and H_{BSEi} respectively (both positive values). The bump stop terminal stiffness is specified by parameters K_{BSCi} and K_{BSEi}. The smooth transition region uses a negative exponential function with coefficients S_{BSCi} and S_{BSEi}. In the compression region, the bump stop force F_{BSij} is given by:

$$
\begin{aligned}
&\textit{If } z_{Sij} > -H_{BSCi} \textit{ then} \\
&\quad F_{BSij} = \left(-H_{BSCi} - z_{Sij}\right) \cdot K_{BSCi} \cdot \left(1 - e^{\left(S_{BSCi} \cdot \left(z_{Sij} + H_{BSCi}\right)\right)}\right) \\
&\textit{Else If } z_{Sij} > -H_{BSEi} \textit{ then} \\
&\quad F_{BSij} = \left(H_{BSEi} - z_{Sij}\right) \cdot K_{BSEi} \cdot \left(1 - e^{\left(S_{BSEi} \cdot \left(z_{Sij} + H_{BSEi}\right)\right)}\right) \\
&\textit{Else} \\
&\quad F_{BSij} = 0 \\
&\textit{End If}
\end{aligned}
\tag{A-27}
$$

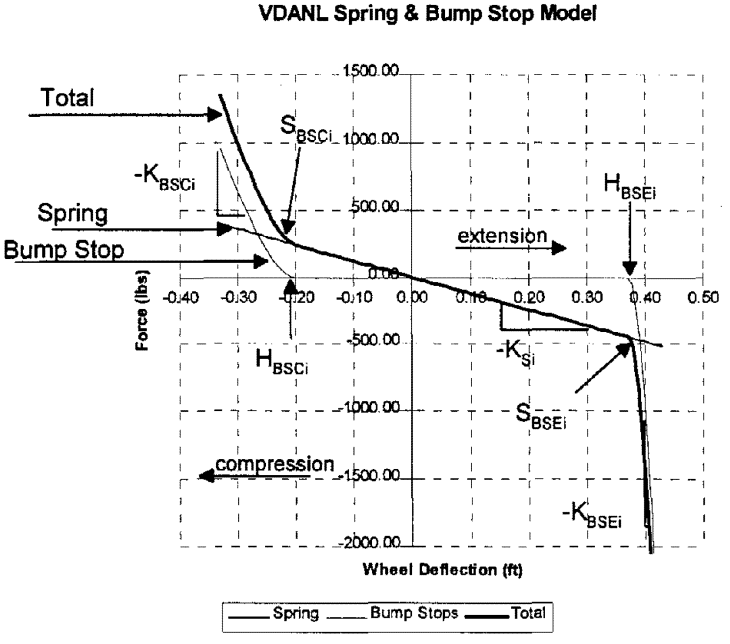

Figure A-10. VDANL Spring and Bump Stop Model Plot

H. SUSPENSION AND STEERING GEOMETRY FUNCTIONS

The suspension and steering geometry defines the relative motions between the four wheels and the sprung mass body. The length and orientation of its links could be used to compute a vehicle's suspension kinematics. However, suspension geometry is so varied and sometimes complex that it would be very difficult to put all measurement data into one consistent organized scheme.

To avoid this problem, all suspension and steering affects are defined in terms of motions at the tire contact point on the road surface. This makes the estimation of all parameters consistent and simple, and allows their determination by simple static tests of wheel motions at the ground contact point as described in Appendix C. This composite approach is also consistent with keeping the equations of motion mathematics as simple and direct as possible, since all the F_x, F_y, F_z, M_z force inputs to the vehicle are defined at this same tire contact point on the road surface.

The composite parameter approach includes the following effects:

1. Wheel camber angle as a function of suspension deflection, which produces tire side force.
2. Suspension squat and lift forces, as a function of F_x, F_y, F_z forces at the tire contact point, which are affected by suspension deflection geometry.
3. Individual wheel steer angle as a function of:
   a) Suspension deflection
   b) Ackerman steer function
   c) Aligning torque applied to steering system compliance
   d) Lateral tire force compliance
   e) Steering axis offset
   f) Steering system dynamics
4. Finally, the individual wheel steer angles, along with $v, u, \dot{\psi}, \dot{\phi}_s$, are used to compute the tire sideslip (α_{ij}) at each tire, which then produce tire side forces.

With all these above-listed effects defined at the tire contact point on the road surface, very straightforward static tests can be done to measure $\delta_w, \gamma, x, y, z$ motion relationships at each wheel (see Figure A-11.

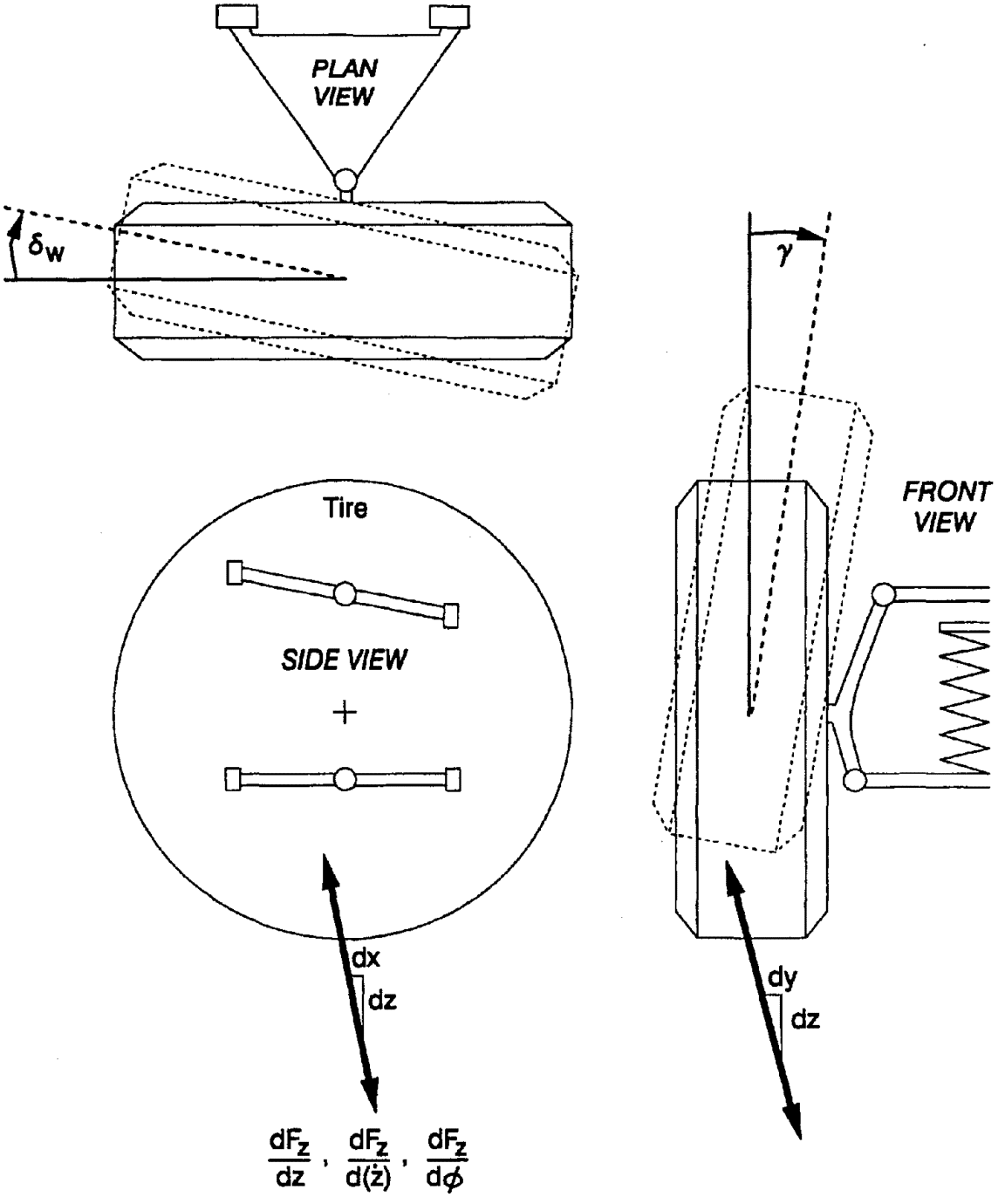

Figure A-11. Static Test on Wheel Motions

The following sections will describe in detail how these motion relationships are specified by math equations, and how the static test data relate to the equation parameters.

1. Wheel Camber Angle Versus Suspension Deflection

Typical wheel camber curves are shown in Figure A-12, and can be represented by a second order equation in relation to the sprung mass body. Since the body also can have a roll angle, the wheel camber angle relative to the road surface is:

For independent suspension

$$\begin{aligned} \gamma_{LF} &= \phi_s - \phi_{T_{LF}} + D_F\, z_{SLF} + E_F\, z_{SLF}^2 \\ \gamma_{RF} &= \phi_s - \phi_{T_{RF}} - D_F\, z_{SRF} - E_F\, z_{SRF}^2 \\ \gamma_{LR} &= \phi_s - \phi_{T_{LR}} + D_R\, z_{SLR} + E_R\, z_{SLR}^2 \\ \gamma_{RR} &= \phi_s - \phi_{T_{RR}} - D_R\, z_{SRR} - E_R\, z_{SRR}^2 \end{aligned} \qquad \text{(A-28)}$$

For solid or beam angle suspension

$$\gamma_{ij} = \phi_{uj} - \phi_{T_{ij}} \qquad \begin{matrix} i = L \text{ or } R \\ \text{j} = F \text{ or } R \end{matrix} \qquad \text{(A-29)}$$

Where ϕ_{Tij} is the angle of the roadway about the tire's X axis (road side slope for straight driving) and γ_{ij} is used in the tire model (Appendix E) to compute side force.

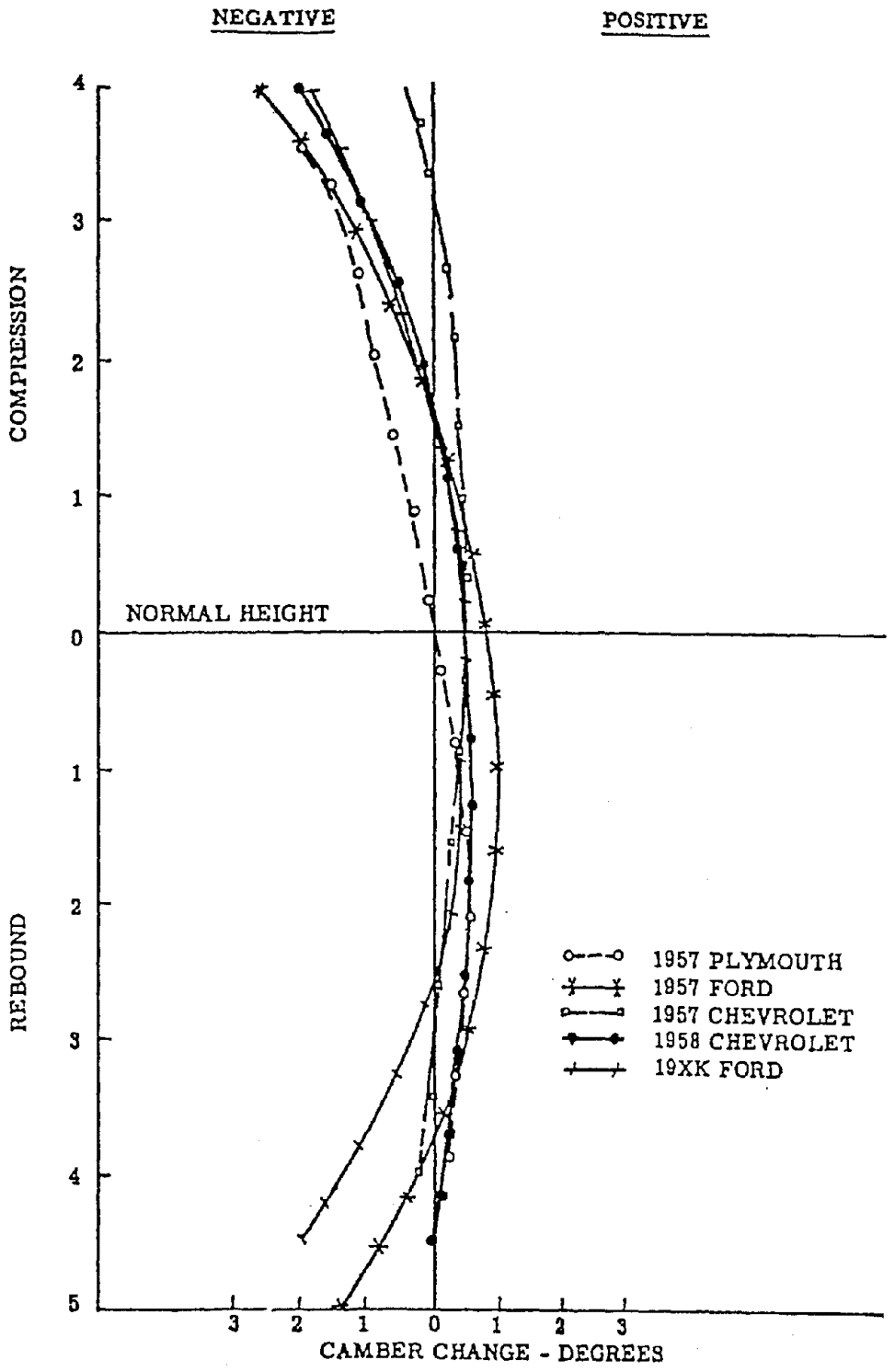

Figure A-12. Chamber Change vs. Suspension Position

2. Suspension Squat and Lift Forces

The mechanism of squat/lift forces is associated with the concept of the chassis roll axis. With solid axle suspensions there is a specific pivot point about which the sprung mass rolls, and which a single-axle side force is transmitted to the sprung mass. For this case, the roll axis is specified at h_{RAF}, h_{RAR}, and there are no squat/lift reactions due to applied side forces.

However, with independent suspensions, there is no single roll axis pivot, in which the axle side forces are transmitted to the sprung mass. There is the tendency to represent this case as having an equivalent or imaginary roll axis location, at which the side forces can be assumed to be acting. But if analyzed this way, the squat/lift effects at each suspension are bypassed. A more direct analysis of the side force and moment application at each individual suspension will not only carry them through more accurately, but also will show that vertical suspension forces are reduced or increased, which in turn causes the suspension to squat or lift.

The key geometry feature that causes squat/lift forces is the slope of the tire contact patch path in vertical motion, relative to pure vertical. In this regard, all multi-link suspensions can be reduced to a single swing arm suspension with the same tire patch path (slope and path arc radius) as illustrated in Figure A-13. In the following analysis, it is shown that the effect of this geometric slope is to produce squat/lift forces in the suspension from applied side forces, while the side forces are effectively being applied at ground level for determination of roll moments to sprung mass.

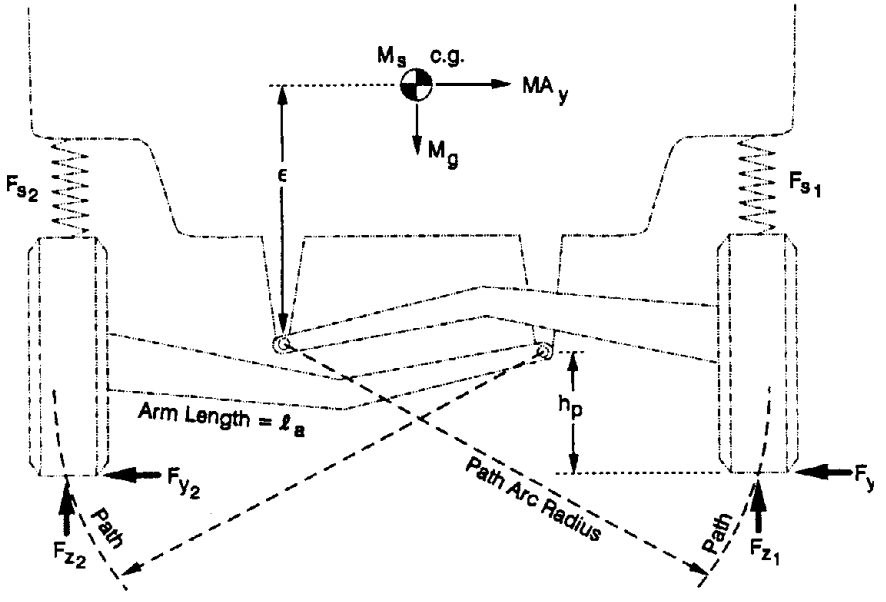

Figure A-13. Equivalent Single Swing Arm Approximation for a Multilink Suspension Showing Suspension Geometry Forces and Moments

Moments about m_s cg come from springs, dampers, bump stops, and anti-roll bars, and suspension arm pivot points. Summing the moments about the cg yields:

$$\begin{aligned}\Sigma m_{x_s} &= \left(F_{s_2} - F_{s_1}\right)\frac{T}{2} + F_{y_1}\left(\varepsilon + h_p\right) + F_{y_2}\left(\varepsilon + h_p\right) \\ &\quad + F_{y_1}\frac{h_p}{\ell_a}\left(\frac{T}{2}\right) - F_{y_2}\frac{h_p}{\ell_a}\frac{T}{2}\end{aligned} \tag{A-30}$$

The $(\varepsilon + h_p)$ distance means that F_{y_1} and F_{y_2} are effectively acting at ground level in producing the roll moment, $(\varepsilon + h_p) = h_s$. The leftover terms acting at *T/2* are effectively the squat/lift forces acting at the suspension.

As summarized in Figure A-14, the lift forces bypass the springs and act up on the sprung mass and down on the tire. This reduces the load needed on the suspension spring; therefore, it can extend, or lift up, until it reaches equilibrium. Note that the $h_p \ell_a$ ratio is merely the slope of the tire patch path relative to vertical, for any type of independent suspension.

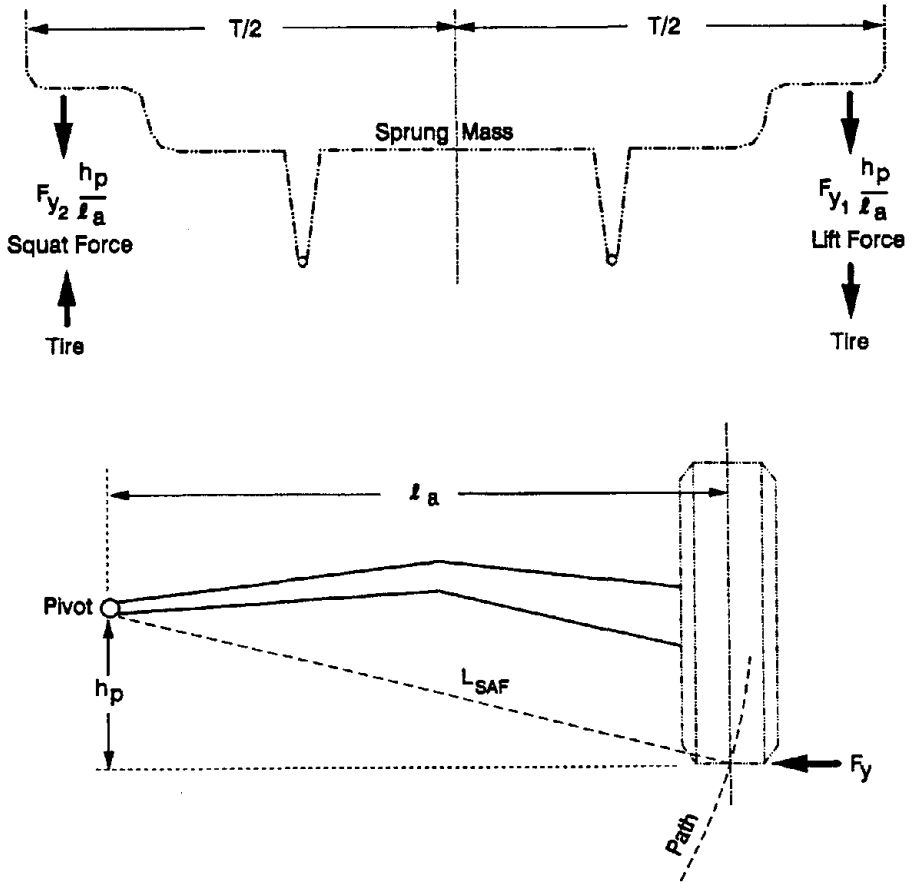

Figure A-14. Squat/Lift Forces and Slope of Tire Patch Path

In the math model, this slope is $\frac{h_p}{\ell_a} = K_{SLj}$, and to provide for changes in slope as the suspension moves up or down, the change to the initial slope as a function of suspension deflection is added. This slope at any z_{Sij} = is given by $K_{SLj} + \frac{z_{SLj}}{L_{SAj}}$. The side force in the body axis system multiplied by this slope then gives the squat/lift force at each suspension. For each suspension point, this force is given by:

$$F_{SQij} = \left[K_{SLj} + \frac{z_{Sij}}{L_{SAj}} \right] \left(F_{Y_{ij}} \cos\phi_s - F_{Z_{ij}} \sin\phi_s \right) \tag{A-31}$$

where i = Left or Right and j = Front or Rear.

A final reason for applying the forces in this way is that F_{SQij} acts at the same place as the spring, damping, auxiliary roll stiffness, and bump stop forces. In this way, there is no need to specify suspension pivot locations different for each vehicle, to pass these forces through. The composite suspension force approach allows all forces to act at one point and avoids the specification of detailed suspension geometry. Note that the net lift force per axle is $\left(F_{y_{Lj}} - F_{y_{Rj}} \right) \frac{h_p}{\ell_a}$ and this becomes significant only when $F_{y_1} >>> F_{y_2}$ in hard cornering.

The swing arm suspension is used in the analysis to show the effect of a given arc radius and path slope of tire patch motion. It is shown below that MacPherson strut, double A arm, and any other multi-link suspensions will have an equivalent tire patch motion slope and arc radius, and produce the same squat/lift reactions.

For the McPherson Strut Suspension in Figure A-15, the only steady state force possible at the upper strut mount, F_{USM}, is at 90° to the strut axis. For the lower arm, this force, F_{LA}, must be in line with the arm pivots. These two forces also act through the instantaneous center of motion. Taking moments about this center: $F_y h_{ic} = \left(F_z - F_s \right) L_{ic}$, the additional lift force is $F_z - F_s = F_y \frac{h_{i_c}}{L_{ic}}$, where $\frac{h_{ic}}{L_{ic}} L_{ic}$ is the line slope from center to tire patch. This is also the slope of tire patch motion relative to vertical.

The forces at the instant center are therefore F_y laterally and $F_z - F_s$ vertically.

The moment on the sprung mass is therefore:

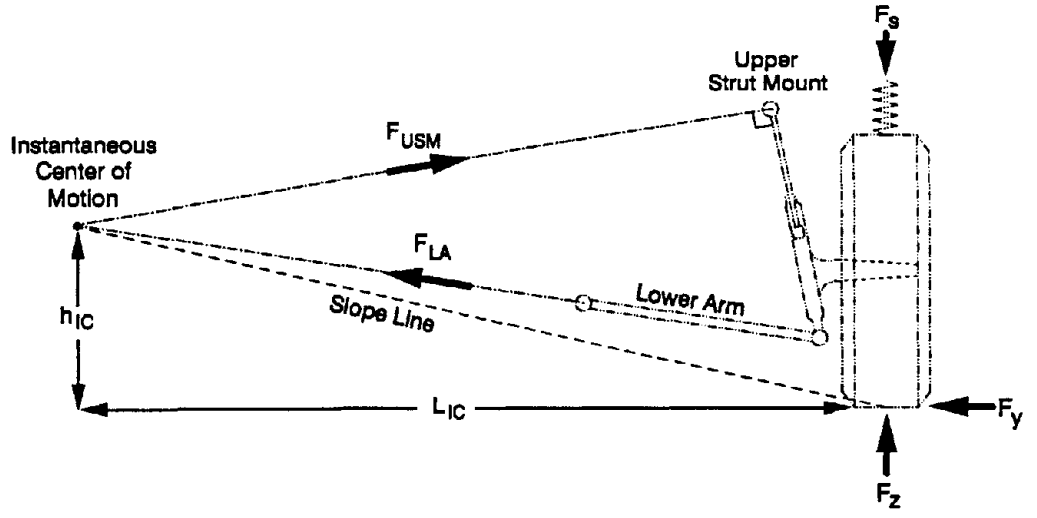

Figure A-15. McPherson Strut Suspension Steady State Forces

$$\begin{aligned}\Sigma m_{x_S} &= F_y(h_s - h_{ic}) - (F_z - F_s)\left(\frac{T}{2} - L_{ic}\right) - F_s\frac{T}{2} \\ &= F_y\left[h_s - h_{ic} - \left(\frac{T}{2} - L_{ic}\right)\right] - F_s\frac{T}{2} \\ &= F_y h_s - F_y\left(\frac{h_{ic}}{L_{ic}}\right)\frac{T}{2} - F_s\frac{T}{2}\end{aligned} \tag{A-32}$$

This is identical to the right-hand suspension terms for the single arm suspension, with the lift force, $F_y\left(\frac{h_{ic}}{L_{ic}}\right)$, applied at the composite suspension point.

A major difference with the MacPherson strut suspension occurs because the tire patch motion arc radius is usually very small. This means that the patch path slope changes very fast with small suspension deflection. This effect of the changing slope is covered by the z_{Sij} / L_{SAi} terms in equations (A-33). L_{SAi} is the path arc radius as shown in Figure A-16, which is a graphical solution for the tire path arc radius, L_{SAi}. Note how short L_{SAi} is, and how fast the slope changes; whereas, the distance to the instant center is fairly long.

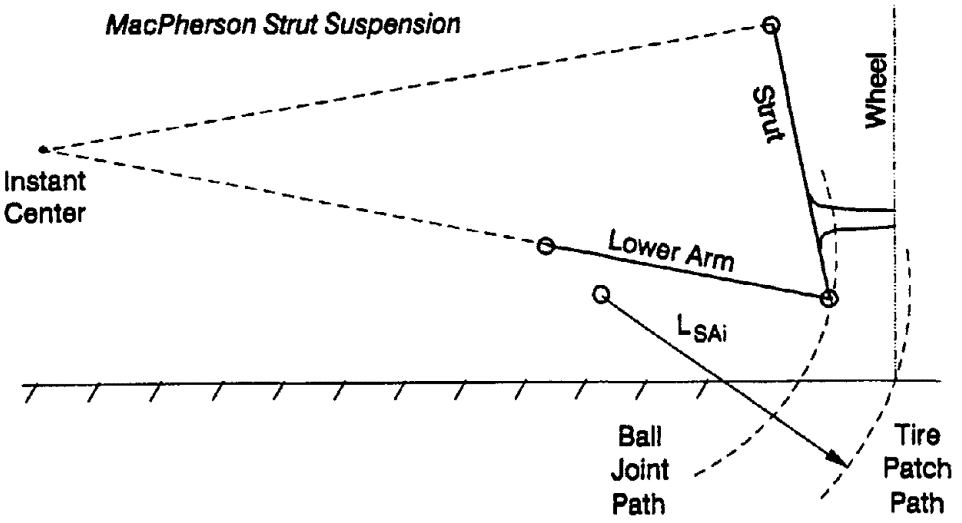

Figure A-16. Equivalent Tire Patch Radius for a McPherson Strut Suspension

Other suspension types, short and long arm, or multi-link, would have the same layout, analysis, and result as the MacPherson strut. All that is needed is to place the upper (short) arm, or the upper link, on the same line as F_{USM}, as shown Figure A-16. This upper arm force acts directly at the instantaneous center of motion, and produces the same analytical result.

Following from the above discussion, the simulation equations with the lift forces can be stated as follows. In the front view, the slope at the operating point defines how much squat or lift force will be generated by the application of an F_y cornering force:

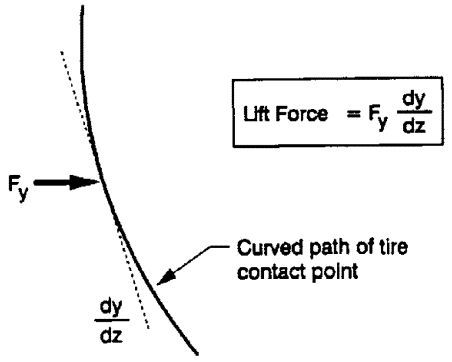

In the side view, a similar curved path can result in squat/or lift forces when F_x braking forces are applied at the tire contact point:

$$\text{Lift force} = F_x \frac{dx}{dz}$$

These forces are then combined into one equation for each wheel and suspension (see Figure A-17)

$$
\begin{aligned}
F_{SQLF} &= \left(K_{SLF} + \frac{z_{SLF}}{L_{SAF}}\right)\left(F_{y_{LF}} \cos\phi_s - F_{Z_{LF}} \sin\phi_s\right) - F_{xN_{LF}} K_{SADF} \\
F_{SQRF} &= \left(K_{SLF} + \frac{z_{SRF}}{L_{SAF}}\right)\left(-F_{y_{RF}} \cos\phi_s + F_{Z_{RF}} \sin\phi_s\right) - F_{xN_{RF}} K_{SADF} \\
F_{SQLR} &= \left(K_{SLR} + \frac{z_{SLR}}{L_{SAR}}\right)\left(F_{y_{LR}} \cos\phi_s - F_{Z_{Lr}} \sin\phi_s\right) + F_{xN_{LR}} K_{SADR} \\
F_{SQRR} &= \left(K_{SLR} + \frac{z_{SRR}}{L_{SAR}}\right)\left(-F_{y_{RR}} \cos\phi_s + F_{Z_{RR}} \sin\phi_s\right) + F_{xN_{RR}} K_{SADR}
\end{aligned}
\qquad \text{(A-33)}
$$

where K_{SLj} = Lateral Slope of equivalent single arm at curb load

L_{SAj} = Length of equivalent Single Arm at curb load

K_{SADj} = Anti Dive Slope

These F_{SQij} forces are added to the suspension force equations, (A-25) and (A-26). Suspension slopes for different conditions can be set as indicated in Table A-2.

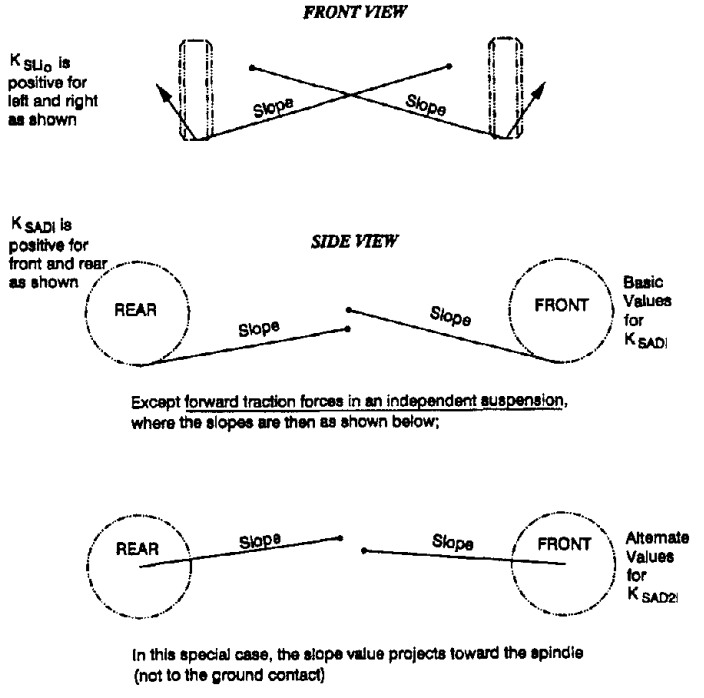

Figure A-17. Squat/Lift Function Slope Definitions

Table A-2 . Squat/Lift Slopes for Various Maneuvering Conditions

	Cornering	Braking (Neg. F_x)		Forward ACC (Pos. F_x)		
Suspension	Independent	Solid Axle	Independent	Solid Axle	Independent	Solid Axle
	As shown in Equations	$K_{SLj} = 0$ $L_{SAj} = \infty$	K_{SADj}	K_{SADj}	Switch to K_{SAD2j}	K_{SADj}

The above parameters can be preset for all cases, except that for forward acceleration (Forward ACC) with an Independent (IND) suspension, the K_{SADj} parameter must be changed to the alternate value K_{SAD2j}.

$$K_{SADj} \rightarrow K_{SA2Dj} \text{ for pos. } F_x \text{ ind. susp.}$$

3. Individual Wheel Steer Angle

a. Due to Suspension Deflection

There are two classes of suspensions here: the solid or beam axle, and fully independent. Figure A-18 is an example of wheel steer vs. suspension deflection for a fully independent suspension.

For a solid or bean axle, as the sprung mass rolls, the path of the lower pivot has a slope of $\frac{h}{L}$.

Vertical deflection of this pivot is $= \phi \frac{W_{SB}}{2}$

Longitudinal movement of pivot is $= \phi \left(\frac{W_{SB}}{2}\right)\left(\frac{h}{L}\right)$

Axle steer angle with body roll $= \frac{\text{Long Movement}}{\frac{W_{SB}}{2}} = \phi \frac{h}{L}$

Thus, $\frac{h}{L}$ is the roll steer coefficient.

However, this can be generalized for any situation of suspension squat/lift due to braking or acceleration forces where $h = h_o + z_s$ when average across left and right suspension deflection, the complete roll steer effect can be stated as follows:

$$\Delta\delta w_{ij} = \left[\frac{h_j + .5\left(z_{SLj} + z_{SRj}\right)}{L_j}\right]\left(\phi_s - \phi_{uj}\right) \qquad \text{(A-34)}$$

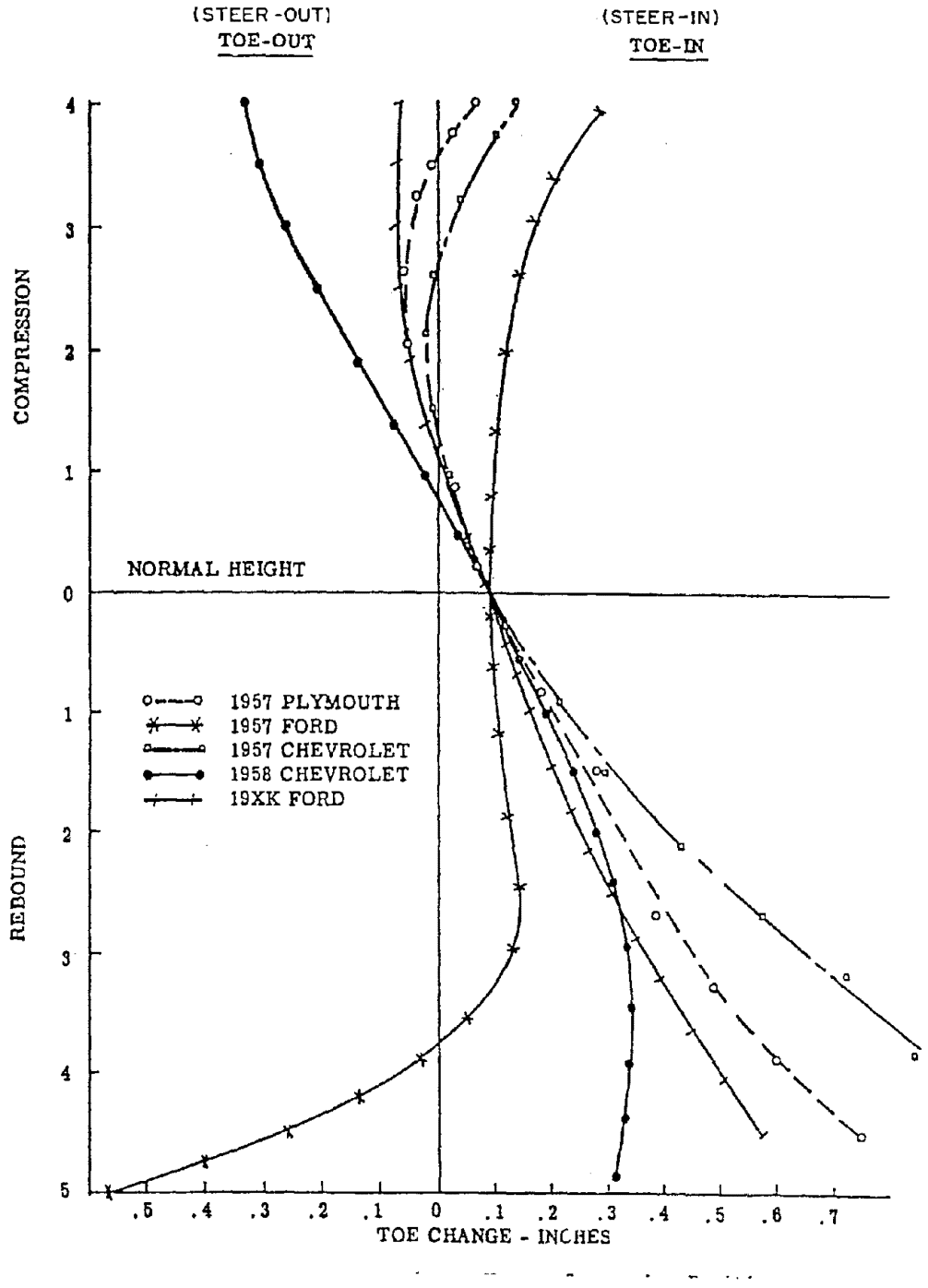

Figure A-18. Toe Change vs. Suspension Position

This accounts for changes in roll steer, when suspension squat/or lift is present via z_{sij}, where h, L are suspension arm parameters in side view as shown in Figure A-19.

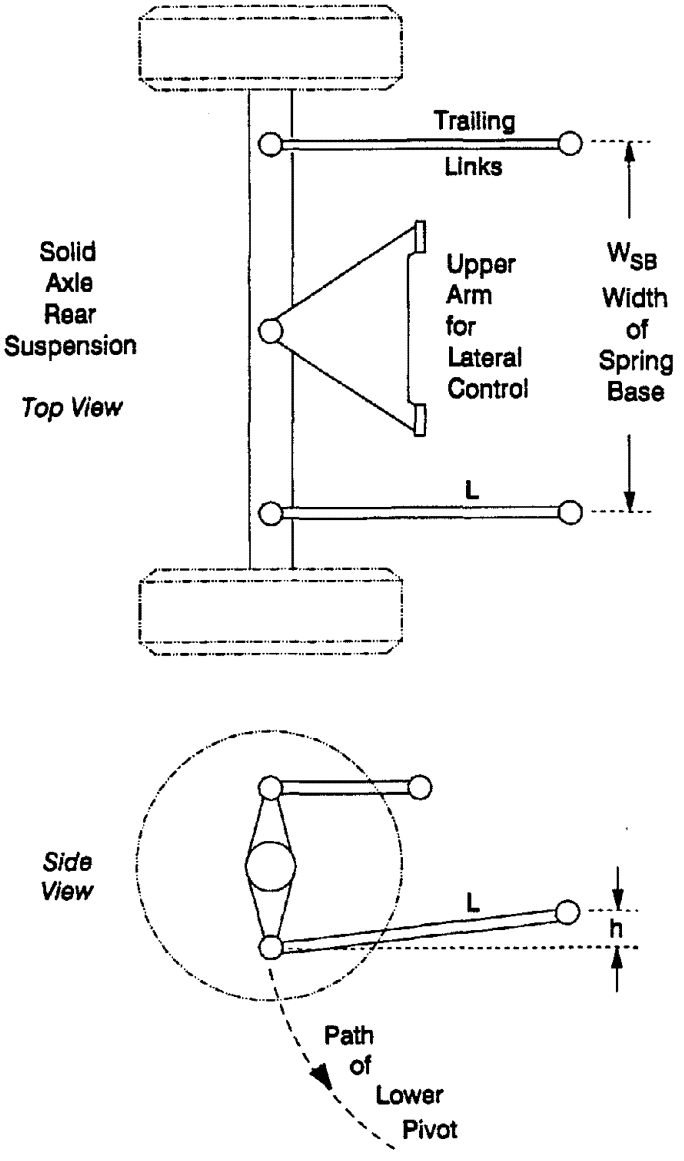

Figure A-19. Solid Axle or Beam Axle Suspensions with Ttrailing Links Controlling Axle Steer Angle

For independent suspensions, the steer effect is a nonlinear function of deflection z_{sij}, which can be approximated with a quadratic:

$$\Delta\delta_{w_{ij}} = A_{ij} + B_{ij}\, z_{Sij} + C_{ij}\, z_{Sij}^2 \qquad \text{(A-35)}$$

The A_{ij} component is static toe in, which is supposed to be zero, in motion. Therefore we can ignore this. The B_{ij} and C_{ij} are curve fitting parameters, which are simply opposite sign identical values for the left and right wheels.

$$\begin{aligned}
\Delta\delta_{w_{LF}} &= B_F\, z_{SLF} + C_F\, z_{SLF}^2 \\
\Delta\delta_{w_{RF}} &= -B_F\, z_{SRF} - C_F\, z_{SRF}^2 \\
\Delta\delta_{W_{LR}} &= B_R\, z_{SLR} + C_R\, z_{SLR}^2 \\
\Delta\delta_{w_{RR}} &= -B_R\, z_{SRR} - C_R\, z_{SRR}^2
\end{aligned} \tag{A-36}$$

Positive values of B_F steer the $\delta_{w_{LF}}$ to the left with negative z_{SLF}, and $\delta_{w_{RF}}$ to the left with positive z_{SRF}. Thus, in a right-hand turn, roll to the left will produce roll understeer.

b. Ackermann Steer Effects

Front wheel steer geometry is commonly designed for turning the inside wheel more than the outside wheel, for sharp small-radius turns as summarized in Figure A-20, where:

$$\begin{aligned}
\tan\delta_{AVG} &= \frac{\ell}{\sqrt{R^2 - \ell^2}} \\
\tan\delta_{w_L} &= \frac{\ell}{\sqrt{R^2 - \ell^2} + \frac{T_j}{2}} = \frac{\tan\delta_{\text{AVG}}}{1 + \frac{T_j}{2\ell}\tan\delta_{\text{AVG}}} \\
\tan\delta_{w_R} &= \frac{\ell}{\sqrt{R^2 - \ell^2} - \frac{T_j}{2}}
\end{aligned} \tag{A-37}$$

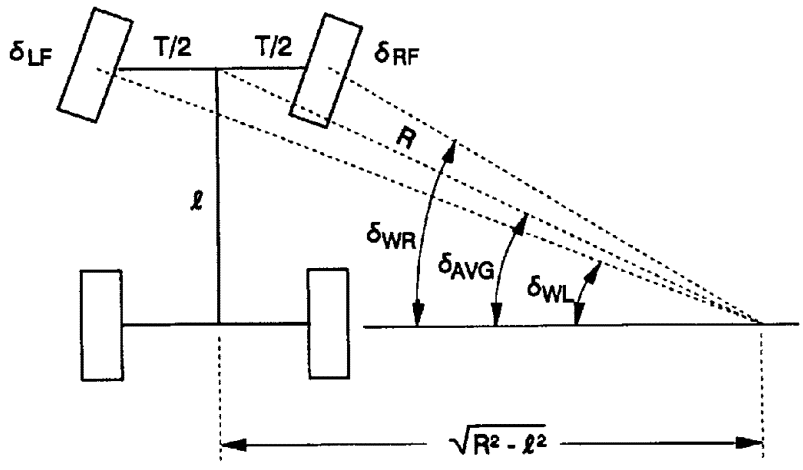

Figure A-20. Ackermann Steer Relationship's

For small angle approximations (to avoid $\tan^{-1}$ calculations), use $tan\left(\delta_w\right) \cong \delta_w$

$$\therefore \delta_{w_L} \approx \frac{\delta_{\text{AVG}}}{1+\frac{T_j}{2\ell}\delta_{\text{AVG}}} \approx \delta_{\text{AVG}}\left(1-\frac{T_j}{2\ell}\delta_{\text{AVG}}\right)$$
$$\delta_{w_R} \approx \delta_{\text{AVG}}\left(1+\frac{T_j}{2\ell}\delta_{\text{AVG}}\right) \tag{A-38}$$

To make this into a general case, we can change $\frac{T_j}{2\ell} = K_{ACK}$, so that this can be changed to any value.

$$\delta_{w_{LF}} = \delta_{w_F}\left(1-K_{ACK}\delta_{w_F}\right)$$
$$\delta_{w_{RF}} = \delta_{w_F}\left(1+K_{ACK}\delta_{w_F}\right) \tag{A-39}$$

c. Aligning Torque Steer

This is the deflection in the steering gear due to total aligning torque applied at the wheels.

$$\Delta\delta_{w_F} = \left(M_{z_{LF}} + M_{z_{RF}}\right)K_{SCF} \tag{A-40}$$

M_{ziF} are the sum of the tire aligning and the steer moment due to F_x (see e. below).

d. Lateral Force Compliance Steer

This is the deflection of the wheel steer angle due to lateral forces acting on compliant suspension components.

$$\Delta\delta_{wij} = F_{y_{ij}}K_{c_j} \tag{A-41}$$

e. Steer moments due to the F_x

Referring to Figure A-21, in most vehicle steering systems the ball-joint steer axis (kingpin axis) is offset laterally from the tire centerline at the tire contact patch. Longitudinal tire forces thus cause a moment about the ball-joint steer axis that acts on the front suspension aligning torque compliance. During cornering, the tire contact patch deforms laterally as shown in Figure A-21. The moment acting about the bass-joint axis is $= F_{xN_{iF}}\left(L_{SO} - K_{LT}F_{y_{iF}}\right)$

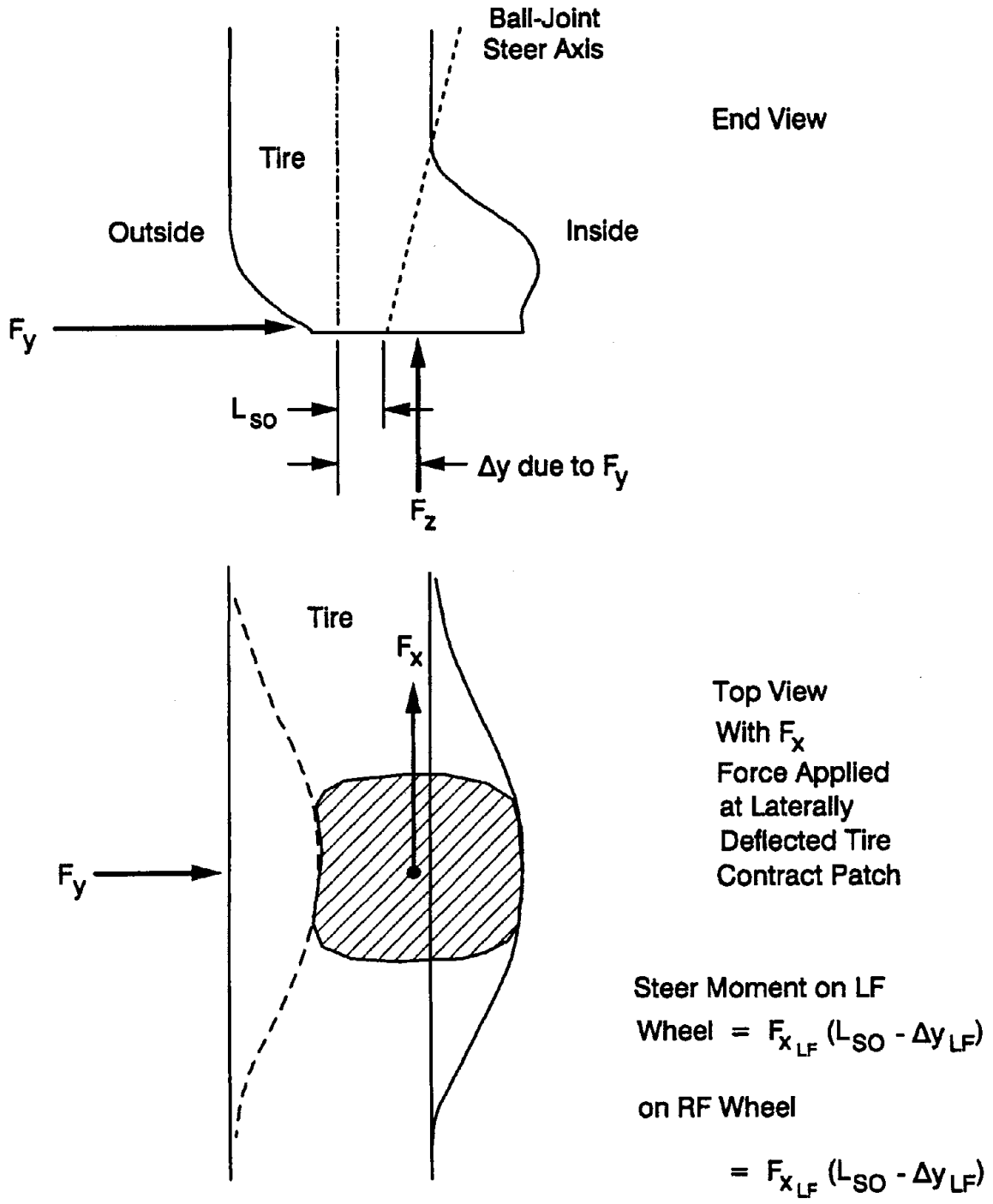

Figure A-21. Tire Lateral Deflection Due to Cornering (Side) Forces

f. Steering System Lag in Response Due to I_w, K_{SCF}

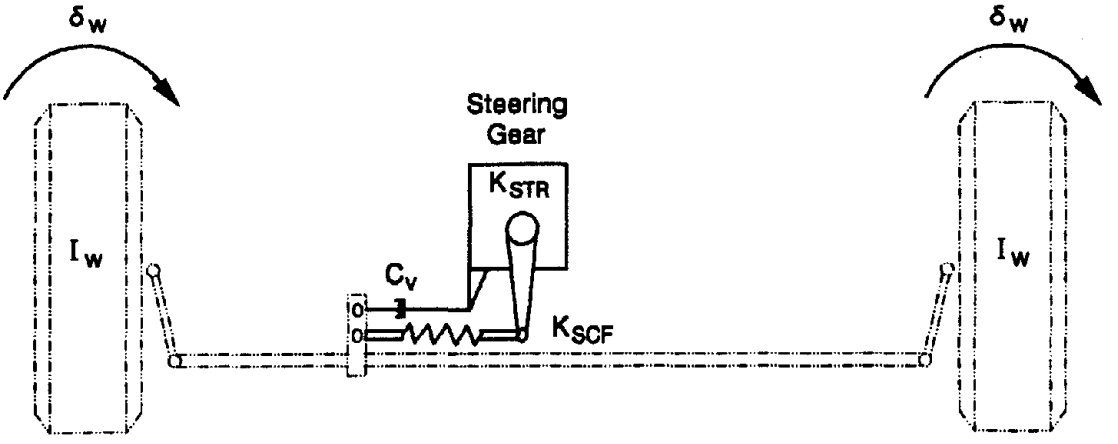

Figure A-22. Simplified Steering System

K_{SCF} = Steer gear compliance
K_{STR} = Steer gear ratio
C_v = Steering system damping

The transient dynamic moment equation for steering motions can be expressed as:

$$2\ I_w \ddot{\delta}_w = \left(\frac{\delta_{SW}}{K_{STR}} + \begin{bmatrix}\text{ROLL}\\ \text{STEER}\end{bmatrix} - \delta_W\right)\frac{1}{K_{SCF}} - C_v\dot{\delta}_w + \begin{pmatrix}\text{STEER}\\ \text{MOMENTS}\\ \text{FROM TIRES}\end{pmatrix}$$

Taking the Laplace transform:

$$\delta_W = \frac{\frac{\delta_{sw}}{K_{STR}} + \begin{pmatrix}\text{ROLL}\\ \text{STEER}\end{pmatrix} + \begin{pmatrix}\text{STEER}\\ \text{MOMENTS}\end{pmatrix}(K_{SCF})}{2\ I_w K_{SCF} S^2 + C_v K_{SCF} S + 1}$$

Thus, the steering system lag is a second order system,

where, $\omega_m = \dfrac{1}{\sqrt{2\ I_w K_{SCF}}}$ and $\zeta = C_v\sqrt{\dfrac{K_{SCF}}{8\ I_w}}$

Combining all these effects into the steering equations:

$$\delta_{w_F} = \frac{\left\{\begin{array}{c} \dfrac{\delta_{SW}}{K_{STR}} + \dfrac{K_{SAF}}{L_F}\left[h_F + \left(\dfrac{Z_{SLF} + Z_{SRF}}{2}\right)\right](\phi_s - \phi_{uF}) \\ +\left[M_{z_{LF}} + M_{z_{RF}} + F_{xN_{LF}}\left(L_{SO} - K_{LT}F_{y_{LF}}\right) - F_{xN_{RF}}\left(L_{SO} + K_{LT}F_{y_{RF}}\right)\right]K_{SCF} \end{array}\right\}}{\dfrac{S^2}{\omega_n^2} + \dfrac{2\zeta S}{\omega_n} + 1} \quad \text{(A-42)}$$

$$\delta_{w_R} = \delta_{SWB} + \frac{K_{SAR}}{L_R}\left(h_R + \frac{[z_{SLR} + z_{SRR}]}{2}\right)(\phi_S - \phi_{UR}) + \left(M_{Z_{LR}} + M_{Z_{RR}}\right)K_{SCR} \quad \text{(A-43)}$$

$$\begin{aligned} \delta_{w_{LF}} &= \delta_{w_F}\left(1 - K_{ACK}\,\delta_{w_F}\right) + B_F\, z_{SLF} + C_F\, z_{SLF}^2 + F_{y_{LF}}\, K_{CF} \\ \delta_{w_{RF}} &= \delta_{w_F}\left(1 - K_{ACK}\,\delta_{w_F}\right) - B_F\, z_{SRF} - C_F\, z_{SRF}^2 + F_{y_{RF}}\, K_{CF} \\ \delta_{w_{LR}} &= \delta_{w_R} + B_R\, z_{SLR} + C_R\, z_{SLR}^2 + F_{y_{LR}}\, K_{CR} \\ \delta_{w_{RR}} &= \delta_{w_R} - B_R\, z_{SRR} - C_R\, z_{SRR}^2 + F_{y_{RR}}\, K_{CR} \end{aligned} \quad \text{(A-44)}$$

For independent suspensions, set B_j, C_j values, and set K_{SAj} = zero.

For solid axle suspensions, set K_{SAj}, h_j, L_j values and set B_j, C_j = zero.

I. TIRE FORCES

The tire model described in Appendix E requires four independent inputs: normal load, longitudinal slip, lateral slip angle, and camber angle. The computation of camber angle is described above in section H. The computation of tire normal loads as discussed below. The generation of the longitudinal and lateral slip variables is also described below, including the computation of the tire lateral relaxation time constant which delays tire side forces relative to the side slip input.

1. Vertical (normal) Tire Loads

Tire load, defined perpendicular to the road surface, depends on compression of the tire casing and its spring stiffness (see Figure A-23).

$$\begin{aligned}
\Delta z_{ij} &= \left(z_{Uj} + RR_j\left[\cos\phi_{Uj} - 1\right] \pm \frac{T_j}{2}\sin\phi_{Uj} - h_{T_{Lj}} \right) \\
\Delta \dot{z}_{ij} &= \left(\dot{z}_{Uj} - \dot{\phi}_{Uj}\left(\frac{T_j}{2}\cos\phi_{Uj} \pm RR_j \sin\phi_{Uj} \right) - \dot{h}_{T_{Lj}} \right) \\
F_{Zij} &= F_{Zij_0} + \Delta z_{ij} K_{ZT_{ij}} + \Delta \dot{z}_{ij} K_{DZT_{ij}}
\end{aligned} \tag{A-45}$$

$$\begin{aligned}
F_{ZLF} &= F_{ZLF_0} + \left(z_{UF} + RR_F\left[\cos\phi_{UF} - 1\right] - \frac{T_F}{2}\sin\phi_{UF} - h_{T_{LF}} \right) K_{ZT_{LF}} \\
&\quad + \left(\dot{z}_{UF} - \dot{\phi}_{UF}\left(\frac{T_F}{2}\cos\phi_{UF} + RR_F \sin\phi_{UF} \right) - \dot{h}_{T_{LF}} \right) K_{DZT_{LF}}
\end{aligned} \tag{A-46}$$

$$\begin{aligned}
F_{ZRF} &= F_{ZRF_0} + \left(z_{UF} + RR_F\left[\cos\phi_{UF} - 1\right] + \frac{T_F}{2}\sin\phi_{UF} - h_{T_{RF}} \right) K_{ZT_{RF}} \\
&\quad + \left(\dot{z}_{UF} + \dot{\phi}_{UF}\left(\frac{T_F}{2}\cos\phi_{UF} - RR_F \sin\phi_{UF} \right) - \dot{h}_{T_{RF}} \right) K_{DZT_{RF}}
\end{aligned} \tag{A-47}$$

$$\begin{aligned}
F_{ZLR} &= F_{ZLR_0} + \left(z_{UR} + RR_R\left[\cos\phi_{UR} - 1\right] - \frac{T_R}{2}\sin\phi_{UR} - h_{T_{LR}} \right) K_{ZT_{LR}} \\
&\quad + \left(\dot{z}_{UR} - \dot{\phi}_{UR}\left(\frac{T_R}{2}\cos\phi_{UR} + RR_R \sin\phi_{UR} \right) - \dot{h}_{T_{LR}} \right) K_{DZT_{LR}}
\end{aligned} \tag{A-48}$$

$$\begin{aligned}
F_{ZRR} &= F_{ZRR_0} + \left(z_{UR} + RR_R\left[\cos\phi_{UR} - 1\right] + \frac{T_R}{2}\sin\phi_{UR} - h_{T_{RR}} \right) K_{ZT_{RR}} \\
&\quad + \left(\dot{z}_{UR} + \dot{\phi}_{UR}\left(\frac{T_R}{2}\cos\phi_{UR} - RR_R \sin\phi_{UR} \right) - \dot{h}_{T_{RR}} \right) K_{DZT_{RR}}
\end{aligned} \tag{A-49}$$

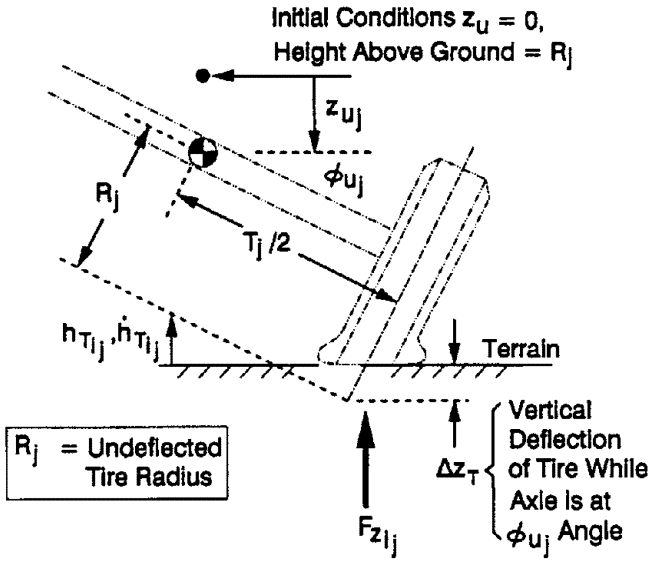

Figure A-23. Tire Vertical Deflection Characteristics

To prevent tire normal load from going negative, the following logic evaluation is performed at each time step after the computation of tire normal load for each wheel:

$$\begin{aligned} &if \quad F_{Zij} < 0 \quad then \\ &\qquad F_{Zij} = 0 \\ &end\,if \end{aligned} \tag{A-50}$$

2. Tire Side Slip and Side Force Lag

First order differential equations are used to model tire slip angle as proposed by Bernard (Refs. A.4 and A.5). Bernard's model in terms of $\tan(\alpha_{ij})$ is:

$$\frac{d}{dt}\left(\tan\alpha'_{ij}\right) + \frac{|u_{ij}|}{K_{TLij}}\tan\alpha'_{ij} = \frac{v_{ij}}{K_{TLij}} \tag{A-51}$$

Where u_{ij} is the longitudinal tire contact patch velocity, v_{ij} is the lateral tire contact patch velocity, and K_{TLij} is the tire relaxation length. The longitudinal and lateral contact patch velocities for each tire are given by:

$$\begin{aligned} V_{TERM_F} &= v + a\dot{\psi} - \dot{\phi}_{uF}\left(R_F - z_{uF} + 0.5\left(h_{T_{LF}} + h_{T_{RF}}\right)\right) \\ V_{TERM_R} &= v - b\dot{\psi} - \dot{\phi}_{uR}\left(R_R - z_{uR} + 0.5\left(h_{T_{LR}} + h_{T_{RR}}\right)\right) \end{aligned} \tag{A-52}$$

$$u_{LF} = \left(u + \dot{\psi}\frac{T_F}{2}\right)\cos\left(\delta_{W_{LF}}\right) + V_{TERM_F}\sin\left(\delta_{W_{LF}}\right)$$
$$v_{LF} = -\left(u + \dot{\psi}\frac{T_F}{2}\right)\sin\left(\delta_{W_{LF}}\right) + V_{TERM_F}\cos\left(\delta_{W_{LF}}\right) \quad \text{(A-53)}$$

$$u_{RF} = \left(u - \dot{\psi}\frac{T_F}{2}\right)\cos\left(\delta_{W_{RF}}\right) + V_{TERM_F}\sin\left(\delta_{W_{RF}}\right)$$
$$v_{RF} = -\left(u - \dot{\psi}\frac{T_F}{2}\right)\sin\left(\delta_{W_{RF}}\right) + V_{TERM_F}\cos\left(\delta_{W_{RF}}\right) \quad \text{(A-54)}$$

$$u_{LR} = \left(u + \dot{\psi}\frac{T_R}{2}\right)\cos\left(\delta_{W_{LR}}\right) + V_{TERM_R}\sin\left(\delta_{W_{LR}}\right)$$
$$v_{LR} = -\left(u + \dot{\psi}\frac{T_R}{2}\right)\sin\left(\delta_{W_{LR}}\right) + V_{TERM_R}\cos\left(\delta_{W_{LR}}\right) \quad \text{(A-55)}$$

$$u_{RR} = \left(u - \dot{\psi}\frac{T_R}{2}\right)\cos\left(\delta_{W_{RR}}\right) + V_{TERM_R}\sin\left(\delta_{W_{RR}}\right)$$
$$v_{RR} = -\left(u - \dot{\psi}\frac{T_R}{2}\right)\sin\left(\delta_{W_{RR}}\right) + V_{TERM_R}\cos\left(\delta_{W_{RR}}\right) \quad \text{(A-56)}$$

α_{ij} is now computed by integrating Equation (A-45), to get tan(α_{ij}), and taking the inverse tangent. This formulation of slip angle adds a first order lag to both tire lateral force and aligning moment, with characteristic distance K_{TLij}. It also removes the longitudinal velocity from the denominator, thus avoiding the conventional slip angle model which overflows at low vehicle speeds. Along with the zero speed logic described by Bernard (Ref. A.5), VDANL is now stable at zero speed, and can start/stop on sloped roads.

Lateral acceleration at the longitudinal cg is defined at the unsprung mass so that the computed motions are directly usable in defining side slip at the tires, without having to correct for sprung mass roll motions.

$$a_{y_U} = \dot{v} + u\dot{\psi} \quad \text{(A-57)}$$

which is used to solve for v

where, at the longitudinal cg

$$a_{y_U} = a_{y_S} - \varepsilon\left(\cos\phi_s\right)\ddot{\phi}_s \quad \text{(A-58)}$$

ε = vertical distance between the M_s cg and the roll axis.

This ε normally $= h_s - \frac{b}{\ell}(h_{RAF}) - \frac{a}{\ell}(h_{RAR})$

However, the h_{RAj} parameter is not used (set = 0) for independent suspensions in order to model squat/lift effects.

For independent suspensions $h_{RAj} = K_{SLj}\left(\frac{T_j}{2}\right)$

Therefore, compute ε using $h_{RAj} = K_{SLj}\left(\frac{T_j}{2}\right)$ for ind. susp. $= h_{RAj}$ for solid susp.

3. Tire Longitudinal Slip and Wheel Spin Mode

Wheel spin dynamics are simulated in order to compute longitudinal slip ratio. Wheel rotational speed and longitudinal tire slip are modeled as first order differential equations as proposed by Bernard (Refs. A.4 and A.5). In Figure A-24 angular acceleration of the wheel (ω) is proportional to the sum of the applied braking, engine and road torques:

$$I_{yw_{ij}}\dot{\omega}_{ij} = -R_j \cdot F_{x_{ij}} + T_{B_{ij}} + T_{E_{ij}} \tag{A-59}$$

The differential equation for longitudinal tire slip is:

$$\dot{S}_{ij} + \frac{|u_{ij}|}{\sigma_{x_{ij}}} S_{ij} = \frac{|u_{ij}| - R_j\omega_{ij}sign(u_{ij})}{\sigma_{x_{ij}}} \tag{A-60}$$

Where S_{ij} is the longitudinal slip ratio, σ_{xij} is the first order longitudinal time constant. Reference A.5 provides a detailed description of the solution methods for equations (A-59) and (A-60). Like the differential equation for slip angle, this formulation removes the tire longitudinal velocity from the denominator, and with the addition of zero speed logic described in Ref. A.5) is stable at zero vehicle speed. The tire model formulation does not allow the absolute value of longitudinal slip to reach a value of one. This is prevented within the simulation using the following logic evaluation:

$$
\begin{aligned}
&\textit{if} \quad |S_{ij}| \geq 1 \quad \textit{then} \\
&\qquad S_{ij} = 0.99 \cdot sign(S_{ij}) \\
&\textit{end if}
\end{aligned}
\tag{A-61}
$$

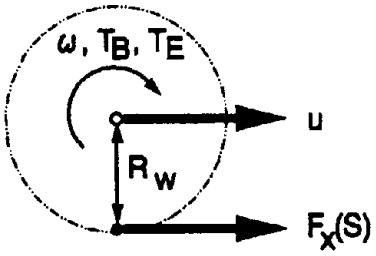

Figure A-24. Wheel Spin Mode

J. COMPLIANT PIN JOINTS BETEEEN M_s and M_u

To avoid computational instabilities, the F_{RAF}, F_{RAR} forces acting at the roll axis between M_s and M_{ui} will be passed through compliant pin joints as illustrated in Figure A-25. This is also true in real cars, as the lateral positioning members in the suspension have rubber cushioning pivot bushings.

This means that the F_{RAF}, F_{RAR} forces will be computed as follows, if ϕ_s = zero.

$$F_{RAj} = \left(y_{u_j} - y_{s_j}\right) K_{RAS} + \left(\dot{y}_{u_j} - \dot{y}_{s_j}\right) K_{RAD} \tag{A-62}$$

where
$$\begin{aligned} y_{u_j} &= \int \dot{y}_{u_j} \quad y_{s_j} = \int \dot{y}_{s_j} \\ \dot{y}_{u_j} &= \int A_{y_{Uj}} \\ \dot{y}_{s_F} &= \int\left(A_{y_s} + a\ddot{\psi}\right) \\ \dot{y}_{s_R} &= \int\left(A_{y_s} - b\ddot{\psi}\right) \end{aligned}$$

$$\Delta_j = \left(\Delta z_j \tan\phi_s - \Delta y_j\right)\cos\phi_s - \left(h_{RAj} - R_j\right)\sin\Delta\phi_j \tag{A-63}$$

where
$$\begin{aligned} \Delta\phi_j &= \phi_s - \phi_{uj} \\ \Delta y_j &= y_s - y_{uj} \\ \Delta z_j &= h_s - R_j + z_{uj} - z_s \end{aligned}$$

$$\begin{aligned} \dot{\Delta}_j = {} & \left[\Delta z_j \cos\phi_s + \Delta y_j \sin\phi_s\right]\dot{\phi}_s + \dot{\Delta} z_j \sin\phi_s \\ & - \dot{\Delta} y_j \cos\phi_s - \left(h_{RA_j} - R_j\right)\cos\Delta\phi_j\left(\dot{\Delta}\phi_j\right) \end{aligned} \tag{A-64}$$

$$F_{RAj} = \Delta_j K_{RAS} + \dot{\Delta}_j K_{RAD} \tag{A-65}$$

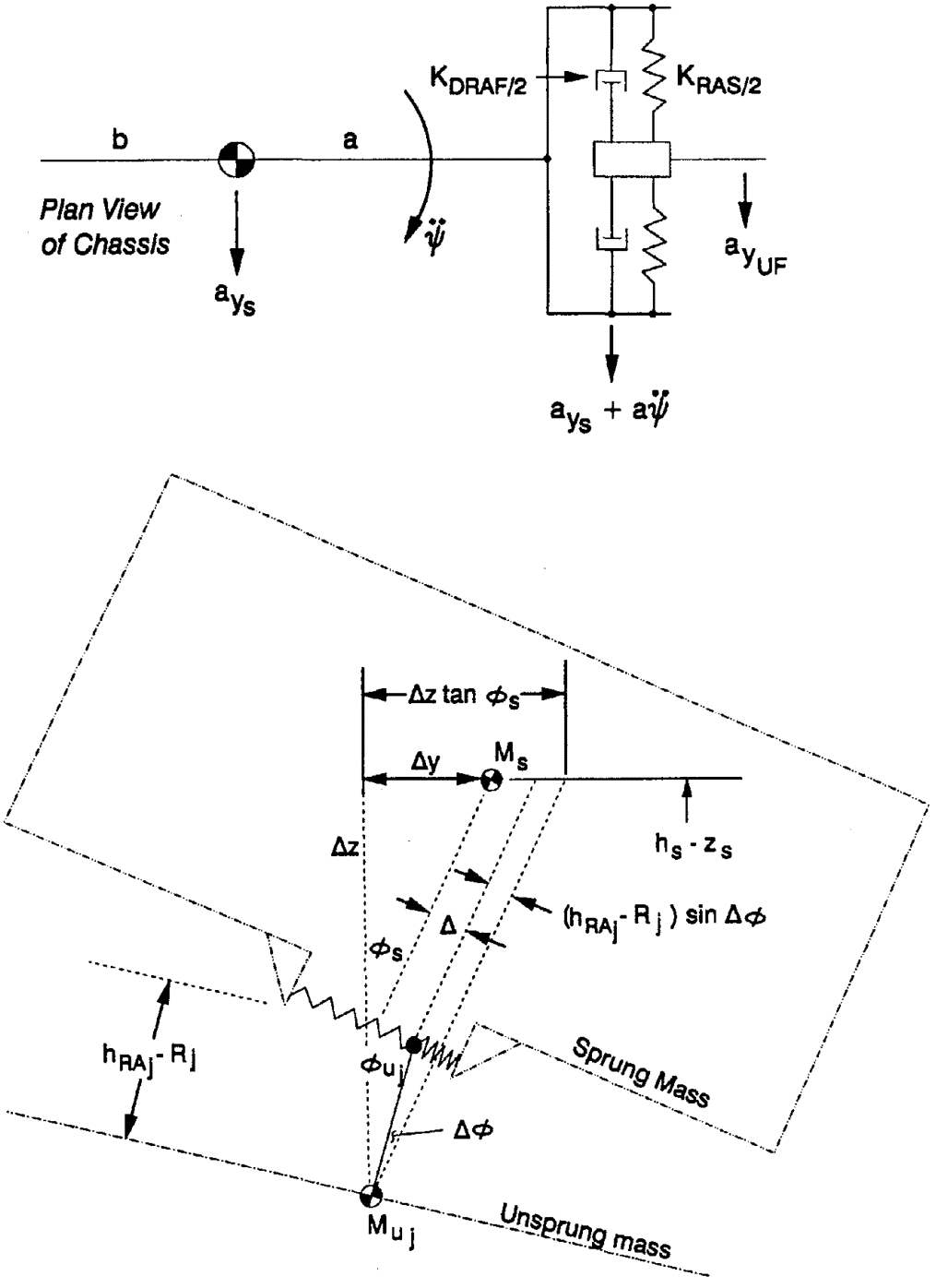

Figure A-25. Compliant Pin Joints Connecting Unsprung and Sprung Masses

K. INITIAL CONDITIONS

To avoid startup transients in simulation, the initial loads on the tires and in the suspension have to be set in at the startup.

Initial conditions for suspension loads F_{Sij_o}

$$\begin{aligned} F_{SLF_0} &= F_{SRF_0} = \frac{M_s g\left(b - \sin(\theta)\right) + F_{Z_{HITCHI}}(d-b)}{2\ell} \\ F_{SLR_0} &= F_{SRR_0} = \frac{M_s g\left(a + \sin(\theta)\right) + F_{Z_{HITCHI}}(d+a)}{2\ell} \end{aligned} \tag{A-66}$$

For tire F_z forces

$$\begin{aligned} F_{ZLF_0} &= F_{ZRF_0} = F_{SLF_0} + \frac{M_{UF}\, g}{2} \\ F_{ZLR_0} &= F_{ZRR_0} = F_{SLR_0} + \frac{M_{UR}^2\, g}{2} \end{aligned} \tag{A-67}$$

For wheel rotational velocity

$$\dot{\omega}_{ij} = \frac{u_{initial}}{RR_j} \tag{A-68}$$

L. TRAILER HITCH MODELING

Hitch forces between the tractor and trailer in the X, Y, and Z directions are transmitted through a spring/damper. The velocities of the hitch point on the tow vehicle and the trailer are computed in the global coordinate system. For the tow vehicle:

$$\begin{aligned} V_X &= u + \dot{\theta}\, H_H \cos(\theta) + d\dot{\theta}\sin(\theta) \\ V_Y &= v - d\dot{\psi} \\ V_Z &= \dot{z}_S + d\dot{\theta}\cos(\theta) - \dot{\theta}\, H_H \sin(\theta) \end{aligned} \tag{A-69}$$

For the trailer:

$$\begin{aligned} T_X &= u^T + \dot{\theta}^T\, {H_H}^T \cos(\theta^T) - e\dot{\theta}^T \sin(\theta^T) \\ T_Y &= v^T + e\dot{\psi}^T \\ T_Z &= \dot{z}_S{}^T - e\dot{\theta}^T \cos(\theta^T) + \dot{\theta}^T {H_H}^T \sin(\theta^T) \end{aligned} \tag{A-70}$$

Where the superscript symbol, ^{T}, denotes trailer variables. The articulation angle about the body Z axis between the tow vehicle and the trailer is computed by:

$$\eta = \psi - \psi^T \tag{A-71}$$

The relative velocities in each direction are compute from:

$$\begin{aligned}
\Delta V_X &= V_X - \left(V_X{}^T \cos(\eta) + V_Y{}^T \sin(\eta)\right) \\
\Delta V_Y &= V_Y - \left(-V_X{}^T \sin(\eta) + V_Y{}^T \cos(\eta)\right) \\
\Delta V_Z &= V_Z - V_Z{}^T
\end{aligned} \tag{A-72}$$

The relative hitch velocities are integrated to compute relative hitch deflections $\Delta x, \Delta y$, and Δz. Hitch force reaction on the tow vehicle is computed form:

$$\begin{aligned}
F_{x_{HITCH}} &= -\Delta_X K_{HITCH} - \Delta V_X C_{HITCH} \\
F_{y_{HITCH}} &= -\Delta_Y K_{HITCH} - \Delta V_Y C_{HITCH} \\
F_{z_{HITCH}} &= \Delta_Z K_{HITCH} + \Delta V_Z C_{HITCH} + F_{z_{HITCH}}
\end{aligned} \tag{A-73}$$

And the reaction on the trailer:

$$\begin{aligned}
F^T_{x_{HITCH}} &= -\left(F_{x_{HITCH}} \cos(\eta) - F_{y_{HITCH}} \sin(\eta)\right) \\
F^T_{y_{HITCH}} &= -\left(F_{x_{HITCH}} \sin(\eta) + F_{y_{HITCH}} \cos(\eta)\right) \\
F^T_{z_{HITCH}} &= -F_{z_{HITCH}}
\end{aligned} \tag{A-74}$$

For tractor semi-trailer vehicles, a fifth wheel hitch is used. The derivation of the fifth wheel kinematics and force transmission follows. The fifth wheel connection between the tractor and the semi-trailer provides the kinematic link between the two chassis, and transfers all forces and moments between them. The fifth wheel constrains the translational motion between the tractor and trailer in the horizontal plane and in the vertical direction. Yaw motion between the tractor and trailer is unconstrained. The constraints about the roll and pitch axis are more complex. The fifth wheel pitch axis is fixed to the tractor frame, so the tractor is always free to pitch. The tractor is constrained in roll by the fifth wheel, relative to the trailer, however the relative roll angle of this constraint is dependent on the articulation angle between the tractor and trailer. For the trailer, at zero articulation angle, its roll motion is

constrained relative to the tractor, while its pitch motion is unconstrained. When the articulation angle is ninety degrees, the trailer's roll motion is unconstrained (the trailers X-axis is now parallel to the pitch axis of the fifth wheel), and its pitch axis in constrained by the fifth wheel relative to the roll angle of the tractor. All of the fifth wheel constraints between the tractor and trailer have some stiffness, and will be modeled as linear springs. Nonlinearities such as non-linear stiffness, lash, and Coulomb friction will not be included in the fifth wheel model.

The kinematics of the tractor and trailer relative to each other and the global coordinate system are shown in Figure A-26 in the pitch plane, Figure A-27 in the yaw plane, and Figure A-28 in the roll plane. The subscript "G" is used to denote the global coordinate system, the subscript "V" is used to denote the coordinate system attached to the tractor chassis, and the subscript "T" is used to denote the coordinate system attached to the trailer chassis. The yaw angle between the tractor's x-axis and the global x-axis is denoted by "ψ", and for the trailer, the yaw angle is denoted by "V^T". The pitch angle between the tractor's x-axis and the global x-axis is denoted by "θ_s", and for the trailer, the pitch angle is denoted by "$\theta_s{}^T$". The roll angle between the tractor's y-axis and the global y-axis is denoted by "ϕ_s", and for the trailer, the roll angle is denoted by "$\phi_s{}^T$".

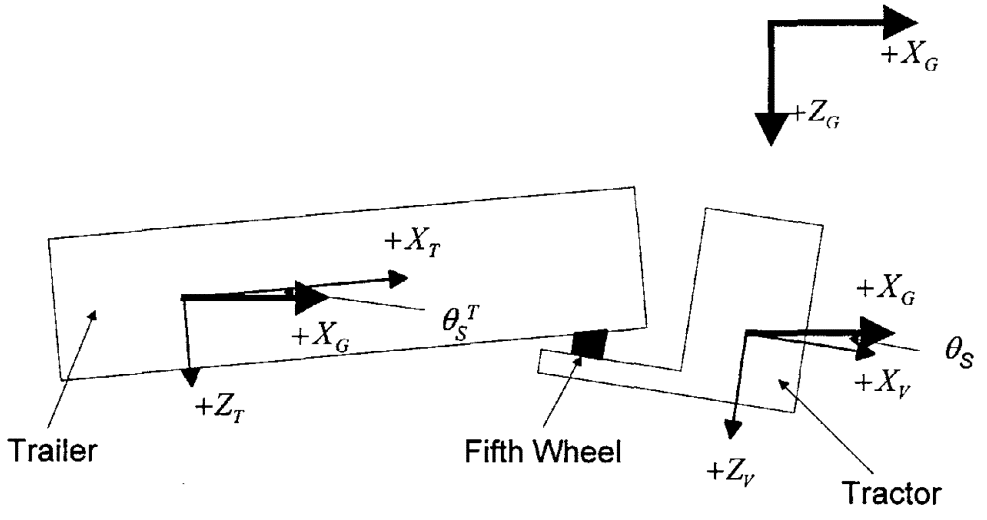

Figure A-26. Pitch Plane Diagram of Tractor/Semi-Trailer

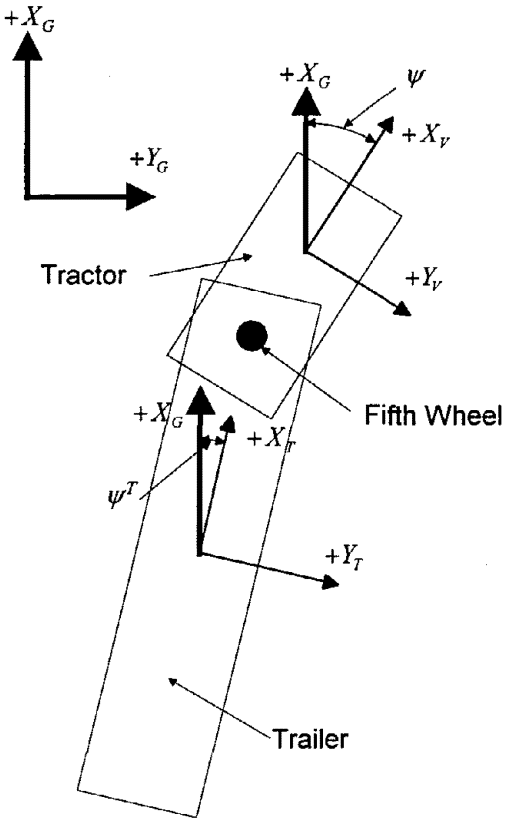

Figure A-27. Yaw Plane Diagram of Tractor/Semi-Trailer

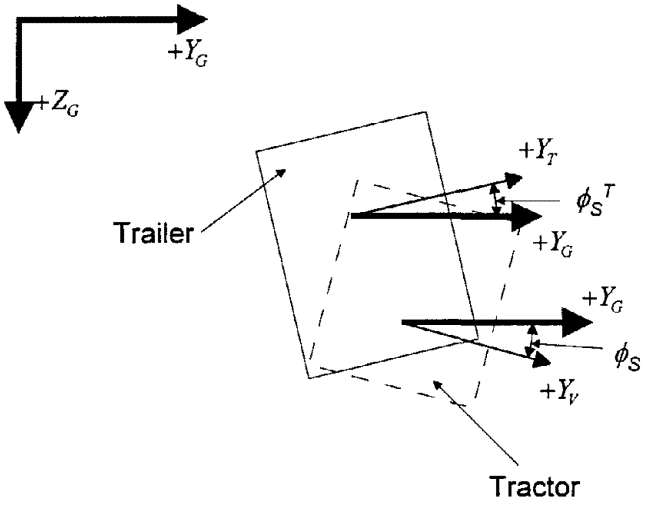

Figure A-28. Roll Plane Diagram of Tractor/Semi-Trailer

The pitch/roll kinematics of the fifth wheel can now be derived. The measured torsional stiffness of the fifth wheel about the tractor's x-axis at zero articulation angle ($\psi - \psi^T = 0$) will be denoted by KT_{FIFTH}. For the tractor, the roll angle between the tractor and the trailer is given by:

$$\phi_{FIFTH} = (\phi_S - \phi_S^T)\cos(\psi - \psi^T) + (\phi_S + \theta_S^T)\sin(\psi - \psi^T) \tag{A-75}$$

This equation says that at zero articulation angle, the roll angle between the tractor and the trailer is the difference between their roll angles. When the articulation angle reaches 90 degrees, the trailer's pitch angle becomes oriented in the roll direction of the tractor, so the roll angle between the tractor and the trailer (as seen by the tractor) is the difference between the tractor's roll angle, and the trailer's pitch angle. Since the orientation of the fifth wheel relative to the tractor remains constant, it will be assumed that the torsional stiffness of the fifth wheel will remain constant. The roll moment applied to the tractor by the fifth wheel is:

$$M_{xFIFTH} = -KT_{FIFTH} \cdot \phi_{FIFTH} \tag{A-76}$$

The pitching moment applied to the tractor by the fifth wheel is always zero since the fifth wheel's pitch axis is fixed to the tractor.

For the trailer, the roll angle of the fifth wheel between the tractor and the trailer will be slightly different, and is given by:

$$\phi_{FIFTH}^T = (\phi_S - \phi_S^T)\cos(\psi - \psi^T) + (\phi_S^T - \theta_S)\sin(\psi - \psi^T) \tag{A-77}$$

Torsional twisting of the fifth wheel can apply both roll and pitch moments to the trailer. The roll moment applied to the trailer is:

$$M_{xFIFTH}^T = KT_{FIFTH} \cdot \phi_{FIFTH}^T \cdot \cos(\psi - \psi^T) \tag{A-78}$$

The pitching moment applied to the trailer is:

$$M_{yFIFTH}^T = KT_{FIFTH} \cdot \phi_{FIFTH}^T \cdot \sin(\psi - \psi^T) \tag{A-79}$$

M. BRAKE SYSTEM MODEL

A schematic of the hydraulic brake system model is shown in Figure A-29. Brake pedal force is the input to a bi-linear vacuum booster. The booster has a limiting point above which the brake system acts

like a manual brake system. The output of the booster is front brake line pressure. For the front axle, this pressure is multiplied by the front brake effectiveness to compute front brake torque. For the rear axle, a bi-linear proportioning valve is used to reduce the rear brake line pressure (Figure A-29). The equations are shown below.

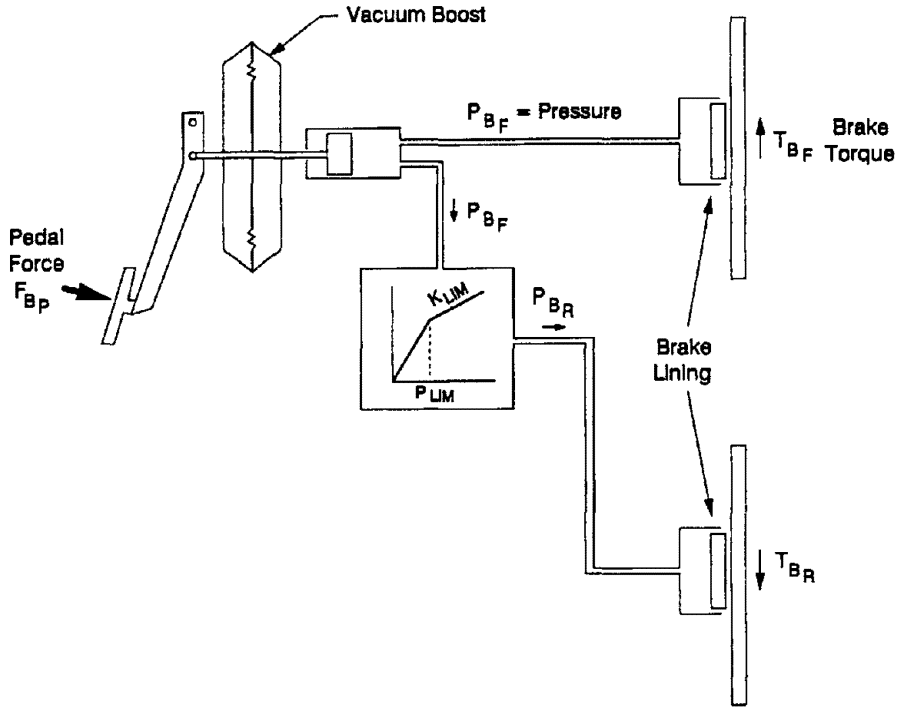

Figure A-29. Brake System Model

$$P_{LIM} = \frac{R_F\, F_{XLIM}}{2\, K_{BTF}}$$

$$K_{BTR} = K_{BTF}\, K_1$$

$$K_{LIM} = \frac{K_2}{K_1}$$

$$P_{B_F} = f\left(F_{B_P},\ \text{Lever Ratio},\ \text{Vac Boost},\ \text{Mast. Cyl Pist Diam}\right)$$

$$P_{B_F} = K_{VB}\, F_{BP},\ \text{for } F_{BP} \le F_{BPVL}$$

$$= K_{VB}\, F_{BPVL} + K_{MB}\left(F_{BP} - F_{BPVL}\right) \quad \text{for } F_{BP} > F_{BPVL}$$

$$P_{B_R} = P_{B_F} \text{for } P_{B_F} \le P_{LIM}$$

$$= P_{LIM} + K_{LIM}\left(P_{B_F} - P_{LIM}\right) \text{for } P_{B_F} > P_{LIM}$$

$$T_{B_F} = [K_{BTF}]P_{B_F}$$
$$T_{B_R} = [K_{BTR}]P_{B_R}$$

For vehicles with an air brake system (heavy trucks) the brake model is somewhat different. The brake proportioning parameters used in the hydraulic brake model to describe the proportioning valve (K_1 and K_2) are used to for the front axle brake effectiveness (K_1) and the drive and trailer axle brake effectiveness (K_2) as shown in Figure A-30.

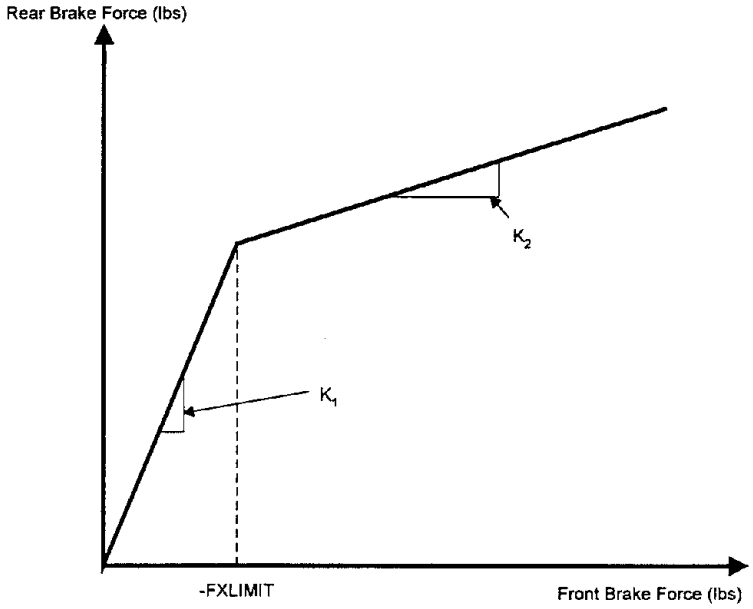

Figure A-30. Truck Brake Proportioning

$T_{B_F} = [K_1]P_{B_F}$ front brake torque torque, per wheel
$T_{B_R} = [K_2]P_{B_R}$ drive brake torque torque, per wheel
$T_{B_T} = [K_2]P_{B_R}$ trailer brake torque torque, per whee

The air brake model also contains a thermal model used to estimate the brake temperatures. The following describes the heavy truck thermal model. Parameter K_{fade} is specified in the trailer parameter file.

In Reference A.6, an energy balance for an individual brake was derived as:

$$m_B C \frac{dT}{dt} = \frac{HP_B - hA_c(T - T_\infty)}{3600} \qquad \text{(A-80)}$$

Where m_B (*lbm*) is the effective mass of the brake system components that can store heat, C (*Btu/lbm-°F*) is the specific heat capacity of the brake components, T (*°F*) is the temperature of the brake components, t (*sec*) is time, HP_B (*Btu/hr*) is the power input into the brakes, h (*Btu/hr-ft²-°F*) is the effective heat transfer coefficient accounting for convection, conduction, and radiant heat transfer, and T_∞ (90 *°F*) is the temperature of the surrounding air. In [A.6], this equation was analytically integrated assuming that HP_B was constant, and using experimental data, the parameters were estimated. The results were:

$$hA_c = 0.1 + 0.00208\overline{V}\left(\frac{hp}{^\circ F}\right) \tag{A-81}$$

$$\frac{hA_c}{m_B C} = 1.23 + 0.0256\overline{V}\left(\frac{1}{hr}\right) \tag{A-82}$$

Where $\overline{V}$ is vehicle longitudinal velocity in mph. Converting these equations to VDANL's units of ft, lbm, and sec, and rearranging terms gives:

$$hA_c = 254.55 + 3.61\,u\left(\frac{Btu}{hr^\circ F}\right) \tag{A-83}$$

$$m_B C = 0.0813\left(\frac{Btu}{^\circ F}\right) \tag{A-84}$$

The power input to the brakes is the brake torque multiplied by the wheel angular velocity given by:

$$HP_{Bj} = T_{Bj}\omega_{ij}\left(\frac{ft \cdot lb}{\sec}\right) = 4.628 T_{Bj}\omega_{ij}\left(\frac{Btu}{hr}\right) \tag{A-85}$$

Where T_B is the brake torque in (*ft-lb*) and ω_{ij} is the wheel angular velocity in (*rad/sec*). If Equation (A-80) is solved for the derivative of temperature as:

$$\frac{dT}{dt} = \frac{\left(HP_B - hA_c(T - T_\infty)\right)m_B C}{3600} \tag{A-86}$$

It can be integrated at each time step to give brake temperature in degrees Fahrenheit. Brake torque, wheel angular velocity, and vehicle longitudinal velocity can be used from the previous simulation time

step. Since the braking system will be modeled using one effectiveness value for the front axle, and one for the rest of the axles, two brake temperatures will have to be computed. This makes the assumption that the wheel angular velocities are not very different from each other (the time constant of the brake temperature is very slow compared to the wheel rotational dynamics).

Temperature affects on brake torque are modeled as a linear function of brake temperature as:

$$T_{Bfade} = T_B\left[1 - K_{fade}(T - T_\infty)\right] \qquad \text{A-87)}$$

Where T_B is the commanded brake torque (air pressure multiplied by effectiveness), T_{Bfade} is the actual brake torque, and K_{fade} *(%/°F)* is the parameter that determines the loss in brake torque due to brake temperature rise. This equation is computed for each axle.

Because of mass, friction, and compressibility affects, vehicle braking systems do not act instantaneously. To model this behavior, first order lags with time constants BRAKLAG(1/2/3) for the brakes on the front (1) and rear (2) axles tractor axles, and the trailer axles (3) are used to model the delay in the brake line pressure versus brake pedal input response. For heavy truck air brake systems, the time lags will get longer as the axle gets farther from the brake pedal.

The basic brake system model and parameters assume that the left and right brake torque on each axle are equal. This assumes an idealized vehicle, which rarely exists. To allow left/right brake torque differences to be modeled, a brake torque multiplier parameter is specified for each wheel. After the brake torque for each wheel is computed using the above models, the final brake torque is modified by:

$$T_{B_{ij}} = T_{B_{ij}} \cdot BRAKMULT_{ij} \qquad \text{(A-88)}$$

If $BRAKMULT_{ij}$ is set to 1, then there is no affect. Setting $BRAKMULT_{ij}$ to 0.5 will reduce the brake torque at that wheel to 50% of its value computed by the brake system model.

N. OTHER DYNAMIC VARIABLES

The sideslip angle of the sprung mass at its cg and its derivative are computed from:

$$\beta = \tan^{-1}\left(\frac{v}{u}\right)$$
$$\dot{\beta} = \tan^{-1}\left(\frac{u\dot{v} - v\dot{u}}{u^2 + v^2}\right) \qquad \text{A-89)}$$

Accelerations measured by an accelerometer attached to chassis Z_{ACC} above the roll axis and X_{ACC} forward of the sprung mass cg:

$$\begin{aligned} A_{y_{MEAS}} &= a_{y_U}\cos(\phi_S) - g_{ys}\sin(\phi_S) + Z_{ACC}\ddot{\phi}_S + X_{ACC}\ddot{\psi} \\ A_x &= \dot{u} - v\dot{\psi} \end{aligned} \tag{A-90}$$

Total vehicle lateral velocity:

$$V_{LAT} = \int\left(a_{y_U} - \dot{\psi}u\right) \tag{A-91}$$

Total lateral load transfer:

$$LOAD_{TRANS} = 100\left[\frac{F_{ZRF} + F_{ZRR} - F_{ZLF} - F_{ZLR}}{F_{ZRF} + F_{ZRR} + F_{ZLF} + F_{ZLR}}\right] \tag{A-92}$$

Trailer off-tracking:

$$Y_{OffTrack} = \left(e + b^T\right)\sin(\eta) \tag{A-93}$$

Longitudinal tire force with rolling drag:

$$\begin{aligned} R_{DRAG_{ij}} &= DRAGC_{ij} \cdot F_{z_{ij}} \\ F_{xN_{ij}} &= F_{x_{ij}} R_{DRAG_{ij}} \end{aligned} \tag{A-94}$$

Where F_{xij} is the longitudinal tire force computed by the tire model, and F_{xNij} is the longitudinal tire force with rolling drag included.

O. POWER AND DRIVE TRAIN MODELS

1. Overview

The power and drive train models include the elements summarized in Figure A-31. Further detail for the engine and transmission is given in Figure A-32. The power produced by the engine and transformed by the transmission is then distributed to the front and/or rear axles as torques and angular velocities as illustrated in Figure A-33. The transmission gearing provides torque and angular velocity to the driveline. For four-wheel drive the torque is split by a center differential to the front and rear axles. For front wheel or rear wheel only drive, and torque is sent to the driven axle. The front and rear differentials can also be set up for limited slip operation. Component descriptions are given below.

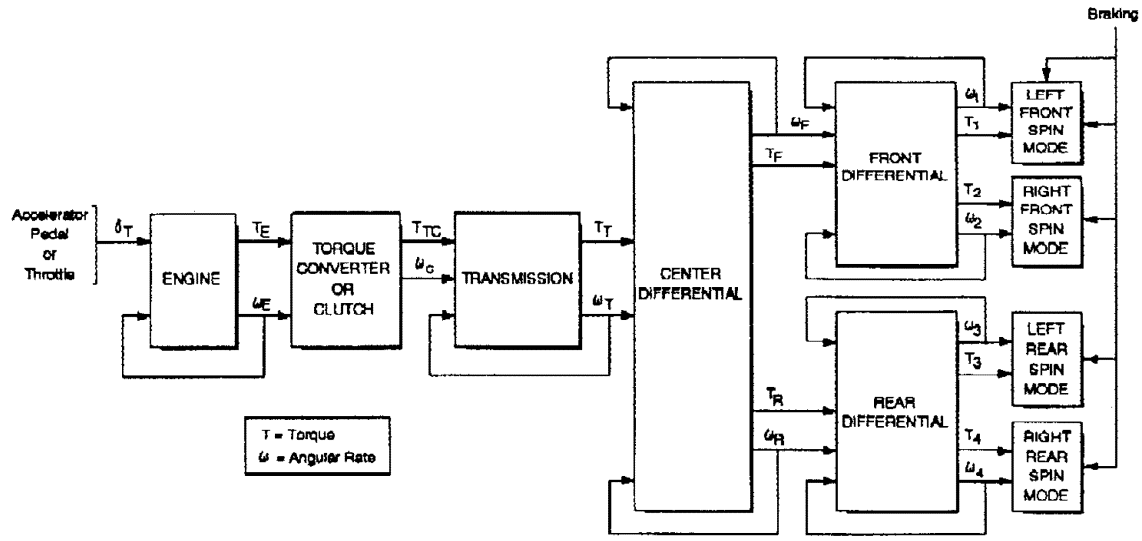

Figure A-31. Power and Drive Train Model

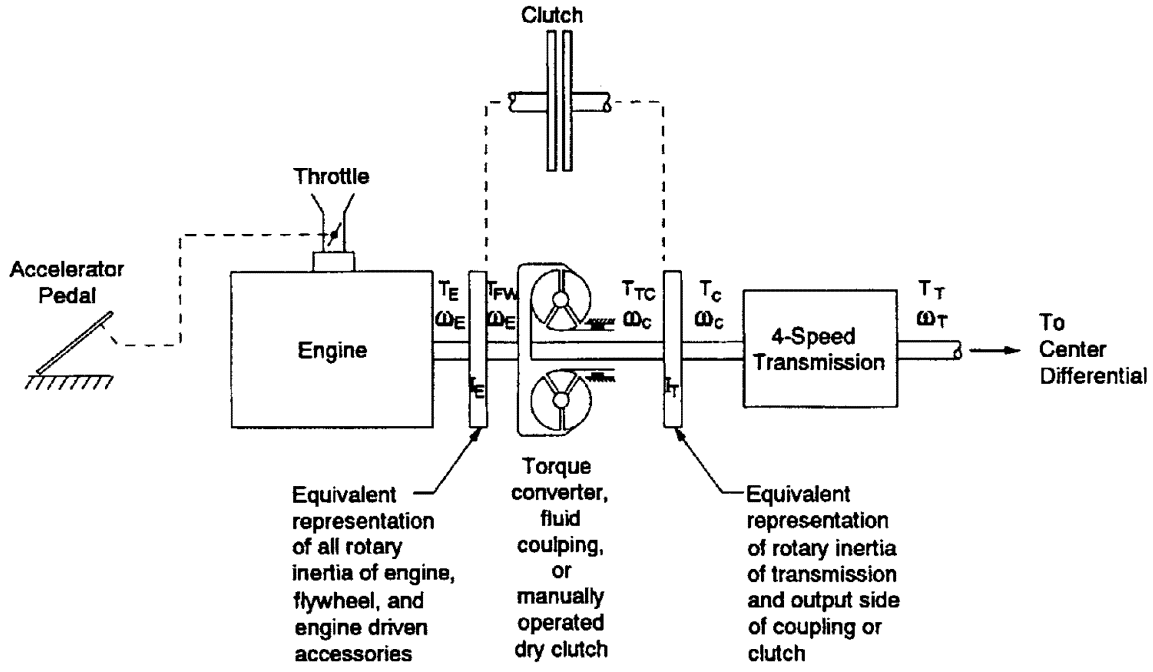

Figure A-32. Engine/Transmission Model

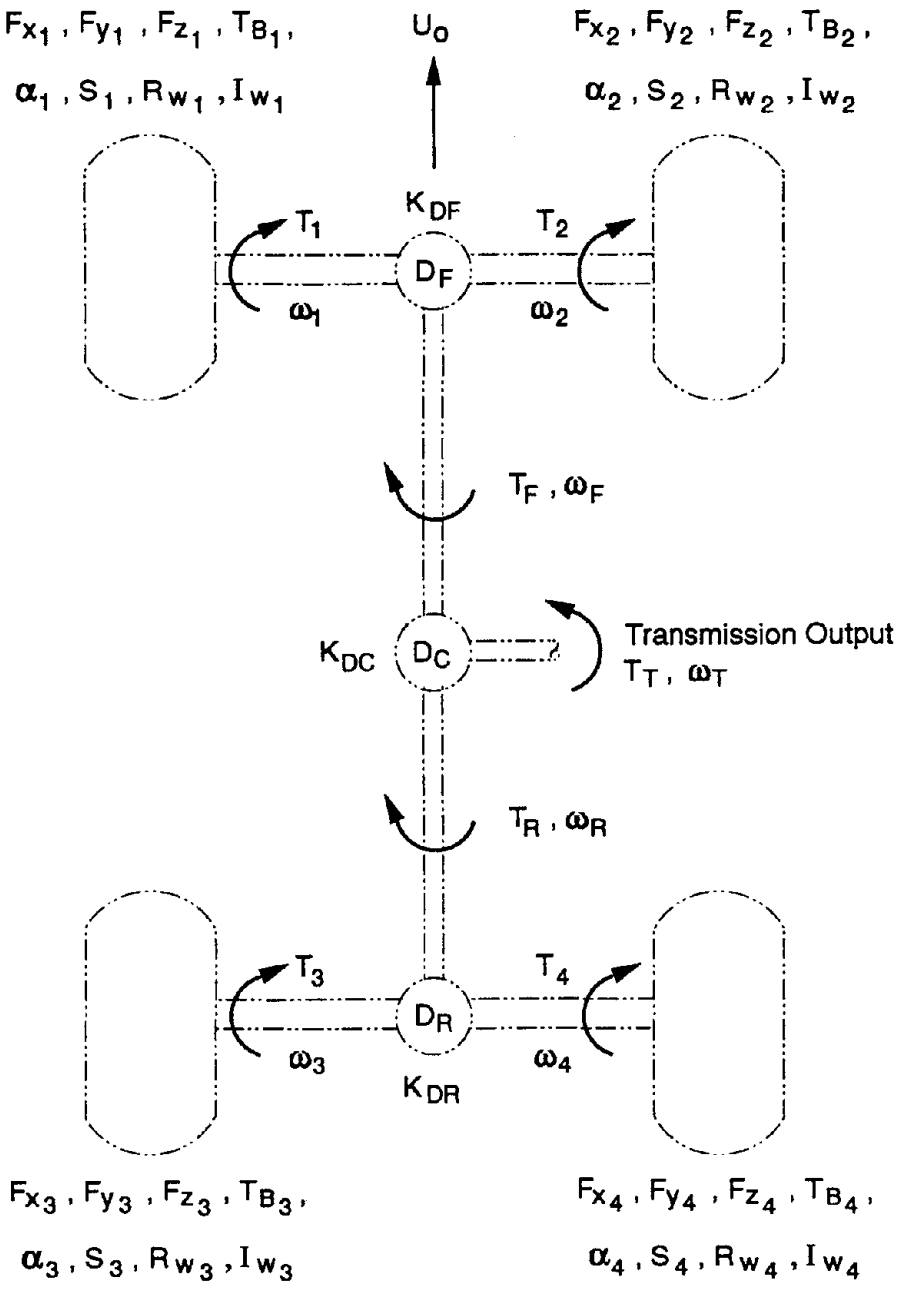

Figure A-33. Forces, Torques and Angular Velocities in Drive Train

2. Engine Power Functions

Maximum engine torque output can be closely modelled by a second order function as shown in Figure A-34, where.

$$T_{E_{\max}} = K_{E_1} + K_{E_2}\omega_E + K_{E_3}\omega_E^2 \tag{A-95}$$

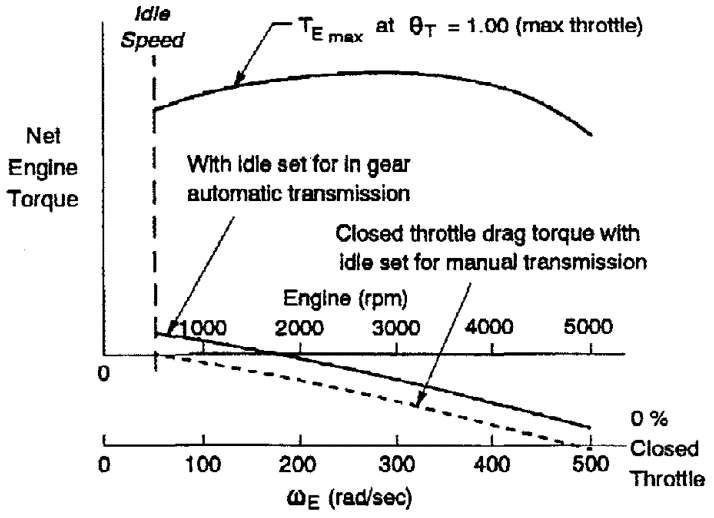

Figure A-34. Maximum Torque at Full and Closed Throttle

However, at closed throttle, there is an increasing negative drag torque as engine speed increases. This is the net internal friction drag, (engine and accessories) and pumping losses (due to throttling) at closed throttle. This is the net drag torque above the condition at idle, so that at idle the net torque is zero. But to cover the condition of an automatic transmission in-gear with a torque load from the converter, the throttle must be opened enough to maintain engine speed with this torque load.

Engine drag torque can be modeled with a similar function as max torque:

$$\text{Engine Drag Torque} = K_{E_4} + K_{E_5}\omega_E + K_{E_6}\omega_E^2 \tag{A-96}$$

Actual torque would then be modulated between this drag torque (minimum) and the maximum torque, according to throttle position θ_T.

$$\begin{aligned} T_E &= \left(T_{E_{\max}} - T_{E_{\text{drag}}}\right)\theta_T + T_{E_{\text{drag}}} \\ T_E &= \left(K_{E_1} + K_{E_2}\omega_E + K_{E_3}\omega_E^2\right)\theta_T + \left(K_{E_4} + K_{E_5}\omega_E + K_{E_6}\omega_E^2\right)\left(1-\theta_T\right) \end{aligned} \tag{A-97}$$

Engine torque then passes through the rotary inertia, such that during acceleration the torque delivered is less than when at constant speed.

$$T_{FW} = T_E - I_E\dot{\omega}_E \tag{A-98}$$

3. Torque Converter Functions

$$\begin{aligned} T_{FW} &= \frac{\omega_E^2}{K_{TC}} \qquad \text{For} \quad \frac{\omega_C}{\omega_E} \le 0.9 \\ T_C &= T_{FW} \qquad \text{For} \quad \frac{\omega_C}{\omega_E} > 0.9 \\ K_{TC} &= \left(K_{TC_o}\right) f\left(\omega_{C/\omega_E}\right) \end{aligned} \tag{A-99}$$

The torque converter function $f(\omega_C / \omega_E)$ is illustrated in Figure A-35, the complete torque Converter equations are as follows

$$\begin{aligned} K_{TC} &= 123\left(1+\tfrac{5}{3}\left[\frac{\omega_C}{\omega_E}\right]^3\right) \\ T_{FW} &= \frac{\omega_E^2}{K_{TC_o}\left(1+\tfrac{5}{3}\left[\frac{\omega_C}{\omega_E}\right]^3\right)} \end{aligned} \tag{A-100}$$

$$\text{with } K_{TC_o} = 123, \qquad \text{For} \frac{\omega_C}{\omega_E} \le 0.90$$

$$\begin{aligned} T_C &= \left[SR_o\left(1-\frac{\omega_C/\omega_E}{0.9}\right)+\frac{\omega_C/\omega_E}{0.9}\right](T_{FW}) \\ \text{with} \quad SR_o &= 2.1, \qquad \text{For} \frac{\omega_C}{\omega_E} \le 0.90 \end{aligned} \tag{A-101}$$

The final equation for the torque converter is when $\omega_C / \omega_E > 0.9$, at which point the stator is free-running (off the over-running clutch) and the impeller and turbine elements are now acting as a simple fluid coupling. The equation for this is;

$$T_{FW} = K_c\left(\frac{\omega_E+\omega_C}{2}\right)^2\left(\frac{\omega_E-\omega_C}{\omega_E}\right) \qquad \text{For} \frac{\omega_C}{\omega_E} > 0.9 \tag{A-102}$$

In order to make for smooth transition between torque converter and fluid coupling operation;

$$T_{FW_{TC}} = T_{FW_{FC}} \text{ at } \frac{\omega_C}{\omega_E} = 0.90$$

$$\frac{\omega_E^2}{K_{TC_o}\left(1+\frac{5}{3}[.9]^3\right)} = K_c\left(\frac{\omega_E+.9\omega_E}{2}\right)^2(1-.9) \qquad \text{(A-103)}$$

$$\text{or } K_c = \frac{5.00}{K_{TC_o}}$$

Note that for coasting down, with engine drag slowing down the vehicle where, $\omega_C / \omega_E > 1.00$, the torque converter functions act only as a simple coupling, (i.e., there is no torque ratio as in engine power application for acceleration).

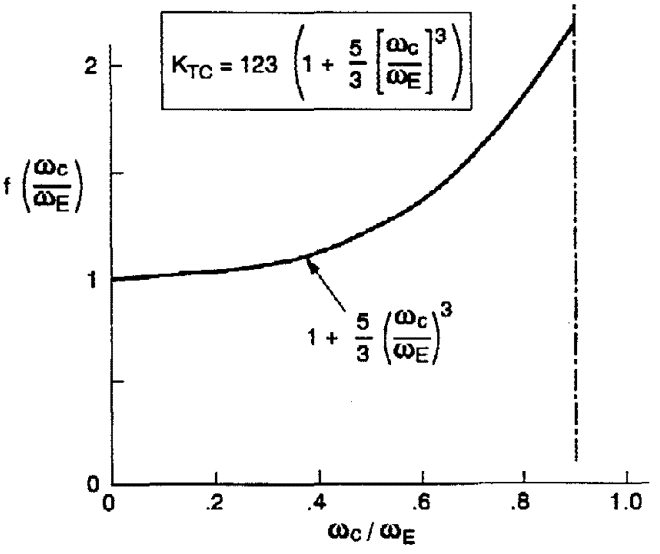

Figure A-35. Torque Converter Function

4. Automatic Transmission

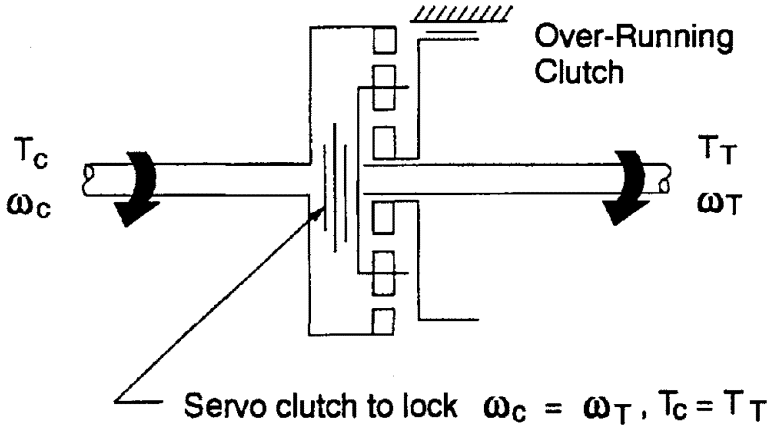

Figure A-36. A Typical Planetary Gear Set

To Lock $\omega_C = \omega_T : T_C = T_T$ Sun Gear Radius - R Planet Gear Radius = r

$$\text{Then Gear Ratio} = \frac{2(R+r)}{R+2r} = \text{Typically about 1.5}$$

The servo clutch will engage direct drive over a Δt time interval, up to the point where the torque reaction at the overrunning clutch goes to zero and it releases as illustrated in Figure A-37.

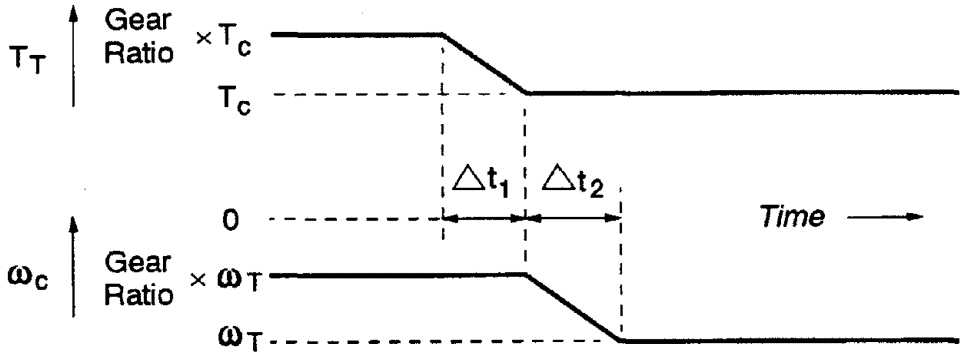

Figure A-37. Torque and Angular Rate Over Time

At the point where the overrunning clutch release ω_c is still $= G.R.x\omega_T$. Thus a further time interval Δt_2 is needed for the servo clutch to bring input speed, ω_c, down to output speed ω_T.

To avoid excessive complications we will have these torque and speed change transitions occur simultaneously, but over a preset time interval as illustrated in Figure A-38.

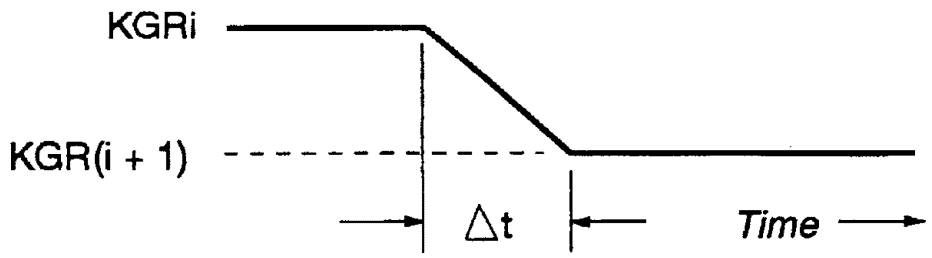

Figure A-38. Gear Ratio Change Over Time

We will allow for up to 10 gear ratios in the transmission.

Each gear ratio is identified by *KGRi* with i =1, ----- to 10.

The Δt time for shift transition is identified by "Shift Time," in seconds.

Thus, in the above example, the gear ratio will change from *KGRi* to the next gear choice $i + 1$, which is *KGR* ($i + 1$,over a Δt time interval.

The input-output relationships are as follows:

A reduction in torque transmitted, due to accelerating rotary inertia of transmission.

$$T_c = T_{TC} - I_T \dot{\omega}_c$$

$$T_T = K_{GRi} T_c \qquad \text{(A-104)}$$

$$\omega_c = K_{GRi} \omega_T$$

The automatic upshifts and downshifts will occur at θ_T (load) and ω_T (speed) control points.

For illustration we will use a 4 speed transmission, with shift points described by the equations A-105 and Figure A-39, and to avoid excessive up and down shift cycling, the downshift points must be lower by a predetermined downshift threshold, "DS."

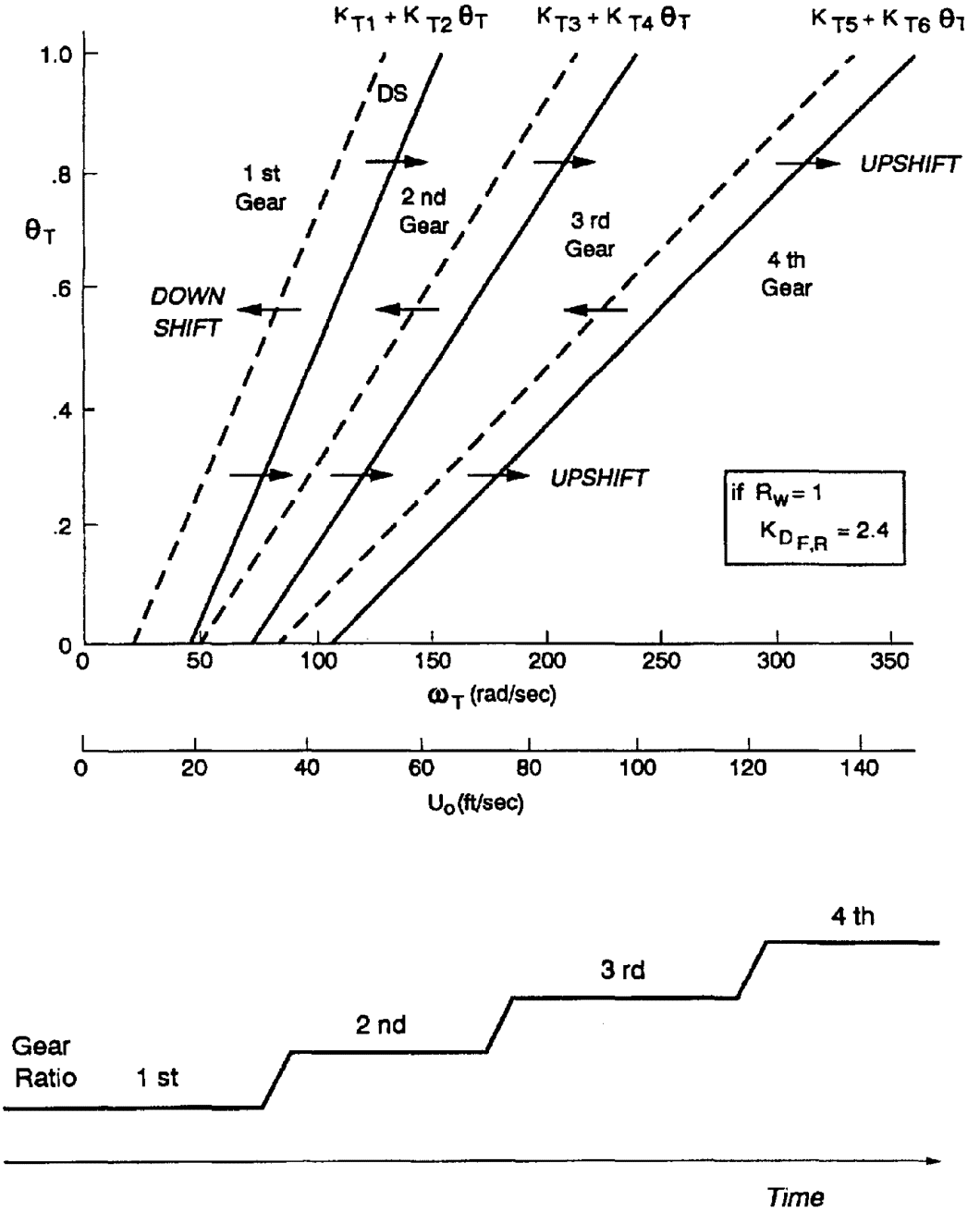

Figure A-39. Shift Sequence and Timing for Example Four Speed Transmission

If in first Gear

Shift up to second gear if,

$$\omega_T > \left(K_{T1}(1) + K_{T2}(1)\theta_T\right)$$

If in Second Gear

If $\omega_T > \left(K_{T1}(2) + K_{T2}(2)\theta_T\right)$, shift up to 3rd gear

If $\omega_T < \left(K_{T1}(1) + K_{T2}(1)\theta_T - DS\right)$, shift down to 1st gear (A-105)

If in Third Gear

If $\omega_T > \left(K_{T1}(3) + K_{T2}(3)\theta_T\right)$, shift up to 4th gear

If $\omega_T < \left(K_{T1}(2) + K_{T2}(2)\theta_T - DS\right)$, shift down to 2nd gear

If in Fourth Gear

If $\omega_T < \left(K_{T1}(3) + K_{T2}(3)\theta_T - DS\right)$, shift down to 3rd gear

For manual shift operation, the fluid coupling would be removed, and the transmission shifts would occur in a sequence in time as specified by a gear shift input file.

P. TABLES OF VARIABLES AND PARAMETERS, WHERE THEY ARE DEFINED, GIVEN A SIGN CONVENTION, AND AXIS SYSTEM

Variables Defined

i = $L_{(left)}$ or $R_{(right)}$: j = $F_{(front)}$, or $R_{(rear)}$: ij = LF, RF, LR, RR : # 1 to 8

Variable	Units	Mnemonic	Definition	Sign Convention For Positive Value	Axis System
L_A	ft-lb	VD.AEROTERML	Aerodynamic Roll Moment	clockwise	body
N_A	ft-lb	VD.AEROTERMN	Aerodynamic Yaw Moment	clockwise	body
X_A	lb	VD.AEROTERMX	Aerodynamic Drag Moment	back	body
Y_A	lb	VD.AEROTERMY	Aerodynamic Side Moment	right	body
A_{yMEAS}	ft/s^2	VD.AYMEAS	Measured lateral acceleration	right	body
a_{yS}	ft/s^2	VD.AYS	Lateral acceleration of m_S	Right	Horizontal to road plane and perpendicular to body centerline
a_{uF}	ft/s^2	VD.AYUF	Lateral acceleration of m_{uF}	Right	Horizontal to road plane and perpendicular to body centerline
a_{uR}	ft/s^2	VD.AYUR	Lateral acceleration of m_{uR}	Right	Horizontal to road plane and perpendicular to body centerline
β	rad	VD.BETA	Sideslip angle of m_S at CG	clockwise	body
$\dot{\beta}$	rad/s	VD.BETADOT	Rate of change of Sideslip angle	clockwise	body
$F_{xCOLLISION}$	lb	VD.COLLISIONFX	External force applied to m_S CG	forward	body
$F_{yCOLLISION}$	lb	VD.COLLISIONFY	External force applied to m_S CG	right	body
$F_{zCOLLISION}$	lb	VD.COLLISIONFZ	External force applied to m_S CG	down	body
$M_{xCOLLISION}$	ft-lb	VD.COLLISIONMP	External moment applied to m_S CG	clockwise	body
$M_{yCOLLISION}$	ft-lb	VD.COLLISIONMQ	External moment applied to m_S CG	clockwise	body
$M_{zCOLLISION}$	ft-lb	VD.COLLISIONMR	External moment applied to m_S CG	clockwise	body
Δ_F	ft	VD.DELYF	Deflection of front pin joint	right	body
Δ_R	ft	VD.DELYR	Deflection of rear pin joint	right	body
$\dot{\Delta}_F$	ft/s	VD.DELYFD	Velocity of front pin joint	right	body
$\dot{\Delta}_R$	ft/s	VD.DELYRD	Velocity of rear pin joint	right	body
δ_{SW}	radians	VD.DSW	Steering wheel angle	clockwise	
δ_{SCR}	radians	VD.DSWB	Steering control input at rear	to the right	
δ_{WF}	radians	VD.DWF	Steer angle of front road wheels without Ackerman or kinematics	clockwise	

Variables Defined

i = $L_{(left)}$ or $R_{(right)}$: j = $F_{(front)}$, or $R_{(rear)}$: ij = LF, RF, LR, RR : # 1 to 8

Variable	Units	Mnemonic	Definition	Sign Convention For Positive Value	Axis System
δ_{WB}	radians	VD.DWB	Steer angle of front road wheels wthout Ackerman or kinematics	clockwise	
ε	ft	VD.EPAR	Vertical distance from Ms CG to roll axis	up	body
F_{BP}	lb	VD.FBP	Brake pedal force input		
F_{BSij}	lb	VD.FBS$_{ij}$	Bump stop force		body
F_{RAj}	lb	VD.FRA$_j$	Pin joint force	right	body
F_{Sij}	lb	VD.FS$_{ij}$	Total suspension force		body
G	ft/s^2	VD.GRAV	Gravity vector	down	world
g_x	ft/s^2	VD.GRAVX	Gravity vector component in body X axis	forward	body
g_{yF}	ft/s^2	VD.GRAVYF	Gravity vector component in front m_{sF} Y axis	right	body
g_{yR}	ft/s^2	VD.GRAVYR	Gravity vector component in rear m_{sF} Y axis	right	body
g_{yS}	ft/s^2	VD.GRAVYS	Gravity vector component in m_s Y axis	right	body
g_{zF}	ft/s^2	VD.GRAVZF	Gravity vector component in front m_{sF} Z axis	down	body
g_{zR}	ft/sec^2	VD.GRAVZR	Gravity vector component in rear m_{sF} Z axis	down	body
g_{zS}	ft/sec^2	VD.GRAVZS	Gravity vector component in m_s Z axis	down	body
H_H	ft	VD.HH	Hitch height	up	body
F_{xHITCH}	lb	VD.HITCHFX	Hitch force along m_s X axis	forward	body
F_{yHITCH}	lb	VD.HITCHFY	Hitch force along m_s Y axis	right	body
F_{zHITCH}	lb	VD.HITCHFZ	Hitch force along m_s Z axis	down	body
$F_{zHITCHI}$	lb	VD.HITCHFZI	Initial hitch force along m_s Z axis	down	body
K_{BTR}	ft-lb/ psi	VD.KBTR	Rear brake effectiveness		
K_{LIM}	-	VD.KLIM	Ratio of BRAKPROP2 to BRAKPROP1		
a_{y_U}	ft/s^2	VD.LATAC	Lateral acceleration at the roll axis	right	Horizontal to road plane and perpendicular to body centerline
$LOAD_{TRANS}$	%	VD.LOADTRANS	Total lateral load transfer		

Variables Defined

i = $L_{(left)}$ or $R_{(right)}$: j = $F_{(front)}$, or $R_{(rear)}$: ij = LF, RF, LR, RR : # 1 to 8

Variable	Units	Mnemonic	Definition	Sign Convention For Positive Value	Axis System
Y	ft	VD.LATPOS	Lateral position in global coordinate system		global
V_{LAT}	ft/sec	VD.LATVEL	Total vehicle lateral velocity		global
A_x	ft/sec^2	VD.LONGAC	Longitudinal acceleration at CG	forward	Horizontal to road plane and parallel to body centerline
X	ft	VD.LONGP	Longitudinal position in global coordinate system		global
U	ft/sec	VD.LONGVEL	Total vehicle longitudinal velocity	forward	body
M_{xFIFTH}	ft-lbs	VD.MXFIFTH	Fifth wheel torque about X axis	clockwise	body
M_{yFIFTH}	ft-lbs	VD.MYFIFTH	Fifth wheel torque about Y axis	clockwise	body
η	rad	VD.NETA	Articulation angle between vehicle and trailer	clockwise	body
$Y_{OffTrack}$	ft	VD.OFFTRACKING	Lateral offset of rear trailer axle from vehicle X axis	right	body
P_{BF}	psi	VD.PBF	Front brake line pressure		
P_{BR}	psi	VD.PBR	Rear brake line pressure		
ϕ_S	rad	VD.PHIS	Sprung mass roll angle	clockwise	body
$\dot{\phi}_S$	rad/sec	VD.PHISD	Sprung mass roll velocity	clockwise	body
$\ddot{\phi}_S$	rad/sec^2	VD.PHISDD	Sprung mass roll acceleration	clockwise	body
ϕ_V	rad	VD.PHISV	Global sprung mass roll angle		global
ϕ_{T_F}	rad	VD.PHITERF	Terrain "roll" angle at front axle		global
ϕ_{T_R}	rad	VD.PHITERR	Terrain "roll" angle at rear axle		global
ϕ_{T_S}	rad	VD.PHITERS	Terrain "roll" angle at CG		global
$\ddot{\phi}_{Uj}$	rad/sec^2	VD.PHIUDDj	Unsprung mass roll acceleration	clockwise	body
$\dot{\phi}_{Uj}$	rad/sec	VD.PHIUDj	Unsprung mass roll velocity	clockwise	body
ϕ_{Uj}	rad	VD.PHIUj	Unsprung mass roll angle	clockwise	body

Variables Defined

$i = L_{(left)}$ or $R_{(right)}$: $j = F_{(front)}$, or $R_{(rear)}$: ij = LF, RF, LR, RR : # 1 to 8

Variable	Units	Mnemonic	Definition	Sign Convention For Positive Value	Axis System
ψ	rad	VD.PSI	Total vehicle yaw angle	clockwise	body
$\dot{\psi}$	rad/sec	VD.PSID	Total vehicle yaw velocity	clockwise	body
$\ddot{\psi}$	rad/sec^2	VD.PSIDD	Total vehicle yaw acceleration	clockwise	body
RR_j	ft	VD.RRj	Average axle rolling radius		
ΣL_S	ft-lbs	VD.SUML	Sum of roll moments on sprung mass	clockwise	body
ΣL_{Uj}	ft-lbs	VD.SUMLj	Sum of roll moments on unsprung masses	clockwise	body
ΣN	ft-lbs	VD.SUMN	Sum of yaw moments on total vehicle	clockwise	body
ΣM_S	ft-lbs	VD.SUMQ	Sum of pitch moments on sprung mass	clockwise	body
ΣX	lbs	VD.SUMX	Sum of longitudinal forces on total vehicle	forward	body
ΣY_S	lbs	VD.SUMY	Sum of lateral forces on sprung mass	right	body
ΣY_{Uj}	lbs	VD.SUMYj	Sum of lateral forces on unsprung masses	right	body
ΣZ_S	lbs	VD.SUMZ	Sum of vertical forces on sprung mass	down	body
ΣZ_{Uj}	lbs	VD.SUMZj	Sum of vertical forces on unsprung masses	donw	body
θ_S	rad	VD.THE	Sprung mass pitch angle	clockwise	body
$\dot{\theta}_S$	rad/sec	VD.THED	Sprung mass pitch velocity	clockwise	body
$\ddot{\theta}_S$	rad/sec^2	VD.THEDD	Sprung mass pitch acceleration	clockwise	body
$\dot{u}$	ft/sec^2	VD.UDOT	Sprung mass longitudinal acceleration	forward	body
v_g	ft/sec	VD.VG	Wind gust velocity	right	body
$Y_{\alpha j}$	lbs/rad	VD.YALPHAj	Total front axle tire cornering stiffness		
y_S	ft	VD.YS	Sprung mass lateral deflection	right	body
$\dot{y}_S$	ft/sec	VD.YSD	Sprung mass lateral velocity	right	body

Variables Defined

i = $L_{(left)}$ or $R_{(right)}$: j = $F_{(front)}$, or $R_{(rear)}$: ij = LF, RF, LR, RR : # 1 to 8

Variable	Units	Mnemonic	Definition	Sign Convention For Positive Value	Axis System
y_{Sj}	ft	VD.YUj	Unsprung mass lateral deflection	right	body
$\dot{y}_{Sj}$	ft/sec	VD.YUDj	Unsprung mass lateral velocity	right	body
z_S	ft	VD.ZS	Sprung mass vertical deflection	down	body
$\dot{z}_S$	ft/sec	VD.ZSD	Sprung mass vertical velocity	down	body
$\ddot{z}_S$	ft/sec^2	VD.ZSDD	Sprung mass vertical acceleration	down	body
z_{Sij}	ft	VD.Zsij	Suspension deflection	extension	
$\dot{z}_{Sij}$	ft/sec	VD.ZsijD	Suspension velocity	extension	
z_{Uj}	ft	VD.Zuj	Unsprung mass vertical deflection	down	body
$\dot{z}_{Uj}$	ft/sec	VD.ZUDj	Unsprung mass vertical velocity	down	body
$\ddot{z}_{Uj}$	ft/sec^2	VD.ZSDD	Unsprung mass vertical acceleration	down	body
α_{ij}	radians	WT(#).ALPHA	Tire slip angle	clockwise	body
T_{Bj}	ft-lbs	WT(#).BRT2	Wheel brake torque		
δ_{Wij}	radians	WT(#).DW	Steer angle of road wheel	clockwise	
F_{sij0}	lbs	WT(#).FS0	Initial suspension force	+ comp.	body
F_{xij}	lbs	WT(#).FX	Longitudinal tire force without rolling resistance	forward	tire
F_{xNij}	lbs	WT(#).FXN	Longitudinal tire force with rolling resistance	forward	tire
F_{yij}	lbs	WT(#).FY	Lateral tire force	right	tire
F_{zij}	lbs	WT(#).FZ	Vertical tire force	positive	tire
F_{zij0}	lbs	WT(#).FZ0	Initial vertical tire force	positive	tire
γ_{ij}	radians	WT(#).GAMMA	Tire camber angle	clockwise	body
SN_0	–	WT(#).MUNOM	Surface friction at tire		

Variables Defined

$i = L_{(left)}$ or $R_{(right)}$: $j = F_{(front)}$, or $R_{(rear)}$: ij = LF, RF, LR, RR : # 1 to 8

Variable	Units	Mnemonic	Definition	Sign Convention For Positive Value	Axis System
ω_{ij}	rad/sec	WT(#).OMEGA	Tire rotational velocity	clockwise	tire
R_{DRAG}	lbs	WT(#).RDRAG	Tire rolling drag	Opposes u_{ij}	tire
S_{ij}	–	WT(#).S	Longitudinal slip	+ braking	tire
M_{zij}	ft-lbs	WT(#).TAU	Tire aligning moment	clockwise	tire
v_{ij}	ft/sec	WT(#).WLATVEL	Tire lateral velocity	right	body
u_{ij}	ft/sec	WT(#).WLONVEL	Tire longitudinal velocity	forward	body
X_{ij}	ft	WT(#).XAXELP	Global tire X position		global
Y_{ij}	ft	WT(#).YAXELP	Global tire Y position		global
$\partial F_X/\partial S\big\vert_S$	–	WT(#).XSLIP	Longitudinal tire stiffness		tire
$Y_{\alpha ij}$	lbs/rad	WT(#).YALPHA	Tire cornering stiffness $\partial F_Y/\partial \alpha\big\vert_\alpha$		tire
Δz_{ij}	ft	WT(#).TIREDEF	Tire deflection		
$\Delta \dot{z}_{ij}$	ft/sec	WT(#).TIREVEL	Tire deflection rate		

Notes:

1. Mnemonic prefix definitions:

VD.	Vehicle Dynamic variables
TRD.	TRailer Dynamic variables
WT().	Wheel and Tire variables
DTD.	DRiveTrain Dynamic variables
TM.	Terrain Model variables
DRT.	DRiveTrain parameters
DRI.	DRIver model parameters
V.	Vehicle model parameters
TR.	TRailer model parameters
TIRE().	TIRE model parameters

Variables Defined

$i = L_{(left)}$ or $R_{(right)}$: $j = F_{(front)}$, or $R_{(rear)}$: ij = LF, RF, LR, RR : # 1 to 8

2. Wheel numbering is denoted by # symbol:

1	Left Front wheel of vehicle
2	Right Front wheel of vehicle
3	Left Rear wheel of vehicle
4	Right Rear wheel of vehicle
5	Left Front wheel of trailer
6	Right Front wheel of trailer
7	Left Rear wheel of trailer
8	Right Rear wheel of trailer

Parameters Defined

i = $L_{(left)}$ or $R_{(right)}$: j = $F_{(front)}$, or $R_{(rear)}$: ij = LF, RF, LR, RR : # 1 to 8

PARAMETERS	SOURCE CODE MNEMONIC	UNITS	DEFINITION
a	v.vlena	ft	X distance from m_s c.g. to front axle
a	v.refarea	ft^2	Frontal area of vehicle, used for longitudinal drag
b	v.vlenb	ft	X distance from m_s c.g. to rear axle
b_j	v.bf, v.br	1/ft	first order coefficient for change in wheel steer angle with suspension deflection
c_j	v.cf, v.cr	$1/ft^2$	second order coefficient for wheel steer with suspension deflection
c_d	v.cdx		longitudinal drag coefficient
d_j	v.df,v. dr	1/ft	first order coefficient for change in wheel camber angle, with suspension deflection
e_j	v.ef, v.er	$1/ft^2$	second order coefficient for wheel camber angle with suspension deflection
h_j	v.hf, v.hr	ft	l_i times slope of trailing link in trailing arm suspension
h_{cg}	v.hcg	ft	c.g. height of total mass
h_{rai}	v.hraf, v.hrar	ft	height of roll axis above ground for solid axle suspension
h_s	v.hs	ft	m_s c.g. height above ground
I_{ϕ_s}	v.ixs	lb ft sec^2	moment of inertia for sprung mass in roll
I_{xz_S}	v.ixz	lb ft sec^2	cross product of inertia for sprung mass about x-z axis
i_{uj}	v.ixuf, v.ixur	lb ft sec^2	moment of inertia for unsprung mass about x axis
I_{y_S}	v.iys	lb ft sec^2	moment of inertia for sprung mass about y axis
i_z	v.izz	lb ft sec^2	moment of inertia for entire mass about z axis
k_{ack}	v.kack	ft/ft	ackerman steer coefficient
k_{ci}	v.kcf	$\frac{\text{rad}}{\text{lb}}$	lateral force steering compliance for suspension and steer linkage
k_{lt}	v.klt	ft/lb	lateral compliance rate, of tire, wheel, and suspension, per tire
k_{rad}	v.kradp	lb-sec/ft	damping rate at compliant pin joint between m_s and m_u
k_{ras}	v.kras	lbs/ft	lateral spring rate at compliant pin joint between m_s and m_u
k_{saj}	v.ksaf, v.ksar		= 1.0 for solid axle, = 0.0 for independent suspension
k_{sadj}	v.ksadf, v.ksadr	ft/ft	anti dive coefficient, or slope in side view of an equivalent single suspension arm
k_{sad2j}	v.ksad2f, v.ksad2r	ft/ft	special case for k_{sadi} when there is positive f_x with independent suspension
k_{sj}	v.ksf, v.ksr	lbs/ft	suspension spring rate equivalent at each wheel
k_{scj}	v.kscf, v.kscb	rad-lbs/ft	steering compliance for steering gear

Parameters Defined

i = $L_{(left)}$ or $R_{(right)}$: j = $F_{(front)}$, or $R_{(rear)}$: ij = LF, RF, LR, RR : # 1 to 8

PARAMETERS	SOURCE CODE MNEMONIC	UNITS	DEFINITION
k_{sdj}	v.ksdf, v.ksdr	lbs-sec/ft	suspension damping rate equivalent at each wheel
k_{slj}	v.kslf, v.klsr	ft/ft	lateral slope of an equivalent single suspension arm, at curb load
k_{str}	v.kstr	rad/rad	overall steering ratio
k_{tl}	v.ktl	ft	tire lag, expressed in rolling distance
k_{zt}	v.tspringr	lbs/ft	vertical spring rate of tire
k_{tsj}	v.ktsf, v.ktsr	ft-lbs/rad	auxiliary torsional roll stiffness per axle, (normally negative)
l_j	v.lf, v.lr	ft	length of trailing link, in a trailing arm suspension
l_{saj}	v.lsaf, v.lsar	ft	length of the k_{slj} arm
l_{so}	v.lso	ft	lateral steering axis offset from king pin to tire patch center (positive if tire c.l. is outside king pin axis)
m	v.mass	slugs	total vehicle mass
m_s	v.smass	slugs	sprung mass
m_{ui}	v.umassf, v.umassr	slugs	front, or rear, unsprung mass
r_{ij}	wt(#).rr	ft	effective wheel/tire radius, and same as c.g. height of m_{ui}
t_i	v.trwf, v.trwr	ft	track width
ω_{n_s}	v.sww	rad/rad	natural frequency for second order steering system lag
ζ_s	v.swz		damping ratio for steering system lag
$\partial L_A / \partial v$	v.dladv	ft-lbs/ft/sec	aerodynamic roll moment coefficient
$\partial N_A / \partial v$	v.dnadv	ft-lbs/ft/sec	aerodynamic yaw moment coefficient
$\partial Y_A / \partial v$	v.dyadv	lbs/ft/sec	aerodynamic lateral force coefficient
ρ	v. density	lbs/ft^3	air density
u_{aero}	v. aerovel	ft/sec	aerodynamic reference speed
x_{acc}	v. xacc	ft	distance of accelerometer ahead of sprung mass c.g.
z_{acc}	v. zacc	ft	distance of accelerometer above vehicle roll axis
k_{btf}	v.kbtf	ft-lbs/psi	front brake effectiveness
k_{vb}	v.kvb	psi/lbs	brake gain in vacuum boost range
k_{vm}	v.kvm	psi/lbs	brake gain in manual range
f_{bpvl}	v.fbpvl	lbs	pedal force where vacuum boost runs out
k_1	v.brakprop1	lbs/lbs, or ft-lbs/psi	hydraulic: initial f/r brake force slope, air - front axle brake effectiveness
k_2	v.brakprop2	lbs/lbs, or ft-lbs/psi	hydraulic: final f/r brake force slope, air – drive and trailer axle brake effectiveness
f_{xlim}	v.fxlimit	lbs	hydraulic: front brake force at knee in rear vs. front

Parameters Defined

i = $L_{(left)}$ or $R_{(right)}$: j = $F_{(front)}$, or $R_{(rear)}$: ij = LF, RF, LR, RR : # 1 to 8

PARAMETERS	SOURCE CODE MNEMONIC	UNITS	DEFINITION
			brake force curve (entered as a negative number)
c_{cf}	v. dampcomf	lbs-sec/ft	front shock compression damping
c_{rf}	v. dampextf	lbs-sec/ft	front shock rebound or extension damping
c_{cr}	v. dampcomr	lbs-sec/ft	rear shock compression damping
c_{rr}	v. dampextr	lbs-sec/ft	rear shock rebound or extension damping
airbrakes	v.airbrakes	0 or 1	air brake model flag: 0 - off, 1 - on
τ_f	v.braklag1	sec	front axle brake force time constant
τ_r	v.braklag2	sec	drive axle brake force time constant
τ_t	v.braklag3	sec	trailer axle brake force time constant
d	tr. lend	ft	distance from vehicle sprung mass c.g. to hitch
e	tr. lene	ft	distance from trailer sprung mass c.g. to hitch
h_h	tr.thh	ft	trailer hitch height above ground
k_{hitch}	tr. hitchsp	lbs/ft	hitch deflection spring stiffness
c_{hitch}	tr. hitchspd	lbs-sec/ft	hitch deflection damping
k_{tfifth}	tr.ktfifth	ft-lbs/rad	hitch torsional stiffness
k_{fade}	tr.kfade	%/°f	brake temperature fade parameter
n_{drwhl}	tr.ndrwhl	#	number of tires at each end of drive axle
n_{trwhl}	tr.tdrwhl	#	number of tires at each end of trailer axle
suspensionf	v.suspensionf	0 or 1	front suspension type: 0 - solid axle, 1 - independent
suspensionr	v.suspensionr	0 or 1	rear suspension type: 0 - solid axle, 1 - independent
k_{bscj}	v.kbscj	lb/ft	compression bump stop stiffness
h_{bscj}	v.hbscj	ft	compression bump stop contact point
s_{bscj}	v.sbscj	-	compression bump stop transition term
k_{bsej}	v.kbsej	lb/ft	extension bump stop stiffness
h_{bsej}	v.hbsej	ft	extension bump stop contact point
s_{bsej}	v.sbsej	-	extension bump stop transition term
t_w	tire(#).twidth	ft	tire contact patch width
a_0	tire(#).ka0	lbs/rad	cornering stiffness vs. load constant term
a_1	tire(#).ka1	1/rad	cornering stiffness vs. load linear term
a_2	tire(#).ka2	Lbs	cornering stiffness vs. load squared term
a_3	tire(#).ka3	1/rad	camber stiffness vs. load linear term
a_4	tire(#).ka4	Lbs	camber stiffness vs. load squared term
k_a	tire(#).ka	–	contact patch elongation with fx
$k_{\mu y}$	tire(#).kmu	–	decay in lateral friction with increasing slip angle
t_p	tire(#).tpres	Psi	tire inflation pressure
b_{1y}	tire(#).kb1	1/lbs	peak lateral friction vs. load linear term

Parameters Defined

i = $L_{(left)}$ or $R_{(right)}$: j = $F_{(front)}$, or $R_{(rear)}$: ij = LF, RF, LR, RR : # 1 to 8

PARAMETERS	SOURCE CODE MNEMONIC	UNITS	DEFINITION
b_{3y}	tire(#).kb3	–	peak lateral friction vs. load constant term
b_{4y}	tire(#).kb4	$1/lbs^2$	peak lateral friction vs. load squared term
k_γ	tire(#).kgamma	–	falloff of camber thrust at high slip
cs/fz	tire(#).csfz	–	Normalized longitudinal tire force stiffness
μ_{0y}	tire(#).munomin	–	Lateral friction of vehicle test surface
f_{zt}	tire(#).fztrl	lbs	tire design load
k_1	tire(#).kk1	ft/lbs	Aligning torque stiffness vs. load
c_1	tire(#).var1	–	Shaping coefficient, c1, for force saturation function (-)
c_2	tire(#).var2	–	Shaping coefficient, c2, for force saturation function (-)
c_3	tire(#).var3	–	Shaping coefficient, c3, for force saturation function (-)
c_4	tire(#).var4	–	Shaping coefficient, c4, for force saturation function (-)
c_5	tire(#).var5	–	Shaping coefficient, c5, for force saturation function (-)
g_1	tire(#).graphk1	–	Aligning moment shaping parameter, g1
g_2	tire(#).graphk2	–	Aligning moment shaping parameter, g2
σ_x	tire(#).tlonglag	sec	Longitudinal slip ratio time constant
α_0	tire(#).plysteer	rad	slip angle offset for zero lateral tire force
b_{1x}	tire(#).kb1x	1/lbs	peak longitudinal friction vs. load linear term
b_{3x}	tire(#).kb3x	-	peak longitudinal friction vs. load constant term
b_{4x}	tire(#).kb4x	$1/lbs^2$	peak longitudinal friction vs. load squared term
$k_{\mu x}$	tire(#).kmux	–	Decay in longitudinal friction with increasing slip
$dragc_{ij}$	tire(#).dragc	–	Rolling drag coefficient
$brakmult_{ij}$	tire(#).brakmult	–	Brake torque multiplier
k_{dc}	drt.kdc	–	center differential gear ratio
k_{df}	drt.kdf	–	front differential gear ratio
k_{db}	drt.kdb	–	rear differential gear ratio
k_{cp}	drt. kcp	$\frac{ft \cdot lbs \cdot \sec}{rad}$	center viscous coupling pressure coefficient
k_{cpf}	drt. kcpf	$\frac{ft \cdot lbs \cdot \sec}{rad}$	front viscous coupling pressure coefficient
k_{cpb}	drt. kcpb	$\frac{ft \cdot lbs \cdot \sec}{rad}$	rear viscous coupling pressure coefficient
k_{rf}	drt.krf	-	front torque split differential coefficient
k_{rb}	drt.krb	-	rear torque split differential coefficient
$k_{e\ k=1\ to\ 6}$	drt.$ke_{k=1\ to\ 6}$	-	coefficients for the engine torque curve

Parameters Defined

i = $L_{(left)}$ or $R_{(right)}$: j = $F_{(front)}$, or $R_{(rear)}$: ij = LF, RF, LR, RR : # 1 to 8

PARAMETERS	SOURCE CODE MNEMONIC	UNITS	DEFINITION
k_{tc0}	drt.ktc0	$\frac{rad}{ft \cdot lbs \cdot \sec}$	torque converter coefficient
sr_0	drt.sr0	-	torque converter stall ratio
i_e	drt.enginei	ft-lbs-sec^2	engine rotary inertia
i_t	drt. transmissioni	ft-lbs-sec^2	transmission rotary inertia
Δt	drt.shifttime	sec	time interval for transmission gear shift
speedk1	drt.speedk1	$\frac{throttle}{\Delta V_{ERROR}}$	proportional automatic speed control gain
speedk2	drt.speedk2	$\frac{throttle}{\int \Delta V_{ERROR}}$	integral automatic speed control gain
ω_{idle}	drt.idle	rad/sec	engine idle speed
difftype	drt.difftype	-	center differential type, choices: 1 - limited slip differential, 2 - locked differential
dg(k)	drt.dg(k), k=1 to 10	-	if the center differential is locked, then dg(1) is the drive shaft spring stiffness in ft-lbs-sec^2, and dg(2) is the drive shaft damping in ft-lbs-sec/rad otherwise all are zero
numgear	drt.numgear	-	number of transmission gear ranges (max=10)
ds	drt. downshift	rad/sec	downshift threshold
k_{gri}	drt.kgr(k), k=1 to 10	-	gear ratios
$k_{ti,i=1,3,5,7...}$	drt.kt1(k), k=1 to 10	rad/sec	minimum upshift speed from gear k to k+1
$k_{ti,i=2,4,6,8...}$	drt.kt2(k), k=1 to 10	rad/sec	maximum minus minimum upshift speed k to k+1
τ_a	dri.taua	sec	the driver's look ahead distance reaction time delay
τ_r	dri.taur	sec	the motion feedback time delay
k_y	dri.ky	1/(ft-sec^2)	trim loop gain
k_r	dri.kr	-	motion feedback gain (yaw rate feedback gain)
τ_l	dri.tl	sec	driver curvature error lead compensation term
k_ψ	dri.kpsi	ft/sec	steering loop yaw rate command gain
ζ_n	dri.zn	-	the damping ratio of the driver's neuromuscular dynamics
ω_n	dri.wn	rad/sec	the frequency of the driver's neuromuscular dynamics
k_a	dri.ka	1/sec	the driver's look ahead distance constant ($x_a = k_a * u$)
$k_{\psi 2}$	dri.kpsi2	ft/sec	steering loop yaw rate command gain when in high side slip conditions (scheduled with k_ψ)
τ_{l2}	dri.tl2	sec	driver curvature error lead compensation term when in high side slip conditions (scheduled with τ_l)

Parameters Defined

i = $L_{(left)}$ or $R_{(right)}$: j = $F_{(front)}$, or $R_{(rear)}$: ij = LF, RF, LR, RR : # 1 to 8

PARAMETERS	SOURCE CODE MNEMONIC	UNITS	DEFINITION
k_{a2}	dri.ka2	1/sec	the driver's look ahead distance constant when in high side slip conditions (scheduled with k_a)
$k_{\Delta\beta 1}$	dri. kdelb11	1/rad	proportional throttle due to side slip angle error (β-β_c) control gain (only used during high side slip maneuvering)
$k_{\Delta\beta 2}$	dri. kdelb12	1/(rad-sec)	integral throttle due to side slip angle error (β-β_c) control gain (only used during high side slip maneuvering)
$K_{\Delta\dot{\beta}1}$	dri. kdelbd1	sec	throttle due to sideslip angular rate (only used during high sideslip maneuvering)
$K_{\Delta\dot{\beta}2}$	dri. kdelbd2	sec	throttle due to sideslip angular rate (only used during high sideslip maneuvering).
$k_{c\delta T}$	dri.kcdelt	ft/sec	curvature to throttle compensation gain
$k_{\beta\delta sw}$	dri.kbdsw	-	beta to steering wheel compensation gain
	dri. thlag	sec	throttle lag term when in high sideslip conditions
β_c	dri.betac	rad	the side slip angle that the driver would like to maintain during high sideslip maneuvers
ontime	dri.ontime	sec	the moment in time when the driver begins to counter steer during high sideslip conditions
δ_{tmax}	dri.throttlemax	-	the maximum throttle available during high side slip maneuvers
$k_{\Delta\beta 1\_2}$	dri. kdelb2	1/rad	proportional throttle due to side slip angle error (β-β_c) control gain (only used during high side slip maneuvering)
$K_{\dot{\beta}}$	dri. kbddsw	sec	beta rate to steering wheel compensation gain
	dri.fbkay		collision avoidance feedback loop gain
$K_{\dot{y}}$	dri.kydot	sec	lane position rate feedback gain
k_{stab}	dri.kstabf	rad/ft/sec^2	vehicle's stability factor
a_{yd}	dri.ayd	ft/sec^2	3d terrain desired cornering ay
u_{limit}	dri.speedlimit	ft/sec	3d terrain speed limit
$k_{c'}$	dri.kcprime		3d terrain trim integrator gain
$k_c \cdot m$	dri.kcvelm		3d terrain proportional throttle gain multiplied by mass
k_{sff}	dri.ksff		3d terrain steering feed forward gain
τ_b	dri.taub	sec	3d terrain braking time delay
k_{fbp}	dri.kfbp	lbs/throttle	3d terrain braking gain
k_{as}	dri.kas	sec	3d terrain driver steering look ahead time
k_{ab}	dri.kab	sec	3d terrain driver speed control look ahead time
y_c	dri.yc	ft	3d terrain commanded lane position

Parameters Defined

i = $L_{(left)}$ or $R_{(right)}$: j = $F_{(front)}$, or $R_{(rear)}$: ij = LF, RF, LR, RR : # 1 to 8

PARAMETERS	SOURCE CODE MNEMONIC	UNITS	DEFINITION
smi	nl.smi	-	wheel spin mode integration rate multiplier
endvel	nl.endvel	ft/sec	longitudinal velocity below which the program will automatically shut off
I_{y_W}	nl.iyw	lb ft sec^2	wheel inertia about spin axis
δ_{swmax}	nl.dswmax	rad	maximum value the steering wheel may be turned in either direction
fbp_{max}	nl. Braktmax	lbs	the maximum limiting brake pedal force
antibf	nl.antibf	0 or 1	front axle anti-lock brake flag: 0 - off, 1 - on
antiblimf	nl. Antiblimf	-	longitudinal slip ratio limit where the anti-lock braking routine for the front turns on and off
k_{antibf}	nl. Kantibf	ft-lbs/s	anti-lock braking gain for front the brakes
k_{antibr}	nl.antibr	0 or 1	rear axle anti-lock brake flag: 0 - off, 1 - on
antiblimr	nl. Antiblimr	-	longitudinal slip ratio limit where the anti-lock braking routine for the rear turns on and off
k_{antibr}	nl. Kantibr	ft-lbs/s	anti-lock braking gain for rear the brakes
siunits	nl.siunits	0 or 1	flag for plotting and saving data in si units: 0 - u.s., 1 - si
saverate	nl.saverate	hz	output data save rate
rollover	nl.rollover	rad	vehicle roll angle where simulation stops
distplot	nl.distplot	0 or 1	change plotting and saving data from time base to distance based: 0 - time, 1 - distance
	dtd.eng2trans	ft-lbs	torque the engine sends the transmission
t_c	dtd.engtorque	ft-lbs	engine torque
ω_c / ω_e	dtd.func1	-	ratio of transmission input speed to engine speed
Gear	dtd.gear	-	current gear number
ω_c	dtd.omegac	rad/sec	transmission input shaft speed
ω_e	dtd.omegae	rad/sec	engine speed
$\dot{\omega}_E$	dtd.omegaed	rad/sec^2	engine acceleration
ω_r	dtd.omegatb	rad/sec	rear differential speed
ω_f	dtd.omegatf	rad/sec	front differential speed
ω_t	dtd.omegatt	rad/sec	center differential speed
	dtd.sgear	-	previous gear (used during shifting)
$t_{\#}$	dtd.shafttorq(#)	ft/lbs	torque in axle shaft
θ_t	dtd.throttle	0 to 1	total throttle position used by engine model
θ_a	dtd.throttlea	0 to 1	additional throttle from driver model or speed control
θ_c	dtd.throttlec	0 to 1	open-loop throttle command

Parameters Defined

$i = L_{(left)}$ or $R_{(right)}$: $j = F_{(front)}$, or $R_{(rear)}$: ij = LF, RF, LR, RR : # 1 to 8

PARAMETERS	SOURCE CODE MNEMONIC	UNITS	DEFINITION
g.r.	dtd.trangr	-	current transmission gear ratio
	dtd.transmission	0 or 1	transmission type: 0 - automatic, 1 - manual
t_t	dtd. Trantorq	ft-lbs	torque output from transmission
t_f	dtd. Trantorqf	ft-lbs	front torque output from center differential
t_r	dtd. Trantorqb	ft-lbs	rear torque output from center differential

Q. APPENDIX A REFERENCES

A.1. Allen, R. W., Rosenthal, T. J., and Szostak, H. T., *Analytical Modeling of Driver Response in Crash Avoidance Maneuvering*:

– *Vol. I: Technical Background*, DOT-HS-807 270, April 1988.

– *Vol. II: An Interactive Tire Model for Driver/Vehicle Simulation*, DOT-HS-807 271, April 1988.

– *Vol. III: A Trim Model and Computer Program for Determining Ground Vehicle Steady State Operating Conditions and Quasilinear Stability Coefficients*, DOT-HS-807 272, April 1988.

– *Vol. IV: User's Guide for Linear Analysis, Nonlinear Simulation, Part Task Simulation*, DOT-HS-807 273, April 1988.

A.2. Allen, R. W., Szostak, H. T., Klyde, D. H., Rosenthal, T. J., and Owens, K. J., *Vehicle Dynamic Stability and Rollover*, DOT-HS-807 956, September 1992.

A.3. Allen, R. W., Rosenthal, T. J., and Chrstos, J. P., "A Vehicle Dynamics Tire Model for Both Pavement and Off-Road Conditions," SAE Paper 970559, December 1996.

A.4. Bernard, J. E. and Clover, C. L., "Tire Modeling for Low-Speed and High-Speed Calculations," SAE Paper 950311, February 1995.

A.5. Clover, C. L. and Bernard, J. E., "Longitudinal Tire Dynamics," Iowa State University, Ames, IL, April 1995.

A.6. Myers, Thomas T., *Feasibility of a Grade Severity Rating System*, FHWA-RD-79-116, August 1979.

APPENDIX B

VEHICLE PARAMETER FILE

A. BACKGROUND

In the past, there has always been a problem in finding good parameters for vehicle dynamics simulations. Now, with the current state of development in VDANL, parameter specification is a major consideration, including inertial and compliance parameters, suspension geometry functions, and a tire model that needs tire test data. This appendix is intended to make VDANL parameter selection more straightforward, easier to understand, and make the parameter values more readily available, by offering optional methods for measurement, calculation, or estimation by rules of thumb.

To help make the parameter selection more rational and understandable, the computer simulation mathematics are kept as general as possible, using composite functions in place of endless mechanical details for every possible component found in car designs, such as;

1. For vertical and antiroll spring functions, all suspension springs, shocks, and auxiliary roll stiffness are specified to act at the tire contact patch. This is consistent with the way cars are tested for ride and roll force reactions at each tire, and makes it unnecessary to model the complex suspension mechanisms.
2. Suspension geometry functions for deflection steer, camber angle change, squat-lift forces, and Ackerman steer, are also specified at the wheel. This is also consistent with the static test data for cars, and avoids complex models for many different suspension designs.
3. The tire model used is a rational and direct description of how tires respond undergoing composite slip, while being relatively simple and easy to understand. It only needs accurate "end point" coefficients to be specified from accurate tire test data. The tire model is described in some detail in Appendix E.

Various methods to obtain vehicle parameters can be found in the following references:

1. Measure the vehicle directly (static tests)

   See STI Report WP-1119-4 (Ref. B.1)
   SAE Paper 720473 (Ref. B.2)
   DOT HS-801 800 (Ref. B.3)
   SAE Paper 910232 (Ref. B.4)

2. Simple "rule of thumb" calculated estimates

   See SAE Paper 840561 (Ref. B.5)

SAE Paper 881767 (Ref. B.6)

SAE Paper 870495 (Ref. B.7)

SAE Paper 930897 (Ref. B.8)

SAE Paper 960183 (Ref. B.9)

3. Sources for obtaining direct data on cars.

   Miscellaneous National Highway Traffic Safety Administration (NHTSA) Vehicle Research Test Center (VRTC) reports

   Automotive Industries magazine, the annual Engineering Specifications issue

   Motor Vehicle Manufacturers Association (MVMA) passenger car specifications forms

   Consumer Reports magazine, the annual auto issue

   Car & Driver magazine, buyer's guide

   Motor Trend magazine, automotive yearbook

   Road & Track magazine, road test annual, and buyer's guide

4. Dimensional measurement, via tape measure, an
5. d conversion for suspension geometry functions.
6. Scale parameters up or down, from known car data
7. Tire test data

   Calspan tire test data, as published for NHTSA

   University of Maryland, tire test data

   Adjust data from available tire test data to a new size

These methods are now used in the following section to provide estimating parameters for the vehicle input files for VDANL.

An example of the vehicle parameter input file for a 1994 Ford Taurus is shown in Table B-1.

All parameters are defined in Appendix A.

Note the small distinction or difference between m and m_c. m should be the total mass as tested or to be run in the simulation. However, most static test data on I_{xs}, I_{ys}, I_z etc., are based on empty "curb load" states for the car. Therefore, all estimates for the inertias should use the "curb weight" state = m_c.

Table B-1. Vehicle Parameters for a 1994 Ford Taurus

1) MASS	= 113	24) KSR	= 1200	47) KBTF	= -1.5729
2) SMASS	= 100.8	25) KSDR	= 118.4	48) KVB	= 24.73
3) UMASSF	= 6.72	26) TRWF	= 5.13	49) KMB	= 4.3
4) UMASSR	= 5.45	27) TRWB	= 5.03	50) KBPVL	= 40.1
5) LENA	= 3.175	28) HCG	= 1.78	51) SWZ	= .5
6) LENB	= 5.66	29) KBS	= 9918	52) SWW	= 86
7) UXS	= 322.9	30) HBS	= 0.19	53) KCF	= 0.000005
8) IYS	= 1836.5	31) KTSF	= -76119.3	54) LSO	= -0.031
9) IZZ	= 2248.2	32) KTSR	= -27961	55) KLAGV	= 16.5
10) IXZ	= 0	33) KRAS	= 53000	56) BRAKPROP1	= 0.239
11) KSTR	= 15.97	34) KRADP	= 1000	57) BRAKPROP2	= 0.083
12) KSCF	= 0.000115	35) TSPRINGR	= 15096	58) FXLIMIT	= -544
13) KSCB	= 0.000049	36) HRAF	= 0	59) DAMPCOMF	= 0
14) DLADV	= 0	37) HRAR	= 0	60) DAMPEXTF	= 0
15) DYADV	= 0	38) HS	= 1.87	61) DAMPCOMR	= 0
16) DNADV	= 0	39) IXUF	= 45.8	62) DAMPEXTR	= 0
17) DENSITY	= 0.00237	40) IXUR	= 37.0	63) AIRBRAKES	= 0
18) REFAREA	= 23.23	41) KLT	= 1.036E-5	64) BRAKLAG1	= .25
19) CDX	= 0.372	42) XACC	= 0.23	65) BRAKMULTLF	= 1
20) AEROVEL	= 44	43) ZACC	= 1.52	66) BRAKMULTRF	= 1
21) KTL	= 0.86	44) DRAGC	= -.015	67) BRAKMULTLR	= 1
22) KSF	= 1818	45) LENS	= 0	68) BRAKMULTRR	= 1
23) KSDF	= 167.9	46) LM	= 1		

Then if desired, the inertias can be corrected for the addition of a driver and test equipment to provide the "as-tested" inertias

For I_z, I_{ys} this is not needed, because one driver and test equipment adds less than 1 percent to the I_{zo}, I_{yso} for the empty car.

But for roll inertia, the I_{xs} with the driver and equipment added could be 5 percent to 10 percent larger than I_{xso} empty, so that this difference may be large enough to add this correction into I_{xso}. But one should also realize that the driver is not rigidly attached to the sprung mass, so that the effective I_{xs} in dynamic roll response may be less than nominal calculations suggest.

B. LIST OF VEHICLE PARAMETERS AND ESTIMATION METHODS

The following table is set up with numbers and terms in the same order as they appear in the VDANL computer simulation input files. All units and definitions are shown in Appendix A.

1. m, total mass (slugs)

   Total vehicle mass with driver and test equipment. Or use published weight and add for driver and equipment

2. m_s, sprung mass (slugs)

   Total vehicle mass minus front and rear unsprung masses

   $m_s = m - m_{uF} - m_{uR}$

3. m_{uF}, front unsprung mass (slugs)

   Estimates:

   $m_{UF} = 1+.045\, m_c$ for suspensions with sprung differential

   $m_{UF} = .08\, m_c$ for solid axle suspensions with differential unsprung

   m_c = curb mass, to be used with formula

4. m_{uR}, rear unsprung mass

   Use same formulas as for 3., m_{UF}

5. a, distance from front axle to cg of m_s (ft)

   $$a = (W_R - g m_{UR}) \frac{\ell}{g m_s}$$

   W_R = test vehicle weight at rear axle

   ℓ = wheelbase

6. b, distance from rear axle to cg of m_s (ft)

   $b = \ell - a$

7. I_{xs}, sprung mass roll inertia (ft-lb-s^2)

These data are always difficult to obtain. If published data are available, they are usually for total inertia, I_{xs}. To convert to I_{xs} ,

$$I_{x_s} = I_x - I_{UF} - I_{UR} - m_S\left(h_S - h_{cg}\right)^2 - \left(m_{UF} + m_{UR}\right)\left(h_{cg} - R_W\right)^2$$

$$\left.\begin{aligned} I_{UF} &= m_{UF}\left(\frac{T_F}{2}\right)^2 \\ I_{UR} &= m_{UF}\left(\frac{T_R}{2}\right)^2 \end{aligned}\right\} \text{ For independent suspensions}$$

$$\left.\begin{aligned} I_{UF} &= \tfrac{2}{3} m_{UF}\left(\frac{T_F}{2}\right)^2 \\ I_{UR} &= \tfrac{2}{3} m_{UF}\left(\frac{T_R}{2}\right)^2 \end{aligned}\right\} \text{ For solid axle with differential gear}$$

$$h_s = \frac{m_c h_{cg} - \left(m_{UF} + m_{UR}\right) R_W}{m_s}$$

If no published data are available, then I_{xs} can be estimated from data in Figure B-1, where,

$$I_{xs} = .558\left(m_c\right)^{4/3}$$

For the special cases of unusual body shapes, the following shape-corrected formulas can be used:

$$I_{xs} = \frac{m_c}{18.5}\left(W^2 + [.69H]^2\right) \quad \text{For sedans}$$

$$I_{xs} = \frac{m_c}{18.5}\left(W^2 + [.77H]^2\right) \quad \text{For station wagons and utility vehicles}$$

$$I_{xs} = \frac{m_c}{18.5}\left(W^2 + [.85H]^2\right) \quad \text{For vans}$$

where W = vehicle body width

H = vehicle roof height

8. I_{ys}, sprung mass pitch inertia (ft-lb-s^2)

If published data available are only for total inertia, I_y, then convert to I_{ys},

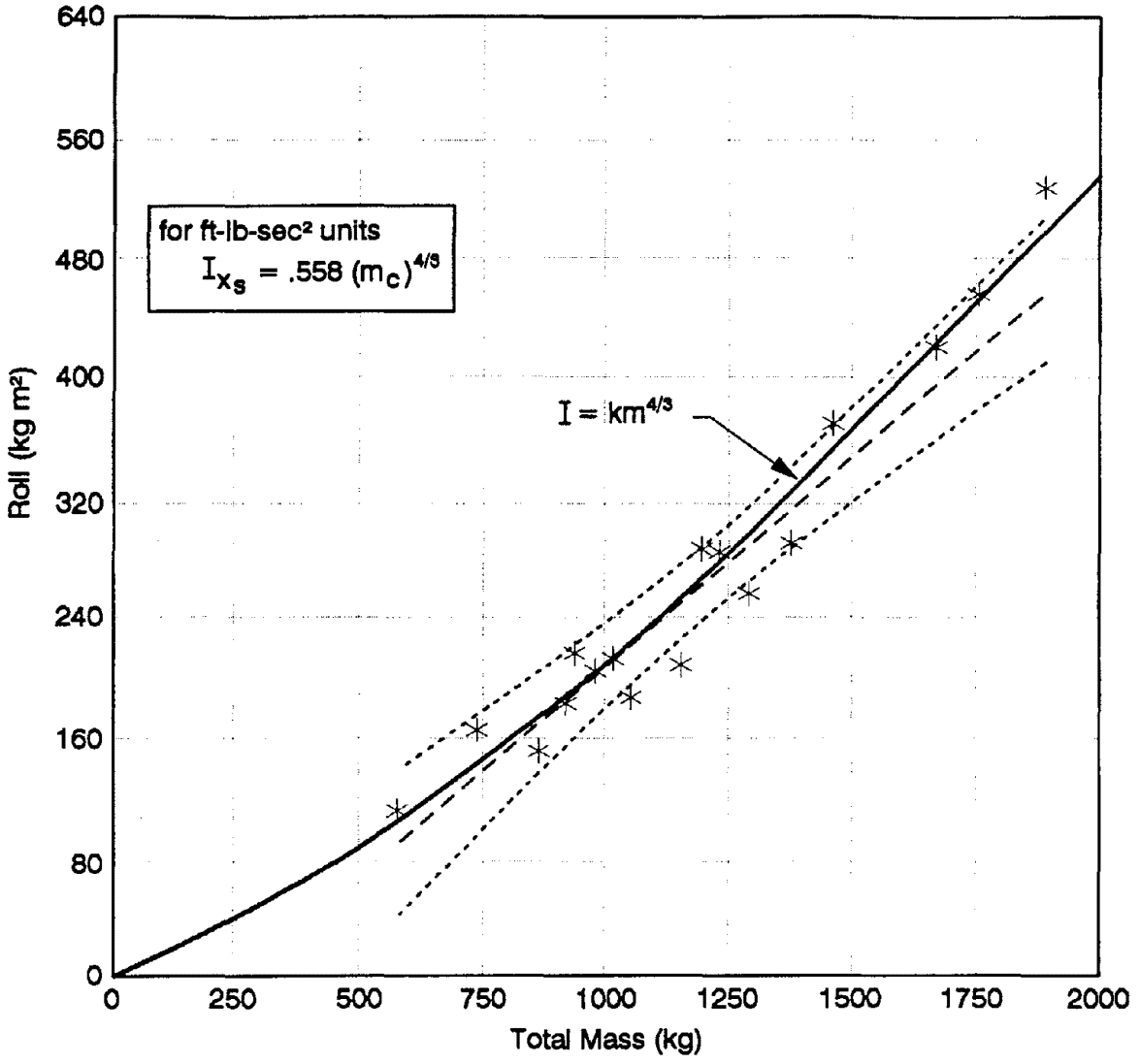

Figure B-1. Sprung Mass Roll Inertia About cg, vs. Total Mass

$$I_{ys} = I_y - m_S\left(h_S - h_{cg}\right)^2 - m_{UR}\left(b^2 + \left[h_{cg} - R_W\right]^2\right) - m_{UF}\left(a^2 + \left[h_{cg} - R_W\right]^2\right)$$

If no published data are available, then I_{ys}, can be estimated from data in Figure B-2,

$$I_{ys} = .733 m_c^{5/3}$$

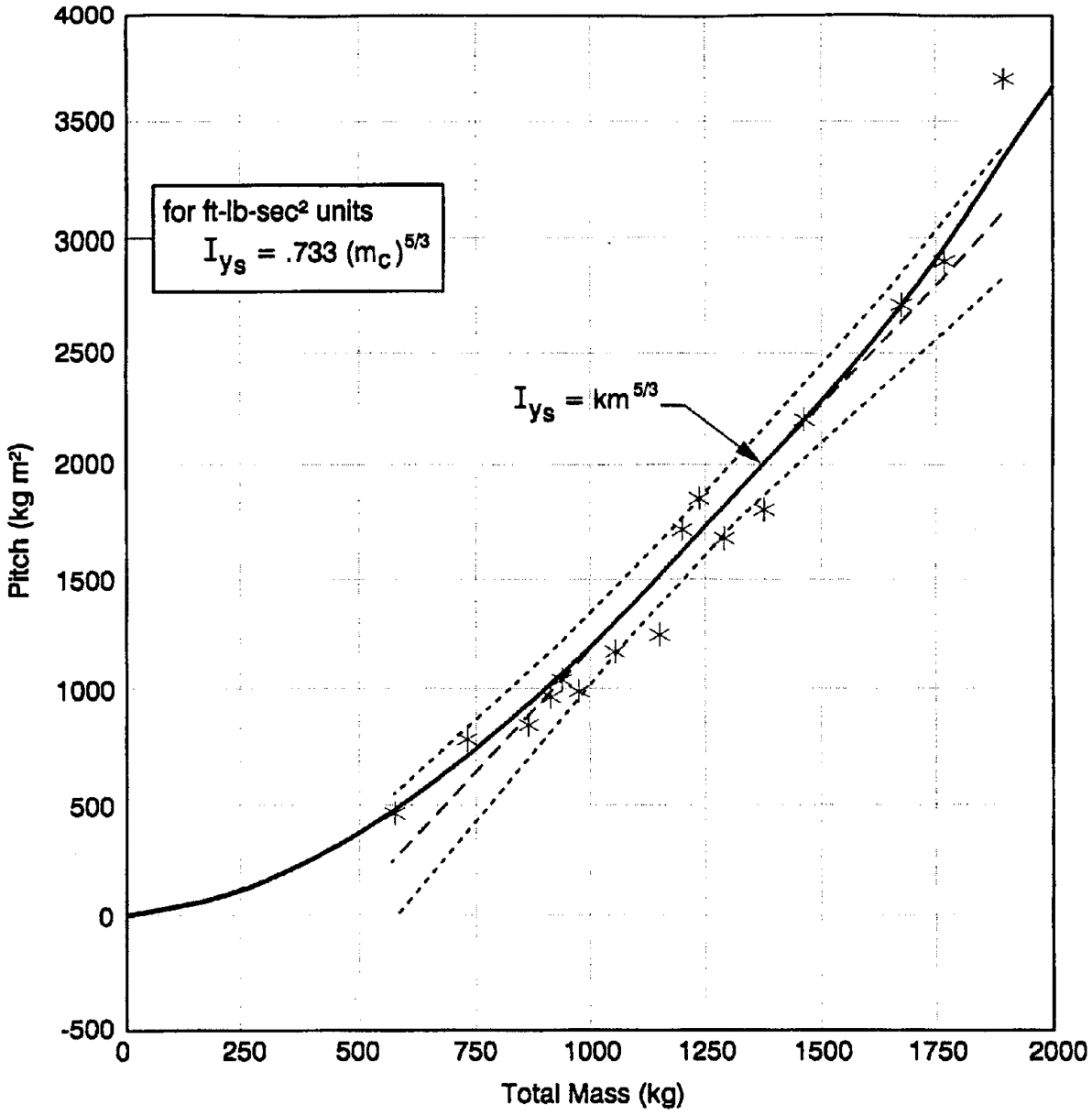

Figure B-2. Sprung Mass Pitch Inertia About cg, vs. Total Mass

9. I_z, total yaw inertia (ft-lb-s^2)

If no published data are available, then $I_z = m_c\, ab$ can be used, or can be estimated from data in Figure B-3.

$$I_z, \quad = \quad .99 m_c^{5/3}$$

This $5/3$ exponential is consistent with vehicle mass varying proportional to ℓ^3. So that ab varies as ℓ^2 or as $m^{2/3}$. Therefore I_z should vary as mab, or $m\ell^2$, or $m^{5/3}$.

However, there is a body shape correction needed for short vs. long body lengths for vehicles of the same mass. This is important when considering short-bodied utility vehicles, as contrasted with sedans with long body overhangs. For these vehicles, I_z can be estimated by,

$$I_z \quad = \quad .0875 m_c \ell^2 + .053 m_c \text{ (overall length)}^2$$

10. I_{xz}, cross product of inertia (ft-lb-s^2)

These data are rarely available, and there is no rationale for estimating it. Since it is often a very small number with little effect on vehicle handling, it can be set equal to zero if the data are not available.

11. K_{STR} overall steering ratio

These data are seldom available and must be tested directly.

12. K_{SCF}, steering gear compliance at front

See Appendix D for test method.

13. K_{SCB}, steering gear compliance at front

K_{SCB}, steering gear compliance at rear

See Appendix E for test method.

14. $\partial L_A / \partial v$, aerodynamic roll moment coefficient (ft-lb-ft/s)

Roll moment applied to cg due to side wind gust

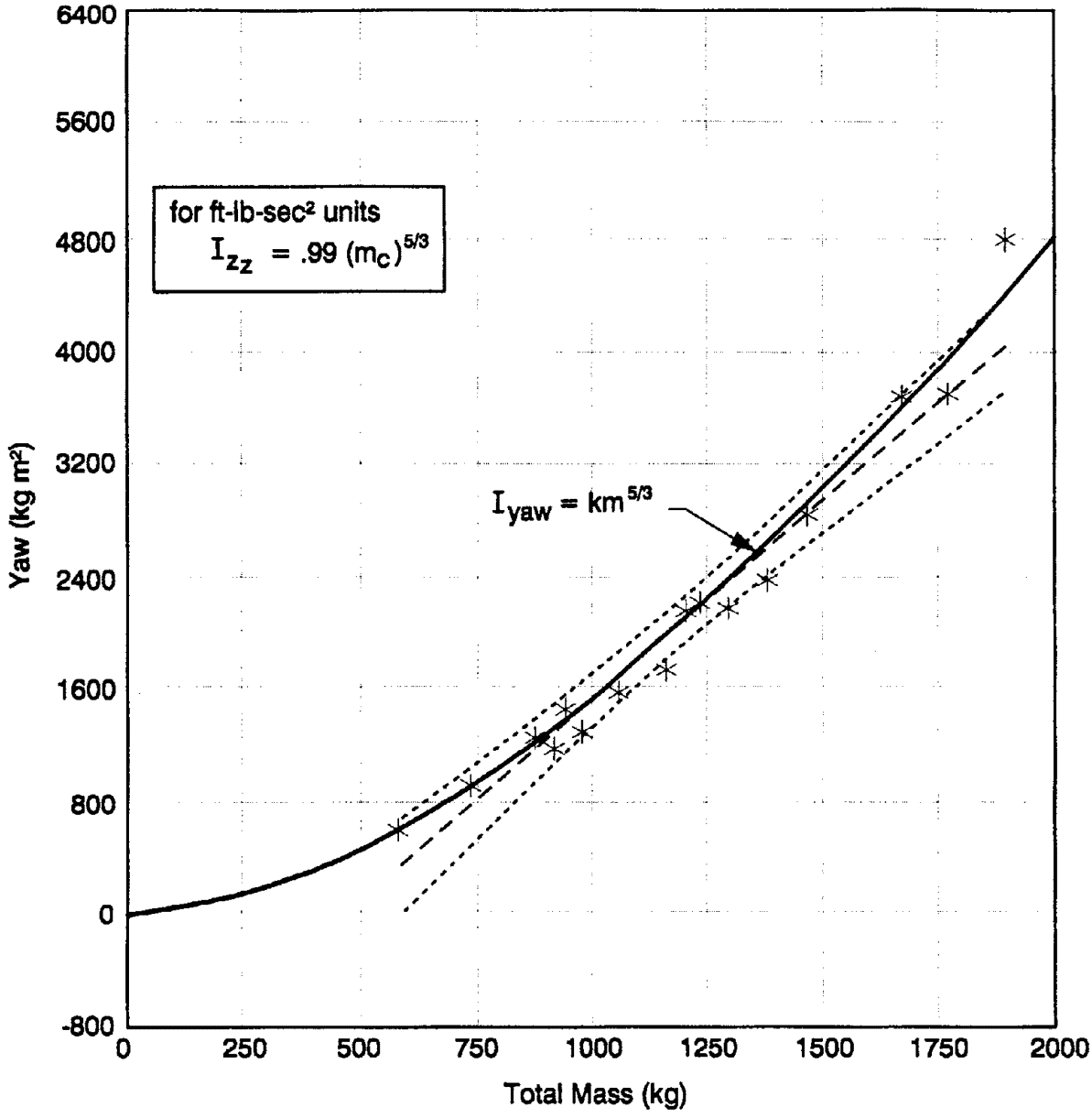

Figure B-3. Total Vehicle Yaw Inertia About cg, vs. Total Mass

15. $\partial Y_A / \partial v$, aerodynamic lateral force coefficient (lb-ft-/s)

    Lateral force applied to c.g. due to side wind gust

16. $\partial N_A / \partial v$, aerodynamic yaw moment coefficient (ft-lb-ft/s)

    yaw moment applied to cg due to side wind gust

17. ρ, atmospheric density (lb-s^2/ft^2)

18. *REFAREA*, front view body cross-section area (ft^2)

    If not available can be estimated from .75 h w

    Where h = body height

    w = body width

19. C_{DX}, drag factor in X direction

    This varies from 0.30 to 0.40 for most new cars and vans and probably about 0.40 to 0.50 for most small trucks and older cars.

20. U_{AERO}, the air velocity where aero coefficients were measured (ft/s)

21. K_{TL}, tire side force development lag (ft)

    This is expressed in feet of rolling tire travel, in which the time constant $= K_{TL} / u$ for a first order system. The tire will roll about 6 times the K_{TL} distance to reach the final value for a step input.

    Therefore, $K_{TL} = \dfrac{\text{Roll distance to S.S.}}{6}$

    Typical values for K_{TL} range from 0.7 to 1.4 ft, which corresponds to a total roll distance of 4.2 to 8.4 ft.

    K_{TL} can also be measured from sinusoidal steering tire test data.

22. K_{SF}. Front suspension spring rate (lb-ft)

    This is the suspension spring rate as measured at the wheel. See Appendix E for test method.

23. K_{SDF}, front suspension damping rate (lb-ft/s)

    No data is available for this, but most cars have ζ =.025 to 0.35 for good ride quality.

choose $\zeta = 0.25$ if ride is soft and floating

$\zeta = 0.35$ if ride is firm

$\zeta = 0.45$ if ride is very stiff and jerky

then,

$$K_{SDF} = 2\zeta\sqrt{(K_{SF})(m_{siF})}$$

where

$$m_{siF} = \frac{m_s \cdot b}{2\ell} = \text{sprung mass over one front wheel}$$

24. K_{SR} , rear suspension spring rate (lb-ft)

This is the spring rate as measured at the wheel. See Appendix D for test method.

25. K_{SR}, rear suspension damping (lb-ft/s)

This is usually somewhat higher than the front.

choose $\zeta = 0.30$ if ride is soft

$\zeta = 0.40$ if ride is firm

$\zeta = 0.50$ if ride is very stiff

then,

$$K_{SDR} = 2\zeta\sqrt{(K_{SR})(m_{siR})}$$

where

$$m_{SiR} = \frac{m_s \cdot a}{2\ell}$$

26. T_F, front track width (ft)

Measure this from tire center to tire center.

27. T_R, rear track width (ft)

Measure this from tire center to tire center.

28. h_{cg}, center of gravity of total vehicle

Use published data, or test method described in Appendix D. or a simple rule of thumb can be used to estimate h_{cg}.

h_{cg} = 0.39 (roof height) for passenger cars

= 0.38 (roof height), for vans

= 0.37 (roof height), for pick up trucks

= 0.39 (roof height), for 4WD utility vehicles

= 0.41 (roof height), for 4WD vehicles designed extra high for clearance from unsprung front axle differential housing

29. K_{bs}, bump stop stiffness (lb-ft)

No longer used. Use new bump stop model (parameters in suspension parameter file)

30. H_{bs}, suspension travel to bump stop (ft)

No longer used. Use new bump stop model (parameters in suspension parameter file)

31. K_{TSF}
32. K_{TSR}

} front and rear auxiliary roll stiffness.

This is seldom available, and must therefore be measured in a static test on the vehicle. See Appendix D for that method. However, this test provides the overall roll stiffness, K_{ORSj}, at each axle. [Note: K_{ORSj} is the slope of the total axle roll torque (ft-lb) versus chassis roll angle (rad) relative to the ground. Using the VDANL sign conventions, this slope will be negative. In the equations below, K_{ORSj} is entered as a negative number]. To compute the net auxiliary roll stiffness, the effects from the tire and suspension spring rates must be removed.

$$K_{TSj} = \frac{K_{ORSj}\,K_{TRSj}}{K_{TRSj} - K_{ORSj}} + \frac{K_{Sj}\,T_j^2}{2}$$

where K_{ORSj} = overall roll stiffness at axle j

T_j = track width

K_{Sj} = suspension spring rate

$$K_{TRSj} = -\frac{K_{ZT}\,T_j^2}{2}$$

K_{ZT} = tire spring rate

Note that roll stiffness coefficients normally have negative values.

33. K_{RAS}, spring rate for compliant pin joint (lb-ft)

This provides for lateral compliance at the suspension pivot and subframe rubber bushing attachments. An additional purpose is to avoid digital computer computational instabilities. Thus, a value needs to be chosen to provide a natural frequency above the region of interest for vehicle handling, but below the region that would interact with the typical computer program sampling interval of 0.005 s.

$$\omega_n = \sqrt{\frac{(m_{UF}\ell + m_s b)\, K_{RAS}}{m_{UF}\, m_s b}}$$

34. K_{RAS}, damping rate for compliant pin joint (lb-ft/s)

K_{RAS} is chosen to provide near critical damping

$$\zeta \approx \frac{K_{RAD}}{2\sqrt{m_{uj}\, K_{RAS}}}$$

35. K_{ZT}, tire spring rate (lb-ft)

This is usually available from Calspan tire test data. If not, this can be estimated from formula;

$$K_{ZT} = 510\left[\text{Wheel Rim Diam} + 2\,(\text{tire sect. size})\right]\frac{\text{Press}}{35}$$

Wheel rim diameter and tire section size need to be in inches, and tire pressure in lb-in^2.

Tire size is given on the side wall, such as P205/75 R15

↑ wheel rim diameter, in in

↑ section size, in mm, which then needs to be converted into in by dividing by 25.4 mm/in.

36. h_{RAF}
37. h_{RAR}

} front and rear roll axis height (ft)

For solid axle or beam axle suspensions, the roll axis height is the height of the lateral control link pivot above ground. This is the pivot about which the sprung mass will rotate in free geometric roll.

For all independent suspensions, where there is no physical roll axis pivot, all forces and moments are carried through each independent suspension. Therefore, for these cases, h_{RAF} and / or h_{RAR} are set = zero. And the force and moment effects are set by suspension geometry parameters, in the suspension parameter files.

38. h_s, sprung mass cg of gravity height (ft)

$$h_s = \frac{m_{hcg} - (m_{UF} + m_{UR})R_W}{m_s}$$

39. I_{uF}
40. I_{uR}

} is the I_x for each axle $\left(\text{ft lb s}^2\right)$

These data are not available, so that estimation by an approximate formula is necessary.

$$I_{uj} = \left(\frac{T_j}{2}\right)^2 m_{uj}$$

where $m_{uj} = 1 + 0.045\, m_c$

The extra mass of an unsprung differential gear is not included, because being at the axle cg center, it does not contribute any significant amount to I_{xu}

41. K_{LT}, lateral compliance of tire and suspension (ft-lb)

This is the total lateral compliance rate of everything that effectively reduces the half-track width (except the compliant pin joint), which plays a direct part in resisting vehicle rollover. This includes tire casing lateral compliance, wheel bending, suspension bending, suspension and subframe bushing deflection, etc.

The tire lateral compliance is given in the Calspan tire test data as the C1 parameter. If this is not available, it can be estimated from a known vertical spring rate of the tire.

$$\approx \frac{1}{.76\, K_{ZT}}$$

Data on the other sources of lateral compliance are difficult to obtain. But all other compliance is probably in the same order of magnitude of the tire compliance. So that if we combine this, we have a rough approximation for total compliance:

$$K_{LT} \approx \frac{2}{.76 K_{ZT}} = \frac{2.6}{K_{ZT}}$$

or if C1 is available,

$$K_{LT} = 2C_1$$

42. X_{ACC}, location of A_y accelerometer forward from sprung mass c.g., in a field test vehicle (ft)
This is used to provide measured A_{yMEAS} values from simulation runs at the same location in the vehicle as used in field testing.

43. $Z_{ACC,}$ location of A_y accelerometer in distance above roll axis (ft)

This is for same purpose as #42, X_{ACC}, and can be calculated as follows;

$$Z_{ACC} = h_{Z_{ACC}} - h_{RAR} + \frac{(b + X_{ACC})}{\ell}(h_{RAR} - h_{RAF})$$

where

$h_{Z_{ACC}}$ = A_y accelerometer height above ground

h_{RAF}, h_{RAR} = front and rear roll axis heights, which are items 36, 37 if it is for solid axle suspensions.

If it is an independent suspension,

$$h_{RAF} = K_{SLF}\left(\frac{T_F}{2}\right)$$
$$h_{RAR} = K_{SLR}\left(\frac{T_R}{2}\right)$$

where

K_{SLj} = suspension motion slope as defined in suspension input file, items 17, 18.

44. $DRAGC$, rolling drag coefficient.

No longer used. Rolling drag coefficient for each tire is specified in tire parameter file.

45. $LENS$, is the distance from the vehicle rear axle back to the side slip sensor trolley wheels (ft)

This is so the simulation β can be compared to a field test vehicle with a side slip sensing trolley.

46. LM, is the length of the trailing arm (lateral swing arm) of the side slip sensing trolley (ft)

This is used to define the sensor response lag.

47. K_{BTF}, front brake effectiveness (ft-lb-psi)

This is the slope of the front brake torque versus front brake line pressure curve.

48. K_{VB}, brake gain in vacuum boost range (psi/lb)

This is the initial slope of the front brake line pressure versus pedal force curve.

49. K_{VB}, brake gain in manual range (psi/lb)

This is the final slope of the front brake line pressure versus pedal force curve.

50. F_{PBVL}, pedal force where vacuum boost runs out (lb)

This is the pedal force at the knee between the K_{VB} and K_{MB} slopes.

51. SWZ, }
52. SWW, } are the damping ratio and natural frequency for the vehicle's steering system response lag.

These can be determined from an instrumented tire kick test while the front wheels of a stationary car are free and off the ground, and the steering wheel is clamped solid in a fixed position this is the natural dynamic response of the two front wheel's inertial mass about the steering (ball joints) axis, while flexing against the steering system compliance, or can be estimated as follows;

$$SWZ = \zeta \text{ is nominally set } = 0.5$$

$$SWW = \omega_n = \frac{1}{\sqrt{2\, I_W\, K_{SCF}}}$$

I_W will range from about 1.0 ft-lb-s^2 for smaller wheels, up to 2.0 ft-lb-s^2 for larger wheels.

K_{SCF} is parameter #12

53. K_{CF}, is lateral force compliance steer (rad/lb)

This is mainly centered in relative suspension deflections in the lateral direction. This can be measured directly, as shown in WP-1119-4. Or it can be assumed that for most vehicle designs, the manufacturer tries to minimize these effects, as they could cause handling problems in certain circumstances. Therefore set K_{CF} = zero.

The exception to this is when the steering linkages are placed in front of the suspension arms. Then there will tend to be a significantly large compliance understeer effect due to soft suspension bushings. In this case, the static test should be done to measure this effect.

54. L_{SO}, steering axis lateral offset (ft)

This is the offset of the steering axis (ball joints) inboard of the wheel centerline at the road surface as shown in Figure B-4. It is used to compute torque steer effects due to braking or traction from front wheel drive.

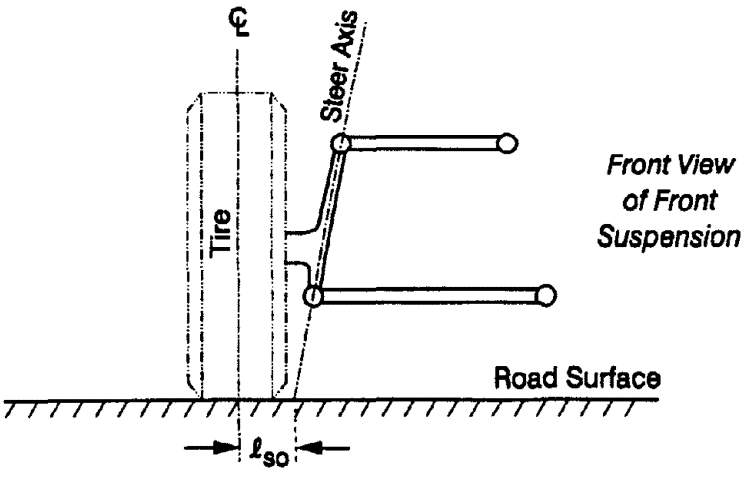

Figure B-4. Steering Axis Lateral Offset

55. K_{lagv}, no longer used

56. K_1, initial rear to front brake force slope (-)

    This is the initial slope of the rear brake force versus front brake force curve

57. K_2, final rear to front brake force slope (-)

    This is the final slope of the rear brake force versus front brake force curve

58. F_{XLIM}, front brake force at knee in rear to front brake force curve (lb)

    This is the front brake force at the knee of the rear brake force versus front brake force curve. F_{XLIM} is entered as a negative number.

59. C_{CF}, front wheel compression damping (lb-s/ft)

    When using the bi-linear damper model, this is the compression damping of each front wheel.

60. C_{RF}, front wheel rebound damping (lb-s/ft)

    When using the bi-linear damper model, this is the rebound damping of each front wheel.

61. C_{CR}, rear wheel compression damping (lb-s/ft)

    When using the bi-linear damper model, this is the compression damping of each rear wheel.

62. C_{RR}, rear wheel rebound damping (lb-s/ft)

    When using the bi-linear damper model, this is the rebound damping of each rear wheel.

63. *AIRBRAKES*, flag to activate air brake model (0 or 1)

    Setting *AIRBRAKES* to 1 activates the airbrake model

64. τ_F, brake force time constant for hydraulic brake systems (s)

    This is the first order time constant for brake line pressure response to brake pedal force input. For hydraulic brake models, this is used for both axles.

65. *BRAKMULTLF*, left-front wheel brake torque multiplier

66. *BRAKMULTRF*, right-front wheel brake torque multiplier

67. *BRAKMULTLR*, left-rear wheel brake torque multiplier

68. *BRAKMULTRR*, right-rear wheel brake torque multiplier

C. APPENDIX B REFERENCES

B.1. Szostak, H. T., "Static Test of Chassis Parameters for a 1980 Chevrolet Citation," Systems Technology, Inc., WP-1119-4, June 1980.

B.2. Nedley, A. L. and Wilson, W. J., "A New Laboratory Facility for Measuring Vehicle Parameters Affecting Understeer and Brake Steer," SAE Paper 720473 presented at National Automobile Engineering Meeting, Detroit, MI, 1972.

B.3. Jindra, F., "Mathematical Model of Four-Wheeled Vehicle for Hybrid Computer Vehicle Handling Program," Ultrasystems, Inc., Phoenix, AZ, Interim Report, DOT-HS-801-800, January 1976.

B.4. Chrstos, J. P., "A Simplified Method for the Measurement of Composite Suspension Parameters," SAE Paper 910232 presented at SAE International Congress and Exposition, Detroit, MI, 1991.

B.5. Riede, P. M., Leffert, R. L., and Cobb, W. A., "Typical Vehicle Parameters for Dynamics Studies Revised for the 1980's," SAE Paper 840561 presented at International Congress & Exposition, Detroit, MI, 1984.

B.6. Garrott, W. R., Monk, M. W., and Chrstos, J. P., "Vehicle Inertial Parameters--Measured Values and Approximations," SAE 881767 presented at Passenger Car Meeting and Exposition, Dearborn, MI, 1988.

B.7. Allen, R. W., Rosenthal, T. J., and Szostak, H. T., "Steady State and Transient Analysis of Ground Vehicle Handling," SAE Paper 870495 presented at International Congress & Exposition, Detroit, MI, 1987.

B.8. Garrott, W. R., "Measured Vehicle Inertial Parameters -- NHTSA's Data Through September 1992," SAE Paper 930897 presented at International Congress and Exposition, Detroit, MI, 1993.

B.9. Bixel, R. A., Heydinger, G. J., Guenther, D. A., and Novak, S. J., "Sprung/Unsprung Mass Properties Determination without Vehicle Disassembly," SAE Paper 960183 presented at SAE International Congress and Exposition, Detroit, MI, 1996.

APPENDIX C

SUSPENSION PARAMETER FILE

A. OVERVIEW

Continuing from the Appendix B discussion, this section deals with the suspension parameters. Again, the vehicle dynamics model relies on composite functions rather than specific suspension design variations. Each parameter can be determined from simple external test procedures or definitions. Table C-1 gives an example suspension parameter input file for a 1994 Ford Taurus; the estimation procedures that follow this will use the same numbering and parameter order.

Table C-1. Suspension Parameter Input File for a 1995 Ford Taurus

1) SUSPENSIONF	=1	20) LSAR	= 1.67
2) SUSPENSIONR	=1	21) KSADF	= 0.08
3) HF	= 0	22) KSADR	= 0.1
4) HR	= 0	23)KSAD2F	= 0.054
5) LF	= 1	24) KSAD2R	= 0
6) LR	= 1	25) KACK	= 0.0021
7) KSAF	= 0	26) KBSCF	= 9744
8) KSAR	= 0	27) HBSCF	= 0.19
9) BF	= 0.036	28) SBSCF	= 20
10) BR	= -0.033	29) KBSEF	= 96000
11) CF	= -0.212	30) HBSEF	= 0.217
12) CR	= 0.014	31) SBSEF	= 20
13) DF	= 0.073	32) KBSCR	= 10000
14) DR	= 0.078	33) HBSCR	= 0.216
15) EF	= 0.174	34) SBSCR	= 20
16) ER	= 0.10	35) KBSER	= 96000
17) KSLF	= 0 .17	36) HBSER	= 0.375
18) KSLR	= 0 .14	37) SBSER	= 20
19) LSAF	= 0 .99		

B. LIST OF SUSPENSION PARAMETERS AND ESTIMATION METHODS

1. SUSPENSIONF, set = 1 for independent, = 0 for solid axles

2. SUSPENSIONR, set = 1 for independent, = 0 for solid axles

3. H_F
4. H_R
5. L_F
6. L_R
7. K_{SAF}
8. K_{SAR}

These define the roll steer coefficient for solid axle or beam axle suspension at the front (F), or rear (R) suspension.

Typical axles have two trailing links or leaf springs with an equivalent link, which control the steer angle of the axle. The side view slope of this link in Figure C-1 gives the axle roll steer coefficient.

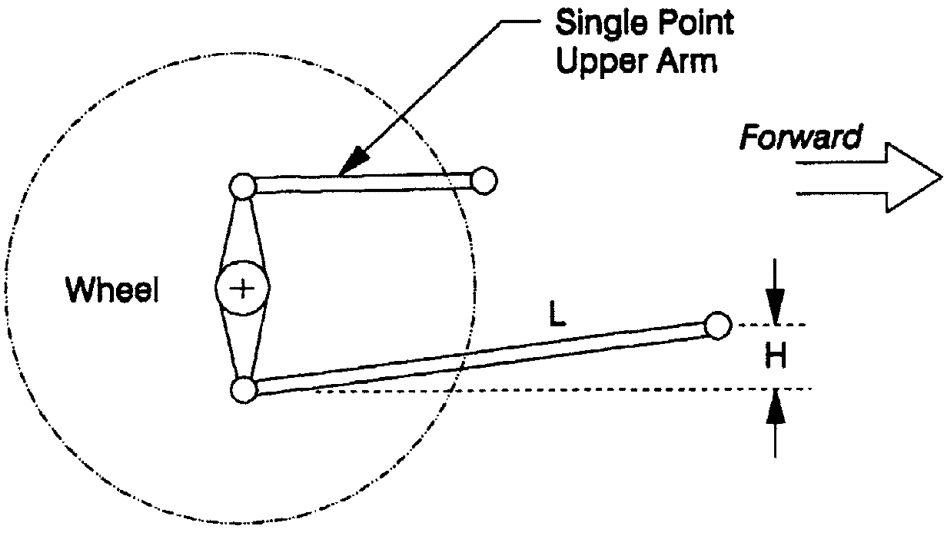

Figure C-1. Suspension Side view Where Roll Steer Function is

$$\Delta\delta_{w_{ij}} = \frac{KSAj}{L_j}\left[h_j + \left(z_{SL_j} + z_{SR_j}\right)\right]\left(\phi_s - \phi_{uj}\right)$$

with H_j = height that forward pivot is above rear pivot (ft)

L_j = length of trailing link (ft)

K_{SAj} = 1.0 to activate function

If, for a front suspension, there are leading links (placed behind the front axle), the L_j should have a negative sign.

For independent suspensions, $H_j = 0$, and set $L_j = 1.0$ to avoid division by zero, and $K_{SAj} = 0$ to remove this function.

9. B_F
10. B_R
11. C_F
12. C_R

These are for the wheel steer functions for vertical suspension deflection.

For solid axle suspensions, these B_j and C_j parameters are set = zero, to remove the functions.

For independent suspensions, the B_j is the first order steer effect, and the C_j is the second order steer effect.

$$\Delta\delta_{w_{LF}} = B_F\, z_{SLF} + C_F\, z_{SLF}^2$$

$$\Delta\delta_{w_{LR}} = B_R\, z_{SLR} + C_R\, z_{SLR}^2$$

See Figure C-2, which shows a suspension with a change in δ_{wij} with vertical wheel motion, z_{Sij}. See Figure C-3 for examples of complex deflection steer.

Most modern suspension designs try to avoid what is sometimes called bump steer, because it tends to be detrimental to predictable handling on certain types of roadway disturbances. And since it is so difficult to obtain reliable test data on deflection steer, we would recommend that these parameters B_j and C_j be set = zero.

If the roll steer coefficient (ε) is known, then $B_j = \dfrac{2 \cdot \varepsilon_j}{T_j}$

If it is suspected that a certain vehicle has a significant amount of deflection steer, then it may be necessary to test for these steer effects. The test is rather straightforward, and measures wheel steer angle change versus forced vertical movement of the sprung mass. Then values of B_j and C_j are chosen so as to fit the function to the test data curve.

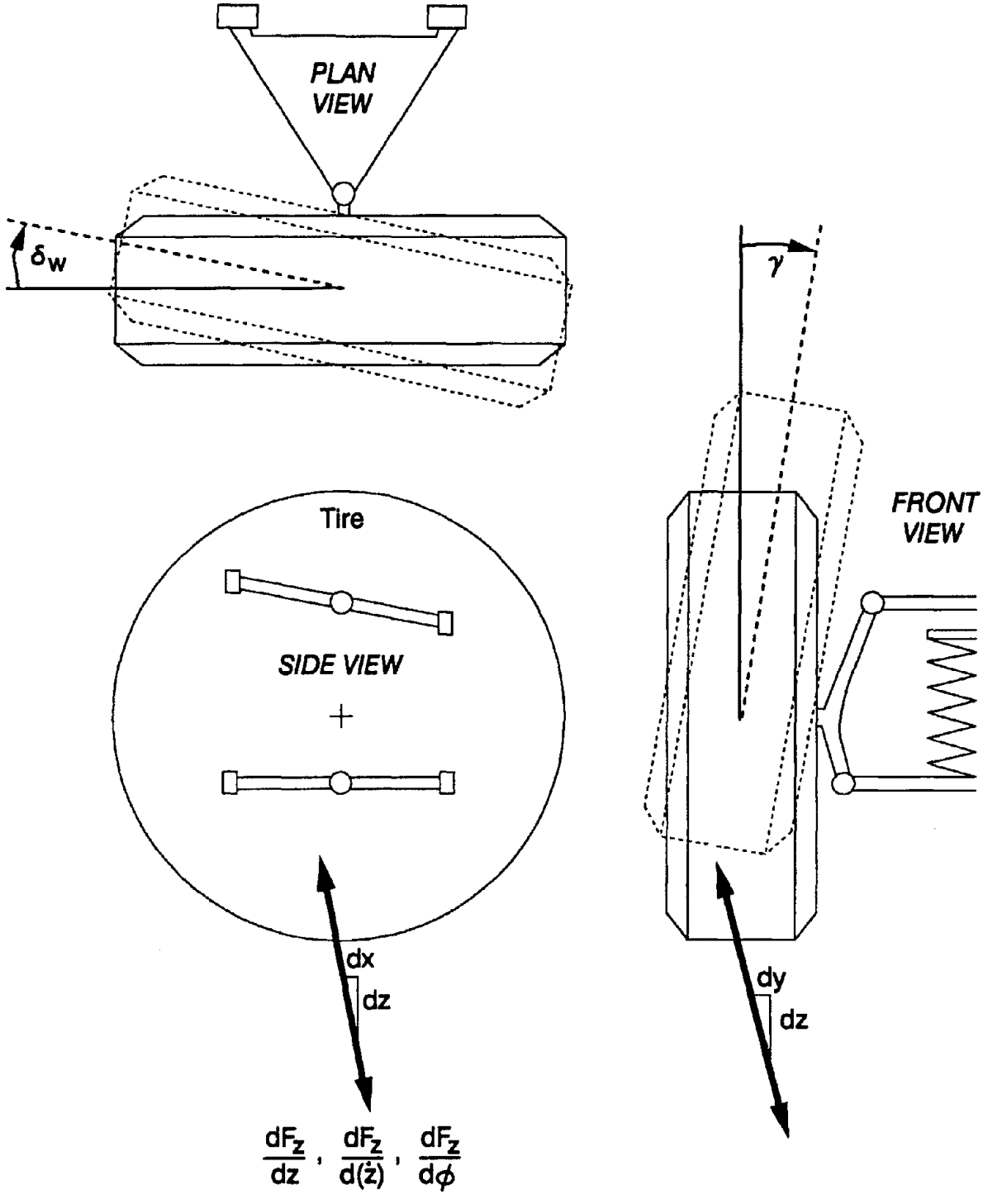

Figure C-2. Static Tests on Wheel Motions

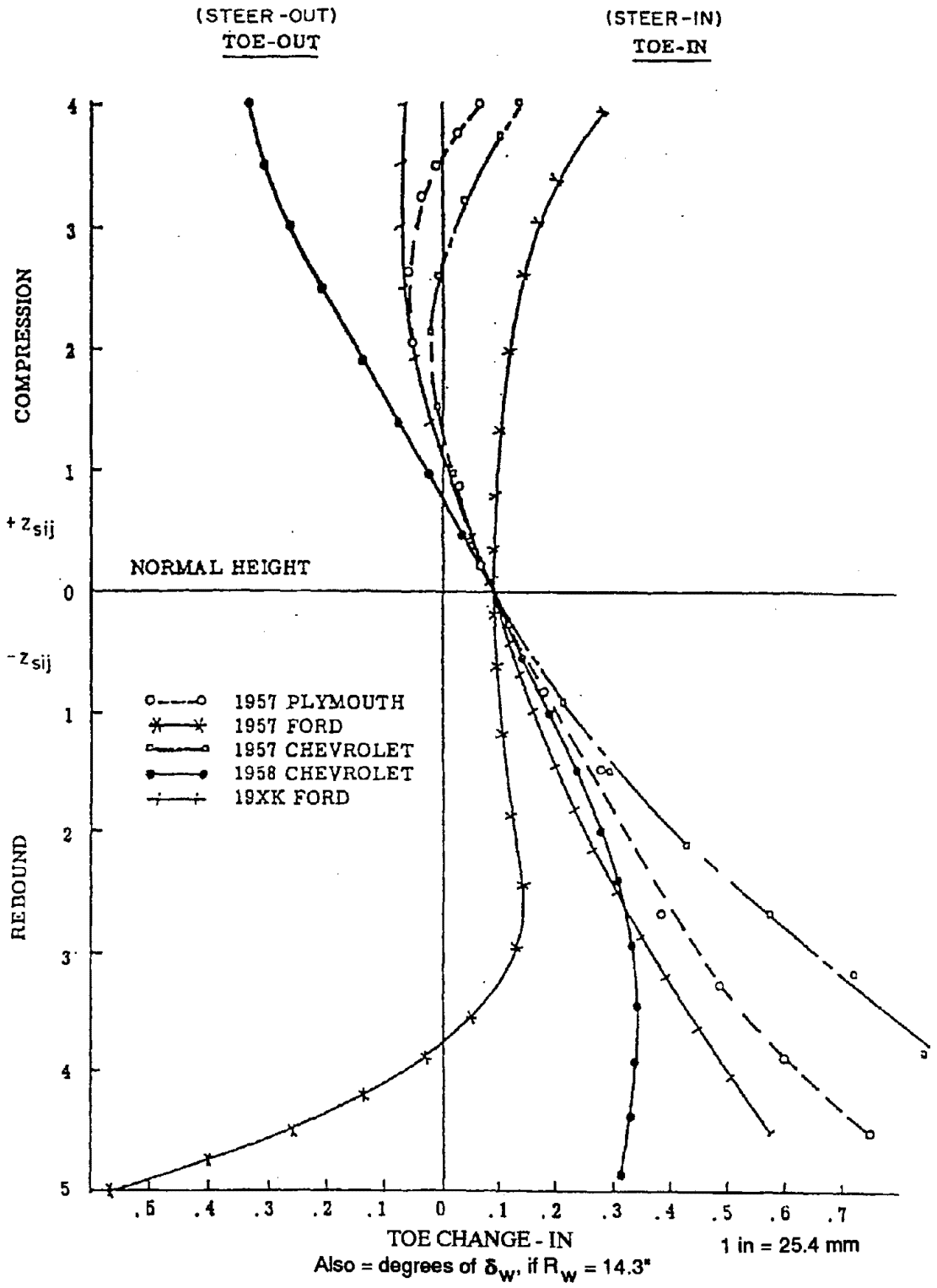

Figure C-3. Toe Change vs. Suspension Position

13. D_F
14. D_R
15. E_F
16. E_R

These are for the camber angle change vs. vertical deflection functions.

See Figure C-2, which shows camber angle γ_{ij} change vs. vertical wheel motion, z_{Sij}. See Figure C-4 for examples of typical camber angle change curves.

The function for camber angle with independent suspension are:

$$\gamma_{LF} = \phi_S + D_F\, z_{SLF} + E_F\, z_{SLF}^2$$
$$\gamma_{LR} = \phi_S + D_R\, z_{SLR} + E_R\, z_{SLR}^2$$

These D_j and E_j coefficients can be estimated by matching the function to static test data, such as in Figure C-4. The static test simply measures camber angle vs. forced vertical motion of the sprung mass.

An alternative is to measure all suspension component pivot locations and link lengths. Then reconstruct the suspension on graph paper, and by plotting the linkage motions on paper, determine the camber angle change by graphical methods.

Also if the camber angle to roll angle coefficient is know, $K_{\gamma/\phi}$, then;

$$D_j = \left[K_{\gamma/\phi} - 1\right]\frac{2}{T_j}$$

For solid axle and beam axle suspensions, these functions are bypassed, such that the D_j and E_j parameters are set = zero.

17. K_{SLF}
18. K_{SLR}
19. L_{SAF}
20. L_{SAR}

These are for the suspension squat/lift functions with lateral forces.

The primary factor in squat/lift reactions is the path direction of the tire contact patch as the wheel moves up and down in suspension motions. These are shown in Figure C-2 as $\Delta y/\Delta z$. And example of test data is shown in Figure C-5.

The function for suspension squat/lift is simply:

$$F_{SQij} = \left[K_{SLj} + \frac{z_{Sij}}{L_{SAj}}\right]F_{y_{ij}}$$

L_{SAj} = arc radius of the tire motion path shown in Figure C-2.

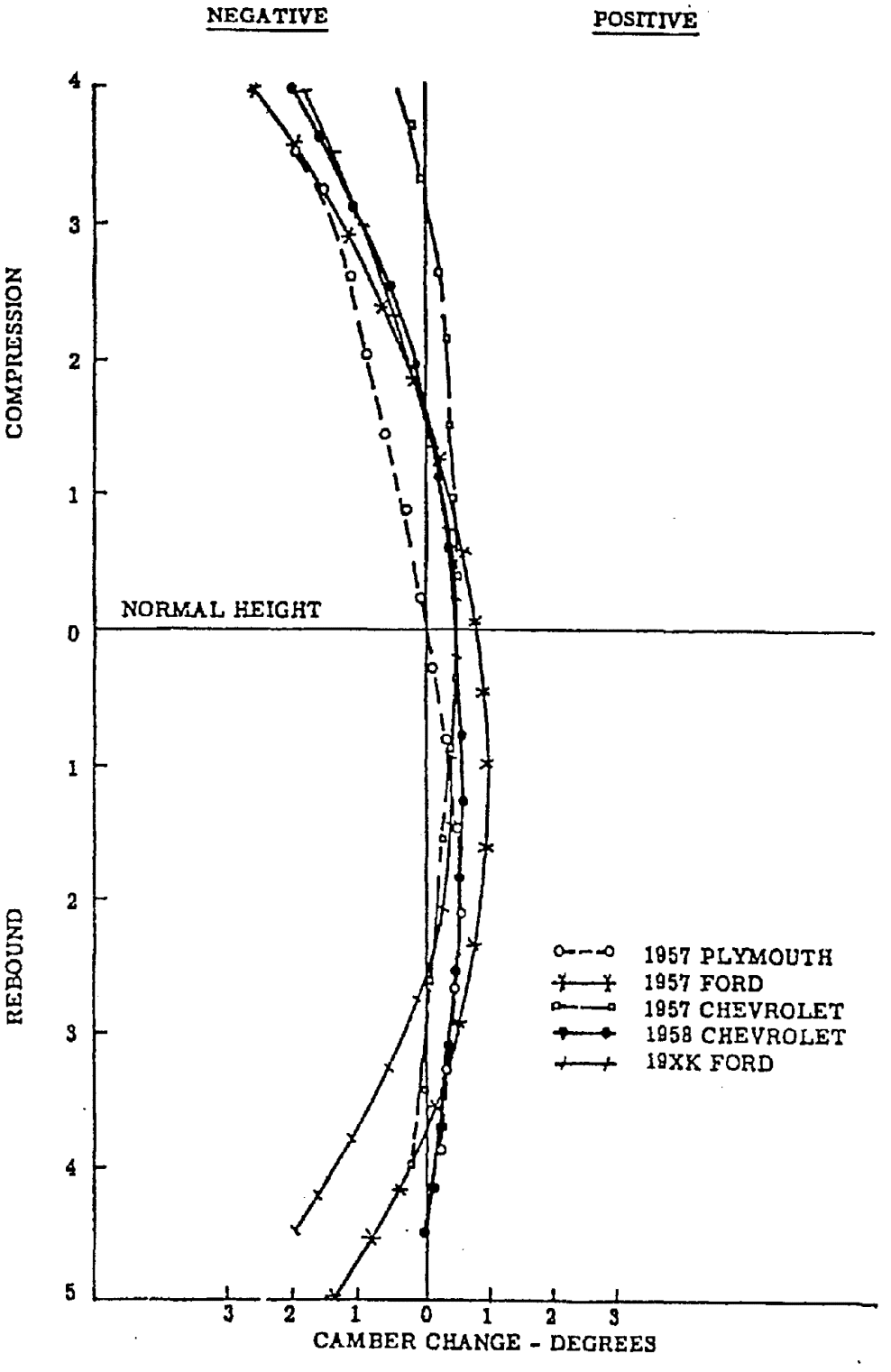

Figure C-4. Camber Change vs. Suspension Position

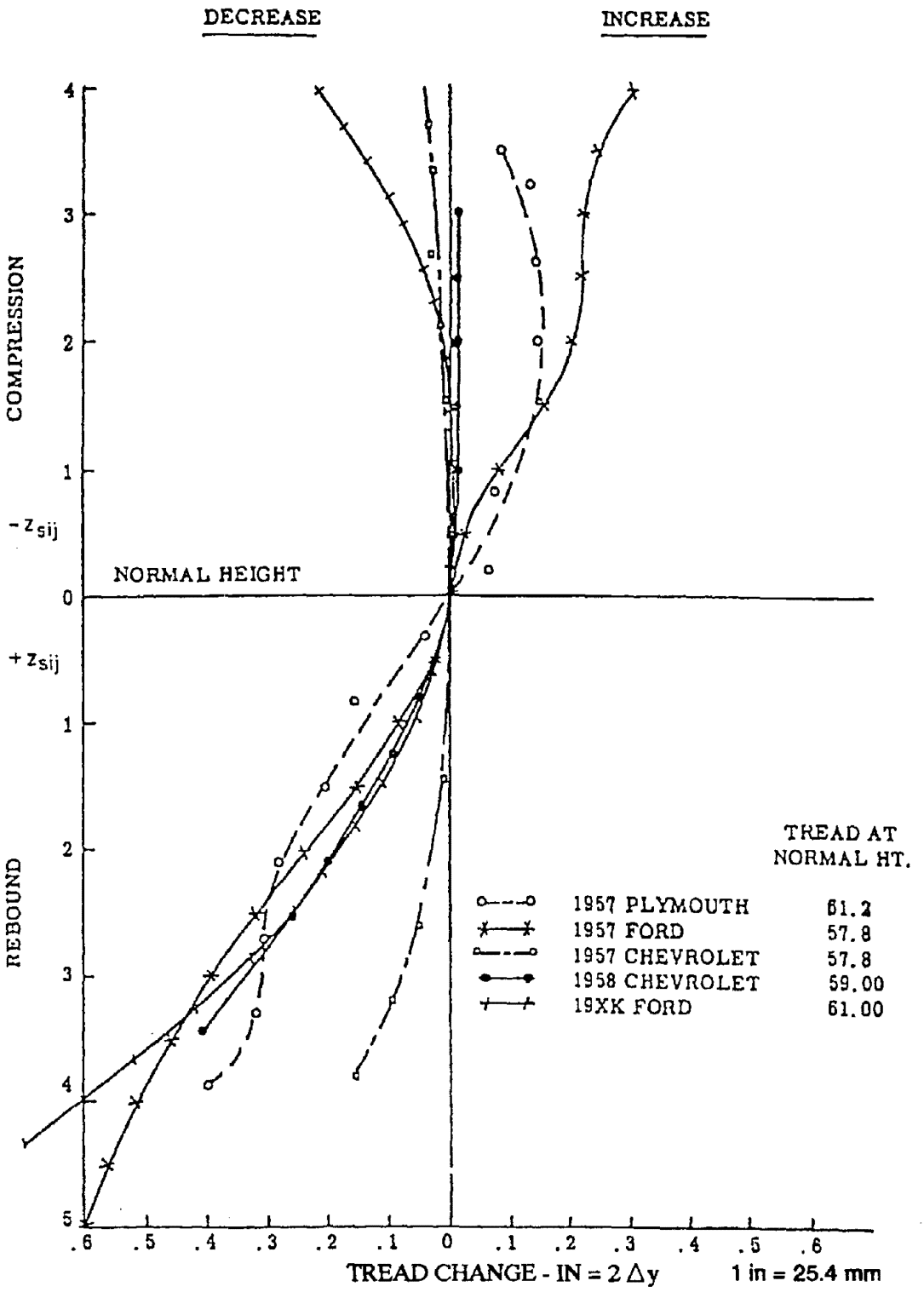

Figure C-5. Tread Change vs. Suspension Position

These squat/lift effects apply only to independent suspensions. It should be explained here, tha t solid axles transmit lateral forces via a well defined roll axis pivot, such that the equations of motion rely on roll axis height parameters to define force application points. Whereas independent suspensions do not have a centrally located roll axis pivot for lateral force application. Rather, these independent suspensions have tires that apply side forces at ground level, so that the roll axis for the equations of motion is set = zero. When independent suspensions are given a specific geometry that produce the effect of an elevated roll axis, what really happens is that the force reactions are carried via suspension squat/lift forces, but not as a force at some imaginary roll axis height and K_{SLj}, is;

$$\text{roll axis height} \quad = \quad K_{SLj}\frac{T_j}{2}$$

These parameters can be obtained from static test data by measuring lateral movement of tire contact patch vs. forced vertical motion of the sprung mass.

An alternative is to measure all suspension component pivot locations and link lengths. Then reconstruct the suspension on graph paper, and by plotting the linkage motions on paper, determining the path of the tire contact patch. An example of this is shown in Figure C-6, where K_{SLj} and L_{SAj} are identified.

Thus, for independent suspensions, K_{SLj} and L_{SAj} must be estimated, while h_{RAj} is set = zero.

And for solid axle and beam axle suspensions, $K_{SLj} = 0$ and L_{SAj} is set to a very large number (1,000) to remove this effect, and h_{RAj} set = to actual roll axis height.

21. K_{SADF}
22. K_{SADR}
23. K_{SAD2F}
24. K_{SAD2R}

These are for the suspension squat/lift functions with longitudinal forces.

These are effects in suspension squat/lift, similar to reactions to lateral forces (in preceding pages), but here are in reaction to longitudinal forces. In this case, we will only use the primary effects of the tire contact patch motion slope, and ignore the insignificant effects due to path curvature.

Static testing for this data would be very difficult. Therefore, it is recommended that graphical representations of the suspensions in the side view be used. By showing the direction of motion of the suspension components in the side view, the motion of the tire contact patch can be projected. The K_{SADi} parameter is the slope of this tire patch path away from pure vertical. Figure C-7 shows some examples of graphically determining K_{SADj} for solid axle and independent suspensions.

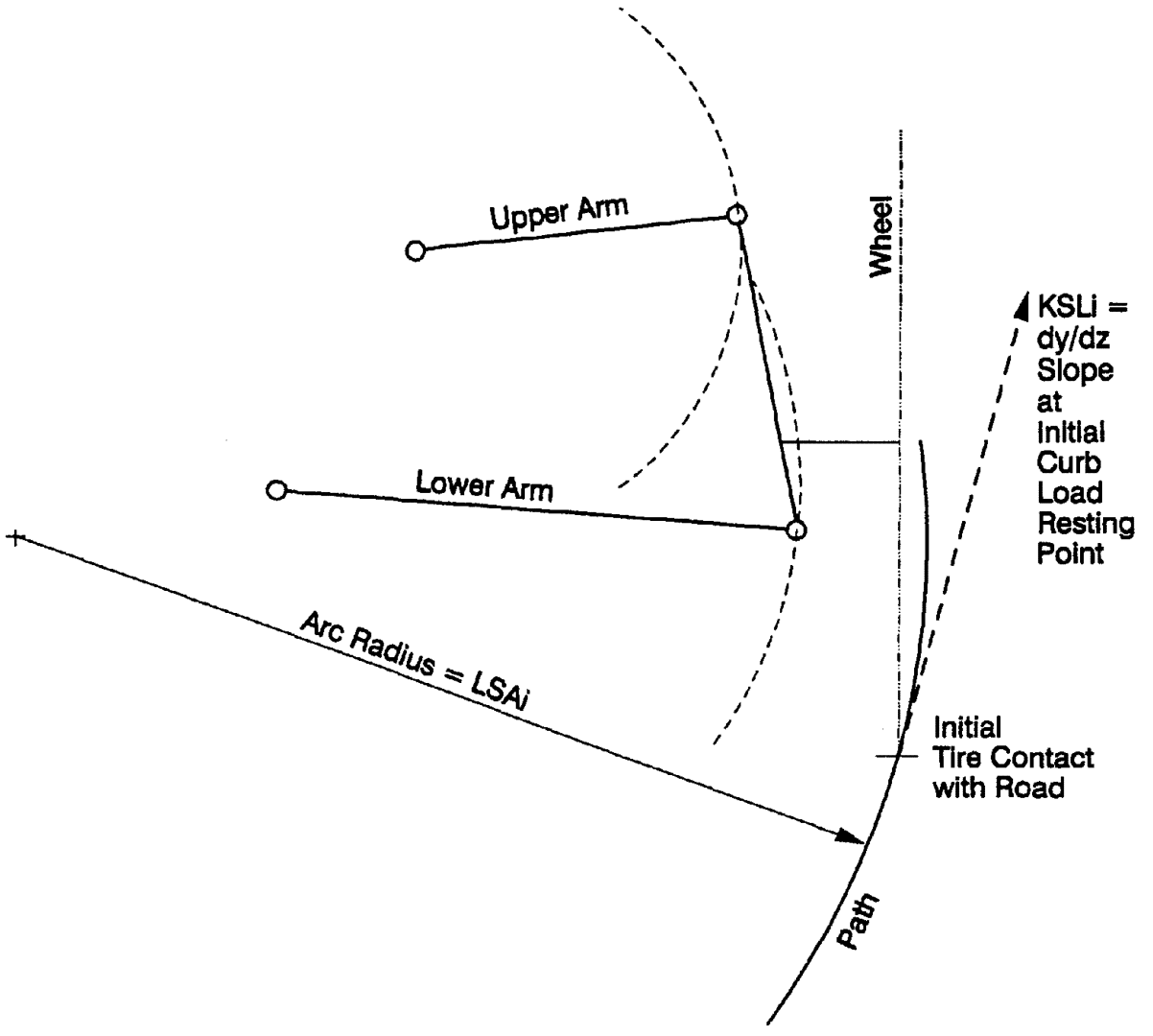

Layout of each suspension member is drawn in to scale from measurements taken according to page C-9. Then move 3 bar linkage to generate curved path at tire contact point.

Figure C-6. Suspension Geometry Plot of Motion

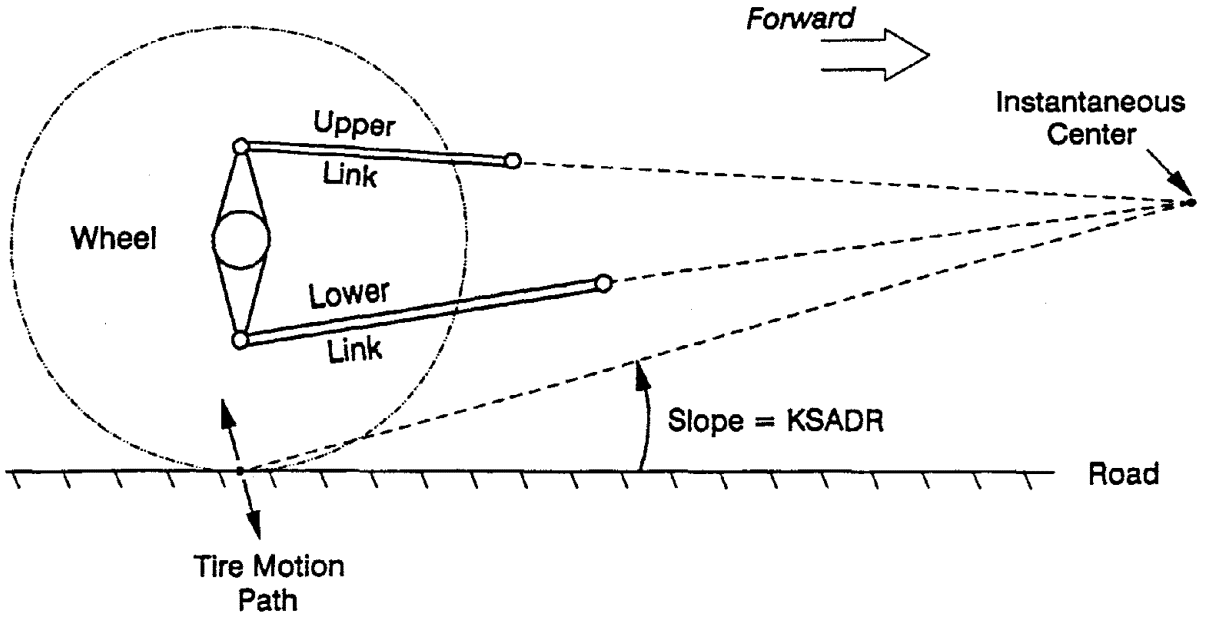

Side View of Solid Axle Rear Suspension

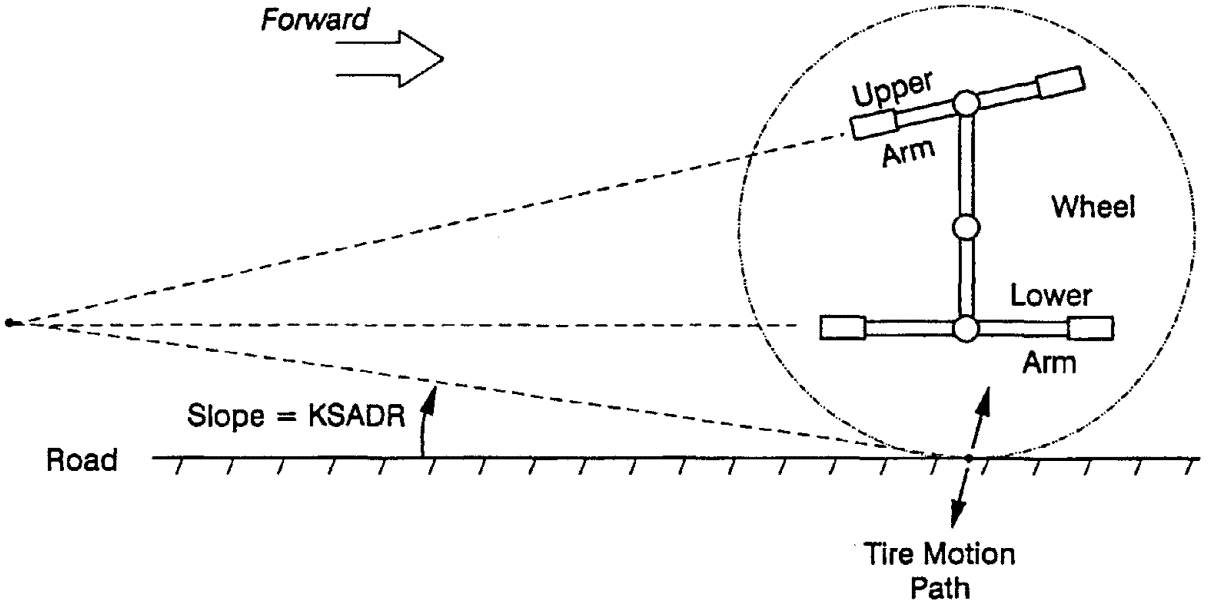

Side View of Independent Front Suspension

Figure C-7. Suspension Geometry Plot of Motion

Finally it needs to be pointed out that the K_{SADj} parameters apply to cases where brake torque is applied and reacted to by the suspension members. Also for engine power applied to a solid axle, where the reaction torque is taken by the suspension.

A special case arises when applying engine power via an independent suspension, where the reaction torque is taken by the sprung mass mounted differential gears. In this case, the only force on the suspension is the drive thrust applied at the wheel axle center. Therefore, the applicable slope for this case is the motion path of the wheel center, and is utilized in the VDANL input file as the K_{SA2Dj} parameters. These come into play whenever engine power application is called for with an independent suspension.

25. K_{ACK}, this controls the difference in δ_{WLF} *vs.* δ_{WRF} due to Ackerman steer geometry.

This is explained and developed in Appendix A. For most straight away high speed handling test runs, the steering angle levels are too small to result in any significant Ackerman steer effect. So that for these cases, parallel steering can be assumed and K_{ACK} set = zero. For low speed maneuvering, Ackerman steering might have some effect, and K_{ACK} can be set by the following method.

From the steering ratio test described in appendix E, the steer angles of the front wheels when the steering wheel is turned 360° to the right, can be used in the following formula to estimate K_{ACK}. With Ackerman steering, the right hand wheel normally turns to a larger angle than the left-hand wheel, for a right hand turn.

$$K_{ACK} = \frac{2\left(\delta_{W_{RF}} - \delta_{W_{LF}}\right)}{\left(\delta_{W_{LF}} + \delta_{W_{RF}}\right)^2}$$

26. K_{BSEF}
27. H_{BSEF}
28. S_{BSEF}
29. K_{BSCR}
30. H_{BSCR}
31. S_{BSCR}
32. K_{BSER}
33. H_{BSER}
34. S_{BSER}

These are for the suspension bump stop model.

The bump stop model in nonsymmetric, and nonlinear. The H_{BSdj} parameters are the contact points with the compression ($d = C$) and extension ($d = E$) bump stops. K_{BSdj} are the terminal stiffnesses of the bump stops, and S_{BSdj} are shaping parameters that control how quickly the stiffness of the bump stop approaches K_{BSdj}.

The bump stop force F_{BSij} is given by:

$$If\ z_{Sij} > -H_{BSCj}\ then$$

$$F_{BSij} = \left(-H_{BSCj} - z_{Sij}\right) \cdot K_{BSCj} \cdot \left(1 - e^{\left(S_{BSCj} \cdot \left(z_{Sij} + H_{BSCj}\right)\right)}\right)$$

$$Else\ If\ z_{Sij} > -H_{BSEj}\ then$$

$$F_{BSij} = \left(H_{BSEj} - z_{Sij}\right) \cdot K_{BSEj} \cdot \left(1 - e^{\left(S_{BSEj} \cdot \left(z_{Sij} + H_{BSEj}\right)\right)}\right)$$

$$Else$$

$$F_{BSij} = 0$$

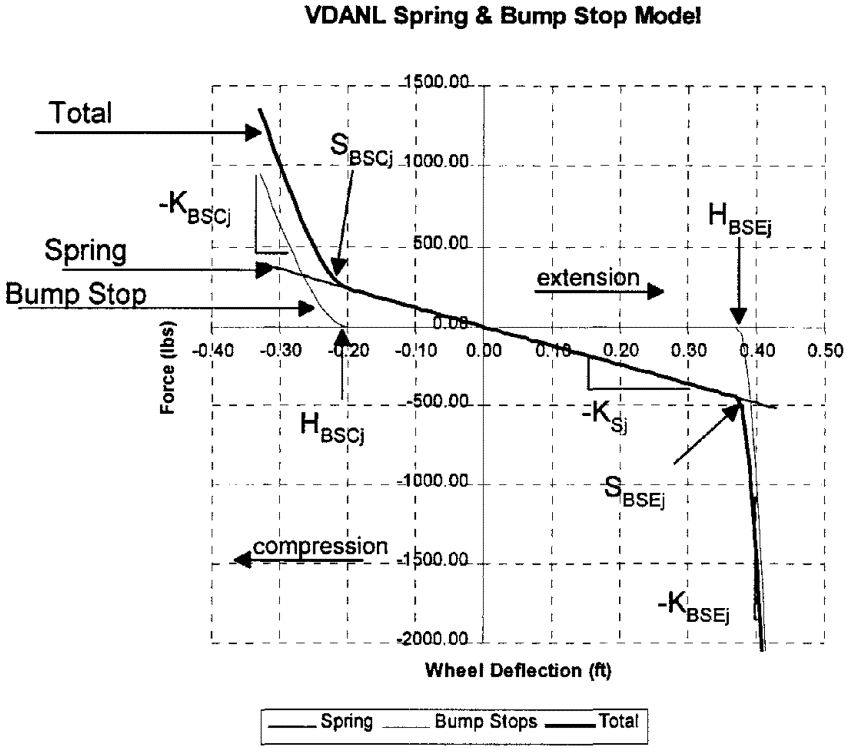

Figure C-8. VDANL Spring and Bump Stop Model Plot

APPENDIX D

VEHICLE PARAMETER MEASUREMENT TEST METHODS

A. OVERVIEW

The following methods can be used to measure vehicle parameters that are required in vehicle dynamics simulation.

1. Center of Gravity Height Test

The vehicle wheels are placed on individual platform scales, with one axle on a vehicle hoist so that it can be raised up to a significant height above ground. Measure heights and weights while level, and raised up. Because suspension deflection changes while lifting up will affect the apparent cg, height, it is necessary to measure changes in suspension height and correct for this. Figure D-1 shows the basic layout in the lifted state. Figure D-2 shows the effects of suspension deflection change on apparent cg height.

Start with car level where

$$F_{z_{F_o}} = \frac{Wb}{\ell} \text{ and } \quad F_{z_{R_o}} = \frac{Wa}{\ell}$$

With one end of car up h_1

$$F_{z_F} = \frac{Wb\left(\cos\theta - \left[h_{cg} - R_W\right]\sin\theta\right)}{\ell\cos\theta}$$

$$\Delta F_z = F_{z_{F_o}} - F_{z_F} = \frac{W}{\ell}\left[h_{cg} - R_W\right]\tan\theta = \frac{W}{\ell}\left[h_{cg} - R_W\right]\frac{h_1}{\sqrt{\ell^2 - h_1^2}}$$

or $$h_{cg} = \frac{\left(\Delta F_z\right)\ell\sqrt{\ell^2 - h_1^2}}{Wh_1} + R_W$$

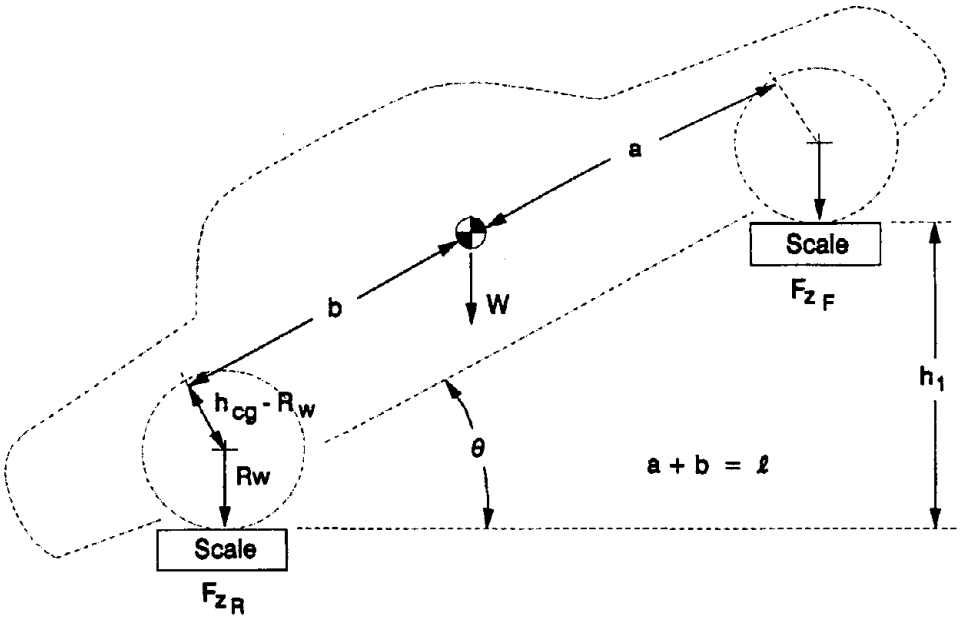

Figure D-1. Center of Gravity Height Test

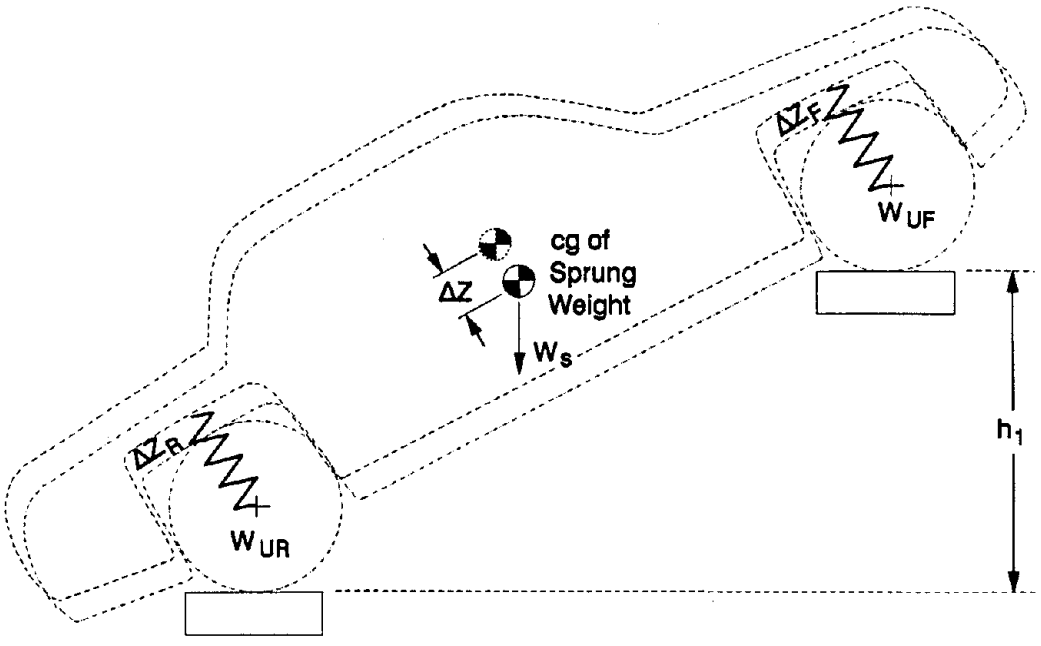

Figure D-2. Correction for Effects of Suspension Extension When One Axle is Raised Off the Ground

ΔZ_F = Change in front suspension riding height

ΔZ_R = Change in rear suspension riding height

ΔZ = resultant change in height of sprung mass cg

$\Delta Z = Z_{i_2} - Z_{i_1}$, where Z_i is measured from fender opening down to bottom of wheel rim

a = horizontal distance W_s cg to front axle

b = horizontal distance of W_s cg to rear axle

ℓ = wheelbase length

W_s = sprung weight = $S - W_{UR} - W_{UF}$

W = total weight

Therefore, the following equations can be used to compute the cg height.

$$\Delta_Z = \Delta Z_F\left(\frac{b}{\ell}\right) + \Delta Z_R \frac{a}{\ell} \tag{D-1}$$

Thus, the actual test data are for a cg height that is higher than normal because W_s center of mass was higher by ΔZ.

$$\text{Test } h'_{cg} = \frac{W_s(h_s + \Delta Z) + (W_{UF} + W_{UR})R_W}{W}$$

$$\text{True } h_{cg} = \frac{W_s h_s + (W_{UF} + W_{UR})R_W}{W} \tag{D-2}$$

$$\therefore \text{ True } h_{cg} = \text{Test } h'_{cg} - \frac{W_s\ \Delta Z}{W}$$

$$\text{True } h_{cg} = \frac{(\Delta F_Z)\ell\sqrt{\ell_2^2 - h_1^2}}{W h_1} + R_W - \frac{W_s\ \Delta Z}{W}$$

where ΔF_z is changed in F_Z at either axle, which can be an average of the change at the front axle and at the rear axle.

h_1 = change in height of lifted axle

R_W = wheel/tire radius under curb load

a, b, W_s are values for the sprung weight, which differs slightly from total weight values. These can be estimated using the following equations:

$$\frac{a W_s}{\ell} = W_R - W_{UR}$$

$$W_s = W - W_{UF} - W_{UR} \qquad \text{(D-3)}$$

$$a = \frac{(W_R - W_{UR})\ell}{W - W_{UF} - W_{IR}}$$

$$b = \ell - a \qquad \text{(D-4)}$$

and the unsprung weights can be estimated from equations based on typical data

$$W_{Ui} = 32.2 + .045W \qquad \text{(D-5)}$$

if the drive train differential is carried in the sprung weight

$$W_{Ui} = .08W \qquad \text{(D-6)}$$

if the axle differential is carried in the unsprung weight.

2. Roll Stiffness Test

For this test, a moment is applied to the sprung mass, and the reaction moment at each axle is measured by the changing load at the individual scales each wheel is resting on. The sprung mass roll angle is measured independently. The slope of the plotted data is the overall roll stiffness at each axle (K_{orsi}), with the tire spring rate included. Figure D-3 shows the experimental setup and computations to obtain data for plotting. Figure D-4, and Figure D-5 show a sample of plotted test data.

3. Steering Compliance Test

With steering wheel clamped in straightahead position, with the engine running for power steering, apply pure moments to one front wheel about its steer axis, in 44.4 newton (10lb) pull increments, as shown in Figure D-6. Then reverse the procedure back to zero pull.

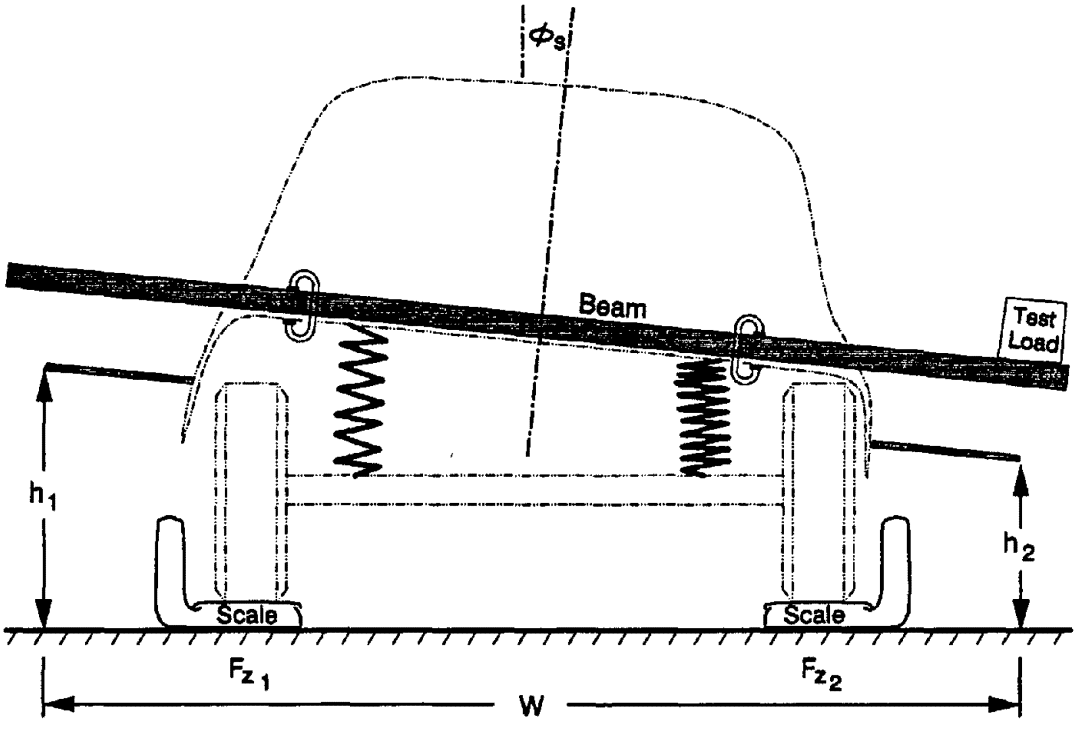

Beam is clamped solid to body, to support test load

Since the beam bends under load, a separate rod is attached to body to measure h_1, h_2 above ground

Test load is constant, but is shifted from right to left and back again, in small increments

h_1 , h_2 is measured at each load position, and wheel loads on scales also recorded

$$\text{Roll Angle} = \frac{h_1 - h_2}{W} = \phi$$

$$\text{Roll Moment (per axle)} = (F_{z_1} - F_{z_2}) \frac{\text{Track}}{2} = M_x$$

Plot M_x vs ϕ

Slope of $dM_x/d\phi$ = overall roll stiffness including tires, per axle

Figure D-3. Roll Stiffness Test

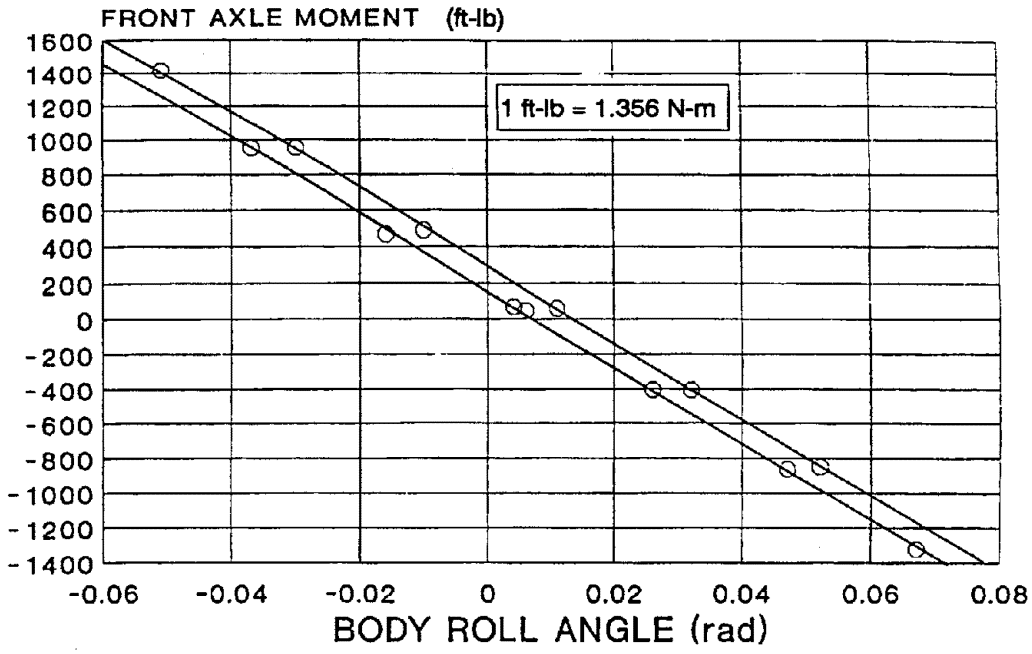

Figure D-4. Front Axle Roll Stiffness for Datsun 200SX
(3060/ .14 = 21,850)

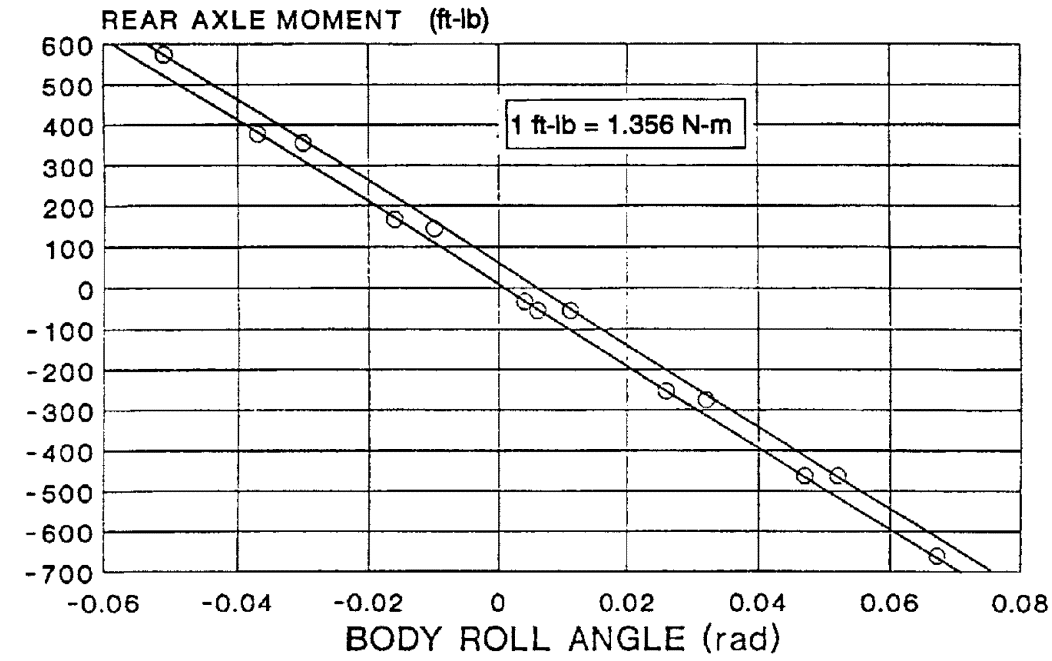

Figure D-5. Rear Axle Roll Stiffness for Datsun 200SX
(1400/ .14 = 10,000)

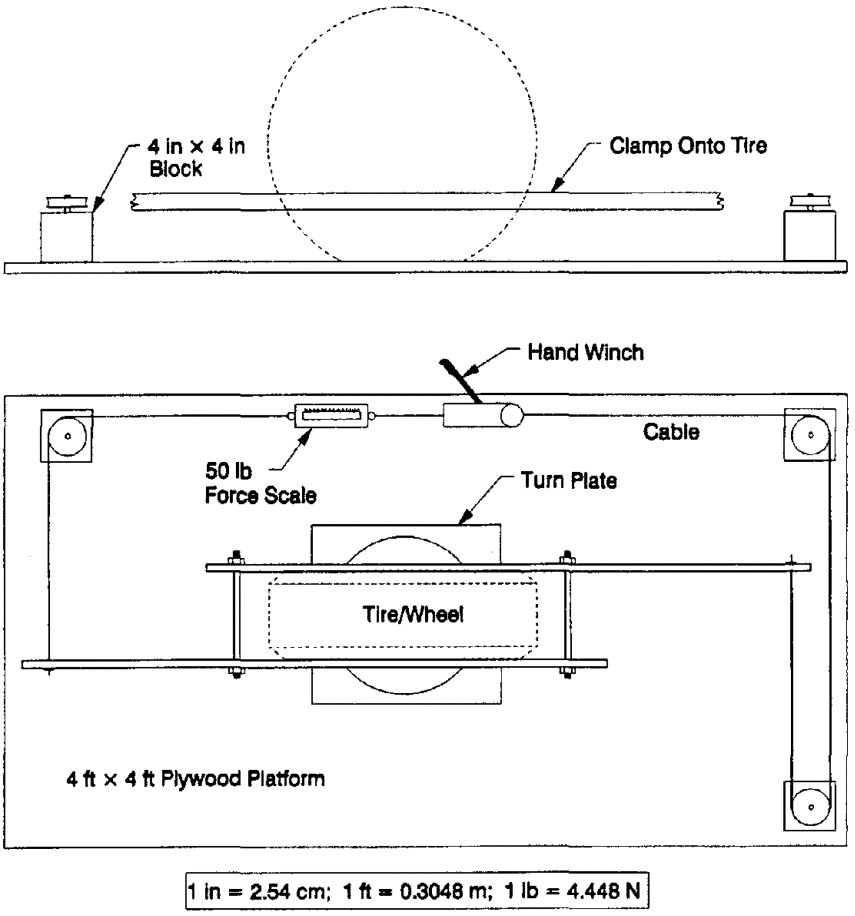

Figure D-6. Steering Compliance Test for Drive

Read the pull scale force and steer angle of the opposite tire, and the length of moment arm from cable end to cable end. The steer angle deflection must be read at the wheel without the clamped load on it because the wheel with the clamped load on it will have tire casing deflection that can add up to 5° more angle at the turn plate than is true for the wheel angle only.

The resulting data plot of moment vs. angle will have a hysteresis loop because of steering free play and friction in the system. The hysteresis is to be ignored, and only the consistent slope used for estimate of steering compliance.

$$K_{sc} = \frac{d\,\delta W}{d\,m_W}$$

An example of plotted data is shown in Figure D-7.

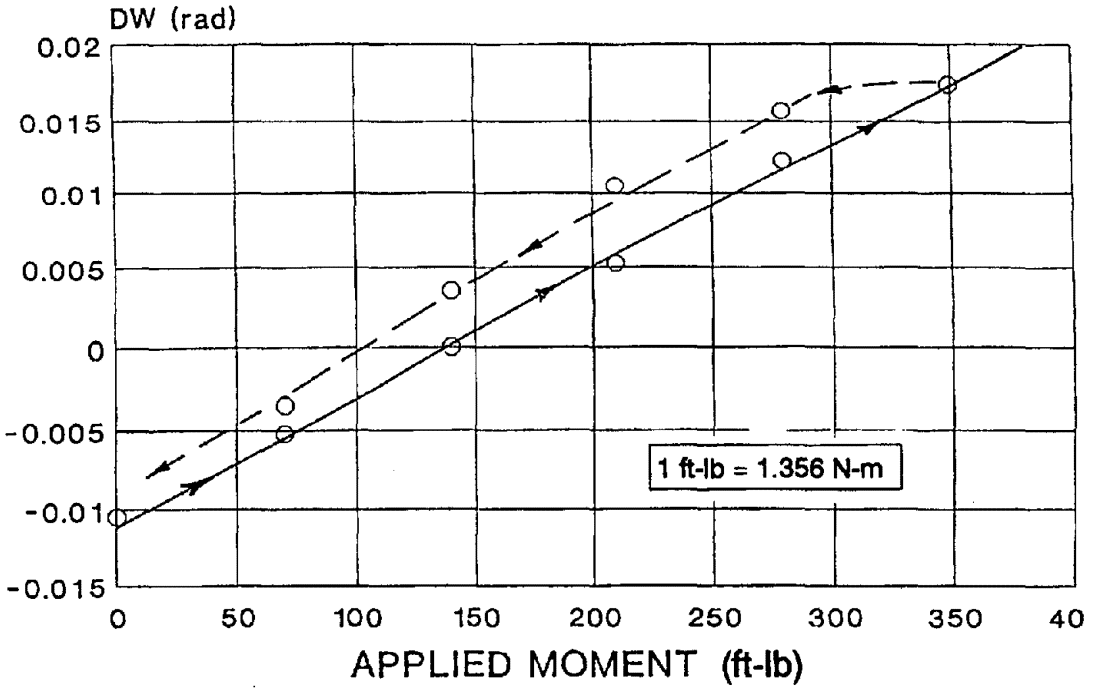

Figure D-7. Steering Compliance Test for Datsun 200SX
(.02/ 250 = 00008)

4. Suspension Geometry Measurements

The *X, Y, Z* locations of the suspension pivots are measured as shown in Figure D-8, Figure D-9, Figure D-10 and Figure D-11. These dimensions are then used in the suspension geometry parameter estimation procedures described in Appendix C. This converts raw dimensions into parameters for composite suspension geometry functions that are used in the vehicle dynamics simulation model described in Appendix A.

Of the many types of suspensions, of that the most common are shown in Figure D-12 and Figure D-13. On some of these, the pivot locations have different implications for the composite function parameters, and this is explained in Appendix C.

5. Steering Ratio Test

The steering ratio is moved in increments of 90° to ±360° and both front-wheel angles are measured on ball-bearing free turn plates. The engine is running for power steering. The slope of the averaged data gives the overall steering ratio. An example of plotted data is shown in Figure D-14.

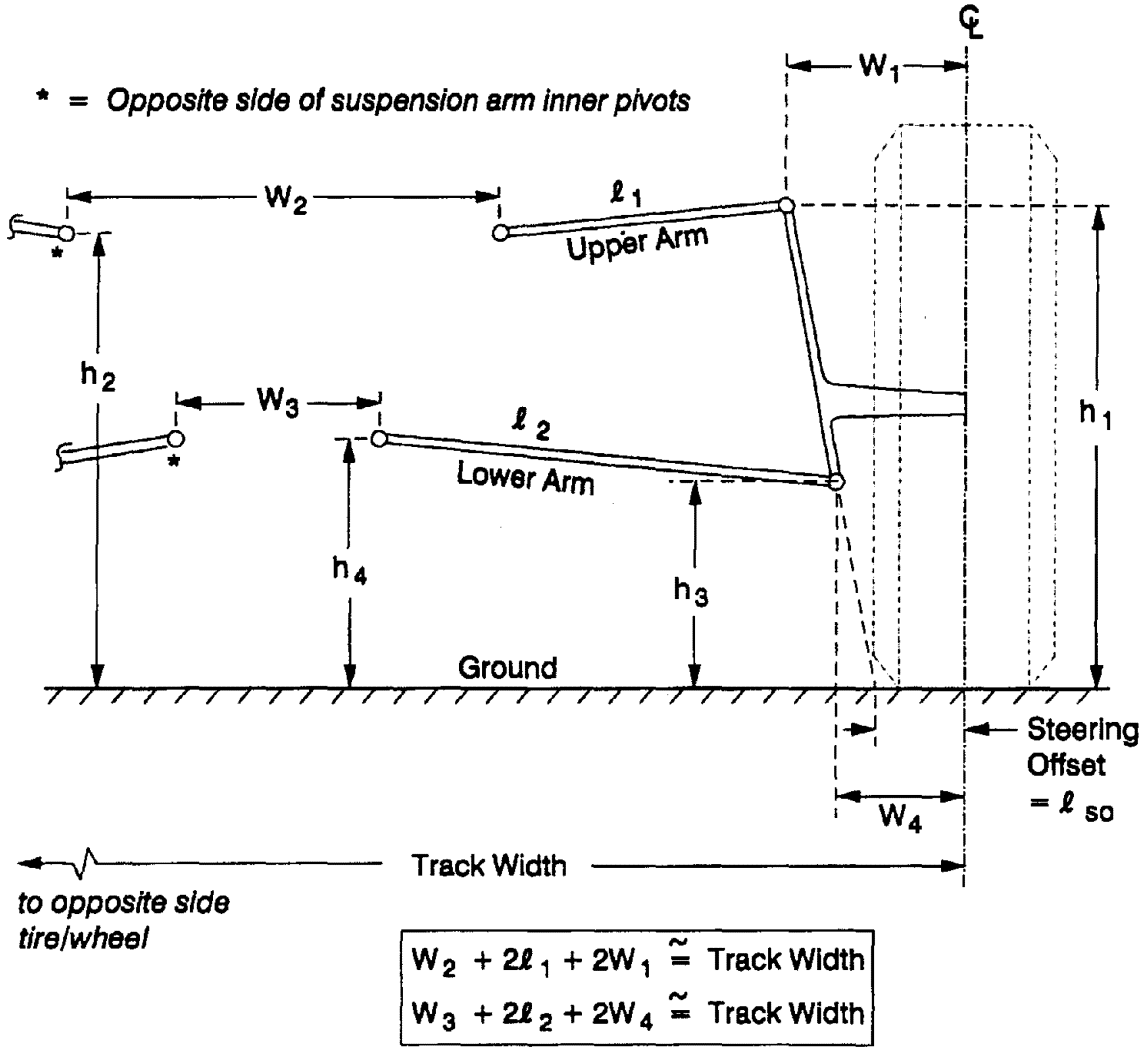

Mcphearson strut suspensions are identical, with the upper arm ball joint pivot at W_1, h_1 now becoming the location for the upper mounting point of the strut, and $\ell_1 = \infty$ in length and at 90° to the spindle/strut line

Figure D-8. Measurements to be Taken on the Vehicle's Suspension Components, From Front View

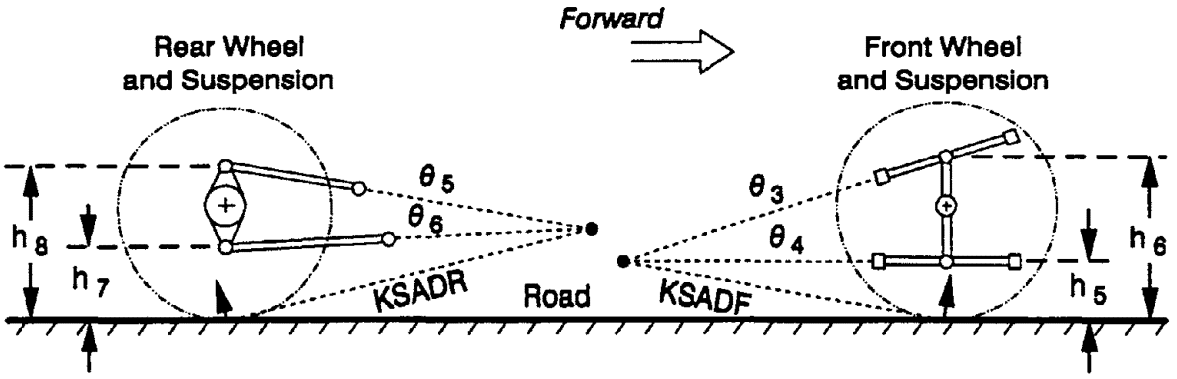

The vertical dimensions of all suspension arms and linkages need to be measured in order to identify the dx/dz path (slope) of wheel spindle ball joints or axle pivot points, (θ_i). From these, the slope or dx/dz of the tire contact point path can be calculated (assuming a brake-locked wheel). KSADF is the slope of the line shown from the instantaneous center to the tire contact point, for the front wheel, (positive value as shown). KSADR is slope for rear. The θ_3, θ_4, θ_5, θ_6 are all positive, if the line shown is going upwards toward the wheel.

$$\text{then} \quad \text{KSADF (slope)} = \frac{h_5\,\theta_3 - h_6\,\theta_4}{h_6 - h_5}$$

$$\text{KSADF (slope)} = \frac{h_7\,\theta_5 - h_8\,\theta_6}{h_8 - h_7}$$

Figure D-9. Measurements to be Taken on Vehicle's Suspension From Side View

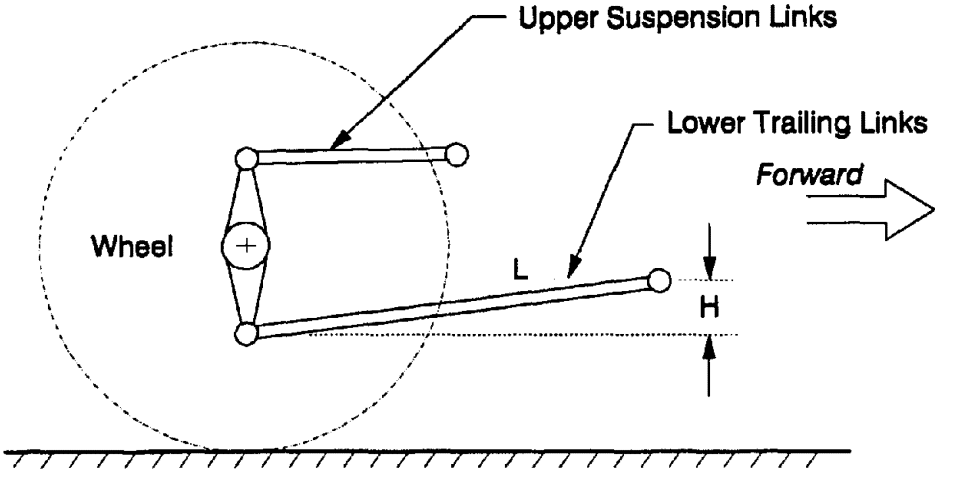

Typical axles have two trailing links that control the axle steer angle during body roll, and the side-view slope (H/L) gives the roll steer coefficient for this axle:

L = length of trailing link
H = height of front pivot above rear pivot

Figure D-10. Measurements to be Taken for Solid or Beam Axle Roll Steer Functions

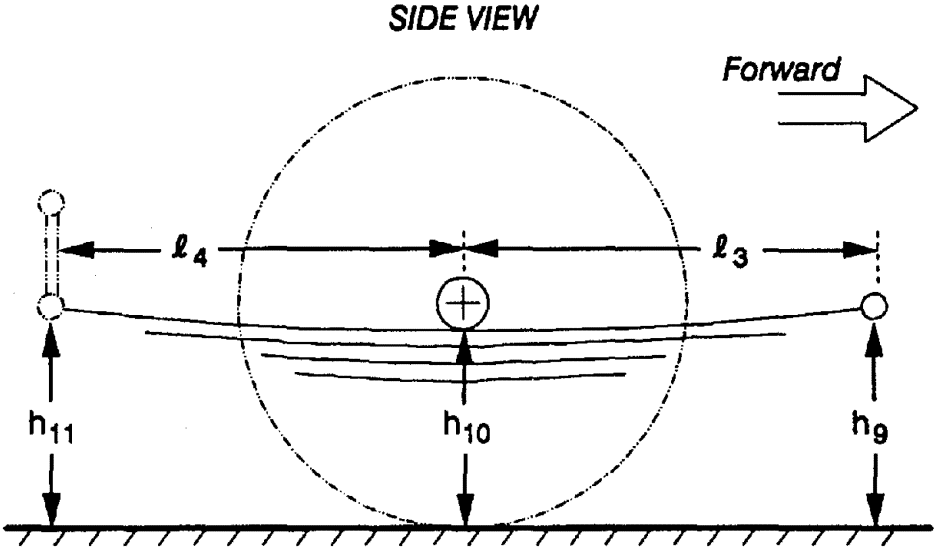

Figure D-11. Special Case for Leaf Spring on Solid Axle Suspension

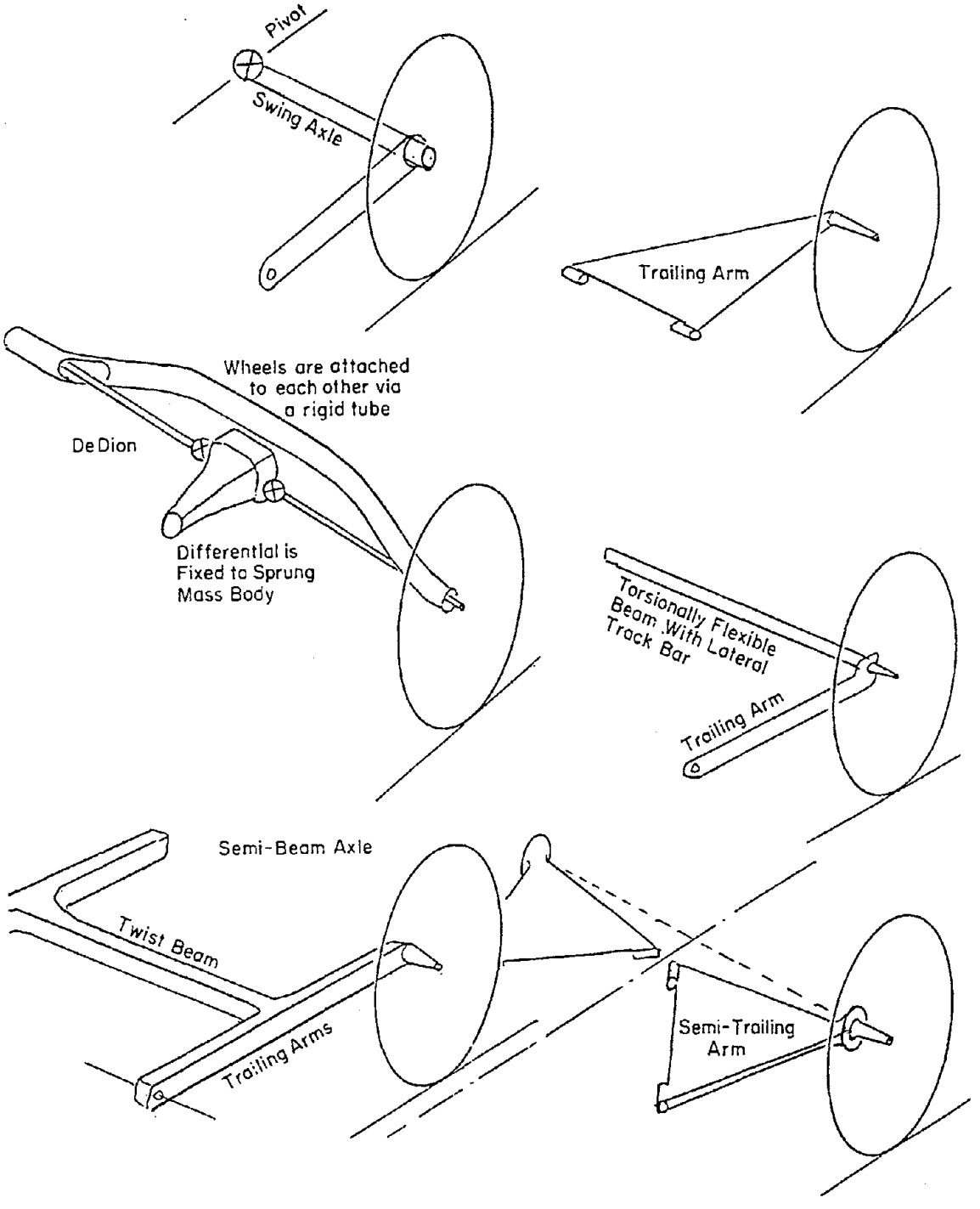

Figure D-12. Typical Examples of Suspension Geometry Layouts

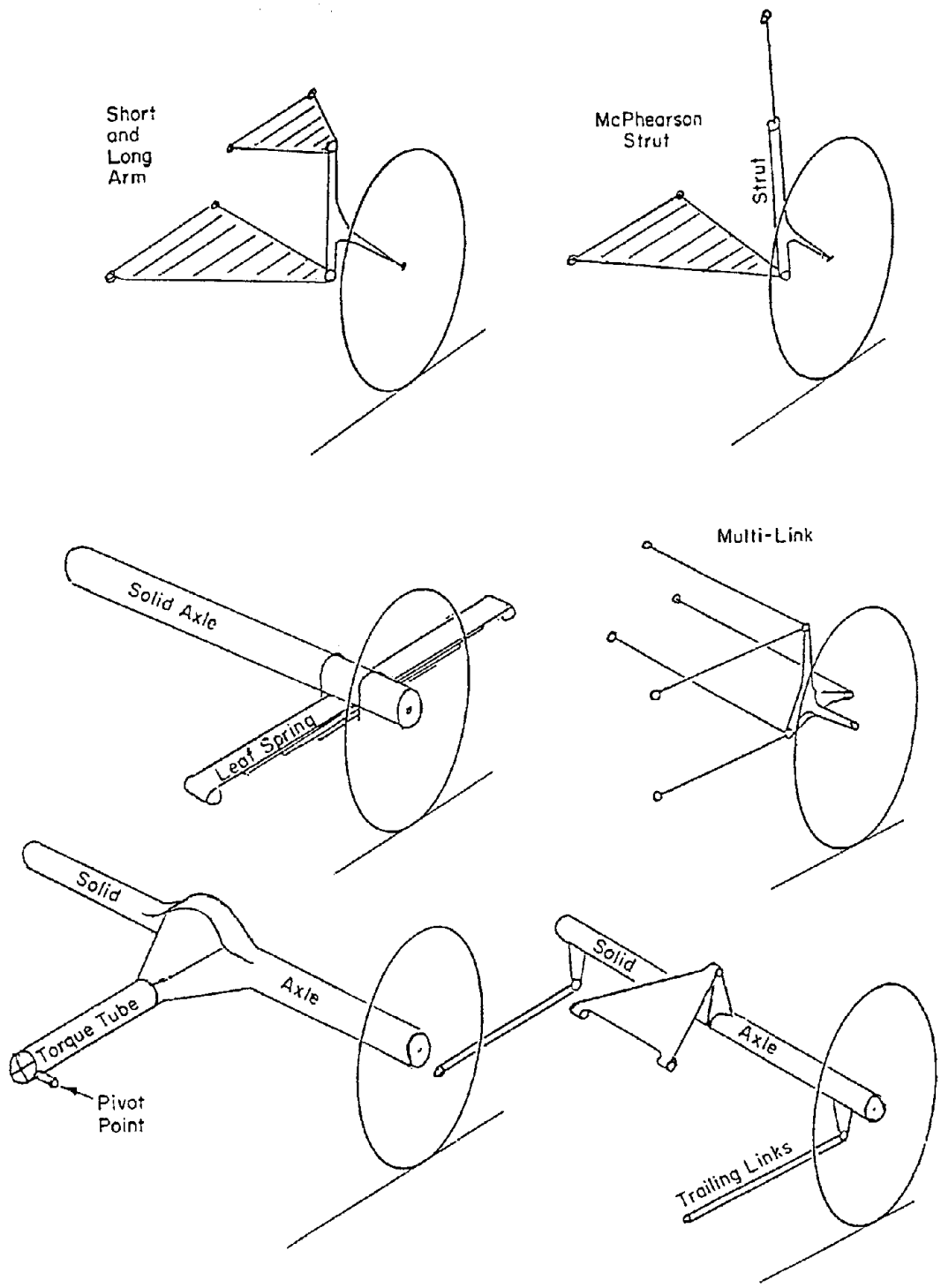

Figure D-13. Typical Examples of Suspension Geometry Layouts

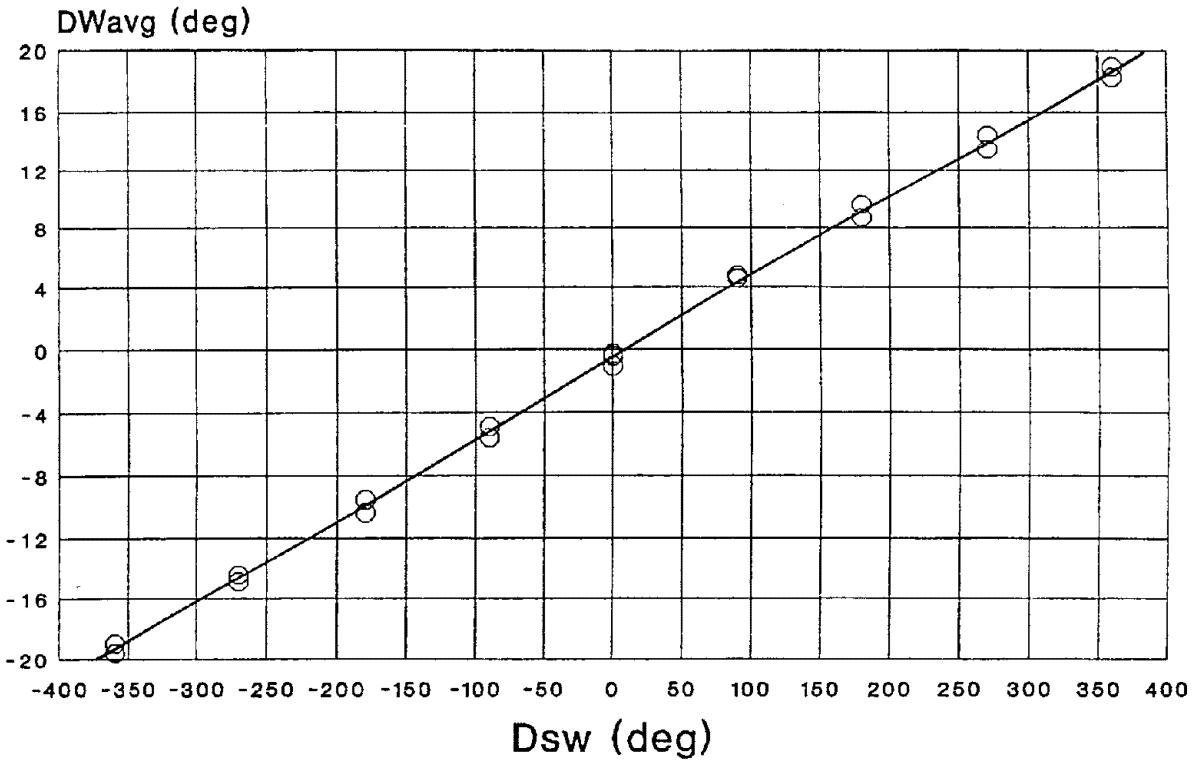

Figure D-14. Steering Ratio Test for Datsun 200SX
(800/43.3 = 18.5)

6. Suspension Spring Rate Test

The suspension is moved up and then down about ± .0.5m by loading and unloading the vehicle sprung mass. Changes in wheel loads are recorded from individual wheel platform scales, and changes in suspension deflection are measured between each wheel and fender. The averaged data slope gives the equivalent suspension spring rate at the wheel. The tire spring rate is not involved here. An example of plotted data is shown in Figure D-15 and Figure D-16.

7. Vehicle Weight and Longitudinal cg Location

Individual wheel loads are measured by individual platform scales, with empty vehicle (curb load) but with a full gas tank.

$$a = \frac{(\text{weight on rear axle})\ell}{\text{total weight}}$$

$$b = \frac{(\text{weight on front axle})\ell}{\text{total weight}}$$

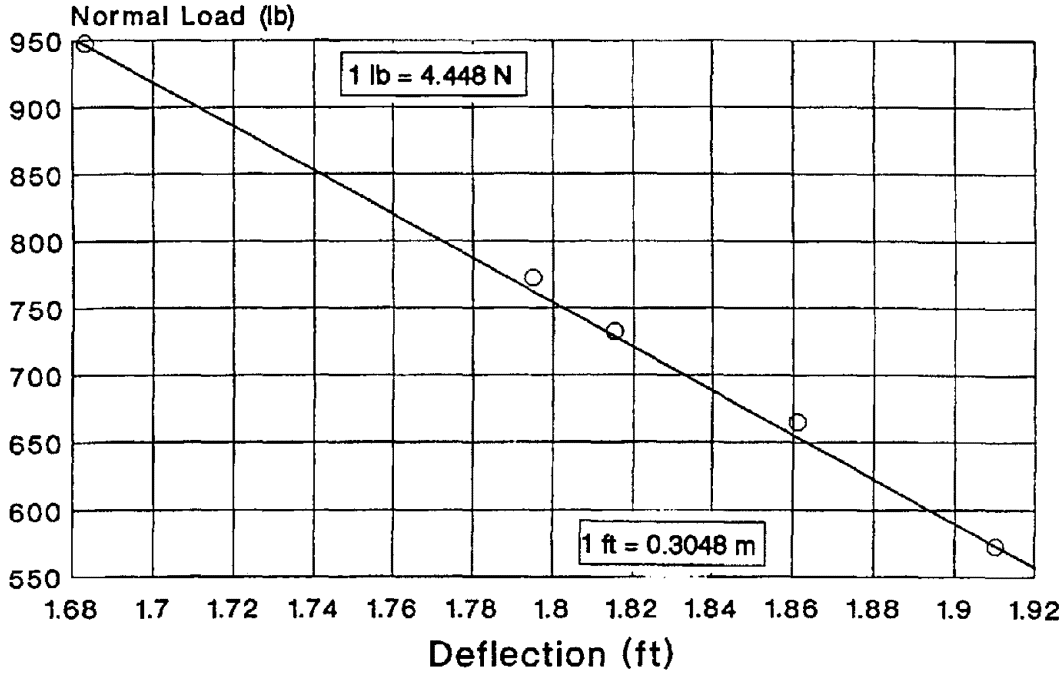

Figure D-15. Front Suspension Spring Rate for Datsun 200SX

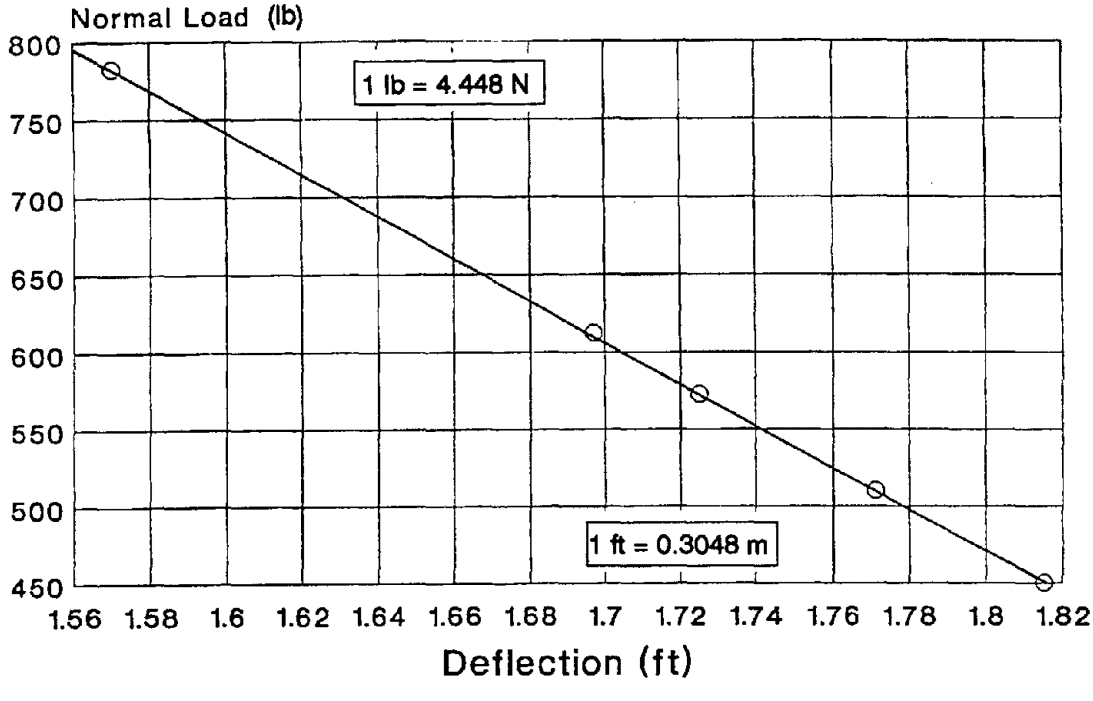

Figure D-16. Rear Suspension Spring Rate for Datsun 200SX

8. **Track width** is measured from tire center to tire center, for each axle.

9. **Wheelbase** is measured from front wheel center to rear wheel center, and averaged for both sides.

10. **Tire loaded radius**, at curb load, is measured from wheel center to ground, and averaged for the four wheels.

11. **Spring base width** is measured whenever there is a solid or beam axle suspension.

12. **Roof height** is measured from the highest point on the roof to the ground.

APPENDIX E

STIREMOD – THE VDANL TIRE MODEL

A. OVERVIEW

This appendix describes a tire model designed for the full range of operating conditions under both on- and off-road surface conditions. The operating conditions include longitudinal and lateral slip, camber angle, and normal load. The model produces tire forces throughout the adhesion range up through peak coefficient of friction, and throughout the saturation region to limit slide coefficient of friction. Beyond the peak coefficient of friction region, the off-road portion of the model simulates plowing of deformable surfaces at large side slip angles, which can result in side forces significantly above the normal load (e.g., equivalent coefficients of friction greatly exceeding unity).

The model allows changing the saturation function depending on the surface currently encountered by a given tire in the vehicle dynamics model. Saturation functions can vary from the sharp peak function associated with radial tires on paved surfaces to the exponential-like saturation associated with various off-road surfaces. Smooth transition functions are provided between the adhesion and saturation regions, and logic is provide to ensure that tire force always opposes slip velocity no matter what operating condition is encountered.

This appendix describes the model functional characteristics and response to a range of operating conditions. Data sources for the model are discussed. Cases are run with a vehicle dynamics model to illustrate model response to changing surface conditions.

B. INTRODUCTION

The basic purpose of the tire modeling discussed in this Appendix is to provide appropriate tire/surface forces for vehicle dynamics simulation. To this extent, the model must account for tire input conditions defined by surface characteristics and motions, loads, and orientations defined at individual wheels. Given these input conditions the tire model must then produce forces in each local wheel/terrain plane that will be applied to the vehicle dynamics. Tire modeling for paved surfaces is a relatively mature discipline [e.g., (Refs. E.1 to E.7)]. Modeling off-road tire characteristics through the full range of operating conditions, particularly in combination with paved surface behavior, has had limited attention, e.g., (Ref. E.8).

In addition to describing a model for paved surfaces (Refs E.6 and E.7), this appendix will discuss extensions for approximating forces on unpaved surfaces as developed by Metz (Ref. E.8). Tire modeling for unpaved surfaces is useful for the analysis of highway vehicle dynamics during shoulder and side slope

incursions, and for the analysis of off-road vehicle dynamics under a range of surface conditions. The general vehicle dynamics problem involving varying surface conditions requires knowledge of the location of each tire and setting tire model parameters according to the local tire/surface conditions. This generally involves a change in the lateral and longitudinal force versus slip characteristics, high lateral forces under high load, high slip angle, loose soil conditions where a tire can dig in or bull doze the surface.

Some background will be given next for current modeling approaches for paved and unpaved surfaces. Subsequent sections will then discuss the details of an on-road/off-road tire model and means for establishing typical model parameters.

C. BACKGROUND

Paved surface tire modeling has been reasonably well developed over the past two decades (Ref. E.1 to E.7). The general characteristics that have been modeled are summarized in Figure E-1. Generally these characteristics involve force versus slip functions in the adhesion region, peak coefficient of friction as the tire reaches saturation, and force reduction at higher post saturation slip conditions out to the limit slide coefficient of friction. Typically these characteristics are all functions of tire normal load, and can vary considerably with tire brand, size, and construction.

Tire/surface conditions can also significantly alter tire response characteristics. For example, different firm surfaces that resist deformation or shear can vary in their apparent peak and slide coefficients of friction. Examples include icy and snowy paved surfaces and firm dirt or gravel surfaces, which are summarized in Table E-1 (Ref. E.9). Beyond basic coefficient of friction, various soil conditions also result in particular force versus slip conditions as summarized by Metz (Ref. E.8).

Table E-1. Typical Tire/Surface Coefficients of Friction (Ref. E.9)

Surface	Peak Value μ_p	Siding Value μ_s
Asphalt and concrete (dry)	0.8-0.9	0.75
Asphalt (wet)	0.5-0.7	0.45-0.6
Concrete (wet)	0.8	0.7
Gravel	0.6	0.55
Earth road (dry)	0.68	0.65
Earth road (wet)	0.55	0.4-0.5
Snow (hard-packet) 0.1	0.07	
Ice	0.1	0.07

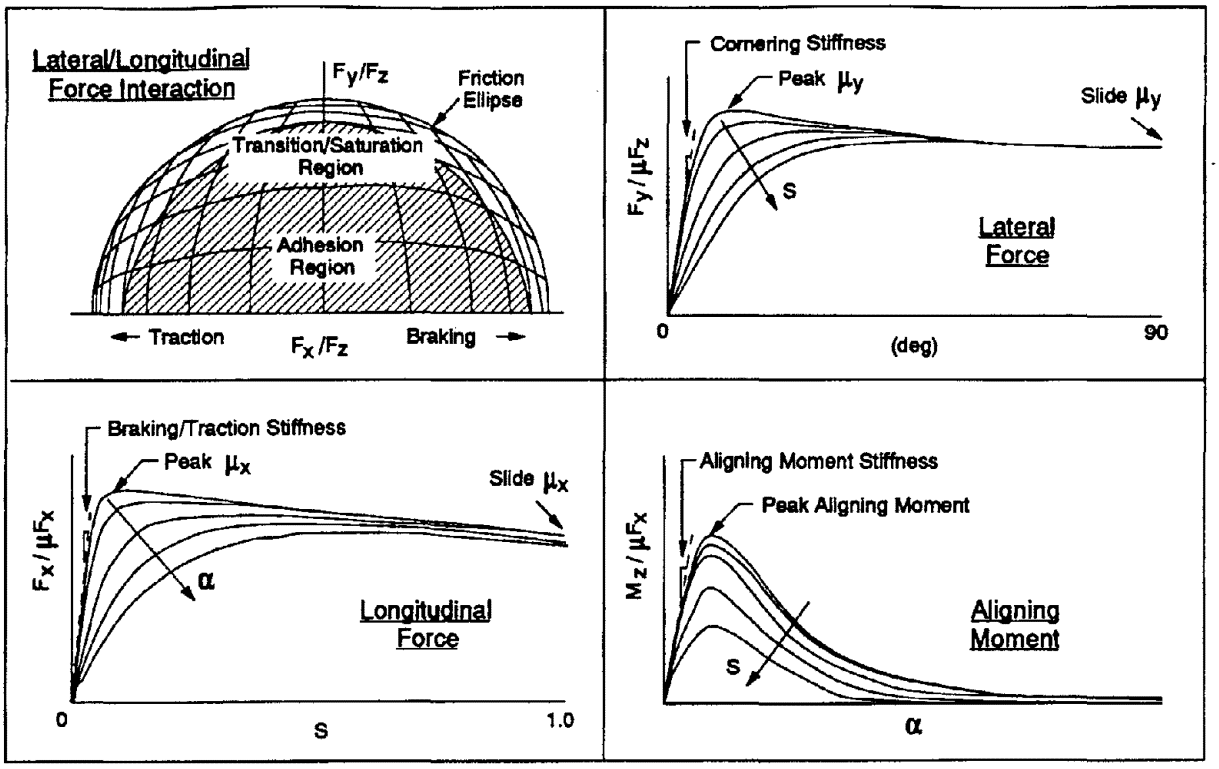

Figure E-1. Typical Tire Response Characteristics

Under soft terrain conditions, tires can also penetrate the surface-depending on the tire load and the amount of shear displacement. These effects have been analyzed by Wong and Bekker e.g., (Refs. E.9 to E.11). In this case, the tire terrain penetration results in increased rolling resistance and plowing forces due to soil displacement. The rolling resistance amounts to a force required to roll the tire forward, and is typically a function of normal load. Plowing forces occur under high side slip conditions (Refs. E.12 and E.13), and can result in apparent high lateral coefficient of friction out in the region where, on a firm surface, we would expect reduced coefficient of friction described by the limiting slide value.

Next we summarize the basic equations required to produce tire forces and moments over the full range of input operating conditions, i.e., normal load, camber, lateral and longitudinal slip, and speed.

D. BASIC MODEL

1. Adhesion Region

The basic derivation and equations for a composite slip tire model (STIREMOD) have previously been developed by Szostak (Ref. E.6 and generally derive from the developments of Sakai (Ref. E.3), Schallenmach and Grosch (Ref. E.14) and Pacejka (Ref. E.15). Without going into detail, the tire model

computes a composite slip parameter, which is a function of both tire slip angle and longitudinal slip ratio. This composite slip is then used in a force saturation function, controlled by five shaping parameters. From the force saturation function, tire lateral and longitudinal forces are computed.

The STIREMOD equations are based on a composite slip formulation, which is basically a quadratic function of lateral and longitudinal slip. Lateral slip is expressed as the ratio of the side slip velocity of the tire patch relative to the longitudinal speed of the tire patch, which is the equivalent of the tangent of the tire patch slip angle. Longitudinal slip is defined as the ratio S of the differential tire patch to ground longitudinal velocity divided by the longitudinal velocity of the wheel hub relative to the ground.

Composite Slip

$$\sigma = \frac{\pi a_p^2}{8\mu_o F_z}\sqrt{K_s^2 \tan^2\alpha + K_c^2\left(\frac{S}{1-S}\right)^2} \qquad \text{(E-1)}$$

This formulation accounts for changes in tire patch length, a_p, which is dependent on lateral and longitudinal force response:

Tire Contact Patch Length

$$a_p = a_{po}\left(1 - K_a\frac{F_x}{F_z}\right) \qquad \text{(E-2)}$$

where the initial patch length a_{po} is dependent on normal load (F_z), design load (F_{ZT}), tire width (T_w) and tire pressure (T_p):

$$a_{p0} = \frac{\sqrt{F_z \cdot F_{ZT}}}{T_W \cdot T_p}(ft) \qquad \text{(E-3)}$$

The tire patch length dependency on longitudinal force has been noted [chapters 5 (Fig. 5.75) and 8 (Fig. 8.2.65) of (Ref. E.1). The sensitivity coefficient K_a is used as a fitting parameter in STIREMOD to accommodate the asymmetrical lateral force response under traction versus braking conditions. The initial patch length formula derives from the relationship between pressure and normal load: $F_z = a_o \cdot T_W \cdot T_p$. Patch length does not vary linearly with normal load, however. Normal load is a near linear function of vertical deflection [chapter 8 (Figs. 8.2.20 to 23 in Ref. E.1), which results in a convenient linear tire spring constant. Tire patch length tends to be a square root function of vertical deflection, however [chapter 5 Figs.

5.27 and 28 in Ref. E.1 so that patch length is thus proportional to the square root of normal load $a_o \cong k_1\sqrt{F_z}$. Thus, in order to utilize this relationship while maintaining consistent units, we partition F_z so that $a_o \cong k_2\sqrt{F_z \cdot F_{ZT}}$ where F_{ZT} is the maximum tire loading. In equation E-3 the $\sqrt{F_z}$ term is assumed to vary while $\sqrt{F_{ZT}}$ remains constant.

The composite slip formulation also accounts for the relative stiffness of the tire force production between lateral and longitudinal slip. Longitudinal stiffness (K_C) is generally greater than lateral stiffness (K_S) since tires typically saturate at a longitudinal slip of around 0.10, while lateral slip saturation occurs in the region of 0.20 to 0.25 radians. The stiffness coefficients are a function of normal load, according to Calspan formulations (Ref. E.16) and are expressed as follows:

Lateral Stiffness Coefficient

$$K_s = \frac{2}{a_{po}^2}\left[A_0 + A_1 F_Z - \frac{A_1}{A_2} F_Z^2 + K_x\left(\frac{|F_{Xest}|}{F_Z}\right)\right] \tag{E-4}$$

The last term is a new addition to STIREMOD that permits increased cornering stiffness under hard braking conditions which is evident in tire test data where $F_{Xest} = CS/FZ \cdot F_Z \cdot S$ and $CS/FZ = (dF_x/dS)/F_z$.

Longitudinal Stiffness Coefficient

$$K_c = \frac{2}{a_{po}^2} F_z\left(\frac{CS}{FZ}\right) \tag{E-5}$$

Given a composite slip function, we now define a force saturation function. This function is expressed as a ratio of numerator and denominator polynomials with two important properties: (1) as slip increases from zero there is a positive slope; (2) the function ratio reaches an asymptote at high slip conditions. The roots of the numerator and denominator polynomials can be located to give a wide variation in the shape of the saturation function to accommodate the full range of pavement and off-road surface conditions. This function is a ratio of polynomials that define a load normalized composite force:

Force Saturation Function

$$f(\sigma) = \frac{F_c}{\mu F_z} = \frac{C_1\sigma^3 + C_2\sigma 2 + C_5\sigma}{C_1\sigma^3 + C_3\sigma^2 + C_4\sigma + 1}1 \tag{E-6}$$

Given the normalized composite force, we then define the normalized lateral and longitudinal forces without cambering in terms of the stiffness weighted lateral and longitudinal slip ratios. With camber γ, the normalized side force also includes an additional camber component where $Y_\gamma = dF_y / d\gamma$:

Normalized Side Force

$$\frac{F_y}{\mu F_z} = \frac{-f(\sigma) K_s \tan\alpha}{\sqrt{K_s^2 \tan^2\alpha + K_{\bar{c}}^2 S^2}} + Y'_\gamma \gamma \tag{E-7}$$

The primed camber stiffness Y'_γ 2 accounts for saturation effects discussed further on, and according to Calspan convention (Ref. E.16), camber stiffness is a quadratic function of normal load:

$$Y_\gamma = A_3 F_z - \frac{A_3}{A_4} F_z^2 \tag{E-8}$$

Normalized Longitudinal Force

$$\frac{F_x}{\mu F_z} = \frac{-f(\sigma) K'_c S}{\sqrt{K_s^2 \tan^2\alpha + K_c'^2 S^2}} \tag{E-9}$$

The primed quantity K'_c accounts for saturation effects discussed below.

Aligning moment is considered a basic function of side force operating on a "pneumatic trail" moment arm. Under saturation (i.e., high slip) conditions, aligning moment approaches zero as the pneumatic trail goes to zero. The aligning moment is expressed as the product of two functions:

Aligning Moment

$$M_z = \frac{K_m a_p^2 \tan\alpha}{\left(1 + G_1 \sigma^2\right)^2} \left[\frac{K_s}{2} - G_2 K_c \frac{S}{1-S} \left(2 + \sigma^2\right) \right] \tag{E-10}$$

where the aligning moment stiffness K_m is a function of normal load:

$$K_m = K_1 F_z \tag{E-11}$$

The first function gives an initial linear slope of aligning moment as a function of lateral slip ratio, which then falls off at higher slips due to the denominator quadratic in composite slip. The shaping coefficient G_1

allows fitting the peak and fall off of aligning torque at high slips. The second function and shaping coefficient G_2 allow accounting for combined cornering and breaking effects on aligning moment due to tire patch lateral offset.

2. Transition and Saturation Regions

As noted in Figure E-1, on paved surfaces tire forces reach a peak at relatively low slip conditions then fall off with further increases in slip out in the saturation region of force production. This peak coefficient of friction can be different for lateral and longitudinal force production, and can be interpreted in the sense of a friction ellipse. STIREMOD has been expanded to include separate lateral and longitudinal slip to slide transition equations for coefficient of friction:

$$\mu_x = \mu_{px}\left(1 - K_{\mu x}\sqrt{\sin^2\alpha + S^2\cos^2\alpha}\right);\ \mu_y = \mu_{py}\left(1 - K_{\mu y}\sqrt{\sin^2\alpha + S^2\cos^2\alpha}\right) \quad \text{(E-12)}$$

where μ_x, μ_y are the equivalent of "slide" coefficients of friction, μ_{px}, μ_{py} are the peak coefficients of friction, is the tire slip angle, and S is the longitudinal slip ratio. In terms of friction ellipse interpretation, μ_{px}, μ_{py} define the limit force ellipse conditions, and the above equations provide the transition throughout the saturation region. Under paved surface conditions the limit slip coefficients of friction are referred to as slide coefficients of friction and are typically 10 to30 percent below the low slip peaks depending on speed as defined by the $K_{\mu x}$ and $K_{\mu y}$ parameters. By setting $K_{\mu x}$ and $K_{\mu y}$ to negative values, tire forces can also be caused to increase beyond the peak transition region, which can be used to produce forces due to surface deformation under high slip conditions.

The peak coefficients of friction are a function of normal load:

$$\mu_{px} = \left(B_{1x}F_z + B_{3x} + B_{4x}F_z^2\right)\frac{SN_o}{SN_T};\ \mu_{py} = \left(B_{1y}F_z + B_{3y} + B_{4y}F_z^2\right)\frac{SN_o}{SN_T} \quad \text{(E-13)}$$

where SN_T is the measurement skid number (i.e., 100 x coefficient of friction) while SN_o is the skid number of the simulated surface.

In the slip to slide transition region two other saturation functions are also defined. The longitudinal stiffness coefficient K_C merges to the lateral stiffness coefficient K_S for symmetry in the limit locked wheel condition:

Lateral/Longitudinal Stiffness Transition

$$K_c' = K_c + (K_s - K_c)\sqrt{\sin^2\alpha + S^2\cos^2\alpha} \tag{E-14}$$

Camber force stiffness is also reduced as a function of the force saturation function:

Camber Force Stiffness Transition

$$F_{y_\gamma} = Y_\gamma \gamma\left[1 - K_\gamma f^2(\sigma)\right] \tag{E-15}$$

When K_γ K_γ is set to 1.0 the camber force goes to zero under high slip conditions.

E. OFF-ROAD SHAPING FUNCTIONS

Metz (Ref. E.8) has developed an empirical model to estimate tire lateral forces during off-road running which only considers pure cornering. To employ this development we will set $S = \gamma = 0$ which gives the reduced equations:

$$\sigma = \frac{\pi a_{p0}^2}{8\mu_0 F_z} K_s \tan\alpha \;;\; \frac{F_y}{F_z} = -\mu f(\sigma) \tag{E-16}$$

The Metz model is based on an exponential function of slip angle, with the parameter relating to cornering stiffness being a function of vertical load. The Metz exponential model is given by the following equations:

$$\frac{F_y}{F_z} = A\left(1 - e^{-B\alpha}\right) \;;\; B = \frac{C}{A}\left(\frac{F_{zref}}{F_z}\right)^m + \frac{D}{A} \tag{E-17}$$

where A is the equivalent of maximum lateral force (sliding friction); B is the equivalent of cornering stiffness (1/deg); C & D are empirical coefficients for variation of B with F_Z (1/deg); m is an empirical exponent; α is tire slip angle (deg); and F_{zref} is rated tire load (lb).

To make STIREMOD emulate an off-road tire model, force saturation function shaping parameters can be determined to match the exponential shape of Metz's model. The following derives equivalent shaping parameters C_1 through C_5 for the case of pure cornering. These shaping parameters can then be used in STIREMOD to predict tire forces during off-road operation.

To compute the equivalent Cs for a particular set of Metz coefficients, the equation must be set equal to equation. Metz's equation for F_y is a function of slip angle (α) in degrees, while STIREMOD's equation for

F_y is a function of composite slip, which is nearly proportional, as illustrated in Figure E-2 since $\alpha \cong \tan\alpha$ for small slip angles. The slope of σ versus α at a given normal load is designated *DsDa*. Metz's equation for F_y can now be put in the domain of composite slip by:

$$\frac{F_y}{F_z} = A\left[1 - e^{-\frac{B\sigma}{DsDa}}\right] \tag{E-18}$$

Now, equation E-16 must be related to equation E-17. Performing an exponential expansion, and rearranging terms, the equation can be written as:

$$\frac{F_y}{F_z} = A\frac{\frac{\left(\frac{B}{DsDa}\right)^3}{6}\sigma^3 + \frac{\left(\frac{B}{DsDa}\right)^2}{2}\sigma^2 + \left(\frac{B}{DsDa}\right)\sigma}{\frac{\left(\frac{B}{DsDa}\right)^3}{6}\sigma^3 + \frac{\left(\frac{B}{DsDa}\right)^2}{2}\sigma^2 + \left(\frac{B}{DsDa}\right)\sigma + 1} \tag{E-19}$$

Therefore:

$$C_1 = \frac{\left(\frac{B}{DsDa}\right)^3}{6}; C_2 = C_3 = \frac{\left(\frac{B}{DsDa}\right)^2}{2}; C_4 = C_5 = \left(\frac{B}{DsDa}\right) \tag{E-20}$$

Table E-2 lists coefficient values given by Metz for various terrain conditions. Figure E-2 illustrates the lateral force as a function of slip angle for each of the Table E-2 terrain types.

Table E-2. Metz's Coefficients For Various Surfaces [Ref. E.8]

Surface	A	B	C	D	M
Pavement	.67	.17	.677	.563	.14
Plowed Field	.65	.07	.267	.222	.14
Gravel .52	.52	.19	.588	.489	.14
Corn Field	.53	.14	.440	.365	.14
Meadow		.88	.15	.784	.652 .14

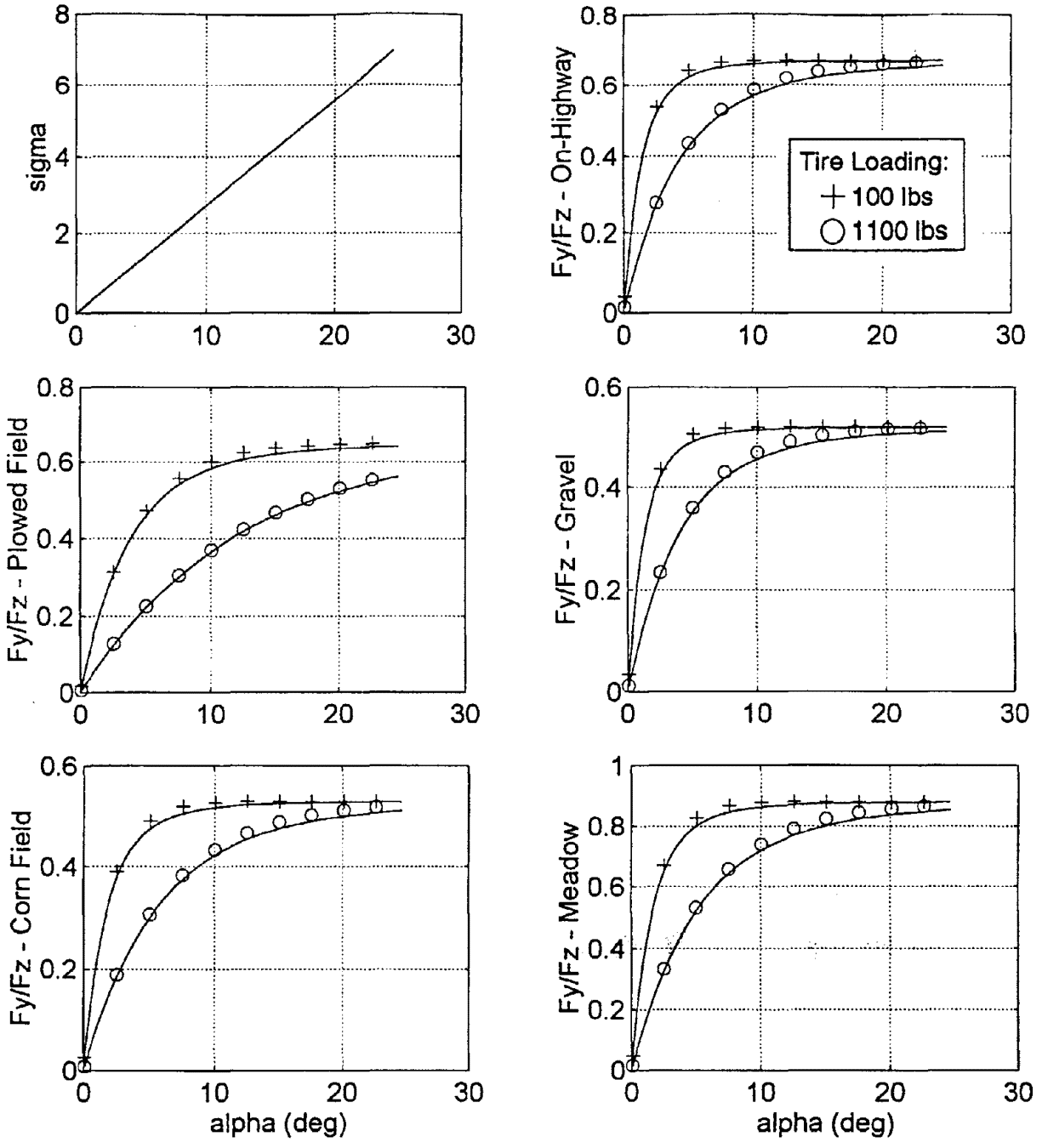

Figure E-2. Later Force Response for Typical Off-Road Terrains

F. HIGH SLIP COEFFICIENT OF FRICTION

There is an additional process that must be considered in generating tire forces in soft soil under high slip conditions having to do with soil mechanics. As developed by Bekker and Wong (Refs. E.9 to E.11), and summarized in Figure E-3, the shear stress, τ, that can be developed by an object varies directly with shear displacement, ΔX_S, and normal pressure, P_Z. The shear stress is given in horizontal force per unit area (i.e., tire patch average pressure over the area of the tire patch, A), which in our case is the composite tire force F_C opposing the direction of soil displacement:

$$\rho = F_c / A \tag{E-21}$$

Shear displacement is the length over which the soil has been compacted. The normal pressure can be expressed as normal load per unit area:

$$P_z = F_z / A \tag{E-22}$$

Now, we note that shear stress ρ is nominally proportional to normal pressure as illustrated in Figure E-3 (Refs. E.9 to E.11). The ratio of these two quantities gives the ratio of composite horizontal force to normal load:

$$\rho / Pz = F_c / F_z \tag{E-23}$$

This last relationship gives normalized tire/soil horizontal force which is the basic output of STIREMOD.

For dry soils, the shear strength (ρ) is proportional to the normal stress on the sheared surface (F) and the angle of internal shearing resistance of the material (φ):

$$\rho = \zeta \tan \varphi \tag{E-24}$$

Here, we will assume that there is an equivalent coefficient of friction corresponding to the ratio of shear strength to normal stress:

$$\mu = \rho / \zeta = tan\ \varphi \tag{E-25}$$

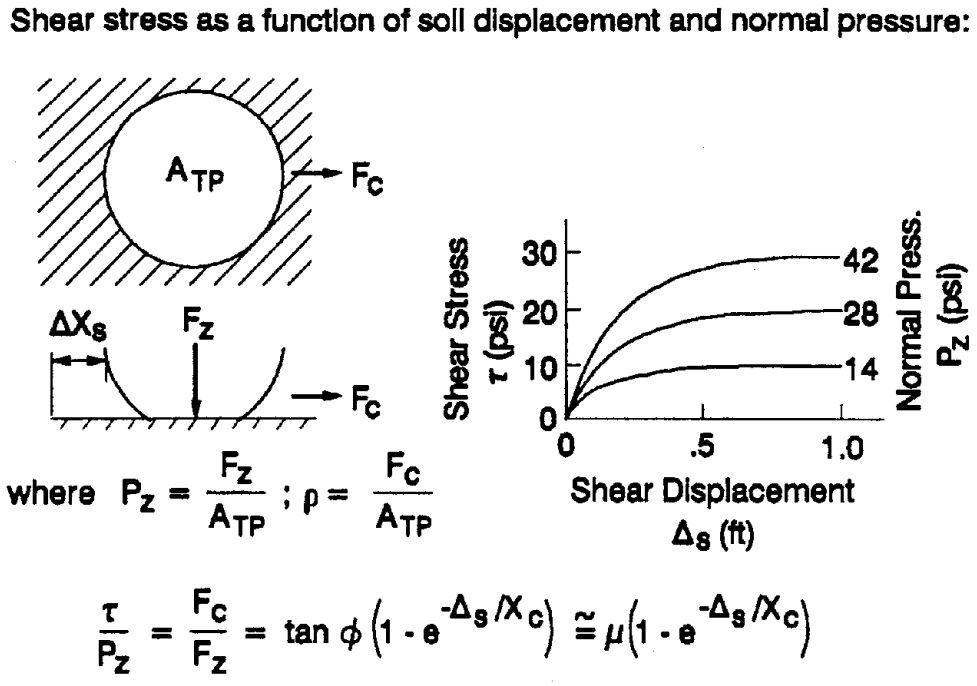

Figure E-3. Off-Road Tire Characteristics Related to Soil Mechanics

For sand, Wong (Ref. E.9) reports measurements resulting in a ratio on the order of 0.7.

Now consider the relationship of shear stress (ρ) to shear displacement (Δ_S). Wong (Ref. E.9) suggests a general exponential relationship for plastic soils (e.g., sand, saturated clay, dry snow):

$$\rho/P_Z = F_C/F_Z = \mu\left[1 - e^{-\Delta_s/X_c}\right] \tag{E-26}$$

In the above expression, X_C is a compaction distance. In loose soils such as sand, when the medium is compacted under pressure without significant disturbance, the compaction distance is on the order of 0.1 ft. For our purpose here, where we are considering plowing or furrowing of the soil surface, the compaction distance will be much longer, perhaps on the order of ft or tens of ft.

The exponential soil shear strength response as a function of distance is analogous to tire side force lag, which is really a distance function related to the tire rolling a characteristic length as the tire patch assumes its new force/slip operating condition. Thus, for each update interval or frame time, T_S, in the vehicle dynamics, the tire moves an incremental distance ΔX based on its velocity, U:

$$\Delta X = U \tag{E-27}$$

The shear force development time constant, T_C, for the tire under soil furrowing conditions will then be given by:

$$T_C = U/X_C \tag{E-28}$$

The characteristic distance for rolling tires on paved surfaces is on the order of their radius, which for passenger cars is on the order of 1 ft. The characteristic distance for tire/soil interaction under furrowing conditions is suspected to be on the order of several ft to tens of ft based on typical marks left by vehicles in off-road encounters, e.g., (Ref. E.12).

Given the development of tire force due to large slip accompanied by soil displacement or plowing, we must now determine the relationship between force and slip. This will be defined by recent measurements discussed further on.

G. TIRE FORCE AND MOMENT MEASUREMENT

1. Paved Surface Characteristics

The tires used to demonstrate parameter identification on paved surfaces are P205/65R15 steel-belted radials (these tires were part of a simulation evaluation program conducted by the National Highway Traffic Safety Administration (Ref. E.15 and E.16). Twenty-six tires were purchased from a single manufacturing batch in an attempt to minimize the tire-to-tire variability. Six of these tires were sent to Smithers Scientific Services, Inc., and were tested on their MTS Flat-Trac II (Ref. E.17) flat-belt tire force and moment measurement machine. A complete description of this testing and its data analysis can be found in (Ref. E.18), and the complete test matrix is documented in Appendix A of this reference.

Five types of tests were used to compute the tire model parameters. Each was run at three normal loads: 560, 930, and 1300 lb. (note: *It is preferable to test a tire at four or five normal loads. Many of the load varying parameters are described by second order polynomials. Much more reliable curve fits are achieved when there are more than three, the minimum, normal loads used*). Measurements during each test included: slip angle, slip ratio, inclination angle, belt speed, spindle height, lateral, longitudinal, and vertical force, and overturning and aligning moment. The five test types were:

1. Quasi-static steering - At each normal load, with zero camber angle and a belt speed of 30 mi/h, slip angle is swept at 1 deg/s between 15 deg.
2. Quasi-static braking/driving - At each normal load, with zero camber angle and a belt speed of 30 mi/h, longitudinal slip ratio is swept at 33 percent s between "50 percent.
3. Quasi-static discrete cambering - At each normal load, with zero slip angle and a belt speed of 30 mi/h, cambers angles of -6, -4, -2, 0, 2, 4, 6 deg.
4. Discrete sinusoidal steering - At 930 lb. normal load, zero camber angle and a belt speed of 30 mi/h, with amplitude of "0.8 deg discrete sinusoidal slip angle frequencies of 0.13, 0.63, 1.25, 1.88, 2.50, 3.13, 3.38, 3.75, 4.38, and 5.00 Hz.
5. Discrete sinusoidal loading - At 930 lb. normal load, zero camber angle and a belt speed of 10 mi/h, with amplitude of 2.4 mm axle height varied sinusoidally at 1 Hz.

Tire Model Parameter Identification

The tire model parameters are computed using the force and moment data described above. The computation of the parameters has been automated using a program written in the MATLAB[7] (Ref. 24) language. The following describes the procedure used to compute each parameter in the order that they are computed.

T_W *Tire Contact Patch Width (in)* - The tire contact patch width is measured using a tape measure with the vehicle at its curb load. T_W is then used in the initial tire patch area (a_o) computation.

T_p *Tire Inflation Pressure (psi)* - This is the tire inflation pressure as tested. T_p is then used in the a_o computation.

F_{ZT} *Tire Design Load (lb.)* - This is the tire design load as marked on the tire side wall.

RR *Tire Rolling Radius at Test Loading (ft)* - The tire rolling radius is the effective tire radius under free rolling conditions at normal driving load. Using data from the 0.13 Hz discrete sinusoidal steering test (at $F_z = 930$ lb.), rolling radius is computed from:

$$RR = mean\left[\frac{BeltSpeed\left(\frac{ft}{s}\right)}{SpindleRotationalVelocity\left(\frac{rad}{s}\right)}\right](ft) \qquad \text{(E-29)}$$

K_γ *Falloff of Camber Thrust at High Slip* - STIREMOD*s camber thrust model is for small camber angles operating at small lateral and longitudinal slip. This parameter determines the degree of camber force saturation.

μ_{ox}, μ_{oy} *Coefficient of Lateral and Longitudinal Friction of Experimental Test Surface* -This is the directional skid number of the pavement on which the vehicle tests were run. A nominal number of 0.85 is chosen for dry pavement.

CS/FZ *Calspan Coefficient for Longitudinal Tire Force Stiffness* 3- *CS/FZ* is computed from the quasi-static braking runs (at F_Z = 560, 930, and 1300). For each test, a straight line is fit to the normalized longitudinal force versus longitudinal slip between zero slip and the slip ratio corresponding to 75 percent of the peak longitudinal force (note: the 75% of the peak longitudinal force limit for the curve fit is chosen as an approximate average region where the *FX/FZ* verses slip ratio curve is linear, and could be changed for a particular tire). The slopes of the three tests are averaged to compute *CS/FZ*.

KB1y, KB3y, KB4y *Calspan Peak Lateral Force versus Normal Load Parameters* - These parameters relate the peak lateral normalized force (*FY/FZ*) to tire normal load in equation E-13. Quasi-static steering tests are used (at F_Z = 560, 930, and 1300), and for each test the average of the peak positive and negative normalized lateral force is computed. A second order polynomial is fit through the three peak normalized forces, and ***KB1y, KB3y, KB4y*** are determined.

KB1x, KB3x, KB4x *Calspan Peak Longitudinal Force versus Normal Load Parameters* - These parameters relate the peak longitudinal normalized force (*FX/FZ*) to tire normal load in equation E-13. Quasi-static braking tests (at F_Z = 560, 930, and 1300) are used, and for each test the average of the peak normalized lateral force is computed. A second order polynomial is fit through the three peak normalized forces, and ***KB1x, KB3x, KB4x*** are determined.

KA0, KA1, KA2 *Calspan Cornering Stiffness versus Normal Load Parameters* - These parameters relate on-center cornering stiffness to tire normal load. Quasi-static steering tests (at F_Z = 560, 930, and 1300) are used, and the cornering stiffness of each is computed for a slip angle range of 2 deg. A second order polynomial is fit through the three cornering stiffnesses, and ***KA0, KA1, KA2*** are determined.

PLYSTEER *Slip Angle Offset for Zero Lateral Tire Force (rad)* - VDANL offsets the slip angle to account for tire plysteer. **PLYSTEER** is the slip angle where the lateral force is zero for the quasi-static steering tests. Using the regression results from the determination of the cornering stiffness parameters ***KA0, KA1,*** and ***KA3***, the average intersection with the slip angle axis is computed.

KK1 *Calspan Coefficient for Aligning Torque Stiffness Variation with Normal Load (ft)* - This parameter relates on-center aligning moment to tire normal load and tire lateral force using equation E-11. This equation is the STIREMOD aligning moment near zero slip angle. Quasi-static steering tests (at F_Z = 560, 930, and 1300) are used, and the slope of each is computed for a slip angle range of 2 degrees. ***KK1*** is the average of the three slopes.

KMUx *Coefficient of the Decay in Longitudinal Friction with Increasing Slip Ratio* - ***KMUx*** is the slope of the normalized longitudinal force (*FX/FZ*) versus slip ratio at high slip ratios. Quasi-static braking tests (at F_Z = 560, 930, and 1300) are used, and a straight line is fit to normalized lateral force versus slip ratio data above slip ratio of 0.2 (chosen to be past the peak longitudinal force). These three slopes are averaged to compute ***KMUx.***

KMUy *Coefficient of the Decay in Lateral Friction with Increasing Slip Angle* - ***KMUy*** is the slope of the normalized lateral force (*FY/FZ*) versus slip angle at high slip angles. Quasi-static steering tests (at F_Z = 560, 930, and 1300) are used, and a straight line is fit to normalized lateral force versus slip angle data above slip angles of 10 deg (chosen to be past the peak lateral force). These three slopes are averaged to compute ***KMUy.***

KA3, KA4 *Calspan Camber Stiffness versus Normal Load Parameters* - These parameters relate on-center camber stiffness to tire normal load using equation E-8. Quasi-static discrete cambering tests (at F_Z = 560, 930, and 1300) are used, and the camber stiffness of each is computed about zero camber angle. A second order polynomial is fit through the three camber stiffnesses, and ***KA3***, ***KA4*** are determined.

C1, C2, C3, C4 *Shaping Coefficients for Force Saturation Function* - The shaping parameters ***C1, C2, C3,*** and ***C4*** can not be determined independently, nor can they be determined from a single tire test. A nonlinear iterative estimation procedure is used to determine the best (in a least squares sense) values for **C1, C2, C3, C4,** and ***kA***.

The estimator uses data from quasi-static steering, braking, and driving tire tests at three normal loads, and uses STIREMOD to compute the tire forces. This estimator is run after all of the load varying parameters have been determined.

KA *Coefficient of Elongation of Tire Contact Patch Due to Longitudinal Force* - This parameter is used to allow asymmetry in the tire's braking/driving while cornering predictions. It is computed during the non-linear curve fitting used to determine the shaping parameters ***C1, C2, C3,*** and ***C4*** (see above for description of procedure).

G1, G2 *Aligning Moment Shaping Parameters* - Parameter ***G1*** determines the shape of the aligning moment curve versus slip angle for zero longitudinal slip. A nonlinear iterative estimation procedure is used to determine the best (in a least squares sense) values for ***G1***. The estimator uses data from quasi-static steering tire tests at three normal loads, and uses STIREMOD to compute the tire forces. This estimator is run after all of the load varying parameters have been determined. ***G2*** adjusts the aligning moment for longitudinal tire forces. A nonlinear iterative estimation procedure is used to determine the best (in a least squares sense) values for ***G2***. The estimator uses data from the combined steering/braking/driving tire tests at the 930 lb. normal load, and STIREMOD to compute the tire forces. This estimator is run after all of the load varying parameters have been determined.

LONGLAG *Longitudinal Slip Ratio Time Constant (s)* - STIREMOD uses a first order dynamic model of longitudinal slip ratio as proposed by Bernard (Ref. E.22). The standard STIREMOD parameter value of 0.25 s was used.

KTL *Tire Lag Constant (ft)* - STIREMOD uses two first order lags on the tire lateral force to model the tire force dynamic characteristics. From the Discrete Sinusoidal Steering tests, the lateral force frequency response to steering angle was computed. The test used was run at 30 mi/h, with a tire normal load of 930 lb. The two first order lags are modeled as a second order lag with damping ratio equal to one, and the phase angle of this system is given by:

$$\phi = \tan^{-1}\left\{2\zeta(\omega/\omega_n)/\left[1-(\omega/\omega_n)^2\right]\right\} \qquad \text{(E-30)}$$

Where N is the phase angle, is the damping ration, T is the input frequency, and T_n is the system natural frequency. From the measured frequency response, the frequency where the phase angle drops 45 deg is found to be $T = 3.4$ Hz. Substituting $N = 45$ deg into and solving for T/T_n gives roots of 0.4142 and 2.41. Since T/T_n can not be negative, $T/T_n = 0.4142$. Substituting T = 3.4 gives $T_n = 8.21$ Hz = 51.58 rad/s. The system time constant, J, is equal to $1/T_n = 0.0194$. In VDANL, $J =$ **KTL**/U, where U is the vehicle speed in ft/s. Solve for **KTL** and substitute in $U = 44$ ft/s (the tire test speed).

TSPRINGR *Tire Spring Rate (lb/ft)* - From the Discrete Sinusoidal Loading Tests, data from a 10-mi/h, and a 1Hz loading frequency, tire normal load is regressed against axle height.

The results of the above identification procedures are summarized in Figure E-4 for several parameters. The overall force and moment fits are summarized in Figure E-5.

2. Off-Road Tire Characteristics

Under small slip conditions below saturation, the tire is represented by the Metz exponential function and typical parameters identified for various soils. Under saturation conditions, the buildup of plowing or tripping forces is represented by a combination of K_F, which allows forces to be increased over the tire/surface coefficient of friction, and the tire side force lag characteristic distance K_{TL}. K_F is a decay factor that reduces coefficient of friction as slip increases beyond saturation, so negative values will be used to obtain higher tire forces due to furrowing or plowing. K_{TL} is usually on the order of 1 ft for unsaturated rolling tires. This characteristic distance will need to be on the order of several ft to tens of ft to represent the distance related build-up of furrowing or plowing forces.

High slip data under off-road conditions is relatively rare, but there are some key sources that can provide some data to get us into the right ball park. Typical friction data often reported for off-road surfaces give coefficients less than for paved surfaces. For example, tire/surface friction values for gravel and sand have been reported in the region of 0.4 to 0.6 (Refs. 9 and 23). These values are for braking and low slip conditions where the soil is not being significantly disturbed. More relevant are measurements reported by Deleys and Brinkman (Ref. 12) made by towing a compact passenger car at different slip angles over sod under free rolling tire conditions. At a slip angle of 39E they obtained an effective friction coefficient value as high as 1.13 with moist sod, while at 90E slip they achieved a maximum value of 0.89. Typical values were about 0.5 on the average with the vehicle being towed at 10 to 15 mi/h. They report a slight trend of increased motion resistance with decreased firmness of soil, and variable forces that can be attributed to local irregularities of the ground surface. In comparing their results with sinkage models they also suggest that the high coefficients are probably due to bulldozing (i.e., plowing or furrowing) effects. Finally, Deleys and Brinkman comment that towing force increase with slip angle is consistent with the assumption that a motion-resistance force is proportional to the projection of the vertical tire/soil interface area in the direction of motion.

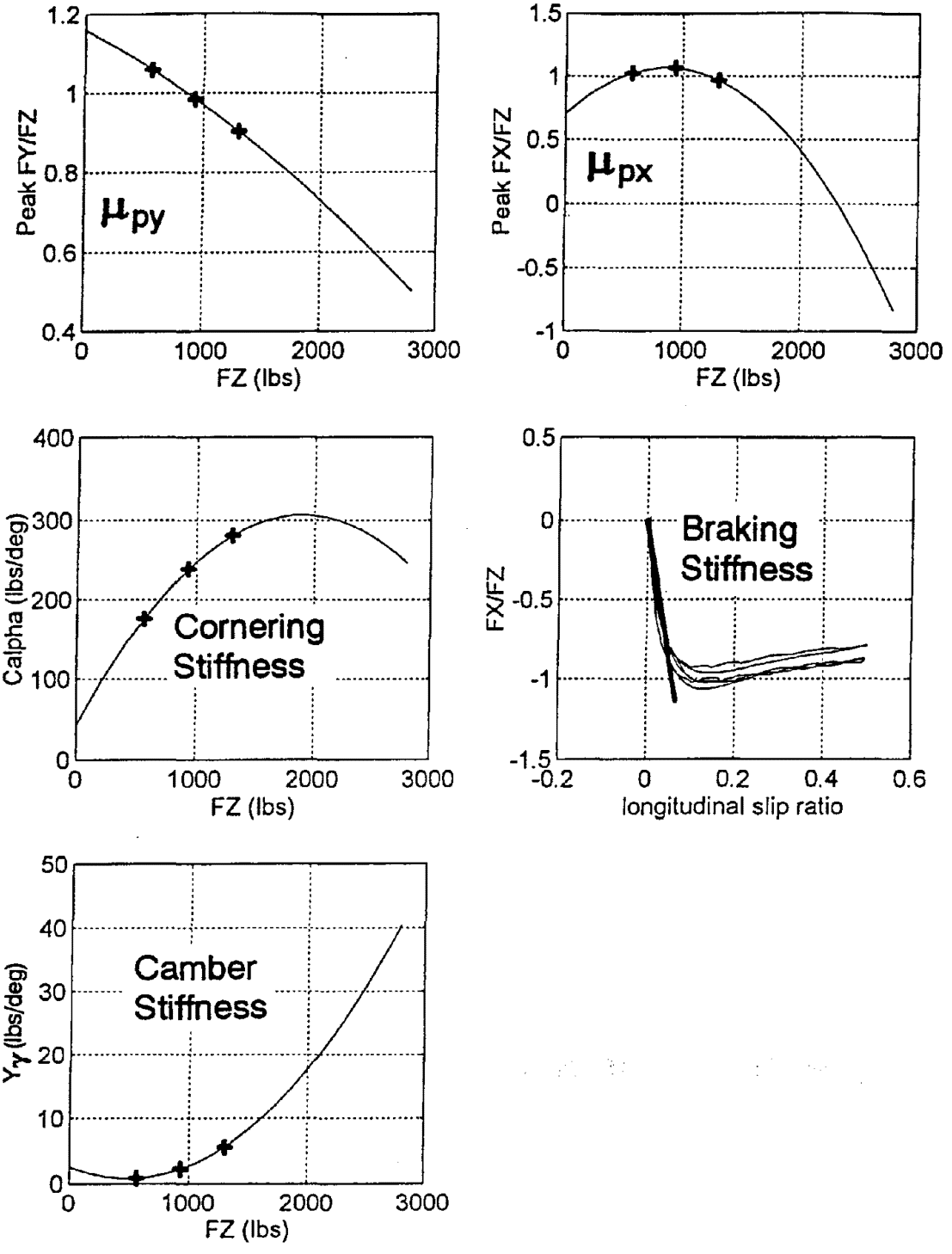

Figure E-4. Tire Parameter Identification Results for P205/65R15 Steel Belted Radial

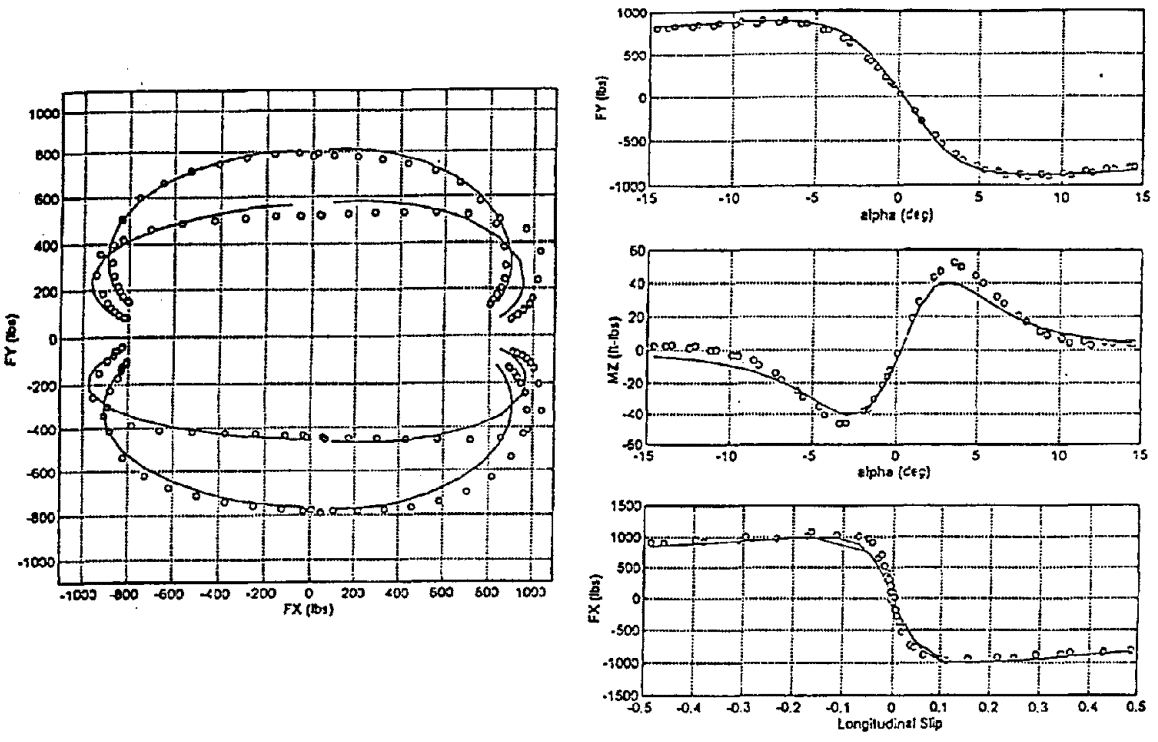

Figure E-5. STIREMOD Validation Data for a General Tire Ameritech St P205/65R15: Normal Load 930 lb., Slip Angles of -4, -2, 2 and 4 deg in F_X, F_Y Plot

Systematically collected data have recently been reported by Christoffersen et al. (Ref. 13) that are directly relevant to our purposes here. In these tests a vehicle was towed over several different types of surfaces at several different slip conditions by a tractor at 0.5 mi/h. As summarized in Figure E-6a, in straight-ahead tests the wheels were locked, which resulted in 100 percent longitudinal slip. In side slip tests (30, 60, and 90E) the wheels were allowed to freely roll, and the tire side slip friction coefficients reported below were obtained from Christoffersen's deceleration factors by resolving through the towing slip angle, as indicated in Figure E-6b. For the cases of 0 and 60E tests, the lateral force and thus friction factor perpendicular to the tires must be larger than the value in the direction of motion as reported by Christoffersen et al. since the free rolling tire will not generate significant longitudinal forces (other than rolling resistance). The friction factors reported below at 30 and 60E slip are larger than reported by Christoffersen by the inverse of sin. For 30E this increase is $(\sin 30E)^{-1} = 2$ and for 90E the increase is $(\sin 60E)^{-1} = 1.15$.

The Christoffersen et al. data reinterpreted based on Figure E-6 are summarized in Figure E-7 for several test surfaces from ranging from asphalt to sand. The asphalt surface behaves as expected, with the

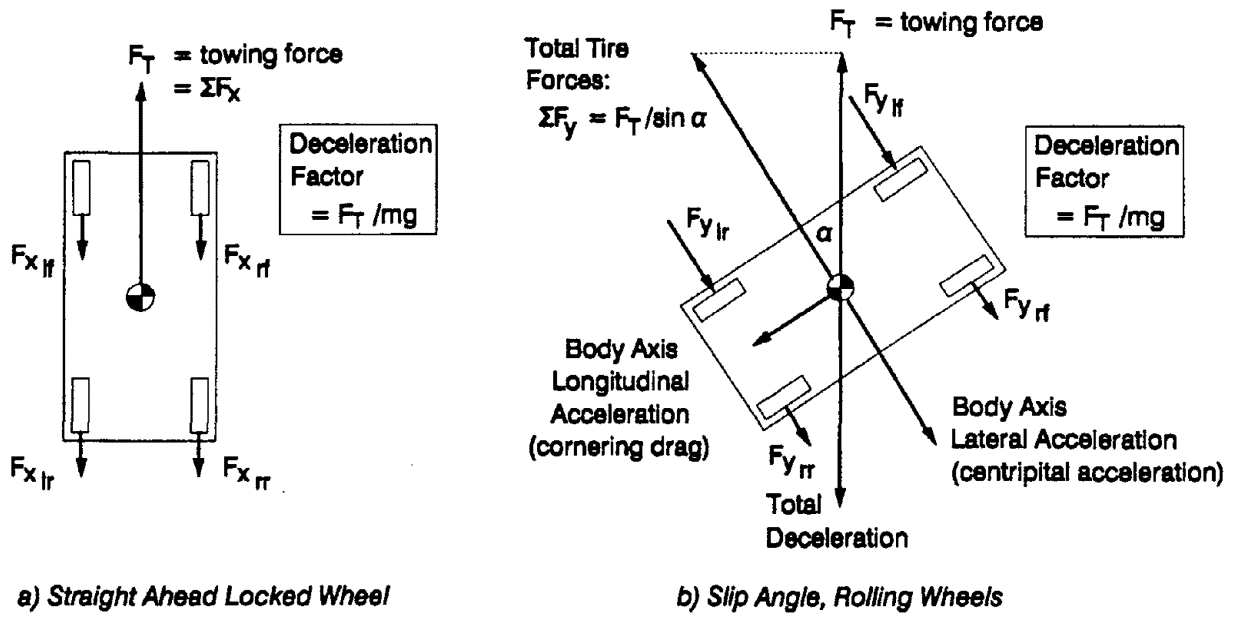

Figure E-6. Slip Conditions, Measurements and Interpretation for Christoffersen, et al. (1995) Deceleration Factor Tow Tests

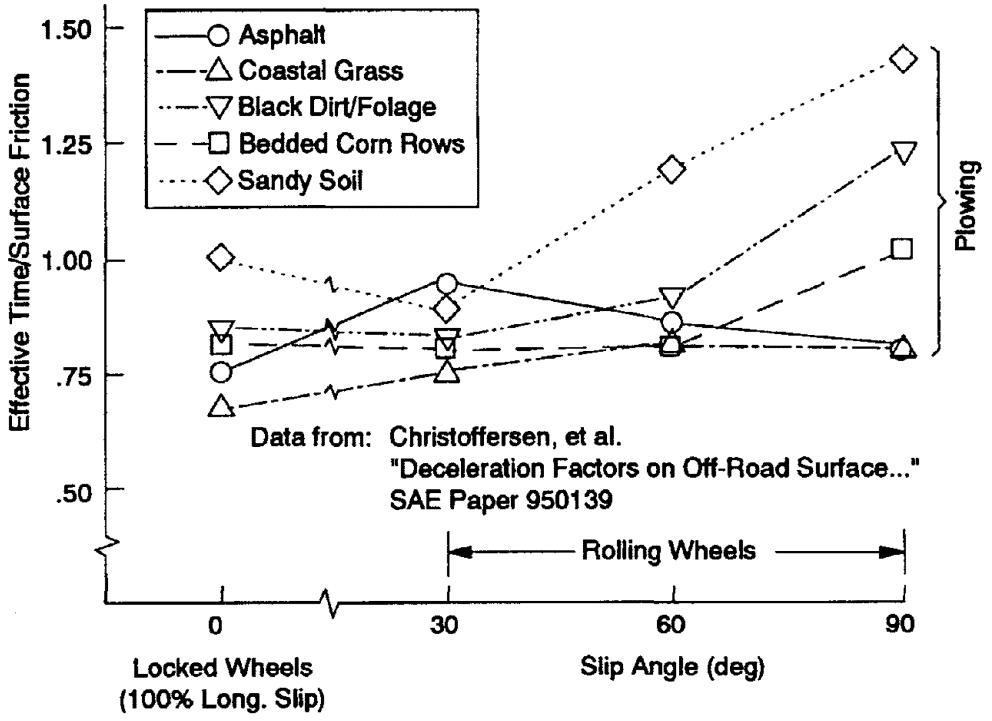

Figure E-7. Tire/Terrain Friction Coefficients for Different Surfaces and Slip Angles as Derived from Christoffersen, et al. (1995) Data

highest friction at 30E, which falls off considerably under locked wheel and high lateral slip conditions. The coastal grass condition gives the lowest friction factors for off road conditions. Sandy soil gives the highest friction factors under high slip conditions. Note, however, for the sand data that under the straight ahead, 100% locked wheel condition, the friction factor is 1.0 while under the 90E (100%) side slip condition the friction factor is 1.41. The other two soil conditions (black dirt/foliage and bedded corn rows) give a similar result in that high lateral slip gives much higher effective friction than the straight-ahead locked wheel (100 percent longitudinal slip) condition.

Christoffersen et al. (Ref. E.13) report that the three soil conditions exhibiting high limit side slip friction coefficients of friction also exhibited plowing that increased with slip angle. Significantly, they also report that the coastal grass condition exhibited no plowing, which, as noted in Figure E-7 has a friction response more similar to asphalt than the other soil conditions.

The response of STIREMOD under off-road conditions for Metz's plowed field condition (Ref. 8) are summarized in Figure E-8. The off-road condition has a much less aggressive saturation curve than paved highway conditions (see Figure E-2) and according to Christoffersen's data reinterpreted in Figure E-7, the peak coefficient of friction exceeds unity at high side slip angles (here we have assumed that Cristoffersen's black dirt/foliage condition in Figure E-7 is the equivalent of Metz's plowed field condition. In Figure E-8 we see that the friction ellipse is narrow longitudinally because of the low peak coefficient of friction for an unpaved surface, but is very high laterally because of the tire's plowing effect under high side slip conditions. Unlike paved surfaces the peak lateral forces occur under 90-degree side slip due to the plowing effect. As discussed earlier, these plowing forces develop as a function of distance that the tire has traveled, analogous to the tire's relaxation distance on pave surfaces that is related to tire diameter. The relaxation distance for the development of plowing forces is related to soil mechanics, and is probably on the order of ft to tens of ft.

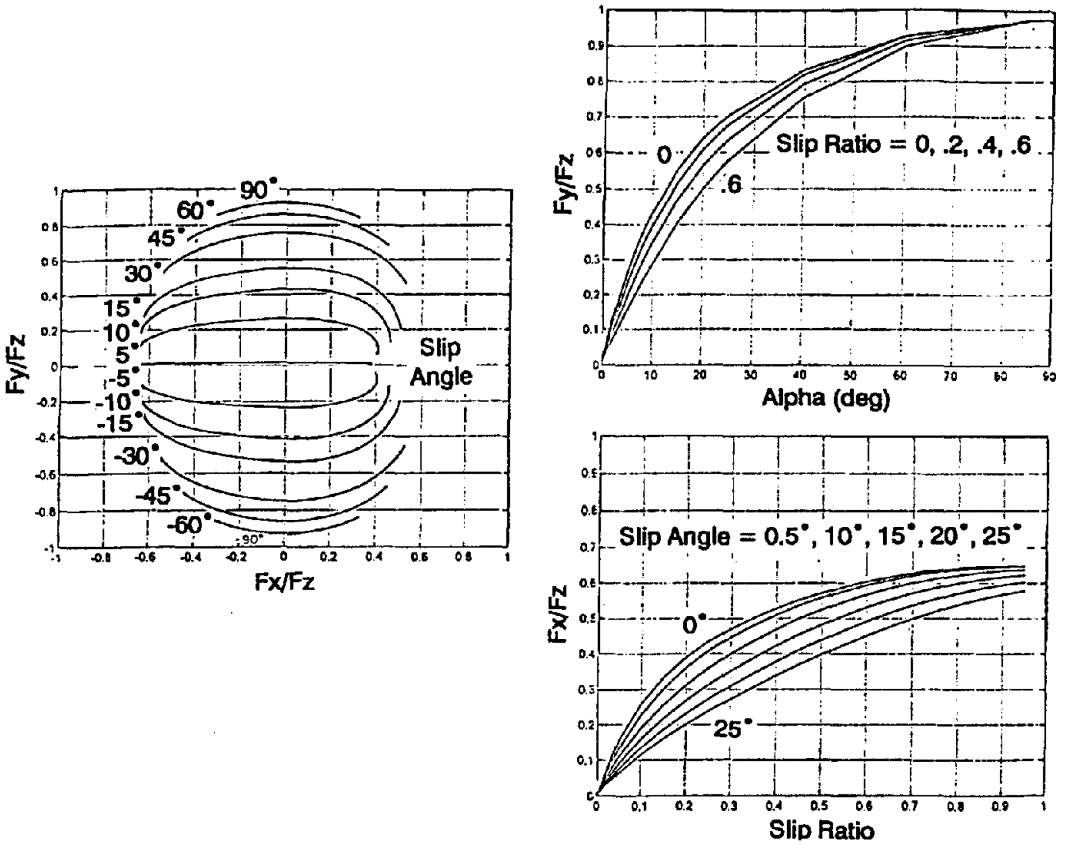

Figure E-8. STIREMOD Response Under Off-Road Conditions: Metz (Ref. E.5} Plowed Field Condition for Adhesion and Transition; Christoffersen, et al. Ref. E.4) "Bedded Corn Rows" for High Slip Angle $\left(K_{\mu y} = 0.5\right)$

H. NOMENCLATURE

a_p - tire patch length under traction/braking conditions

a_{po} - static tire patch length

A - Metz model off-road coefficient of freedom

A_0, A_1, A_2 - quadratic coefficients for lateral stiffness coefficient

A_3, A_4 - quadratic coefficients for camber stiffness coefficient

A_{TP} - tire patch area

B - Metz model off-road cornering stiffness

$B_{1x}, B_{3x}, B_{4x}, B_{1y}, B_{3y}, B_{4y}$ - quadratic coefficients for longitudinal (x) and lateral (y) coefficients of friction

C - Metz off-road tire model shaping coefficient

$C_1, \cdots C_5$ - polynomial coefficients for STIREMOD saturation function

D - Metz off-road tire model shaping coefficient

$DsDa$ - slope of composite slip (σ) versus slip angle (α)

F_x, F_y, F_z - longitudinal, lateral, and vertical tire forces

F_{Xest} - estimated longitudinal force used to increase cornering stiffness under hard braking conditions

F_{ZT} - rated tire design load

G_1, G_2 - shaping coefficients for tire aligning torque

K_1 - coefficient for aligning moment dependence on vertical load

K_a - coefficient for tire patch length dependence on longitudinal force

K_c, K_s - longitudinal and lateral stiffness coefficients

K_m - aligning moment stiffness

K_x - coefficient for cornering stiffness dependence on longitudinal force

K_γ - camber stiffness

$K_{\mu x}, K_{\mu y}$ - coefficients for limit slip change in coefficient of friction

M_z - tire aligning moment

P_z - average tire patch normal pressure

S - longitudinal slip

SN_o, SN_T - skid numbers (%) for simulated surface and tire test, respectively

T_c - tire/soil shear force development time constant

T_p - tire pressure

T_s - simulation frame time or sampling interval

U - wheel hub forward speed

T_W - tire patch width

X_c - characteristic compaction distance

Y_γ - camber stiffness

α - lateral slip angle

Δx - tire longitudinal movement during simulation frame time T_s

Δ_s - soil shear displacement

φ - soil angle of internal shearing resistance

γ - tire camber angle with surface

μ - tire/surface coefficient of friction

μ_{px}, μ_{py} - peak longitudinal (x) and lateral (y) tire/surface coefficients of friction

μ_x, μ_y - peak to slide transition coefficients of friction

ρ - tire/soil shear stress

σ - composite slip

ς - soil shear strength

I. APPENDIX E REFERENCES

E.1. Clarke, S.K. (Ed.), *Mechanics of Pneumatic Tires*, DOT HS 805 952, US Government Printing Office, Washington, DC, 1981.

E.2. Schuring, D.J., Pelz, W., and Pottinger, M.G., "Model for Combined Tire Cornering and Braking Forces," SAE Paper 960180, Society of Automotive Engineers, Warrendale, PA.

E.3. Sakai, H., "Theoretical and Experimental Studies on the Dynamic Properties of Tyres, 1: Review of Theories of Rubber Friction," *International Journal of Vehicle Design*, Vol. 2, No. 1, pp. 78-110, 1981.

E.4. Bakker, E., Pacejka H.B., and Lidner, L., "Tyre Modelling for Use in Vehicle Dynamics Studies," SAE Paper 870432, Society of Automotive Engineers, Warrendale, PA.

E.5. Rad, H.S. and Glemming, D.A., "Normalization of Tire Force and Moment Data," Presented at the Eleventh Annual Meeting of The Tire Society, University of Akron, Akron, OH, March 24-25, 1992.

E.6. Szostak, H.T., *Analytical Modeling of Driver Response in Crash Avoidance Maneuvering Volume II: An Interactive Tire Model for Driver/Vehicle Simulation*, National Highway Traffic Safety Administration Report DOT-HS-807-271, 1988.

E.7. Allen, R.W., Magdaleno, R.E., et al., "Tire Modeling Requirements for Vehicle Dynamics Simulation," SAE Paper 950312, Society of Automotive Engineers, Warrendale, PA.

E.8. Metz, L.D., "Dynamics of Four-Wheel-Steer Off-Highway Vehicles," SAE Paper 930765, Society of Automotive Engineers, Warrendale, PA.

E.9. Wong, J.Y., *Theory of Ground Vehicles*, John Wiley & Sons, New York, 1978.

E.10. Wong, J.Y., *Terramechanics and Off-Road Vehicles*, Elsevier, Amsterdam, 1989.

E.11. Bekker, M.G., *Theory of Land Locomotion*, University of Michigan Press, Ann Arbor, MI, 1956.

E.12. DeLeys, N.J. and Brinkman, C.P., A Rollover Potential of Vehicles on Embankments, Sideslopes, and Other Roadside Features, SAE Paper 87-234, Society of Automotive Engineers, Warrendale,PA, 1987.

E.13. Christoffersen, S.R., et al., Deceleration Factors on Off-Road Surfaces Applicable for Accident Reconstruction, SAE Paper 950139, Society of Automotive Engineers, Warrendale, PA, 1995.

E.14. Schallanmach, A. and Grosch, K., "Tire Traction and Wear," Chapter 6 in Reference 1.

E.15. Pacejka, H., "Analysis of Tire Properties," Chapter 9 in reference 1.

E.16. Schussing, D.J., *Tire Parameter Determination, Vol. I - Summary*, NHTSA DOT HS 802 086, Nov. 1976.

E.17. Chrstos, J.P. and Grygier, P., *Instrumentation and Field Testing of 1994 Ford Taurus GL for NADSdyna Evaluation*, NHTSA Draft Report, 1996.

E.18. Chrstos, J.P., *A Parameter Measurement and Computation Procedures for 1994 Ford Taurus GL*, NHTSA Draft Report, 1996.

E.19. Chrstos, J.P., *Evaluation of the VDANL and VDM RoAD Vehicle Dynamics Simulations*, NHTSA Draft Report, 1996.

E.20. Pottinger, M.G., Flat-Trac II Machine Helps in Tire Force, Moment Measuring, Rubber and Plastic News, March 19, 1990.

E.21. Lee, S., A Development of New Dynamic Tire Model for Improved Vehicle Dynamics Simulation, Ph.D. Dissertation, The Ohio State University, 1994.

E.22. Bernard, J.E. and Clover, C.L., "Tire Modeling for Low-Speed and High-Speed Calculations," SAE Paper No. 950311, 1995.

E.23. *MATLAB*^{7} – *Reference Guide*, The Mathworks, Inc., July 1993.

E.24. Warner, C.Y., et al. "Friction Application in Accident Reconstruction," SAE Paper 830612, Society of Automotive Engineers, Warrendale PA, 1983.

APPENDIX F

AASHTO VEHICLE DATA SETS FOR VDANL

A. OVERVIEW

This appendix summarizes the rationale and sources for the parameter sets for each AASHTO vehicle implemented in VDANL. Appendices B and C give some guidance for measuring and estimating parameters. References at the end of this appendix also give information on parameter measurement and estimation. This appendix describes each of the 12 AASHTO vehicles that are accommodated by VDANL. Some background is given on the method used for establishing the parameter sets. The VDANL parameter sets are also listed for each vehicle. The vehicles accommodated by VDANL and described in this appendix are listed in Table F-1.

Table F-1. AASHTO Vehicles Accommodated By VDANL

	Vehicle Configuration	Symbol
1	Passenger car	P
2	Single-unit truck	SU
3	Single-unit bus	BUS
4	Articulated bus	A-BUS
5	Intermediate semitrailer	WB-40
6	Large semitrailer	WB-50
7	Interstate semitrailer	WB-62
8	Interstate semitrailer	WB-67
9	Motor home	MH
10	Car and camper trailer	P/T
11	Car and boat trailer	P/B
12	Motor home and boat trailer	MH/B

NOTE: This report generally conforms to the metric system for measurements of distance, mass and force. (meters, kilograms, newtons respectively). However, VDANL (the vehicle dynamics simulation) currently requires parameters in English system units. (ft, slugs and pounds). Furthermore, many sources for vehicle parameter data also are given in English units. Therefore, this appendix gives data in English units. English to metric conversion factors are summarized in Table 2.

ENGLISH TO METRIC CONVERSION

DIMENSION	CONVERSION
Length	1 foot = .3048 meters
Mass	1 slug = 14.59 kilograms
Force	1 lb = 4.448 newtons
Velocity	1 mi/h = 1.609 km/h
Acceleration	1 ft/s^2 = .3048 m/s^2
moment (torque)	1 ft-lb = 1.356 N-m
moment of inertia	1 ft-lb-s^2 = 1.355 kg-m-s^2
spring stiffness	1 lb/ft = 14.59 N/m
Pressure	1 psi = 6895 N/m^2 = 6895 pascals

B. VEHICLE PARAMETER SETS

1. Passenger Car - P

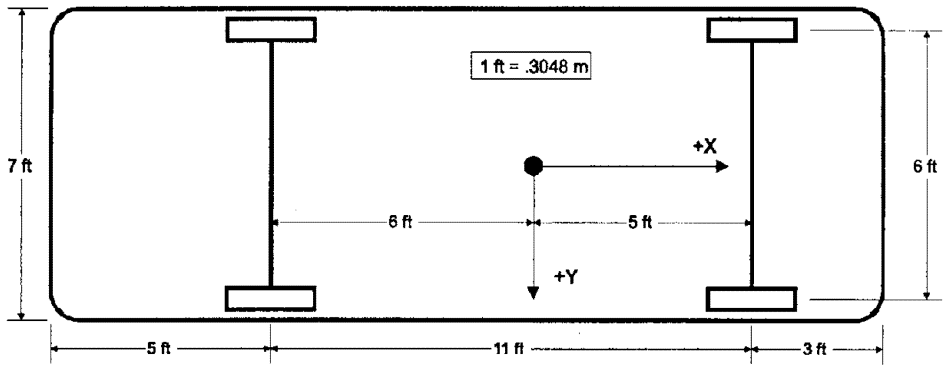

Figure F-1. Dimensions of AASHTO Passenger Car - P

a. Vehicle Parameter File "P.PAR"

It is assumed that this vehicle is a passenger car with independent front suspension, and a solid rear axle.

The following describe parameters in the vehicle file that have been set specific to this vehicle.

MASS Total Vehicle Mass (slugs) - No mass specification is provided by AASHTO. This is a large passenger vehicle, and the weight will be assumed to be 5000 lb. **MASS = 155 slugs.**

SMASS Vehicle Sprung Mass (slugs) - SMASS = MASS - UMASSF - UMASSR. **SMASS = 132.5 slugs**

UMASSF Front Unsprung Mass (slugs) - Ref. F.1 gives the approximation UMASSF = 0.056*MASS+1.097. **UMASSF = 9.8 slugs.**

UMASSR Rear Unsprung Mass (slugs) - Ref. F.1 gives the approximation UMASSR = 0.078*MASS+0.57. **UMASSR = 12.7 slugs.**

LENA Distance from Sprung Mass cg to Front Axle (FT) - Assuming that the vehicle has approximately 55 percent of its weight on the front axle, **LENA = 5 ft.**

LENB Distance from Sprung Mass cg to Rear Axle (FT) - Assuming that the vehicle has approximately 55 percent of its weight on the front axle, **LENB = 6 ft.**

IXS Sprung Mass Roll Inertia (ft-lb-s^2) - Ref. F.1 gives the approximation IXS = 53.7 + 3.075*MASS. **IXS = 530 ft-lb-s^2**

IYS Sprung Mass Pitch Inertia (ft-lb-s^2) - Ref. F.1 gives the approximation IYS = -753.4 + 23.84*MASS. **IYS = 2942 ft-lb-s^2**

IZZ Total Vehicle Yaw Inertia (ft-lb-s^2) - Ref. F.1 gives the approximation IZS = -984.8 + 31.24*MASS. **IZZ = 3858 ft-lb-s^2**

IXZ Total Vehicle Roll/Yaw Cross Product of Inertia (ft-lb-^{2}) - Assumed to be zero.

KSTR Overall Steering Ratio - Steering ratio is assumed to by 20:1. **KSTR = 20**

KSCF Front Aligning Torque Steer Compliance (rad/ft-lb) - Ref. F.1 gives a nominal value of **KSCF = 0.0002 rad/ft-lb.**

KSCR Rear Aligning Torque Steer Compliance (rad/ft-lb) - Assumed to be zero. **KSCR = 0 rad/ft-lb.**

KTL Tire Lag Constant (ft) - A nominal value of 1 ft is used. **KTL = 1 ft.**

Reference F.1 states that the vehicles similar in mass to this AASHTO passenger car have a roll gradient of approximately 8 deg/g, so suspension spring stiffnesses must be computed to achieve this. In Appendix F of Ref. F.2, the steady-state relationship between lateral acceleration and chassis roll angle relative to the ground is derived for a simple vehicle with a roll center. The final equation is:

$$\phi_s = \frac{m_s a_y \varepsilon - \left(K_{FSRS} + K_{RSRS}\right)\dfrac{m a_y h_{CG}}{K_{TSR} T^2}}{K_{FSRS} + K_{RSRS} + m_s g \varepsilon} \qquad \text{(F-1)}$$

where:

m total vehicle mass (slugs)

m_S vehicle sprung mass (slugs)

a_y lateral acceleration (ft/s^2)

K_{FSRS} roll stiffness between front axle and chassis due to springs and anti-roll bars (ft-lb/rad)

K_{RSRS} roll stiffness between rear axle and chassis due to springs and anti-roll bars (ft-lb/rad)

h_{CG} total vehicle cg height above ground (ft)

K_{TSR} tire spring rate (lb/ft)

T track width (ft)

ε vertical distance between roll axis and sprung mass cg (ft)

g acceleration due to gravity (ft/s^2)

Setting ϕ_S = 0.8 deg = 0.0139 rad, a_y = -0.1 g = -3.22 ft/s^2, m = 155 slugs, m_S = 132.5 slugs, h_{CG} = 1.833, K_{TSR} = 15000 lb/ft, T = 6 ft, and ε = 1.475 ft, and solving for the total axle roll stiffness "$K_{FSRS} + K_{RSRS}$", we get $K_{FSRS} + K_{RSRS}$ = -58724.71 ft-lb/rad. The equivalent spring stiffnesses are computed from the equation:

$$K_{RS} = \frac{K_S T^2}{2} \qquad \text{(F-2)}$$

where K_S is the spring stiffness (lb/ft), and K_{RS} is the equivalent axle roll stiffness (ft-lb/rad).

KSF Front Wheel Rate (lb/ft) - Dividing the total roll stiffness between the front and rear axles in the same 55/45 distribution as the weight distribution gives spring stiffnesses of **KSF = 1794 lb/ft**

KSR Rear Wheel Rate (lb/ft) - Dividing the total roll stiffness between the front and rear axles in the same 55/45 distribution as the weight distribution gives spring stiffnesses of **KSR = 1468 lb/ft**

KSDF Front Wheel Damping Rate (lb/ft/s) - Set to a nominal value of: **KSDF = 150 lb/ft/s**

KSDR Rear Wheel Damping Rate (lb/ft/s) - Set to a nominal value of: **KSDR = 150 lb/ft/s**

TRWF Front Track Width (ft) - AASHTO defines vehicle width as 7 ft. Track width is assumed to be 1 ft less than the vehicle width: **TRWF = 6 ft**

TRWR Rear Track Width (ft) - AASHTO defines vehicle width as 7 ft. Track width is assumed to be 1 ft less than the vehicle width: **TRWR = 6 ft**

HCG Total Vehicle cg Height (ft) - HCG was set to a nominal value of: **HCG = 2.0 ft**

KBS Bump Stop Stiffness (lb/ft) - Bump stop stiffness was set to be approximately five times the average wheel rate: **KBS = 8000 lb/ft**

HBS Bump Stop Position (ft) - HBS was set to a nominal value of: **HBS = 0.2 ft**

KTSF Front Auxiliary Roll Stiffness (ft-lb/rad) - All necessary front axle roll stiffness is provided for by the suspension springs, so: **KTSF = 0 ft-lb/rad.**

KTSR Rear Auxiliary Roll Stiffness (ft-lb/rad) - All necessary rear axle roll stiffness is provided for by the suspension springs, so: **KTSR = 0 ft-lb/rad.**

TSPRINGR Tire Spring Rate (lb/ft) - For the P205/65R15 radial tires used, the measured spring rate is: **TSPRINGR = 15000 lb/ft**

HRAR Rear Suspension Roll Center Height (ft) - Rear roll center height is assumed to be: **HRAR = 0.5 ft**

HS Sprung Mass Center-of-Gravity Height (ft) - The unsprung mass cg heights were assumed to be 1 ft, and based on the total vehicle cg height (**HCG**), the sprung mass cg height is computed to be: **HS = 2.17 ft**

IXUF Front Unsprung Mass Roll Inertia (ft-lb-s^2) - Based on past measurements, front unsprung mass roll inertia is estimated to be: **IXUF = 40 ft-lb-s^2**

IXUR Rear Unsprung Mass Roll Inertia (ft-lb-s^2) - Based on past measurements, rear unsprung mass roll inertia is estimated to be: **IXUR = 40 ft-lb-s^2**

KLT Tire Lateral Compliance (ft/lb) - For the P205/65R15 radial tires used, the measured lateral compliance is: **KLT = 1.036E-5 ft/lb**

DRAGC Tire Rolling Drag Coefficient - A nominal value for radial tires is used for rolling drag: **DRAGC = -0.015**

The following braking and steering parameters are from Vehicle #17 in Ref. F.2.

KBTF Front Wheel Brake Effectiveness (ft-lb/psi) - **KBTF = -1.525 ft-lb/psi**

KVB Brake Gain in Vacuum Boost Range (psi/lb) - **KVB = 23.5 psi/lb**

KVM	Brake Gain in Manual Range (psi/lb) - **KVM = 9.4 psi/lb**
FBPVL	Pedal Force when Vacuum Boost Runs Out (lb) - **FBPVL = 55 lb**
SWZ	Steering System Damping Ratio - **SWZ = 0.5**
SWW	Steering System Natural Frequency (rad/s) - **SWW = 70 rad/s**

b. Suspension Parameter File "P.SUS"

It is assumed that this vehicle has no roll steer, no camber change with jounce, no anti-lift/dive forces, and no Ackerman steering geometry. The following are parameters that are set in the suspension file that are specific to this vehicle.

SUSPENSIONF	Front Suspension Type (0 or 1) - **SUSPENSIONF = 1**
SUSPENSIONR	Rear Suspension Type (0 or 1) - **SUSPENSIONR = 0**
KSLF	Front Suspension Squat/Lift Force Due to Lateral Tire Force - The front roll center height is assumed to be 0.5 ft. This is related to KSLF by:

$$KSLF = \frac{2 \cdot H_{RCF}}{T} \qquad \text{(F-3)}$$

where H_{RCF} is the front roll center height. **KSLF = 0.1667.**

c. Tire Parameter File "P.TIR"

The tire parameters used are taken from Ref. F.3 for a General Tire "Ameritech ST" P205/65R15 radial tire.

d. Driver Parameter File "DRIVER.PAR"

The VDANL driver parameter file requires the vehicle stability factor for its adaptive control algorithms. This vehicle's understeer gradient is approximately 4 deg/g, which gives a stability factor of: **KSTABF = 0.002168 rad/ft/s^2**

e. Other Parameters

The AASHTO specifies that the minimum design turning radius of the outside front tire at 10 mi/h is 24 ft, which makes the turning radius of the cg 24-T/2 = 21 ft. Running a slowly increasing steer maneuver at 10 mi/h, and knowing that radius of curvature is equal to forward speed divided by yaw rate, a 21 radius turn is achieved at a steering wheel angle of 10.8 radians. In NONLIN.PAR, **DSWMAX = 10.8**.

f. Parameter Files

Vehicle Parameters

MASS = 155
SMASS = 132.5
UMASSF = 9.8
UMASSR = 12.7
LENA = 5
LENB = 6
IXS = 530
IYS = 2942
IZZ = 3858
IXZ = 0
KSTR = 20
KSCF = 0.0002
KSCB = 0
DLADV = 0
DYADV = 0
DNADV = 0
DENSITY = .00237
REFAREA = 25
CDX = 0.4
AEROVEL = 44
KTL = 1
KSF = 1794
KSDF = 150
KSR = 1468
KSDR = 150
TRWF = 6
TRWB = 6
HCG = 2.0
KBS = 8000
HBS = 0.20
KTSF = 0
KTSR = 0
KRAS = 12000
KRADP = 700
TSPRINGR = 15000
HRAF = 0
HRAR = 0.5
HS = 2.17
IXUF = 40
IXUR = 40
KLT = 1.036E-5
XACC = 0
ZACC = 0
DRAGC = -.015
LENS = 5.4
LM = 1.125
KBTF = -1.525
KVB = 23.5
KMB = 9.4
FBPVL = 55
SWZ = 0.5
SWW = 70
KCF = 0.0
LSO = 0
KLAGV = 16.5
BRAKPROP1 = 0
BRAKPROP2 = 0
FXLIMIT = 0
DAMPCOMF = 0
DAMPEXTF = 0
DAMPCOMR = 0
DAMPEXTR = 0
AIRBRAKES% = 0
BRAKLAG1 = 0
BRAKMULTLF = 1
BRAKMULTRF = 1
BRAKMULTLR = 1
BRAKMULTRR = 1

Suspension Parameters

SUSPENSIONF = 1
SUSPENSIONR = 0
HF = 0
HR = 0
LF = 1
LR = 1000
KSAF = 0
KSAR = 1
BF = 0
BR = 0
CF = 0
CR = 0
DF = 0
DR = 0
EF = 0
ER = 0
KSLF = 0.1667
KSLR = 0
LSAF = 1000
LSAR = 1000
KSADF = 0
KSADR = 0
KSAD2F = 0
KSAD2R = 0
KACK = 0

Tire Parameters

TWIDTH = 5.80
KA0 = 2.4381e+003
KA1 = 1.5990e+001
KA2 = 3.7873e+003
KA3 = -4.2042e-001
KA4 = 9.8425e+002
KA = -0.0699
KMUy = 0.6077
TPRESS = 35.00
KB1y = -1.6516e-004
KB3y = 1.1600e+000
KB4y = -2.5069e-008
KGAMMA = 0.90
CSFZ = 16.7535
MUNOMy = 0.85
FZTRL = 1400
KK1 = -1.1534e-004
RR = 1.025
TIRE = RADIAL
C1 = -0.1641
C2 = 1.8594
C3 = 1.9363
C4 = 0.3134
G1 = 0.9789
G2 = -0.3367
MUNOMx = 0.85
LONGLAG = 0.25
PLYSTEER = -0.0048
KB1x = 8.5700e-004
KB3x = 7.0402e-001
KB4x = -5.0229e-007
KMUx = 0.3984
C5 = 1.2732
Kx = 2218.4231

2. Single Unit Truck - SU

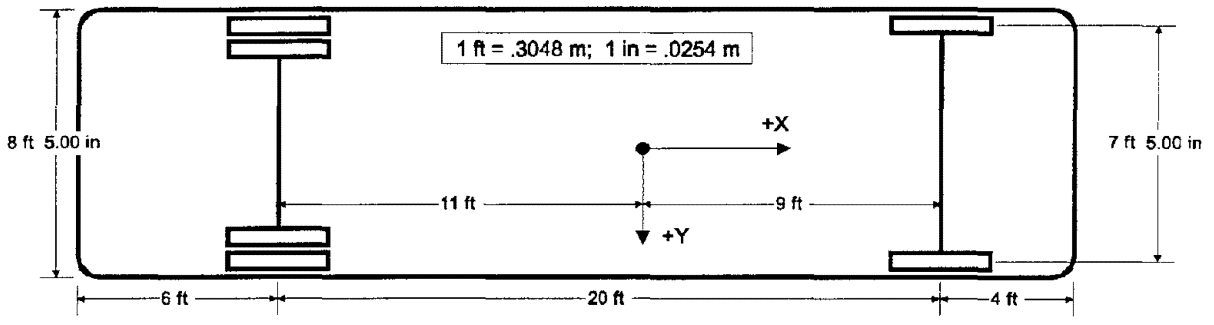

Figure F-2. Dimensions of AASHTO Single Unit Truck - SU

a. Vehicle Parameter File "SU.PAR"

Properties of this single unit truck have been estimated based on representative data from Ref. F.4

MASS Total Vehicle Mass (slugs) - No mass specification is provided by AASHTO. Using Figure 3.2.8 of Ref. F.4, the GM Astro 95 truck mass of 15,750 lb is used. **MASS = 490 slugs.**

SMASS Vehicle Sprung Mass (slugs) - SMASS = MASS - UMASSF - UMASSR. **SMASS = 382 slugs**

UMASSF Front Unsprung Mass (slugs) - Ref. F.4 gives the typical value for a steer axle of 1200 lb. **UMASSF = 37 slugs.**

UMASSR Rear Unsprung Mass (slugs) - Ref. F.4 gives the typical value for a drive axle of 2300 lb. **UMASSR = 71 slugs.**

LENA Distance from Sprung Mass cg to Front Axle (FT) - Ref. F.4 data show that straight trucks are generally slightly front-weight biased. AASHTO gives a wheelbase of 20 ft. **LENA = 9 ft.**

LENB Distance from Sprung Mass cg to Rear Axle (FT) - Wheelbase - LENA: **LENB = 11 ft.**

IXS Sprung Mass Roll Inertia (ft-lb-s^2) - Ref. F.4 gives the typical value to be in the range of, **IXS = 2000 ft-lb-s^2**

IYS Sprung Mass Pitch Inertia (ft-lb-s^2) - Ref. F.4 gives the typical value to be in the range of, **IYS = 20000 ft-lb-s^2**

IZZ Total Vehicle Yaw Inertia (ft-lb-s^2) - Ref. F.4 gives the typical value to be in the range of, **IZZ = 20000 ft-lb-s^2**

IXZ Total Vehicle Roll/Yaw Cross Product of Inertia (ft-lb-s^2) - Assumed to be zero.

KSTR Overall Steering Ratio - Ref. F-5 says that the truck steering ratio's ranges from 22:1 to 36:1. Steering ratio is assumed to by 30:1. **KSTR = 30**

KSCF Front Aligning Torque Steer Compliance (rad/ft-lb) - Ref. F.4 gives the typical value of 10000 in-lb/deg. **KSCF = 0.00002 rad/ft-lb.**

KSCR Rear Aligning Torque Steer Compliance (rad/ft-lb) - Assumed to be zero. **KSCR = 0 rad/ft-lb.**

KTL Tire Lag Constant (ft) - A nominal value of 1 ft is used. **KTL = 1 ft.**

KSF Front Wheel Rate (lb/ft) - Ref. F.4 gives the typical value of 1250 lb/in. **KSF = 15000 lb/ft**

KSR Rear Wheel Rate (lb/ft) - Ref. F.4 gives the typical value of 2000 lb/in. **KSR = 24000 lb/ft**

KSDF Front Wheel Damping Rate (lb/ft/s) - Set to a nominal value of: **KSDF = 1500 lb/ft/s**

KSDR Rear Wheel Damping Rate (lb/ft/s) - Set to a nominal value of: **KSDR = 2400 lb/ft/s**

TRWF Front Track Width (ft) - AASHTO defines vehicle width as 8.5 ft. Track width is assumed to be 1 ft less that the vehicle width: **TRWF = 7.5 ft**

TRWR Rear Track Width (ft) - AASHTO defines vehicle width as 8.5 ft. Track width is assumed to be one foot less that the vehicle width: **TRWR = 7.5 ft**

HCG Total Vehicle cg Height (ft) - Ref. F.4 gives the typical value of 36 in. **HCG = 3.0 ft**

KBS Bump Stop Stiffness (lb/ft) - Bump stop stiffness was set to be approximately five times the average wheel rate: **KBS = 100000 lb/ft**

HBS Bump Stop Position (ft) - HBS was set to a nominal value of: **HBS = 0.2 ft**

KTSF Front Auxiliary Roll Stiffness (ft-lb/rad) - Ref. F.4 gives the typical value for overall front suspension roll stiffness of -20000 in-lb/deg (-95500 ft-lb/rad). This is the combined roll stiffness of the suspension springs and any antiroll bar. The front springs provide a roll stiffness of:

$$K_{RS} = -\frac{K_{SF} TRWF^2}{2} \qquad \text{(F-4)}$$

giving K_{RS} of -421,874 ft-lb/rad. The auxiliary roll stiffness is the total suspension roll stiffness minus the roll stiffness due to the springs. **KTSF = 326374 ft-lb/rad.**

KTSR Rear Auxiliary Roll Stiffness (ft-lb/rad) - Ref. F.4 gives the typical value for overall rear suspension roll stiffness of -60000 in-lb/deg (-286480 ft-lb/rad). This is the combined roll stiffness of the suspension springs and any antiroll bar. The rear springs provide a roll stiffness of:

$$K_{RS} = -\frac{K_{SR} TRWR^2}{2} \qquad \text{(F-5)}$$

giving K_{RS} of -675,000 ft-lb/rad. The auxiliary roll stiffness is the total suspension roll stiffness minus the roll stiffness due to the springs. **KTSR = 388521 ft-lb/rad.**

TSPRINGR Tire Spring Rate (lb/ft) - Ref. F.4 gives a typical value for radial tire spring rate of 4600 lb/in. **TSPRINGR = 55200 lb/ft**

HRAF Front Suspension Roll Center Height (ft) - Ref. F.4 gives a typical value for front roll center height of 19 in. **HRAF = 1.58 ft**

HRAR Rear Suspension Roll Center Height (ft) - Ref. F.4 gives a typical value for rear roll center height of 26 in. **HRAR = 2.17 ft**

HS Sprung Mass cg Height (ft) - The unsprung mass cg heights were assumed to be 1.58 ft, and based on the total vehicle cg height (**HCG**), the sprung mass cg height is computed to be: **HS = 3.4 ft**

IXUF Front Unsprung Mass Roll Inertia (ft-lb-s^2) - The front unsprung mass roll inertia is estimated to be: **IXUF = 300 ft-lb-s^2**

IXUR Rear Unsprung Mass Roll Inertia (ft-lb-s^2) - The rear unsprung mass roll inertia is estimated to be: **IXUR = 650 ft-lb-s^2**

KLT Tire Lateral Compliance (ft/lb) - Tire lateral compliance is estimated to be 76 percent of the tire vertical compliance Ref. F.2: **KLT = 2.3E-5 ft/lb**

KBTF Front Wheel Brake Effectiveness (ft-lb/psi) - Ref. F.4 gives a typical value for front brake effectiveness of -870 in-lb/psi. **KBTF = -72.5 ft-lb/psi**

KVB Brake Gain in Vacuum Boost Range (psi/lb) **KVB = 23.5 psi/lb**

KVM Brake Gain in Manual Range (psi/lb) **KVM = 9.4 psi/lb**

FBPVL Pedal Force when Vacuum Boost Runs Out (lb) **FBPVL = 55 lb**

SWW Steering System Natural Frequency (rad/s) - Because of the stiffness of heavy truck steering systems, the steering system natural frequency will be out of the handling frequency range. Therefore, steering system dynamics will be ignored. **SWW = 0 rad/s**

AIRBRAKE% Air Brake Flag - This truck is assumed to have air brakes. **AIRBRAKE% = 1**

BRAKLAG1 Brake Torque Time Constant (s) - Ref. F.4 gives a typical value of 0.3 s. **BRAKLAG1 = 0.3**

b. Suspension Parameter File "SU.SUS"

It is assumed that this vehicle has no anti-lift/dive forces and no Ackerman steering geometry. The following are parameters that are set in the suspension file that are specific to this vehicle.

SUSPENSIONF Front Suspension Type (0 or 1) - **SUSPENSIONF = 1**

SUSPENSIONR Rear Suspension Type (0 or 1) - **SUSPENSIONR = 1**

HF & LF Front Axle Roll Steer - Ref. F.4 gives a typical value front axle roll steer of 0.2 (understeer). **HF = 0.2 & LF = 1**

HR & LR Rear Axle Roll Steer - Ref. F.4 gives a typical value rear axle roll steer of 0.2 (understeer). **HR = -0.2 & LR = 1**

c. Tire Parameter File "SU.TIR"

The tire parameters used are taken from a General Tire "AMERI*S380" 295/75R22.5 radial tire at 125 psi.

d. Driver Parameter File "DRIVER.PAR"

The VDANL driver parameter file requires the vehicle stability factor for its adaptive control algorithms. This vehicle's understeer gradient is approximately 4 deg/g, which gives a stability factor of: **KSTABF = 0.0022 rad/ft/s^2**

e. Other Parameters

The AASHTO specifies that the minimum design turning radius of the outside front tire at 10 mi/h is 44.1 ft, which makes the turning radius of the center-of-gravity 44.1-T/2 = 40.35 ft. Running a slowly increasing steer maneuver at 10 mi/h, and knowing that radius of curvature is equal to forward speed divided by yaw rate, a 40.35 radius turn is achieved at a steering wheel angle of 14.35 radians. In NONLIN.PAR, **DSWMAX = 14.35**.

f. Parameter Files

Vehicle Parameters
MASS = 490
SMASS = 382
UMASSF = 37
UMASSR = 71
LENA = 11
LENB = 9
IXS = 2000
IYS = 20000
IZZ = 20000
IXZ = 0
KSTR = 30
KSCF = 0.000001
KSCB = 0
DLADV = 0
DYADV = 0
DNADV = 0
DENSITY = 0.00237
REFAREA = 50
CDX = 0.4
AEROVEL = 44
KTL = 2
KSF = 15000
KSDF = 1500
KSR = 24000
KSDR = 2400
TRWF = 7.5
TRWB = 7.5
HCG = 3.0
KBS = 100000
HBS = 0.20
KTSF = 326374
KTSR = 388521
KRAS = 12000
KRADP = 700
TSPRINGR = 55200
HRAF = 1.58
HRAR = 2.17
HS = 3.4
IXUF = 300
IXUR = 650
KLT = 2.3E-5
XACC = 0
ZACC = 0
DRAGC = -.015
LENS = 5.4
LM = 1.125
KBTF = -72.5
KVB = 23.5
KMB = 9.4
FBPVL = 55
SWZ = 0.5
SWW = 0
KCF = 0.0
LSO = 0
KLAGV = 16.5
BRAKPROP1 = 0
BRAKPROP2 = 0
FXLIMIT = 0
DAMPCOMF = 0
DAMPEXTF = 0
DAMPCOMR = 0
DAMPEXTR = 0
AIRBRAKES% = 1
BRAKLAG1 = 0.3
BRAKMULTLF = 1
BRAKMULTRF = 1
BRAKMULTLR = 1
BRAKMULTRR = 1

Suspension Parameters
SUSPENSIONF = 1
SUSPENSIONR = 1
HF = 0.1
HR = 0

LF = 1	KSAD2R = 0	FZTRL = 6175
LR = 1000	KACK = 0	KK1 = -3.0824e-005
KSAF = 1		RR = 1.025
KSAR = 1	**Tire Parameters**	TIRE = RADIAL
BF = 0	TWIDTH = 10.00	C1 = 0.4693
BR = 0	KA0 = 1.9148e+003	C2 = 2.0389
CF = 0	KA1 = 9.1239e+000	C3 = 1.7886
CR = 0	KA2 = 2.6632e+004	C4 = 0.7335
DF = 0	KA3 = 0.0000e+000	G1 = 0.7266
DR = 0	KA4 = 1.0000e+000	G2 = 1.0000
EF = 0	KA = 0.0544	MUNOMx = 0.85
ER = 0	KMUy = 0.3454	LONGLAG = 0.25
KSLF = 0	TPRESS = 125.00	PLYSTEER = -0.0043
KSLR = 0	KB1y = -1.4737e-005	KB1x = -2.9289e-005
LSAF = 1000	KB3y = 6.6176e-001	KB3x = 9.4338e-001
LSAR = 1000	KB4y = -2.5237e-010	KB4x = 1.1202e-009
KSADF = 0	KGAMMA = 0.90	KMUx = 0.3454
KSADR = 0	CSFZ = 6.6412	C5 = 1.2732
KSAD2F = 0	MUNOMy = 0.85	Kx = 0

3. Single Unit Bus - BUS

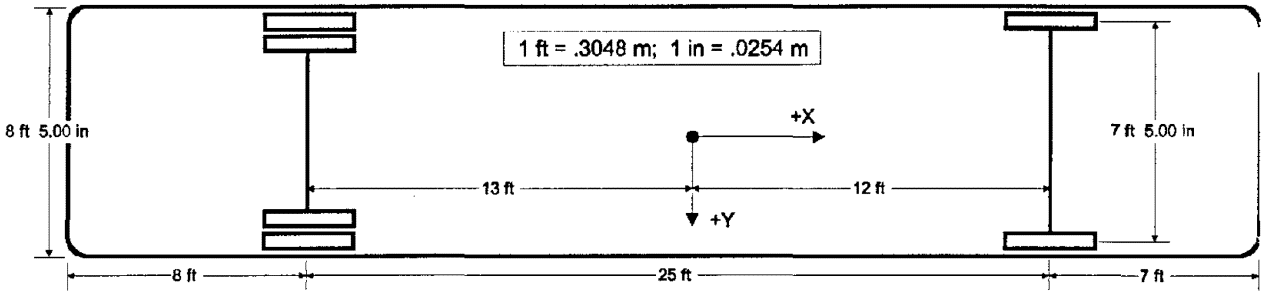

Figure F-3. Dimensions of AASHTO Single Unit BUS - BUS

a. Vehicle Parameter File "BUS.PAR"

Properties of this single unit bus have been estimated based on representative data from Ref. F.4.

MASS Total Vehicle Mass (slugs) - No mass specification is provided by AASHTO. Using Figure 3.2.8 of Ref. F.4, the GM Astro 95 Truck mass of 15,750 lb is used. **MASS = 490 slugs.**

SMASS Vehicle Sprung Mass (slugs) - SMASS = MASS - UMASSF - UMASSR. **SMASS = 382 slugs**

UMASSF Front Unsprung Mass (slugs) - Ref. F.4 gives the typical value for a steer axle of 1200 lb. **UMASSF = 37 slugs.**

UMASSR Rear Unsprung Mass (slugs) - Ref. F.4 gives the typical value for a drive axle of 2300 lb. **UMASSR = 71 slugs.**

LENA Distance from Sprung Mass cg to Front Axle (FT) - Ref. F.4 data show that straight trucks are generally slightly front-weight biased. AASHTO gives a wheelbase of 25 ft. **LENA = 12 ft.**

LENB Distance from Sprung Mass cg to Rear Axle (FT) - Wheelbase - LENA: **LENB = 13 ft.**

IXS Sprung Mass Roll Inertia (ft-lb-s^2) - Ref. F.4 gives the typical value to be in the range of, **IXS = 2000 ft-lb-s^2**

IYS Sprung Mass Pitch Inertia (ft-lb-s^2) - Ref. F.4 gives the typical value to be in the range of, **IYS = 20000 ft-lb-s^2**

IZZ Total Vehicle Yaw Inertia (ft-lb-s^2) - Ref. F.4 gives the typical value to be in the range of, **IZZ = 20000 ft-lb-s^2**

IXZ Total Vehicle Roll/Yaw Cross Product of Inertia (ft-lb-s^2) - Assumed to be zero.

KSTR Overall Steering Ratio - Ref. F-5 says that the truck steering ratio's ranges from 22:1 to 36:1. Steering ratio is assumed to by 30:1. **KSTR = 30**

KSCF Front Aligning Torque Steer Compliance (rad/ft-lb) - Ref. F.4 gives the typical value of 10000 in-lb/deg. **KSCF = 0.00002 rad/ft-lb.**

KSCR Rear Aligning Torque Steer Compliance (rad/ft-lb) - Assumed to be zero. **KSCR = 0 rad/ft-lb.**

KTL Tire Lag Constant (ft) - A nominal value of 1 ft is used. **KTL = 1 ft.**

KSF Front Wheel Rate (lb/ft) - Ref. F.4 gives the typical value of 1250 lb/in. **KSF = 15000 lb/ft**

KSR Rear Wheel Rate (lb/ft) - Ref. F.4 gives the typical value of 2000 lb/in. **KSR = 24000 lb/ft**

KSDF Front Wheel Damping Rate (lb/ft/s) - Set to a nominal value of: **KSDF = 1500 lb/ft/s**

KSDR Rear Wheel Damping Rate (lb/ft/s) - Set to a nominal value of: **KSDR = 2400 lb/ft/s**

TRWF Front Track Width (ft) - AASHTO defines vehicle width as 8.5 ft. Track width is assumed to be 1 ft less than the vehicle width: **TRWF = 7.5 ft**

TRWR Rear Track Width (ft) - AASHTO defines vehicle width as 8.5 ft. Track width is assumed to be 1 ft less than the vehicle width: **TRWR = 7.5 ft**

HCG Total Vehicle cg Height (ft) - Ref. F.4 gives the typical value of 36 in. **HCG = 3.0 ft**

KBS Bump Stop Stiffness (lb/ft) - Bump stop stiffness was set to be approximately five times the average wheel rate: **KBS = 100000 lb/ft**

HBS Bump Stop Position (ft) - HBS was set to a nominal value of: **HBS = 0.2 ft**

KTSF Front Auxiliary Roll Stiffness (ft-lb/rad) - Ref. F.4 gives the typical value for overall front suspension roll stiffness of -20000 in-lb/deg (-95500 ft-lb/rad). This is the combined roll stiffness of the suspension springs and any antiroll bar. The front springs provide a roll stiffness of:

$$K_{RS} = -\frac{K_{SF} TRWF^2}{2} \qquad \text{(F-6)}$$

giving K_{RS} of -421,874 ft-lb/rad. The auxiliary roll stiffness is the total suspension roll stiffness minus the roll stiffness due to the springs. **KTSF = 326374 ft-lb/rad.**

KTSR Rear Auxiliary Roll Stiffness (ft-lb/rad) - Ref. F.4 gives the typical value for overall rear suspension roll stiffness of -60000 in-lb/deg (-286480 ft-lb/rad). This is the combined roll stiffness of the suspension springs and any antiroll bar. The rear springs provide a roll stiffness of:

$$K_{RS} = -\frac{K_{SR} TRWR^2}{2} \qquad \text{(F-7)}$$

giving K_{RS} of -675,000 ft-lb/rad. The auxiliary roll stiffness is the total suspension roll stiffness minus the roll stiffness due to the springs. **KTSR = 388521 ft-lb/rad.**

TSPRINGR Tire Spring Rate (lb/ft) - Ref. F.4 gives a typical value for radial tire spring rate of 4600 lb/in. **TSPRINGR = 55200 lb/ft**

HRAF Front Suspension Roll Center Height (ft) - Ref. F.4 gives a typical value for front roll center height of 19 in. **HRAF = 1.58 ft**

HRAR Rear Suspension Roll Center Height (ft) - Ref. F.4 gives a typical value for rear roll center height of 26 in. **HRAR = 2.17 ft**

HS Sprung Mass cg Height (ft) - The unsprung mass cg heights were assumed to be 1.58 ft, and based on the total vehicle cg height (**HCG**), the sprung mass cg height is computed to be: **HS = 3.4 ft**

IXUF Front Unsprung Mass Roll Inertia (ft-lb-s^2) - The front unsprung mass roll inertia is estimated to be: **IXUF = 300 ft-lb-s^2**

IXUR Rear Unsprung Mass Roll Inertia (ft-lb-s^2) - The rear unsprung mass roll inertia is estimated to be: **IXUR = 650 ft-lb-s^2**

KLT Tire Lateral Compliance (ft/lb) - Tire lateral compliance is estimated to be 76 percent of the tire vertical compliance Ref. F.2: **KLT = 2.3E-5 ft/lb**

KBTF Front Wheel Brake Effectiveness (ft-lb/psi) - Ref. F.4 gives a typical value for front brake effectiveness of -870 in-lb/psi. **KBTF = -72.5 ft-lb/psi**

KVB Brake Gain in Vacuum Boost Range (psi/lb) **KVB = 23.5 psi/lb**

KVM Brake Gain in Manual Range (psi/lb) - **KVM = 9.4 psi/lb**

FBPVL Pedal Force when Vacuum Boost Runs Out (lb) - **FBPVL = 55 lb**

SWW Steering System Natural Frequency (rad/s) - Because the of stiffness of heavy truck steering systems, the steering system natural frequency will be out of the handling frequency range. Therefore, steering system dynamics will be ignored. **SWW = 0 rad/s**

AIRBRAKE% Air Brake Flag - This truck is assumed to have air brakes. **AIRBRAKE% = 1**

BRAKLAG1 Brake Torque Time Constant (s) - Ref. F.4 gives a typical value of 0.3 s. **BRAKLAG1 = 0.3**

b. Suspension Parameter File "BUS.SUS"

It is assumed that this vehicle has no anti-lift/dive forces and no Ackerman steering geometry. The following are parameters that are set in the suspension file that are specific to this vehicle.

SUSPENSIONF	Front Suspension Type (0 or 1) - **SUSPENSIONF = 1**
SUSPENSIONR	Rear Suspension Type (0 or 1) - **SUSPENSIONR = 1**
HF & LF	Front Axle Roll Steer - Ref. F.4 gives a typical value front axle roll steer of 0.2 (understeer). **HF = 0.2 & LF = 1**
HR & LR	Rear Axle Roll Steer - Ref. F.4 gives a typical value rear axle roll steer of 0.2 (understeer). **HR = -0.2 & LR = 1**

c. Tire Parameter File "BUS.TIR"

The tire parameters used are taken from a General Tire "AMERI*S380" 295/75R22.5 radial tire at 125 psi.

d. Driver Parameter File "DRIVER.PAR"

The VDANL driver parameter file requires the vehicle stability factor for its adaptive control algorithms. This vehicle's understeer gradient is approximately 2.2 deg/g, which gives a stability factor of: **KSTABF = 0.0012 rad/ft/s^2**

e. Other Parameters

The AASHTO specifies that the minimum design turning radius of the outside front tire at 10 mi/h is 46.5 ft, which makes the turning radius of the center-of-gravity 46.5-T/2 = 42.75 ft. Running a slowly increasing steer maneuver at 10 mi/h, and knowing that radius of curvature is equal to forward speed divided by yaw rate, a 42.75 radius turn is achieved at a steering wheel angle of 16.5 radians. In NONLIN.PAR, **DSWMAX = 16.5**.

f. Parameter Files

Vehicle Parameters

MASS = 490	KSCF = 0.000001	KSR = 24000
SMASS = 382	KSCB = 0	KSDR = 2400
UMASSF = 37	DLADV = 0	TRWF = 7.5
UMASSR = 71	DYADV = 0	TRWB = 7.5
LENA = 12	DNADV = 0	HCG = 3.0
LENB = 13	DENSITY = 0.00237	KBS = 100000
IXS = 2000	REFAREA = 50	HBS = 0.20
IYS = 20000	CDX = 0.4	KTSF = 326374
IZZ = 20000	AEROVEL = 44	KTSR = 388521
IXZ = 0	KTL = 2	KRAS = 12000
KSTR = 30	KSF = 15000	KRADP = 700
	KSDF = 1500	TSPRINGR = 55200

HRAF = 1.58
HRAR = 2.17
HS = 3.4
IXUF = 300
IXUR = 650
KLT = 2.3E-5
XACC = 0
ZACC = 0
DRAGC = -.015
LENS = 5.4
LM = 1.125
KBTF = -72.5
KVB = 23.5
KMB = 9.4
FBPVL = 55
SWZ = .5
SWW = 0
KCF = 0.0
LSO = 0
KLAGV = 16.5
BRAKPROP1 = 0
BRAKPROP2 = 0
FXLIMIT = 0
DAMPCOMF = 0
DAMPEXTF = 0
DAMPCOMR = 0
DAMPEXTR = 0
AIRBRAKES% = 1
BRAKLAG1 = 0.3
BRAKMULTLF = 1
BRAKMULTRF = 1
BRAKMULTLR = 1
BRAKMULTRR = 1

Suspension Parameters
SUSPENSIONF = 1
SUSPENSIONR = 1
HF = 0.1
HR = 0
LF = 1
LR = 1000
KSAF = 1
KSAR = 1
BF = 0
BR = 0
CF = 0
CR = 0
DF = 0
DR = 0
EF = 0
ER = 0
KSLF = 0
KSLR = 0
LSAF = 1000
LSAR = 1000
KSADF = 0
KSADR = 0
KSAD2F = 0
KSAD2R = 0
KACK = 0

Tire Parameters
TWIDTH = 10.00
KA0 = 1.9148e+003
KA1 = 9.1239e+000
KA2 = 2.6632e+004
KA3 = 0.0000e+000
KA4 = 1.0000e+000
KA = 0.0544
KMUy = 0.3454
TPRESS = 125.00
KB1y = -1.4737e-005
KB3y = 6.6176e-001
KB4y = -2.5237e-010
KGAMMA = 0.90
CSFZ = 6.6412
MUNOMy = 0.85
FZTRL = 6175
KK1 = -3.0824e-005
RR = 1.025
TIRE = RADIAL
C1 = 0.4693
C2 = 2.0389
C3 = 1.7886
C4 = 0.7335
G1 = 0.7266
G2 = 1.0000
MUNOMx = 0.85
LONGLAG = 0.25
PLYSTEER = -0.0043
KB1x = -2.9289e-005
KB3x = 9.4338e-001
KB4x = 1.1202e-009
KMUx = 0.3454
C5 = 1.2732
Kx = 0

4. Articulated Bus - A-BUS

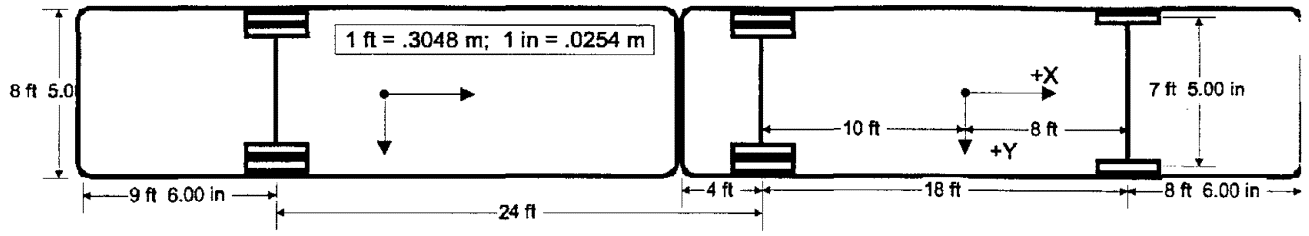

Figure F-4. Dimensions of AASHTO Articulated Bus - A-BUS

a. Vehicle Parameter File "A-BUS.PAR"

Properties of this single unit bus have been estimated based on representative data from Ref. F.4, and scaled from the AASHTO Single Unit Bus model. All parameters are the same as for the BUS model except those shown below.

MASS Total Vehicle Mass (slugs) - No mass specification is provided by AASHTO. MASS has been scaled from the length ratio (75 percent) of the BUS model. **MASS = 370 slugs.**

SMASS Vehicle Sprung Mass (slugs) - SMASS = MASS - UMASSF - UMASSR. **SMASS = 262 slugs**

LENA Distance from Sprung Mass cg to Front Axle (FT) - Ref. F.4. data show that straight trucks are generally slightly front-weight biased. AASHTO gives a wheelbase of 18 ft. **LENA = 8 ft.**

LENB Distance from Sprung Mass cg to Rear Axle (FT) - Wheelbase - LENA: **LENB = 10 ft.**

IXS Sprung Mass Roll Inertia (ft-lb-s^2) - Scaled to 75 percent of BUS model, **IXS = 1500 ft-lb-s^2**

IYS Sprung Mass Pitch Inertia (ft-lb-s^2) - Scaled to 75 percent of BUS model, **IYS = 15000 ft-lb-s^2**

IZZ Total Vehicle Yaw Inertia (ft-lb-s^2) - Scaled to 75 percent of BUS model, **IZZ = 15000 ft-lb-s^2**

b. Suspension Parameter File "A-BUS.SUS"

The suspension model is identical to the BUS model.

c. Trailer Parameter File "A-BUS-TR.PAR"

The trailer geometry is defined by AASHTO. The trailer inertial parameters are assumed to be approximately 50 percent of the tow vehicle, and are scaled accordingly.

MASS Total Vehicle Mass (slugs) - Scaled to 50 percent of tow vehicle. **MASS = 185 slugs.**

SMASS Vehicle Sprung Mass (slugs) - SMASS = MASS - UMASSF - UMASSR. **SMASS = 148 slugs**

UMASSF Front Unsprung Mass (slugs) - Trailer has only a single axle, so front axle parameters are set to zero. **UMASSF = 0 slugs.**

UMASSR Rear Unsprung Mass (slugs) - Ref. F-5 gives the typical value for a non-drive axle of 1200 lb. **UMASSR = 37 slugs.**

LENA Distance from Sprung Mass cg to Front Axle (ft) - **LENA = 0 ft.**

LENB Distance from Sprung Mass cg to Rear Axle (ft) - LENB is set to give a positive tongue weight of 10 percent. AASHTO defines the distance from the hitch to the trailer axle as 20 ft. **LENB = 2.0 ft.**

IXS Sprung Mass Roll Inertia (ft-lb-s^2) - Scaled to 75 percent of A-BUS model **IXS = 1125 ft-lb-s^2**

IYS Sprung Mass Pitch Inertia (ft-lb-s^2) - Scaled to 75 percent of A-BUS model, **IYS = 11250 ft-lb-s^2**

IZZ Total Vehicle Yaw Inertia (ft-lb-s^2) - Scaled to 75 percent of A-BUS model, **IZZ = 11250 ft-lb-s^2**

IXZ Total Vehicle Roll/Yaw Cross Product of Inertia (ft-lb-s^2) - Assumed to be zero.

KTL Tire Lag Constant (ft) - A nominal value of 1 ft is used. **KTL = 1 ft.**

KSR Rear Wheel Rate (lb/ft) - Scaled to 50 percent of A-BUS model, **KSR = 12000 lb/ft**

KSDR Rear Wheel Damping Rate (lb/ft/s) - Scaled to 50 percent of A-BUS model, **KSDR = 1200 lb/ft/s**

TRWR Rear Track Width (ft) - AASHTO defines vehicle width as 8.5 ft. Track width is assumed to be 1 ft less than the vehicle width: **TRWR = 7.5 ft**

HCG Total Vehicle cg Height (ft) - Ref. F.4 gives the typical value of 36 in. **HCG = 3.0 ft**

KBS Bump Stop Stiffness (lb/ft) - Bump stop stiffness was set to be approximately five times the average wheel rate: **KBS = 60000 lb/ft**

HBS Bump Stop Position (ft) - HBS was set to a nominal value of: **HBS = 0.2 ft**

KTSR Rear Auxiliary Roll Stiffness (ft-lb/rad) - Ref. F.4 gives the typical value for overall rear suspension roll stiffness of -60000 in-lb/deg (-286480 ft-lb/rad). This is scaled to 50 percent: -143240 (ft-lb/rad). This is the combined roll stiffness of the suspension springs and any antiroll bar. The springs provide a roll stiffness of:

$$K_{RS} = -\frac{K_{SR} TRWR^2}{2} \qquad \text{(F-8)}$$

giving K_{RS} of -337,500 ft-lb/rad. The auxiliary roll stiffness is the total suspension roll stiffness minus the roll stiffness due to the springs. **KTSR = 194260 ft-lb/rad.**

TSPRINGR Tire Spring Rate (lb/ft) - Ref. F.4 gives a typical value for radial tire spring rate of 4600 lb/in. **TSPRINGR = 55200 lb/ft**

HRAR Rear Suspension Roll Center Height (ft) - Ref. F.4 gives a typical value for rear roll center height of 26 in. **HRAR = 2.17 ft**

HS Sprung Mass cg Height (ft) - The unsprung mass cg height was assumed to be 1.58 ft, and based on the total vehicle cg height (**HCG**), the sprung mass cg height is computed to be: **HS = 3.355 ft**

IXUR Rear Unsprung Mass Roll Inertia (ft-lb-s^2) - The rear unsprung mass roll inertia is estimated to be: **IXUR = 300 ft-lb-s^2**

KLT Tire Lateral Compliance (ft/lb) - Tire lateral compliance is estimated to be 76 percent of the tire vertical compliance [0]: **KLT = 2.3E-5 ft/lb**

SUSPENSIONR Rear Suspension Type (0 or 1) - **SUSPENSIONR = 1**

HR & LR Rear Axle Roll Steer - Ref. F.4 gives a typical value rear axle roll steer of 0.2 (understeer). **HR = -0.2 & LR = 1**

TLEND Longitudinal Distance from Tow Vehicle cg to Hitch (ft) - AASHTO defines the distance from the tow vehicle rear axle to the hitch at 4 ft, and LENB (tow vehicle) is 10 ft, **TLEND = 14 ft**

TLENE Longitudinal Distance from Trailer Vehicle cg to Hitch (ft) - AASHTO defines the distance from the trailer axle to the hitch as 20 ft, and the CG is 2.0 ft ahead of the axle (trailer LENB), **TLENE = 18.0 ft**

THH Initial Height of Hitch Above the Ground (ft) - Initial hitch height is assumed to be approximately at the sprung mass cg height. **THH = 3.4 ft**

HITCHSP Hitch Translational Spring Stiffness (lb/ft) - Hitch stiffness is assumed to be 5000 lb/in, **HITCHSP = 60000 lb/ft**

HITCHSPD Hitch Translational Damping (lb/ft/s) - Hitch damping is assumed to be 100 lb/in/s, **HITCHSPD = 1200 lb/ft/s**

KTFIFTH Fifth Wheel Torsional Stiffness (ft-lb/rad) - Hitch is assumed to allow free rotation between the tow vehicle and trailer, **KTFIFTH = 0 ft-lb/rad**

BRAKLAG1 Brake Torque Time Constant for Steer Axle (s) - Ref. F.4 gives a typical value of 0.3 s. **BRAKLAG1 = 0.3**

BRAKLAG2 Brake Torque Time Constant for Drive Axle (s) - Ref. F.4 gives a typical value of 0.3 s. **BRAKLAG1 = 0.3**

BRAKLAG3 Brake Torque Time Constant for Trailer Axle (s) - Ref. F.4 gives a typical value of 0.3 s. **BRAKLAG1 = 0.6**

NDRWHL Number of Tires on each end of Drive Axle - The AASHTO diagram for the articulated bus shows dual tires on the drive axle. **NDRWHL = 2**

NTRWHL Number of Tires on each end of Trailer Axle(s) - The AASHTO diagram for the articulated bus shows dual tires on the trailer axle. **NTRWHL = 2**

d. Tire Parameter File "A-BUS.TIR"

The tire parameters used are taken from a General Tire "AMERI*S380" 295/75R22.5 radial tire at 125 psi.

e. Driver Parameter File "DRIVER.PAR"

The VDANL driver parameter file requires the vehicle stability factor for its adaptive control algorithms. This vehicle's understeer gradient is approximately 2.2 deg/g, which gives a stability factor of: **KSTABF = 0.0014 rad/ft/s^2**

f. Other Parameters

The AASHTO specifies that the minimum design turning radius of the outside front tire at 10 mi/h is 42.7 ft, which makes the turning radius of the center-of-gravity 42.7-T/2 = 38.95 ft. Running a slowly increasing steer maneuver at 10 mi/h, and knowing that radius of curvature is equal to forward speed divided by yaw rate, a 38.95 radius turn is achieved at a steering wheel angle of 13.5 radians. In NONLIN.PAR, **DSWMAX = 13.9**.

g. Parameter Files

Vehicle Parameters
MASS = 370
SMASS = 262
UMASSF = 37
UMASSR = 71
LENA = 8
LENB = 10
IXS = 1500
IYS = 15000
IZZ = 15000
IXZ = 0
KSTR = 30
KSCF = 0.00002
KSCB = 0
DLADV = 0
DYADV = 0
DNADV = 0
DENSITY = 0.00237
REFAREA = 0
CDX = 0.4
AEROVEL = 44
KTL = 0.5
KSF = 15000
KSDF = 1500
KSR = 24000
KSDR = 2400
TRWF = 7.5
TRWB = 7.5
HCG = 3.0
KBS = 100000
HBS = 0.20
KTSF = 326374
KTSR = 388521
KRAS = 120000
KRADP = 7000
TSPRINGR = 55200
HRAF = 1.58
HRAR = 2.17
HS = 3.4
IXUF = 300
IXUR = 650
KLT = 2.3E-5
XACC = 0
ZACC = 0
DRAGC = 0
LENS = 5.4
LM = 1.125
KBTF = -72.5
KVB = 23.5
KMB = 9.4
FBPVL = 55
SWZ = 0.9
SWW = 100
KCF = -1E-6
LSO = 0
KLAGV = 16.5
BRAKPROP1 = 1
BRAKPROP2 = 1
FXLIMIT = -1000
DAMPCOMF = 0
DAMPEXTF = 0
DAMPCOMR = 0
DAMPEXTR = 0
AIRBRAKES% = 1
BRAKLAG1 = 0.3
BRAKMULTLF = 1
BRAKMULTRF = 1
BRAKMULTLR = 1
BRAKMULTRR = 1

Suspension Parameters
SUSPENSIONF = 1
SUSPENSIONR = 1
HF = 0.2
HR = -0.2
LF = 1
LR = 1
KSAF = 1
KSAR = 1
BF = 0
BR = 0
CF = 0
CR = 0
DF = 0
DR = 0
EF = 0
ER = 0
KSLF = 0
KSLR = 0
LSAF = 1000
LSAR = 1000

KSADF = 0
KSADR = 0
KSAD2F = 0
KSAD2R = 0
KACK = 0
LSAF = 1000
LSAR = 1000
KSADF = 0
KSADR = 0
KSAD2F = 0
KSAD2R = 0
KACK = 0

Trailer Parameters
MASS = 185.0
SMASS = 148.0
UMASSF = 0
UMASSR = 37
LENA = 0
LENB = 2.0
IXS = 1125
IYS = 11250
IZZ = 11250
IXZ = 0
DLADV = 0
DYADV = 0
DNADV = 0
KTL = 1
KSF = 0
KSDF = 0
KSR = 12000
KSDR = 1200
TRWF = 0
TRWB = 7.5
HCG = 3.0
KBS = 60000
HBS = 0.20
KTSF = 0
KTSR = 194260
KRAS = 120000
KRADP = 7000
TSPRINGR = 55200
HRAF = 0
HRAR = 2.17
HS = 3.355
IXUF = 0
IXUR = 300
KLT = 2.3E-5
DRAGC = 0
KLAGV = 25
SUSPENSIONF = 0
SUSPENSIONR = 1
HF = 0
HR = -0.2
LF = 1
LR = 1
KSAF = 0
KSAR = 0
BF = 0
BR = 0
CF = 0
CR = 0
DF = 0
DR = 0
EF = 0
ER = 0
KSLF = 0
KSLR = 0
LSAF = 1
LSAR = 1
KSADF = 0
KSADR = 0
KSAD2F = 0
KSAD2R = 0
TLEND = 14.0
TLENE = 18.0
THH = 3.4
THITCHSP = 60000
THITCHSPD = 1200
KTFIFTH = 0
BRAKLAG1 = 0.3
BRAKLAG2 = 0.3
BRAKLAG3 = 0.6
KFADE = 0.0005
NDRWHL = 2
NTRWHL = 2

Tire Parameters
TWIDTH = 10.00
KA0 = 1.9148e+003
KA1 = 9.1239e+000
KA2 = 2.6632e+004
KA3 = 0.0000e+000
KA4 = 1.0000e+000
KA = 0.0544
KMUy = 0.3454
TPRESS = 125.00
KB1y = -1.4737e-005
KB3y = 6.6176e-001
KB4y = -2.5237e-010
KGAMMA = 0.90
CSFZ = 6.6412
MUNOMy = 0.85
FZTRL = 6175
KK1 = -3.0824e-005
RR = 2.0
TIRE = RADIAL
C1 = 0.4693
C2 = 2.0389
C3 = 1.7886
C4 = 0.7335
G1 = 0.7266
G2 = 1.0000
MUNOMx = 0.85
LONGLAG = 0.25
PLYSTEER = -0.0043
KB1x = -2.9289e-005
KB3x = 9.4338e-001
KB4x = 1.1202e-009
KMUx = 0.3454
DRAGC = 0
C5 = 1.2732
Kx = 0

5. Intermediate Semi-Trailer - WB-40

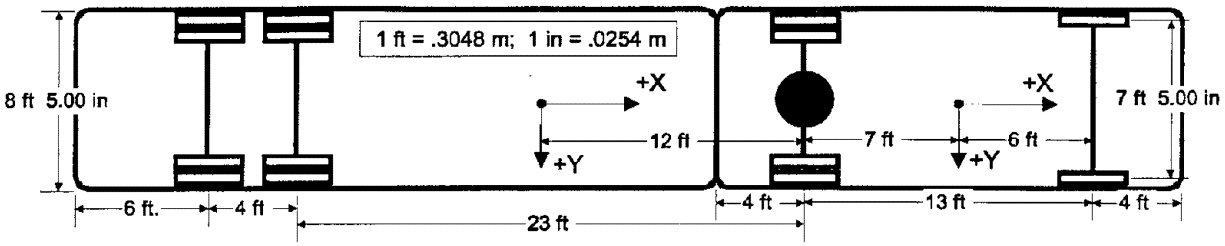

Figure F-5. Dimensions of AASHTO Intermediate Semi-Trailer - WB-40

a. Vehicle Parameter File "WB-40.PAR"

Properties of this intermediate semi-trailer have been estimated based on representative data from Ref. F.4 and F.6. The tractor in Ref. F.6 has two drive axles, and is likely to be larger than the WB-40 tractor. Therefore, inertial data has been scaled to 75 percent of the Ref. F.6 tractor.

MASS	Total Vehicle Mass (slugs) - No mass specification is provided by AASHTO. MASS has been scaled (75 percent) from Ref. F.6 **MASS = 450 slugs.**
SMASS	Vehicle Sprung Mass (slugs) - SMASS = MASS - UMASSF - UMASSR. **SMASS = 338 slugs**
UMASSF	Front Unsprung Mass (slugs) - Ref. F.6 measures the front unsprung mass to be 1255 lb. **UMASSF = 39 slugs.**
UMASSR	Rear Unsprung Mass (slugs) - Ref. F.6 measures the rear unsprung mass to be 2250 lb. **UMASSR = 70 slugs.**
LENA	Distance from Sprung Mass cg to Front Axle (ft) - Ref. F.6 measures the cg to be approximately halfway between the front axle and the fifth wheel (located over the rear axle). AASHTO gives a wheelbase of 13 ft. **LENA = 6 ft.**
LENB	Distance from Sprung Mass cg to Rear Axle (ft) - Wheelbase - LENA: **LENB = 7 ft.**
IXS	Sprung Mass Roll Inertia (ft-lb-s^2) - IXS has been scaled (75 percent) from Ref. F.6 **IXS = 4000 ft-lb-s^2**
IYS	Sprung Mass Pitch Inertia (ft-lb-s^2) - IYS has been scaled (75 percent) from Ref. F.6. **IYS = 20000 ft-lb-s^2**
IZZ	Total Vehicle Yaw Inertia (ft-lb-s^2) - IZZ has been scaled (75 percent) from Ref. F.6. **IZZ = 23000 ft-lb-s^2**
IXZ	Total Vehicle Roll/Yaw Cross Product of Inertia (ft-lb-s^2) - Assumed to be zero.
KSTR	Overall Steering Ratio - KSTR has been measured in Ref.F.6. **KSTR = 12.8**
KSCF	Front Aligning Torque Steer Compliance (rad/ft-lb) - KSCF has been measured in Ref. F.6. **KSCF = 0.000038 rad/ft-lb.**

KSCR Rear Aligning Torque Steer Compliance (rad/ft-lb) - Assumed to be zero. **KSCR = 0 rad/ft-lb.**

KTL Tire Lag Constant (ft) - A nominal value of 1 ft is used. **KTL = 1 ft.**

KSF Front Wheel Rate (lb/ft) - KSF has been measured inRef. F.6. **KSF = 16000 lb/ft**

KSR Rear Wheel Rate (lb/ft) - KSR has been measured in Ref. F.6. **KSR = 54000 lb/ft**

KSDF Front Wheel Damping Rate (lb/ft/s) - Set to a nominal value of: **KSDF = 1600 lb/ft/s**

KSDR Rear Wheel Damping Rate (lb/ft/s) - Set to a nominal value of: **KSDR = 5400 lb/ft/s**

TRWF Front Track Width (ft) - AASHTO defines vehicle width as 8.5 ft. Track width is assumed to be 1 ft less than the vehicle width: **TRWF = 7.5 ft**

TRWR Rear Track Width (ft) - AASHTO defines vehicle width as 8.5 ft. Track width is assumed to be 1 ft less than the vehicle width: **TRWR = 7.5 ft**

HCG Total Vehicle cg Height (ft) - HCG has been measured in Ref. F.6. **HCG = 2.86 ft**

KBS Bump Stop Stiffness (lb/ft) - Bump stop stiffness was set to be approximately five times the average wheel rate: **KBS = 175000 lb/ft**

HBS Bump Stop Position (ft) - HBS was set to a nominal value of: **HBS = 0.2 ft**

KTSF Front Auxiliary Roll Stiffness (ft-lb/rad) - Overall front suspension roll stiffness has been measured in Ref. F.6 as -22,000 in-lb/deg (-105,000 ft-lb/rad). The tractor frame torsional stiffness was measured to be -10,700 in-lb/deg (-51088 ft-lb/rad). Because VDANL does not model frame flexibility directly, the frame torsional stiffness is put in series with the front roll stiffness. The composite front roll stiffness is then 7198 in-lb/deg (-34,380 ft-lb/rad). This is the combined roll stiffness of the suspension springs and any antiroll bar. The front springs provide a roll stiffness of:

$$K_{RS} = -\frac{K_{SF} TRWF^2}{2} \qquad \text{(F-9)}$$

giving K_{RS} of -450,000 ft-lb/rad. The auxiliary roll stiffness is the total suspension roll stiffness minus the roll stiffness due to the springs. **KTSF = 415620 ft-lb/rad.**

KTSR Rear Auxiliary Roll Stiffness (ft-lb/rad) - Overall rear suspension roll stiffness has been measured in Ref. F.6 as -68,000 in-lb/deg (-324,700 ft-lb/rad). This is the combined roll stiffness of the suspension springs and any antiroll bar. The rear springs provide a roll stiffness of:

$$K_{RS} = -\frac{K_{SR} TRWR^2}{2} \qquad \text{(F-10)}$$

giving K_{RS} of -1,518,000 ft-lb/rad. The auxiliary roll stiffness is the total suspension roll stiffness minus the roll stiffness due to the springs. **KTSR = 1193300 ft-lb/rad.**

TSPRINGR Tire Spring Rate (lb/ft) - Ref. F.4 gives a typical value for radial tire spring rate of 4600 lb/in. **TSPRINGR = 55200 lb/ft**

HRAF Front Suspension Roll Center Height (ft) - HRAF has been measured in Ref. F.6. **HRAF = 1.42 ft**

HRAR Rear Suspension Roll Center Height (ft) - HRAR has been measured in Ref. F.6. **HRAR = 2.32 ft**

HS Sprung Mass cg Height (ft) - The unsprung mass cg heights were assumed to be 1.58 ft, and based on the total vehicle cg height (**HCG**), the sprung mass cg height is computed to be: **HS = 3.28 ft**

IXUF Front Unsprung Mass Roll Inertia (ft-lb-s^2) - From measurements in Ref. F.6, the front unsprung mass roll inertia is estimated to be: **IXUF = 500 ft-lb-s^2**

IXUR Rear Unsprung Mass Roll Inertia (ft-lb-s^2) - From measurements in Ref. F.6, the rear unsprung mass roll inertia is estimated to be: **IXUR = 625 ft-lb-s^2**

KLT Tire Lateral Compliance (ft/lb) - Tire lateral compliance is estimated to be 76 percent of the tire vertical compliance Ref. F.2: **KLT = 2.3E-5 ft/lb**

KBTF Front Wheel Brake Effectiveness (ft-lb/psi) – Measurements at VRTC for the Volvo tractor/ Fruehauf semi-trailer give: **KBTF = -57.2 ft-lb/psi**

KVB Brake Gain in Vacuum Boost Range (psi/lb) - Measurements at VRTC for the Volvo tractor/ Fruehauf semi-trailer give: **KVB = 1.4 psi/lb**

KVM Brake Gain in Manual Range (psi/lb) - Measurements at VRTC for the Volvo tractor/ Fruehauf semi-trailer give: **KVM = 1.4 psi/lb**

FBPVL Pedal Force when Vacuum Boost Runs Out (lb) – Not used with airbrake models. **FBPVL = 0 lb**

SWW Steering System Natural Frequency (rad/s) - Because of the stiffness of heavy truck steering systems, the steering system natural frequency will be out of the handling frequency range. Therefore, steering system dynamics will be ignored. **SWW = 0 rad/s**

BRAKPROP1 Steer Axle Brake Gain (ft-lb/lb) - Measurements at VRTC for the Volvo tractor/ Fruehauf semi-trailer give: **80 ft-lb/lb**

BRAKPROP2 Drive/Trailer Axle Brake Gain (ft-lb/lb) - Measurements at VRTC for the Volvo tractor/ Fruehauf semi-trailer give: **200 ft-lb/lb**

AIRBRAKE% Air Brake Flag - This truck is assumed to have air brakes. **AIRBRAKE% = 1**

b. Suspension Parameter File "WB-40.SUS"

It is assumed that this vehicle has no anti-lift/dive forces, and no Ackerman steering geometry. The following are parameters that are set in the suspension file that are specific to this vehicle.

SUSPENSIONF Front Suspension Type (0 or 1) - **SUSPENSIONF = 1**

SUSPENSIONR Rear Suspension Type (0 or 1) - **SUSPENSIONR = 1**

HF & LF Front Axle Roll Steer - Roll steer has been measured in Ref. F.6 as .225 (deg/deg understeer). **HF = 0.225 & LF = 1**

HR & LR Rear Axle Roll Steer - Roll steer has been measured in Ref. F.6 as -.117 (deg/deg understeer). **HR = -0.117 & LR = 1**

c. Trailer Parameter File "WB-40-TR.PAR"

The trailer geometry is defined by AASHTO.

MASS Total Vehicle Mass (slugs) - MASS has been scaled (75percent) from Ref. F.6. It is assumed that a 10,000-lb load is being carried. **MASS = 620 slugs.**

SMASS Vehicle Sprung Mass (slugs) - SMASS = MASS - UMASSF - UMASSR. **SMASS = 520 slugs**

UMASSF Front Unsprung Mass (slugs) - UMASSF has been measured in Ref. F.6. **UMASSF = 50 slugs.**

UMASSR Rear Unsprung Mass (slugs) - UMASSR has been measured in Ref. F.6 **UMASSR = 50 slugs.**

LENA Distance from Sprung Mass cg to Front Axle (ft) - AASHTO defines the distance from the fifth wheel to the front trailer axle as 23 ft. Based on scaling from Ref. F.6, the distance from the sprung mass cg to the fifth wheel has been set to 12 ft. **LENA = -11 ft.**

LENB Distance from Sprung Mass cg to Rear Axle (FT) - AASHTO defines the distance between the trailer axles to be 4 ft. **LENB = 15 ft.**

IXS Sprung Mass Roll Inertia (ft-lb-s^2) - Because of the assumed loading, mass moments of inertia are set equal to the measurements in Ref. F.6. **IXS = 7000 ft-lb-s^2**

IYS Sprung Mass Pitch Inertia (ft-lb-s^2) - Because of the assumed loading, mass moments of inertia are set equal to the measurements in Ref. F.6. **IYS = 122000 ft-lb-s^2**

IZZ Total Vehicle Yaw Inertia (ft-lb-s^2) - Because of the assumed loading, mass moments of inertia are set equal to the measurements in Ref. F.6. **IZZ = 129000 ft-lb-s^2**

IXZ Total Vehicle Roll/Yaw Cross Product of Inertia (ft-lb-s^2) - Assumed to be zero.

KTL Tire Lag Constant (ft) - A nominal value of 1 ft is used. **KTL = 1 ft.**

KSF Front Wheel Rate (lb/ft) - KSF has been measured in Ref. F.6. **KSF = 121000 lb/ft**

KSR Rear Wheel Rate (lb/ft) - KSR has been measured in Ref. F.6. **KSR = 108000 lb/ft**

KSDF Front Wheel Damping Rate (lb/ft/s) - Set to a nominal value of: **KSDF = 2200 lb/ft/s**

KSDR Rear Wheel Damping Rate (lb/ft/s) - Set to a nominal value of: **KSDR = 2200 lb/ft/s**

TRWF Front Track Width (ft) - AASHTO defines vehicle width as 8.5 ft. Track width is assumed to be 1 ft less than the vehicle width: **TRWF = 7.5 ft**

TRWR Rear Track Width (ft) - AASHTO defines vehicle width as 8.5 ft. Track width is assumed to be 1 ft less than the vehicle width: **TRWR = 7.5 ft**

HCG Total Vehicle cg Height (ft) - HCG has been measured in Ref. F.6. **HCG = 5.0 ft**

KBS Bump Stop Stiffness (lb/ft) - Bump stop stiffness was set to be approximately five times the average wheel rate: **KBS = 600000 lb/ft**

HBS Bump Stop Position (ft) - HBS was set to a nominal value of: **HBS = 0.2 ft**

KTSF Front Auxiliary Roll Stiffness (ft-lb/rad) - Overall front suspension roll stiffness has been measured in Ref. F.6 as -175,000 in-lb/deg (-835,000 ft-lb/rad). This is the combined roll stiffness of the suspension springs and any antiroll bar. The front springs provide a roll stiffness of:

$$K_{RS} = -\frac{K_{SF} TRWF^2}{2} \qquad \text{(F-11)}$$

giving K_{RS} of -3,403,000 ft-lb/rad. The auxiliary roll stiffness is the total suspension roll stiffness minus the roll stiffness due to the springs. **KTSF = 2568000 ft-lb/rad.**

KTSR Rear Auxiliary Roll Stiffness (ft-lb/rad) - Overall rear suspension roll stiffness has been measured in Ref. F.6 as -178,000 in-lb/deg (-850,000 ft-lb/rad). This is the combined roll stiffness of the suspension springs and any antiroll bar. The rear springs provide a roll stiffness of:

$$K_{RS} = -\frac{K_{SR} TRWR^2}{2} \qquad \text{(F-12)}$$

giving K_{RS} of -3,037,000 ft-lb/rad. The auxiliary roll stiffness is the total suspension roll stiffness minus the roll stiffness due to the springs. **KTSR = 2187000 ft-lb/rad.**

TSPRINGR Tire Spring Rate (lb/ft) - Ref. F.6 gives a typical value for radial tire spring rate of 4600 lb/in. **TSPRINGR = 55200 lb/ft**

HRAF Front Suspension Roll Center Height (ft) - HRAF has been measured in reference 0. **HRAR = 2.4 ft**

HRAR Rear Suspension Roll Center Height (ft) - HRAR has been measured in Ref. F.6. **HRAR = 2.28 ft**

HS Sprung Mass cg Height (ft) - HS has been measured in Ref. F.6. The additional load cg was assumed to be at the same location as the trailer sprung mass cg. **HS = 5.66 ft**

IXUF Front Unsprung Mass Roll Inertia (ft-lb-s^2) - From measurements in Ref. F.6, the front unsprung mass roll inertia is estimated to be: **IXUF = 570 ft-lb-s^2**

IXUR Rear Unsprung Mass Roll Inertia (ft-lb-s^2) - From measurements in Ref. F.6, the rear unsprung mass roll inertia is estimated to be: **IXUR = 570 ft-lb-s^2**

KLT Tire Lateral Compliance (ft/lb) - Tire lateral compliance is estimated to be 76 percent of the tire vertical compliance Ref. F.2: **KLT = 2.3E-5 ft/lb**

SUSPENSIONF Rear Suspension Type (0 or 1) - **SUSPENSIONF = 1**

SUSPENSIONR Rear Suspension Type (0 or 1) - **SUSPENSIONR = 1**

HF & LF Front Axle Roll Steer - Roll steer has been measured in Ref. F.6 as .035 (deg/deg understeer). **HF = 0.035 & LF = 1**

HR & LR Rear Axle Roll Steer - Roll steer has been measured in Ref. F.6 as .169 (deg/deg understeer). **HR = 0.169 & LR = 1**

TLEND Longitudinal Distance from Tow Vehicle cg to Hitch (ft) - Referring to Figure F-5, the fifth wheel is located over the tractor drive axle, which is 7 ft behind the tractor cg. **TLEND = 7 ft**

TLENE Longitudinal Distance from Trailer Vehicle CG to Hitch (ft) - Referring to Figure F-5, the fifth wheel is located over the tractor drive axle, which is 12 ft ahead of the trailer cg. **TLENE = 12.0 ft**

THH Initial Height of Hitch Above the Ground (ft) - Initial hitch height was measured in Ref. F.6. **THH = 3.6 ft**

HITCHSP Hitch Translational Spring Stiffness (lb/ft) - Hitch stiffness is assumed to be 50000 lb/in, **HITCHSP = 600000 lb/ft**

HITCHSPD Hitch Translational Damping (lb/ft/s) - Hitch damping is assumed to be 200 lb/in/s, **HITCHSPD = 2400 lb/ft/s**

KTFIFTH Fifth Wheel Torsional Stiffness (ft-lb/rad) - Fifth wheel torsional stiffness was measured in Ref. F.6. **KTFIFTH = 1146000 ft-lb/rad**

BRAKLAG1 Brake Torque Time Constant for Steer Axle (s) - Measurements at VRTC for the Volvo tractor/ Fruehauf semi-trailer give: **BRAKLAG1 = 0.31**

BRAKLAG2 Brake Torque Time Constant for Drive Axle (s) - Measurements at VRTC for the Volvo tractor/ Fruehauf semi-trailer give: **BRAKLAG2 = 0.35**

BRAKLAG3 Brake Torque Time Constant for Trailer Axle (s) - Measurements at VRTC for the Volvo tractor/ Fruehauf semi-trailer give:. **BRAKLAG3 = 0.42**

NDRWHL Number of Tires on each end of Drive Axle(s) - The AASHTO diagram for the intermediate semitrailer shows dual tires on the drive axle. **NDRWHL = 2**

NTRWHL Number of Tires on each end of Trailer Axle(s) - The AASHTO diagram for the intermediate semitrailer shows dual tires on each of the trailer axle. **NTRWHL = 2**

d. Tire Parameter File "WB-40.TIR"

The tire parameters used are taken from a General Tire "AMERI*S380" 295/75R22.5 radial tire at 125 psi.

e. Driver Parameter File "DRIVER.PAR"

The VDANL driver parameter file requires the vehicle stability factor for its adaptive control algorithms. This vehicles understeer gradient is approximately 1.5 deg/g, which gives a stability factor of: **KSTABF = 0.0008 rad/ft/s^2**

f. Other Parameters

The AASHTO specifies that the minimum design turning radius of the outside front tire at 10 mi/h is 40.0 ft, which makes the turning radius of the cg 40.0-T/2 = 36.25 ft. Running a slowly increasing steer maneuver at 10 mi/h, and knowing that radius of curvature is equal to forward speed divided by yaw rate, a 36.25 radius turn is achieved at a steering wheel angle of 4.6 radians. In NONLIN.PAR, **DSWMAX = 4.6**.

g. Parameter Files

Vehicle Parameters
MASS = 450
SMASS = 338
UMASSF = 39
UMASSR = 70
LENA = 6
LENB = 7
IXS = 4000
IYS = 20000
IZZ = 23000
IXZ = 0
KSTR = 12.8
KSCF = 0.000038
KSCB = 0
DLADV = 0
DYADV = 0
DNADV = 0
DENSITY = 0.00237
REFAREA = 0
CDX = 0.4
AEROVEL = 44
KTL = 1
KSF = 16000
KSDF = 1600
KSR = 54000
KSDR = 5400
TRWF = 7.5
TRWB = 7.5
HCG = 2.86
KBS = 175000
HBS = 0.20
KTSF = 415620
KTSR = 1193300
KRAS = 120000
KRADP = 7000
TSPRINGR = 55200
HRAF = 1.42
HRAR = 2.32
HS = 3.28
IXUF = 500
IXUR = 625
KLT = 2.3E-5
XACC = 0
ZACC = 0
DRAGC = 0
LENS = 5.4
LM = 1.125
KBTF = -57.21
KVB = 1.4
KMB = 1.4
FBPVL = 100
SWZ = 0.9
SWW = 100
KCF = -1E-6
LSO = 0
KLAGV = 16.5
BRAKPROP1 = 80
BRAKPROP2 = 200
FXLIMIT = 0
DAMPCOMF = 0
DAMPEXTF = 0
DAMPCOMR = 0
DAMPEXTR = 0
AIRBRAKES% = 1
BRAKLAG1 = 0.3
BRAKMULTLF = 1
BRAKMULTRF = 1
BRAKMULTLR = 1
BRAKMULTRR = 1

Suspension Parameters
SUSPENSIONF = 1
SUSPENSIONR = 1
HF = 0.225
HR = -0.117
LF = 1
LR = 1
KSAF = 1
KSAR = 1
BF = 0
BR = 0
CF = 0
CR = 0
DF = 0
DR = 0
EF = 0
ER = 0
KSLF = 0
KSLR = 0
LSAF = 1000
LSAR = 1000
KSADF = 0
KSADR = 0
KSAD2F = 0
KSAD2R = 0
KACK = 0

Trailer Parameters
MASS = 620
SMASS = 520
UMASSF = 50
UMASSR = 50
LENA = -11
LENB = 15
IXS = 7000
IYS = 122000
IZZ = 129000
IXZ = 0
DLADV = 0
DYADV = 0
DNADV = 0
KTL = 1
KSF = 121000
KSDF = 2200
KSR = 108000
KSDR = 2200
TRWF = 7.5
TRWB = 7.5
HCG = 5.0
KBS = 600000
HBS = .20
KTSF = 2568000
KTSR = 2187000
KRAS = 120000
KRADP = 7000
TSPRINGR = 55200
HRAF = 2.4
HRAR = 2.28
HS = 5.66
IXUF = 570
IXUR = 570
KLT = 2.3E-5
DRAGC = 0
KLAGV = 25
SUSPENSIONF = 1
SUSPENSIONR = 1
HF = 0.035
HR = 0.169
LF = 1
LR = 1
KSAF = 0
KSAR = 0
BF = 0

BR = 0
CF = 0
CR = 0
DF = 0
DR = 0
EF = 0
ER = 0
KSLF = 0
KSLR = 0
LSAF = 1
LSAR = 1
KSADF = 0
KSADR = 0
KSAD2F = 0
KSAD2R = 0
TLEND = 7.0
TLENE = 12.0
THH = 3.6
THITCHSP = 600000
THITCHSPD = 2200
KTFIFTH = 1146000

BRAKLAG1 = 0.31
BRAKLAG2 = 0.33
BRAKLAG3 = 0.42
KFADE = 0.0005
NDRWHL = 2
NTRWHL = 2

Tire Parameters
TWIDTH = 10.00
KA0 = 1.9148e+003
KA1 = 9.1239e+000
KA2 = 2.6632e+004
KA3 = 0.0000e+000
KA4 = 1.0000e+000
KA = 0.0544
KMUy = 0.3454
TPRESS = 125.00
KB1y = -1.4737e-005
KB3y = 6.6176e-001
KGAMMA = 0.90
CSFZ = 6.6412

MUNOMy = 0.85
FZTRL = 6175
KK1 = -3.0824e-005
RR = 2.0
TIRE = RADIAL
C1 = 0.4693
C2 = 2.0389
C3 = 1.7886
C4 = 0.7335
G1 = 0.7266
G2 = 1.0000
MUNOMx = 0.85
LONGLAG = 0.25
PLYSTEER = -0.0043
KB1x = -2.9289e-005
KB3x = 9.4338e-001
KB4x = 1.1202e-009
KMUx = 0.3454
DRAGC = 0
C5 = 1.2732
Kx = 0

6. Large Semi-Trailer - WB-50

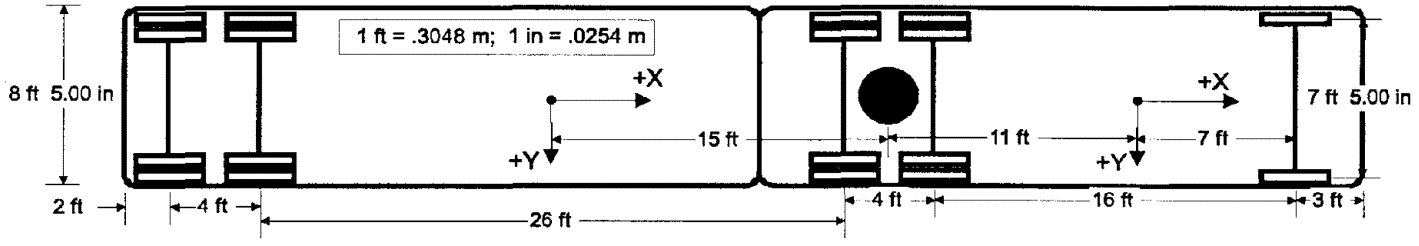

Figure F-6. Dimensions of AASHTO Large Semi-Trailer - WB-50

a. Vehicle Parameter File "WB-50.PAR"

Properties of this large semi-trailer have been estimated based on representative data from Ref. F.4 and F.6.

MASS Total Vehicle Mass (slugs) - No mass specification is provided by AASHTO. MASS from Ref. F.6. **MASS = 600 slugs.**

SMASS Vehicle Sprung Mass (slugs) - SMASS = MASS - UMASSF - UMASSR. **SMASS = 419 slugs**

UMASSF Front Unsprung Mass (slugs) - Ref. F.6 measures the front unsprung mass to be 1255 lb. **UMASSF = 39 slugs.**

UMASSR Rear Unsprung Mass (slugs) - Ref. F.6 measures the total (both axles combined) rear unsprung mass to be 4570 lb. **UMASSR = 142 slugs.**

LENA Distance from Sprung Mass cg to Front Axle (FT) - Ref. F.6 measures the CG to be approximately halfway between the front axle and the fifth wheel (located between the rear axles). AASHTO gives a wheelbase of 18 ft. **LENA = 7 ft.**

LENB Distance from Sprung Mass cg to Rear Axle (ft) - Wheelbase - LENA: **LENB = 11 ft.**

IXS Sprung Mass Roll Inertia (ft-lb-s^2) - IXS from Ref. F.6. **IXS = 5300 ft-lb-s^2**

IYS Sprung Mass Pitch Inertia (ft-lb-s^2) - IYS from Ref. F.6. **IYS = 27000 ft-lb-s^2**

IZZ Total Vehicle Yaw Inertia (ft-lb-s^2) - IZZ from Ref. F.6. **IZZ = 30000 ft-lb-s^2**

IXZ Total Vehicle Roll/Yaw Cross Product of Inertia (ft-lb-s^2) - Assumed to be zero.

KSTR Overall Steering Ratio - KSTR has been measured in Ref. F.6. **KSTR = 12.8**

KSCF Front Aligning Torque Steer Compliance (rad/ft-lb) - KSCF has been measured in Ref. F.6. **KSCF = 0.000038 rad/ft-lb.**

KSCR Rear Aligning Torque Steer Compliance (rad/ft-lb) - Assumed to be zero. **KSCR = 0 rad/ft-lb.**

KTL Tire Lag Constant (ft) - A nominal value of 1 ft is used. **KTL = 1 ft.**

KSF Front Wheel Rate (lb/ft) - KSF has been measured in Ref. F.6. **KSF = 16000 lb/ft**

KSR Rear Wheel Rate (lb/ft) - KSR has been measured in Ref. F.6. **KSR = 54000 lb/ft**

KSDF Front Wheel Damping Rate (lb/ft/s) - Set to a nominal value of: **KSDF = 1600 lb/ft/s**

KSDR Rear Wheel Damping Rate (lb/ft/s) - Set to a nominal value of: **KSDR = 5400 lb/ft/s**

TRWF Front Track Width (ft) - AASHTO defines vehicle width as 8.5 ft. Track width is assumed to be 1 ft less than the vehicle width: **TRWF = 7.5 ft**

TRWR Rear Track Width (ft) - AASHTO defines vehicle width as 8.5 ft. Track width is assumed to be 1 ft less than the vehicle width: **TRWR = 7.5 ft**

HCG Total Vehicle cg Height (ft) - HCG has been measured in Ref. F.6. **HCG = 2.86 ft**

KBS Bump Stop Stiffness (lb/ft) - Bump stop stiffness was set to be approximately five times the average wheel rate: **KBS = 175000 lb/ft**

HBS Bump Stop Position (ft) - HBS was set to a nominal value of: **HBS = 0.2 ft**

KTSF Front Auxiliary Roll Stiffness (ft-lb/rad) - Overall front suspension roll stiffness has been measured in Ref. F.6 as -22,000 in-lb/deg (-105,000 ft-lb/rad). The tractor frame torsional stiffness was measured to be -10,700 in-lb/deg (-51088 ft-lb/rad). Because VDANL does not model frame flexibility directly, the frame torsional stiffness is put in series with the front roll stiffness. The composite front roll stiffness is then 7198 in-lb/deg (-34,380 ft-lb/rad). This is the combined roll stiffness of the suspension springs and any anti-roll bar. The front springs provide a roll stiffness of:

$$K_{RS} = -\frac{K_{SF} TRWF^2}{2} \quad \text{(F-13)}$$

giving K_{RS} of -450,000 ft-lb/rad. The auxiliary roll stiffness is the total suspension roll stiffness minus the roll stiffness due to the springs. **KTSF = 415620 ft-lb/rad.**

KTSR Rear Auxiliary Roll Stiffness (ft-lb/rad) - Overall rear suspension roll stiffness has been measured in Ref. F.6 as -68,000 in-lb/deg (-324,700 ft-lb/rad). This is the combined roll stiffness of the suspension springs and any antiroll bar. The rear springs provide a roll stiffness of:

$$K_{RS} = -\frac{K_{SR} TRWR^2}{2} \quad \text{(F-14)}$$

giving K_{RS} of -1,518,000 ft-lb/rad. The auxiliary roll stiffness is the total suspension roll stiffness minus the roll stiffness due to the springs. **KTSR = 1193300 ft-lb/rad.**

TSPRINGR Tire Spring Rate (lb/ft) - Ref. F.4 gives a typical value for radial tire spring rate of 4600 lb/in. **TSPRINGR = 55200 lb/ft**

HRAF Front Suspension Roll Center Height (ft) - HRAF has been measured in Ref. F.6. **HRAF = 1.42 ft**

HRAR Rear Suspension Roll Center Height (ft) - HRAR has been measured in Ref. F.6. **HRAR = 2.32 ft**

HS Sprung Mass cg Height (ft) - The unsprung mass cg heights were assumed to be 1.58 ft, and based on the total vehicle cg height (**HCG**), the sprung mass cg height is computed to be: **HS = 3.28 ft**

IXUF Front Unsprung Mass Roll Inertia (ft-lb-s^2) - From measurements in Ref. F.6, the front unsprung mass roll inertia is estimated to be: **IXUF = 500 ft-lb-s^2**

IXUR Rear Unsprung Mass Roll Inertia (ft-lb-s^2) - From measurements in Ref. F.6, the rear unsprung mass roll inertia is estimated to be: **IXUR = 1250 ft-lb-s^2**

KLT Tire Lateral Compliance (ft/lb) - Tire lateral compliance is estimated to be 76 percent of the tire vertical compliance Ref. F.2: **KLT = 2.3E-5 ft/lb**

KBTF Front Wheel Brake Effectiveness (ft-lb/psi) – Measurements at VRTC for the Volvo tractor/ Fruehauf semi-trailer give: **KBTF = -57.2 ft-lb/psi**

KVB Brake Gain in Vacuum Boost Range (psi/lb) - Measurements at VRTC for the Volvo tractor/ Fruehauf semi-trailer give: **KVB = 1.4 psi/lb**

KVM Brake Gain in Manual Range (psi/lb) - Measurements at VRTC for the Volvo tractor/ Fruehauf semi-trailer give: **KVM = 1.4 psi/lb**

FBPVL Pedal Force when Vacuum Boost Runs Out (lb) – Not used with airbrake models. **FBPVL = 0 lb**

SWW Steering System Natural Frequency (rad/s) - Because of the stiffness of heavy truck steering systems, the steering system natural frequency will be out of the handling frequency range. Therefore, steering system dynamics will be ignored. **SWW = 0 rad/s**

BRAKPROP1 Steer Axle Brake Gain (ft-lb/lb) - Measurements at VRTC for the Volvo tractor/ Fruehauf semi-trailer give: **80 ft-lb/lb**

BRAKPROP2 Drive/Trailer Axle Brake Gain (ft-lb/lb) - Measurements at VRTC for the Volvo tractor/ Fruehauf semi-trailer give: **200 ft-lb/lb**

AIRBRAKE% Air Brake Flag - This truck is assumed to have air brakes. **AIRBRAKE% = 1**

b. Suspension Parameter File "WB-50.SUS"

It is assumed that this vehicle has no anti-lift/dive forces and no Ackerman steering geometry. The following are parameters that are set in the suspension file that are specific to this vehicle.

SUSPENSIONF	Front Suspension Type (0 or 1) - **SUSPENSIONF = 1**
SUSPENSIONR	Rear Suspension Type (0 or 1) - **SUSPENSIONR = 1**
HF & LF	Front Axle Roll Steer - Roll steer has been measured in Ref. F.6 as 0.225 (deg/deg understeer). **HF = 0.225 & LF = 1**
HR & LR	Rear Axle Roll Steer - Roll steer has been measured in Ref. F.6 as -0.117 (deg/deg understeer). **HR = -0.117 & LR = 1**

c. Trailer Parameter File "WB-50-TR.PAR"

The trailer geometry is defined by AASHTO.

MASS	Total Vehicle Mass (slugs) - MASS has been scaled (75 percent) from Ref. F.6. It is assumed that a 10,000-lb load is being carried. **MASS = 830 slugs.**
SMASS	Vehicle Sprung Mass (slugs) - SMASS = MASS - UMASSF - UMASSR. **SMASS = 730 slugs**
UMASSF	Front Unsprung Mass (slugs) - UMASSF has been measured in Ref. F.6. **UMASSF = 50 slugs.**
UMASSR	Rear Unsprung Mass (slugs) - UMASSR has been measured in Ref. F.6. **UMASSR = 50 slugs.**
LENA	Distance from Sprung Mass cg to Front Axle (FT) - AASHTO defines the distance from the fifth wheel to the front trailer axle as 28 ft. Based on scaling from Ref. F.6, the distance from the sprung mass cg to the fifth wheel has been set to 12 ft. **LENA = -11 ft.**
LENB	Distance from Sprung Mass cg to Rear Axle (ft) - AASHTO defines the distance between the trailer axles to be 4 ft. **LENB = 15 ft.**
IXS	Sprung Mass Roll Inertia (ft-lb-s^2) - Because of the assumed loading, mass moments of inertia are set equal to the measurements in Ref. F.6. **IXS = 7000 ft-lb-s^2**
IYS	Sprung Mass Pitch Inertia (ft-lb-s^2) - Because of the assumed loading, mass moments of inertia are set equal to the measurements in Ref. F.6. **IYS = 122000 ft-lb-s^2**
IZZ	Total Vehicle Yaw Inertia (ft-lb-s^2) - Because of the assumed loading, mass moments of inertia are set equal to the measurements in Ref. F.6. **IZZ = 129000 ft-lb-s^2**
IXZ	Total Vehicle Roll/Yaw Cross Product of Inertia (ft-lb-s^2) - Assumed to be zero.

KTL Tire Lag Constant (ft) - A nominal value of 1 ft is used. **KTL = 1 ft.**

KSF Front Wheel Rate (lb/ft) - KSF has been measured in Ref. F.6. **KSF = 121000 lb/ft**

KSR Rear Wheel Rate (lb/ft) - KSR has been measured in Ref. F.6. **KSR = 108000 lb/ft**

KSDF Front Wheel Damping Rate (lb/ft/s) - Set to a nominal value of: **KSDF = 2200 lb/ft/s**

KSDR Rear Wheel Damping Rate (lb/ft/s) - Set to a nominal value of: **KSDR = 2200 lb/ft/s**

TRWF Front Track Width (ft) - AASHTO defines vehicle width as 8.5 ft. Track width is assumed to be 1 ft less than the vehicle width: **TRWF = 7.5 ft**

TRWR Rear Track Width (ft) - AASHTO defines vehicle width as 8.5 ft. Track width is assumed to be 1 ft less than the vehicle width: **TRWR = 7.5 ft**

HCG Total Vehicle cg Height (ft) - HCG has been measured in Ref. F.6. **HCG = 5.0 ft**

KBS Bump Stop Stiffness (lb/ft) - Bump stop stiffness was set to be approximately five times the average wheel rate: **KBS = 600000 lb/ft**

HBS Bump Stop Position (ft) - HBS was set to a nominal value of: **HBS = 0.2 ft**

KTSF Front Auxiliary Roll Stiffness (ft-lb/rad) - Overall front suspension roll stiffness has been measured in Ref. F.6 as -175,000 in-lb/deg (-835,000 ft-lb/rad). This is the combined roll stiffness of the suspension springs and any antiroll bar. The front springs provide a roll stiffness of:

$$K_{RS} = -\frac{K_{SF} TRWF^2}{2} \qquad \text{(F-15)}$$

giving K_{RS} of -3,403,000 ft-lb/rad. The auxiliary roll stiffness is the total suspension roll stiffness minus the roll stiffness due to the springs. **KTSF = 2568000 ft-lb/rad.**

KTSR Rear Auxiliary Roll Stiffness (ft-lb/rad) - Overall rear suspension roll stiffness has been measured in Ref. F.6 as -178,000 in-lb/deg (-850,000 ft-lb/rad). This is the combined roll stiffness of the suspension springs and any antiroll bar. The rear springs provide a roll stiffness of:

$$K_{RS} = -\frac{K_{SR} TRWR^2}{2} \qquad \text{(F-16)}$$

giving K_{RS} of -3,037,000 ft-lb/rad. The auxiliary roll stiffness is the total suspension roll stiffness minus the roll stiffness due to the springs. **KTSR = 2187000 ft-lb/rad.**

TSPRINGR Tire Spring Rate (lb/ft) - Ref. F.4 gives a typical value for radial tire spring rate of 4600 lb/in. **TSPRINGR = 55200 lb/ft**

HRAF Front Suspension Roll Center Height (ft) - HRAF has been measured in Ref. F.6. **HRAR = 2.4 ft**

HRAR Rear Suspension Roll Center Height (ft) - HRAR has been measured in Ref. F.6. **HRAR = 2.28 ft**

HS Sprung Mass cg Height (ft) - HS has been measured in Ref. F.6. The additional load cg was assumed to be at the same location as the trailer sprung mass cg. **HS = 5.66 ft**

IXUF Front Unsprung Mass Roll Inertia (ft-lb-s^2) - From measurements in Ref. F.6, the front unsprung mass roll inertia is estimated to be: **IXUF = 570 ft-lb-s^2**

IXUR Rear Unsprung Mass Roll Inertia (ft-lb-s^2) - From measurements in Ref. F.6, the rear unsprung mass roll inertia is estimated to be: **IXUR = 570 ft-lb-s^2**

KLT Tire Lateral Compliance (ft/lb) - Tire lateral compliance is estimated to be 76 percent of the tire vertical compliance Ref. F.2: **KLT = 2.3E-5 ft/lb**

SUSPENSIONF Rear Suspension Type (0 or 1) - **SUSPENSIONF = 1**

SUSPENSIONR Rear Suspension Type (0 or 1) - **SUSPENSIONR = 1**

HF & LF Front Axle Roll Steer - Roll steer has been measured in Ref. F.6 as 0.035 (deg/deg understeer). **HF = 0.035 & LF = 1**

HR & LR Rear Axle Roll Steer - Roll steer has been measured in Ref. F.6 as 0.169 (deg/deg understeer). **HR = 0.169 & LR = 1**

TLEND Longitudinal Distance from Tow Vehicle cg to Hitch (ft) - Referring to Figure F-6, the fifth wheel is located over the tractor drive axle, which is 11 ft behind the tractor cg. **TLEND = 11 ft**

TLENE Longitudinal Distance from Trailer Vehicle cg to Hitch (ft) - Referring to Figure F-6, the fifth wheel is located over the tractor drive axle, which is 15 ft ahead of the trailer cg. **TLENE = 15.0 ft**

THH Initial Height of Hitch Above the Ground (ft) - Initial hitch height was measured in Ref. F.6. **THH = 3.6 ft**

HITCHSP Hitch Translational Spring Stiffness (lb/ft) - Hitch stiffness is assumed to be 50000 lb/in, **HITCHSP = 600000 lb/ft**

HITCHSPD Hitch Translational Damping (lb/ft/s) - Hitch damping is assumed to be 200 lb/in/s, **HITCHSPD = 2400 lb/ft/s**

KTFIFTH Fifth Wheel Torsional Stiffness (ft-lb/rad) - Fifth wheel torsional stiffness was measured in Ref. F.6. **KTFIFTH = 1146000 ft-lb/rad**

BRAKLAG1 Brake Torque Time Constant for Steer Axle (s) - Measurements at VRTC for the Volvo tractor/ Fruehauf semi-trailer give: **BRAKLAG1 = 0.31**

BRAKLAG2 Brake Torque Time Constant for Drive Axle (s) - Measurements at VRTC for the Volvo tractor/ Fruehauf semi-trailer give: **BRAKLAG2 = 0.35**

BRAKLAG3 Brake Torque Time Constant for Trailer Axle (s) - Measurements at VRTC for the Volvo tractor/ Fruehauf semi-trailer give:. **BRAKLAG3 = 0.42**

NDRWHL Number of Tires on each end of Drive Axle(s) - The AASHTO diagram for the large semitrailer shows dual tires on the drive axle. **NDRWHL = 4**

NTRWHL Number of Tires on each end of Trailer Axle(s) - The AASHTO diagram for the large semitrailer shows dual tires on each of the trailer axle. **NTRWHL = 2**

d. Tire Parameter File "WB-50.TIR"

The tire parameters used are taken from a General Tire "AMERI*S380" 295/75R22.5 radial tire at 125 psi.

e. Driver Parameter File "DRIVER.PAR"

The VDANL driver parameter file requires the vehicle stability factor for its adaptive control algorithms. This vehicle's understeer gradient is approximately 4.5 deg/g, which gives a stability factor of: **KSTABF = 0.0024 rad/ft/s^2**

f. Other Parameters

The AASHTO specifies that the minimum design turning radius of the outside front tire at 10 mi/h is 45.0 ft, which makes the turning radius of the center-of-gravity 45.0-T/2 = 41.25 ft. Running a slowly increasing steer maneuver at 10 mi/h, and knowing that radius of curvature is equal to forward speed divided by yaw rate, a 41.25 radius turn is achieved at a steering wheel angle of 5.5 radians. In NONLIN.PAR, **DSWMAX = 5.5**

g. Parameter Files

Vehicle Parameters

MASS = 600
SMASS = 419
UMASSF = 39
UMASSR = 142
LENA = 7
LENB = 11
IXS = 5300
IYS = 27000
IZZ = 30000
IXZ = 0
KSTR = 12.8
KSCF = 0.000038
KSCB = 0
DLADV = 0
DYADV = 0
DNADV = 0
DENSITY = 0 .00237
REFAREA = 0
CDX = 0.4
AEROVEL = 44
KTL = 1
KSF = 16000
KSDF = 1600
KSR = 54000
KSDR = 5400
TRWF = 7.5
TRWB = 7.5
HCG = 2.86
KBS = 175000
HBS = 0.20
KTSF = 415620
KTSR = 1193300
KRAS = 120000
KRADP = 7000
TSPRINGR = 55200
HRAF = 1.42
HRAR = 2.32
HS = 3.28
IXUF = 500
IXUR = 1250
KLT = 2.3E-5
XACC = 0
ZACC = 0
DRAGC = 0
LENS = 5.4
LM = 1.125
KBTF = -57.21
KVB = 1.4
KMB = 1.4
FBPVL = 100
SWZ = 0.9
SWW = 100
KCF = -1E-6
LSO = 0
KLAGV = 16.5
BRAKPROP1 = 80
BRAKPROP2 = 200
FXLIMIT = 0
DAMPCOMF = 0
DAMPEXTF = 0
DAMPCOMR = 0
DAMPEXTR = 0
AIRBRAKES% = 1
BRAKLAG1 = 0.3
BRAKMULTLF = 1
BRAKMULTRF = 1
BRAKMULTLR = 1
BRAKMULTRR = 1

Suspension Parameters

SUSPENSIONF = 1
SUSPENSIONR = 1
HF = 0.225
HR = -0.117
LF = 1
LR = 1
KSAF = 1
KSAR = 1
BF = 0
BR = 0
CF = 0
CR = 0
DF = 0
DR = 0
EF = 0
ER = 0
KSLF = 0
KSLR = 0

LSAF = 1000
LSAR = 1000
KSADF = 0
KSADR = 0
KSAD2F = 0
KSAD2R = 0
KACK = 0

Trailer Parameters
MASS = 830
SMASS = 730
UMASSF = 50
UMASSR = 50
LENA = -11
LENB = 15
IXS = 7000
IYS = 122000
IZZ = 129000
IXZ = 0
DLADV = 0
DYADV = 0
DNADV = 0
KTL = 1
KSF = 121000
KSDF = 2200
KSR = 108000
KSDR = 2200
TRWF = 7.5
TRWB = 7.5
HCG = 5.0
KBS = 600000
HBS = .20
KTSF = 2568000
KTSR = 2187000
KRAS = 120000
KRADP = 7000
TSPRINGR = 55200
HRAF = 2.4
HRAR = 2.28
HS = 5.66
IXUF = 570
IXUR = 570
KLT = 2.3E-5
DRAGC = 0
KLAGV = 25
SUSPENSIONF = 1
SUSPENSIONR = 1
HF = 0.035
HR = 0.169
LF = 1
LR = 1
KSAF = 0
KSAR = 0
BF = 0
BR = 0
CF = 0
CR = 0
DF = 0
DR = 0
EF = 0
ER = 0
KSLF = 0
KSLR = 0
LSAF = 1
LSAR = 1
KSADF = 0
KSADR = 0
KSAD2F = 0
KSAD2R = 0
TLEND = 11.0
TLENE = 15.0
THH = 3.6
THITCHSP = 600000
THITCHSPD = 2200
KTFIFTH = 1146000
BRAKLAG1 = 0.31
BRAKLAG2 = 0.35
BRAKLAG3 = 0.42
KFADE = 0.0005
NDRWHL = 4
NTRWHL = 2

Tire Parameters
TWIDTH = 10.00
KA0 = 1.9148e+003
KA1 = 9.1239e+000
KA2 = 2.6632e+004
KA3 = 0.0000e+000
KA4 = 1.0000e+000
KA = 0.0544
KMUy = 0.3454
TPRESS = 125.00
KB1y = -1.4737e-005
KB3y = 6.6176e-001
KB4y = -2.5237e-010
KGAMMA = 0.90
CSFZ = 6.6412
MUNOMy = 0.85
FZTRL = 6175
KK1 = -3.0824e-005
RR = 2.0
TIRE = RADIAL
C1 = 0.4693
C2 = 2.0389
C3 = 1.7886
C4 = 0.7335
G1 = 0.7266
G2 = 1.0000
MUNOMx = 0.85
LONGLAG = 0.25
PLYSTEER = -0.0043
KB1x = -2.9289e-005
KB3x = 9.4338e-001
KB4x = 1.1202e-009
KMUx = 0.3454
DRAGC = 0
C5 = 1.2732
Kx = 0

7. Interstate Semi-Trailer - WB-62

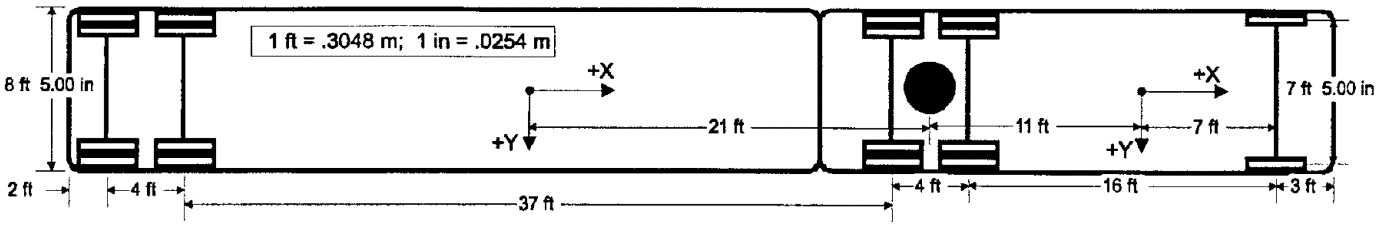

Figure F-7. Dimensions of AASHTO Interstate Semi-Trailer - WB-62

Properties of this interstate semi-trailer have been estimated based on representative data from Ref. F.4 and Ref. F.6. The data set is identical to the large semi-trailer, except the trailer has been lengthened by 11 ft, and the trailer cg has been moved rearward by 6 ft. The following describes the parameters that have been changed.

a. Trailer Parameter File "WB-62-TR.PAR"

The trailer geometry is defined by AASHTO.

LENA Distance from Sprung Mass cg to Front Axle (ft) - AASHTO defines the distance from the fifth wheel to the front trailer axle as 39 ft. Based on scaling from Ref. F.6, the distance from the sprung mass cg to the fifth wheel has been set to 21 ft. **LENA = -18 ft.**

LENB Distance from Sprung Mass cg to Rear Axle (ft) - AASHTO defines the distance between the trailer axles to be 4 ft. **LENB = 22 ft.**

TLENE Longitudinal Distance from Trailer Vehicle CG to Hitch (ft) - Referring to Figure F-7, the fifth wheel is located over the tractor drive axle, which is 21 ft ahead of the trailer cg. **TLENE = 21.0 ft**

b. Driver Parameter File "DRIVER.PAR"

The VDANL driver parameter file requires the vehicle stability factor for its adaptive control algorithms. This vehicle's understeer gradient is approximately 4.0 deg/g, which gives a stability factor of: **KSTABF = 0.0022 rad/ft/s^2**

c. Other Parameters

The AASHTO specifies that the minimum design turning radius of the outside front tire at 10 mi/h is 45.0 ft, which makes the turning radius of the cg 45.0-T/2 = 41.25 ft. Running a slowly increasing steer maneuver at 10 mi/h, and knowing that radius of curvature is equal to forward speed divided by yaw rate, a 41.25 radius turn is achieved at a steering wheel angle of 5.5 radians. In NONLIN.PAR, **DSWMAX = 5.5**

d. Parameter Files

Vehicle Parameters
MASS = 600
SMASS = 419
UMASSF = 39
UMASSR = 142
LENA = 7
LENB = 11
IXS = 5300
IYS = 27000
IZZ = 30000
IXZ = 0
KSTR = 12.8
KSCF = 0.000038
KSCB = 0
DLADV = 0
DYADV = 0
DNADV = 0
DENSITY = 0.00237
REFAREA = 0
CDX = 0.4
AEROVEL = 44
KTL = 1
KSF = 16000
KSDF = 1600
KSR = 54000
KSDR = 5400
TRWF = 7.5
TRWB = 7.5
HCG = 2.86
KBS = 175000
HBS = 0.20
KTSF = 415620
KTSR = 1193300
KRAS = 120000
KRADP = 7000
TSPRINGR = 55200
HRAF = 1.42
HRAR = 2.32
HS = 3.28
IXUF = 500
IXUR = 1250
KLT = 2.3E-5
XACC = 0
ZACC = 0
DRAGC = 0
LENS = 5.4
LM = 1.125
KBTF = -57.21
KVB = 1.4
KMB = 1.4
FBPVL = 100
SWZ = 0.9
SWW = 100
KCF = -1E-6
LSO = 0
KLAGV = 16.5
BRAKPROP1 = 80
BRAKPROP2 = 200
FXLIMIT = 0
DAMPCOMF = 0
DAMPEXTF = 0
DAMPCOMR = 0
DAMPEXTR = 0
AIRBRAKES% = 1
BRAKLAG1 = 0.3
BRAKMULTLF = 1
BRAKMULTRF = 1
BRAKMULTLR = 1
BRAKMULTRR = 1

Suspension Parameters
SUSPENSIONF = 1
SUSPENSIONR = 1
HF = 0.225
HR = -0.117
LF = 1
LR = 1
KSAF = 1
KSAR = 1
BF = 0
BR = 0
CF = 0
CR = 0
DF = 0
DR = 0
EF = 0
ER = 0
KSLF = 0
KSLR = 0
LSAF = 1000
LSAR = 1000
KSADF = 0
KSADR = 0
KSAD2F = 0
KSAD2R = 0
KACK = 0

Trailer Parameters
MASS = 830
SMASS = 730
UMASSF = 50
UMASSR = 50
LENA = -18
LENB = 22
IXS = 7000
IYS = 122000
IZZ = 129000
IXZ = 0
DLADV = 0
DYADV = 0
DNADV = 0
KTL = 1
KSF = 121000
KSDF = 2200
KSR = 108000
KSDR = 2200
TRWF = 7.5
TRWB = 7.5
HCG = 5.0
KBS = 600000
HBS = 0.20
KTSF = 2568000
KTSR = 2187000
KRAS = 120000
KRADP = 7000
TSPRINGR = 55200
HRAF = 2.4
HRAR = 2.28
HS = 5.66
IXUF = 570
IXUR = 570
KLT = 2.3E-5
DRAGC = 0
KLAGV = 25
SUSPENSIONF = 1
SUSPENSIONR = 1
HF = 0.035
HR = 0.169
LF = 1
LR = 1
KSAF = 0
KSAR = 0
BF = 0

BR = 0
CF = 0
CR = 0
DF = 0
DR = 0
EF = 0
ER = 0
KSLF = 0
KSLR = 0
LSAF = 1
LSAR = 1
KSADF = 0
KSADR = 0
KSAD2F = 0
KSAD2R = 0
TLEND = 11.0
TLENE = 21.0
THH = 3.6
THITCHSP = 600000
THITCHSPD = 2200
KTFIFTH = 1146000
BRAKLAG1 = 0.31
BRAKLAG2 = 0.35
BRAKLAG3 = 0.42
KFADE = 0.0005
NDRWHL = 4
NTRWHL = 2

Tire Parameters

TWIDTH = 10.00
KA0 = 1.9148e+003
KA1 = 9.1239e+000
KA4 = 1.0000e+000
KA2 = 2.6632e+004
KA3 = 0.0000e+000
KA = 0.0544
KMUy = 0.3454
TPRESS = 125.00
KB1y = -1.4737e-005
KB3y = 6.6176e-001
KB4y = -2.5237e-010
KGAMMA = 0.90
CSFZ = 6.6412
MUNOMy = 0.85
FZTRL = 6175
KK1 = -3.0824e-005
RR = 2.0
TIRE = RADIAL
C1 = 0.4693
C2 = 2.0389
C3 = 1.7886
C4 = 0.7335
G1 = 0.7266
G2 = 1.0000
MUNOMx = 0.85
LONGLAG = 0.25
PLYSTEER = -0.0043
KB1x = -2.9289e-005
KB3x = 9.4338e-001
KB4x = 1.1202e-009
KMUx = 0.3454
DRAGC = 0
C5 = 1.2732
Kx = 0

8. Interstate Semi-Trailer - WB-67

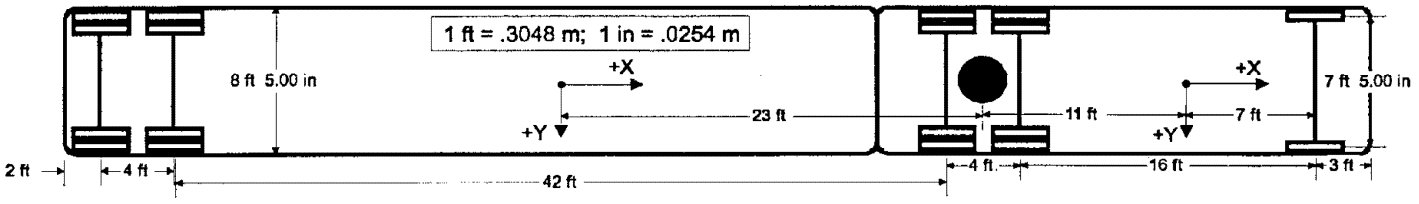

Figure F-8. Dimensions of AASHTO Interstate Semi-Trailer - WB-67

Properties of this interstate semi-trailer have been estimated based on representative data from Ref. F.4 and Ref. F.6. The data set is identical to the interstate semi-trailer WB-62, except the trailer has been lengthened by 5 ft, and the trailer cg has been moved rearward by 2 ft. The following describes the parameters that have been changed.

a. Trailer Parameter File "WB-67-TR.PAR"

The trailer geometry is defined by AASHTO.

LENA Distance from Sprung Mass cg to Front Axle (ft) - AASHTO defines the distance from the fifth wheel to the front trailer axle as 44 ft. Based on scaling from Ref. F.6, the distance from the sprung mass cg to the fifth wheel has been set to 23 ft. **LENA = -21 ft.**

LENB Distance from Sprung Mass cg to Rear Axle (FT) - AASHTO defines the distance between the trailer axles to be 4 ft. **LENB = 25 ft.**

TLENE Longitudinal Distance from Trailer Vehicle cg to Hitch (ft) - Referring to Figure F-7, the fifth wheel is located over the tractor drive axle, which is 23 ft ahead of the trailer cg. **TLENE = 23.0 ft**

b. Driver Parameter File "DRIVER.PAR"

The VDANL driver parameter file requires the vehicle stability factor for its adaptive control algorithms. This vehicle's understeer gradient is approximately 4.0 deg/g, which gives a stability factor of: **KSTABF = 0.0022 rad/ft/s^2**

c. Other Parameters

The AASHTO specifies that the minimum design turning radius of the outside front tire at 10 mi/h is 45.0 ft, which makes the turning radius of the center-of-gravity 45.0-T/2 = 41.25 ft. Running a slowly increasing steer maneuver at 10 mi/h, and knowing that radius of curvature is equal to forward speed divided by yaw rate, a 41.25 radius turn is achieved at a steering wheel angle of 5.5 radians. In NONLIN.PAR, **DSWMAX = 5.5**

d. Parameter Files

Vehicle Parameters
MASS = 600
SMASS = 419
UMASSF = 39
UMASSR = 142
LENA = 7
LENB = 11
IXS = 5300
IYS = 27000
IZZ = 30000
IXZ = 0
KSTR = 12.8
KSCF = 0.000038
KSCB = 0
DLADV = 0
DYADV = 0
DNADV = 0
DENSITY = 0.00237
REFAREA = 0
CDX = 0.4
AEROVEL = 44
KTL = 1
KSF = 16000
KSDF = 1600
KSR = 54000
KSDR = 5400
TRWF = 7.5
TRWB = 7.5
HCG = 2.86
KBS = 175000
HBS = 0.20
KTSF = 415620
KTSR = 1193300
KRAS = 120000
KRADP = 7000
TSPRINGR = 55200
HRAF = 1.42
HRAR = 2.32
HS = 3.28
IXUF = 500
IXUR = 1250
KLT = 2.3E-5
XACC = 0
ZACC = 0
DRAGC = 0
LENS = 5.4
LM = 1.125
KBTF = -57.21
KVB = 1.4
KMB = 1.4
FBPVL = 100
SWZ = 0.9
SWW = 100
KCF = -1E-6
LSO = 0
KLAGV = 16.5
BRAKPROP1 = 80
BRAKPROP2 = 200
FXLIMIT = 0
DAMPCOMF = 0

DAMPEXTF = 0
DAMPCOMR = 0
DAMPEXTR = 0
AIRBRAKES% = 1
BRAKLAG1 = 0.3
BRAKMULTLF = 1
BRAKMULTRF = 1
BRAKMULTLR = 1
BRAKMULTRR = 1

Suspension Parameters
SUSPENSIONF = 1
SUSPENSIONR = 1
HF = 0.225
HR = -0.117
LF = 1
LR = 1
KSAF = 1
KSAR = 1
BF = 0
BR = 0
CF = 0
CR = 0
DF = 0
DR = 0
EF = 0
ER = 0
KSLF = 0
KSLR = 0
LSAF = 1000
LSAR = 1000
KSADF = 0
KSADR = 0
KSAD2F = 0
KSAD2R = 0
KACK = 0

Trailer Parameters
MASS = 830
SMASS = 730
UMASSF = 50
UMASSR = 50
LENA = -21
LENB = 25
IXS = 7000
IYS = 122000
IZZ = 129000
IXZ = 0
DLADV = 0
DYADV = 0
DNADV = 0
KTL = 1
KSF = 121000
KSDF = 2200
KSR = 108000
KSDR = 2200
TRWF = 7.5
TRWB = 7.5
HCG = 5.0
KBS = 600000
HBS = 0.20
KTSF = 2568000
KTSR = 2187000
KRAS = 120000
KRADP = 7000
TSPRINGR = 55200
HRAF = 2.4
HRAR = 2.28
HS = 5.66
IXUF = 570
IXUF = 570
IXUR = 570
KLT = 2.3E-5
DRAGC = 0
KLAGV = 25
SUSPENSIONF = 1
SUSPENSIONR = 1
HF = 0.035
HR = 0.169
LF = 1
LR = 1
KSAF = 0
KSAR = 0
BF = 0
BR = 0
CF = 0
CR = 0
DF = 0
DR = 0
EF = 0
ER = 0
KSLF = 0
KSLR = 0
LSAF = 1
LSAR = 1
KSADF = 0
KSADR = 0
KSAD2F = 0
KSAD2R = 0
TLEND = 11.0
TLENE = 23.0
THH = 3.6
THITCHSP = 600000
THITCHSPD = 2200
KTFIFTH = 1146000
BRAKLAG1 = 0.31
BRAKLAG2 = 0.35
BRAKLAG3 = 0.42
KFADE = 0.0005
NDRWHL = 4
NTRWHL = 2

Tire Parameters
TWIDTH = 10.00
KA0 = 1.9148e+003
KA1 = 9.1239e+000
KA2 = 2.6632e+004
KA3 = 0.0000e+000
KA4 = 1.0000e+000
KA = 0.0544
KMUy = 0.3454
TPRESS = 125.00
KB1y = -1.4737e-005
KB3y = 6.6176e-001
KB4y = -2.5237e-010
KGAMMA = 0.90
CSFZ = 6.6412
MUNOMy = 0.85
FZTRL = 6175
KK1 = -3.0824e-005
RR = 2.0
TIRE = RADIAL
C1 = 0.4693
C2 = 2.0389
C3 = 1.7886
C4 = 0.7335
G1 = 0.7266
G2 = 1.0000
MUNOMx = 0.85
LONGLAG = 0.25
PLYSTEER = -0.0043
KB1x = -2.9289e-005
KB3x = 9.4338e-001
KB4x = 1.1202e-009
KMUx = 0.3454
DRAGC = 0
C5 = 1.2732
Kx = 0

9. Motor Home - MH

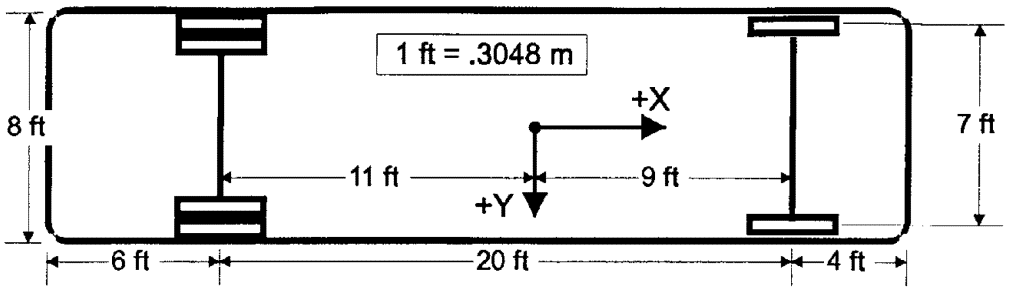

Figure F-9. Dimensions of AASHTO Motor Home - MH

a. Vehicle Parameter File "MH.PAR"

The AASHTO Motor Home size specification is almost identical to the AASHTO single-unit truck, except for overall width being half a foot narrower. Parameter data for recreational vehicles are not common in the literature, so the properties of this motor home have been estimated based on scaling from the single-unit truck. The motor home is assumed to weigh 10,400 lb, which is 66 percent of the single unit truck. All inertial and spring/damper values are scaled accordingly.

MASS Total Vehicle Mass (slugs) - No mass specification is provided by AASHTO. Scaling from the single unit truck data: **MASS = 323 slugs**.

SMASS Vehicle Sprung Mass (slugs) - SMASS = MASS - UMASSF - UMASSR. **SMASS = 252 slugs**

UMASSF Front Unsprung Mass (slugs) - Scaling from the single-unit truck data. **UMASSF = 24 slugs**.

UMASSR Rear Unsprung Mass (slugs) - Scaling from the single-unit truck data. **UMASSR = 47 slugs**.

LENA Distance from Sprung Mass CG to Front Axle (FT) - Ref. F.4 data show that straight trucks are generally slightly front-weight biased. AASHTO gives a wheelbase of 20 ft. **LENA = 9 ft.**

LENB Distance from Sprung Mass cg to Rear Axle (ft) - Wheelbase - LENA: **LENB = 11 ft.**

IXS Sprung Mass Roll Inertia (ft-lb-s^2) - Ref. F.4 gives the typical value to be in the range of, **IXS = 1300 ft-lb-s^2**

IYS Sprung Mass Pitch Inertia (ft-lb-s^2) - Ref. F.4 gives the typical value to be in the range of, **IYS = 130000 ft-lb-s^2**

IZZ Total Vehicle Yaw Inertia (ft-lb-s^2) - Ref. F.4 gives the typical value to be in the range of, **IZZ = 13000 ft-lb-s^2**

IXZ Total Vehicle Roll/Yaw Cross Product of Inertia (ft-lb-s^2) - Assumed to be zero.

KSTR Overall Steering Ratio - Ref. F-5 says that the truck steering ratios range from 22:1 to 36:1. Steering ratio is assumed to be 30:1. **KSTR = 30**

KSCF Front Aligning Torque Steer Compliance (rad/ft-lb) - Ref. F.4 gives the typical value of 10000 in-lb/deg. **KSCF = 0.00002 rad/ft-lb.**

KSCR Rear Aligning Torque Steer Compliance (rad/ft-lb) - Assumed to be zero. **KSCR = 0 rad/ft-lb.**

KTL Tire Lag Constant (ft) - A nominal value of 1 ft is used. **KTL = 1 ft.**

KSF Front Wheel Rate (lb/ft) - Scaling from the single-unit truck data. **KSF = 10000 lb/ft**

KSR Rear Wheel Rate (lb/ft) - Scaling from the single-unit truck data. **KSR = 16000 lb/ft**

KSDF Front Wheel Damping Rate (lb/ft/s) - Set to a nominal value of: **KSDF = 1000 lb/ft/s**

KSDR Rear Wheel Damping Rate (lb/ft/s) - Set to a nominal value of: **KSDR = 1600 lb/ft/s**

TRWF Front Track Width (ft) - AASHTO defines vehicle width as 8.0 ft. Track width is assumed to be 1 ft less thanthe vehicle width: **TRWF = 7.0 ft**

TRWR Rear Track Width (ft) - AASHTO defines vehicle width as 8.0 ft. Track width is assumed to be one ft less than the vehicle width: **TRWR = 7.0 ft**

HCG Total Vehicle cg Height (ft) - Ref. F.4 gives the typical value of 36 in. **HCG = 3.0 ft**

KBS Bump Stop Stiffness (lb/ft) - Bump stop stiffness was set to be approximately five times the average wheel rate: **KBS = 660000 lb/ft**

HBS Bump Stop Position (ft) - HBS was set to a nominal value of: **HBS = 0.2 ft**

KTSF Front Auxiliary Roll Stiffness (ft-lb/rad) - Scaling from the single-unit truck data. **KTSF = 215000 ft-lb/rad.**

KTSR Rear Auxiliary Roll Stiffness (ft-lb/rad) - Scaling from the single unit truck data. **KTSR = 256000 ft-lb/rad.**

TSPRINGR Tire Spring Rate (lb/ft) - Ref. F.4 gives a typical value for radial tire spring rate of 4600 lb/in. **TSPRINGR = 55200 lb/ft**

HRAF Front Suspension Roll Center Height (ft) - Ref. F.4 gives a typical value for front roll center height of 19 in. **HRAF = 1.58 ft**

HRAR Rear Suspension Roll Center Height (ft) - Ref. F.4 gives a typical value for rear roll center height of 26 in. **HRAR = 2.17 ft**

HS Sprung Mass cg Height (ft) - The unsprung mass cg heights were assumed to be 1.58 ft, and based on the total vehicle cg height (**HCG**), the sprung mass cg height is computed to be: **HS = 3.4 ft**

IXUF Front Unsprung Mass Roll Inertia (ft-lb-s^2) - Scaling from the single-unit truck data: **IXUF = 200 ft-lb-s^2**

IXUR Rear Unsprung Mass Roll Inertia (ft-lb-s^2) - Scaling from the single unit truck data: **IXUR = 400 ft-lb-s^2**

KLT Tire Lateral Compliance (ft/lb) - Tire lateral compliance is estimated to be 76 percent of the tire vertical compliance Ref. F.2: **KLT = 2.3E-5 ft/lb**

KBTF Front Wheel Brake Effectiveness (ft-lb/psi) - Ref. F.4 gives a typical value for front brake effectiveness of -870 in-lb/psi. **KBTF = -72.5 ft-lb/psi**

KVB Brake Gain in Vacuum Boost Range (psi/lb) **KVB = 23.5 psi/lb**

KVM Brake Gain in Manual Range (psi/lb) **KVM = 9.4 psi/lb**

FBPVL Pedal Force when Vacuum Boost Runs Out (lb) **FBPVL = 55 lb**

SWW Steering System Natural Frequency (rad/s) - Because of the stiffness of heavy truck steering systems, the steering system natural frequency will be out of the handling frequency range. Therefore, steering system dynamics will be ignored. **SWW = 0 rad/s**

AIRBRAKE% Air Brake Flag - This truck is assumed to have hydraulic brakes. **AIRBRAKE% = 0**

BRAKLAG1 Brake Torque Time Constant (s) - Reference F.4 gives a typical value of 0.3 s. **BRAKLAG1 = 0.3**

b. Suspension Parameter File "MH.SUS"

It is assumed that this vehicle has no anti-lift/dive forces, and no Ackerman steering geometry. The following are parameters that are set in the suspension file that are specific to this vehicle.

SUSPENSIONF Front Suspension Type (0 or 1) - **SUSPENSIONF = 1**

SUSPENSIONR Rear Suspension Type (0 or 1) - **SUSPENSIONR = 1**

HF & LF Front Axle Roll Steer - Ref. F.4 gives a typical value front axle roll steer of 0.2 (understeer). **HF = 0.2 & LF = 1**

HR & LR Rear Axle Roll Steer - Ref. F.4 gives a typical value rear axle roll steer of 0.2 (understeer). **HR = -0.2 & LR = 1**

c. Tire Parameter File "MH.TIR"

The tire parameters used are taken from a General Tire "AMERI*S380" 295/75R22.5 radial tire at 125 psi.

d. Driver Parameter File "DRIVER.PAR"

The VDANL driver parameter file requires the vehicle stability factor for its adaptive control algorithms. This vehicles understeer gradient is approximately 3 deg/g, which gives a stability factor of: **KSTABF = 0.0016 rad/ft/s^2**

e. Other Parameters

The AASHTO specifies that the minimum design turning radius of the outside front tire at 10 mi/h is 40 ft, which makes the turning radius of the cg 40-T/2 = 36.25 ft. Running a slowly increasing steer maneuver at 10 mi/h, and knowing that radius of curvature is equal to forward speed divided by yaw rate, a 36.25 radius turn is achieved at a steering wheel angle of 16.0 radians. In NONLIN.PAR, **DSWMAX = 16.0.**

f. Parameter Files

Vehicle Parameters

MASS = 323
SMASS = 252
UMASSF = 24
UMASSR = 47
LENA = 9
LENB = 11
IXS = 1300
IYS = 13000
IZZ = 13000
IXZ = 0
KSTR = 30
KSCF = 0.00002
KSCB = 0
DLADV = 0
DYADV = 0
DNADV = 0
DENSITY = 0.00237
REFAREA = 50
CDX = 0.4
AEROVEL = 44
KTL = 1
KSF = 10000
KSDF = 1000
KSR = 16000
KSDR = 1600
TRWF = 7.0
TRWB = 7.0
HCG = 3.0
KBS = 660000
HBS = .20
KTSF = 215000
KTSR = 256000
KRAS = 120000
KRADP = 7000
TSPRINGR = 55200
HRAF = 1.58
HRAR = 2.17
HS = 3.4
IXUF = 200
IXUR = 400
KLT = 2.3E-5
XACC = 0
ZACC = 0
DRAGC = -0.015
LENS = 5.4
LM = 1.125
KBTF = -72.5
KVB = 23.5
KMB = 9.4
FBPVL = 55
SWZ = 0.5
SWW = 0
KCF = -1E-6
LSO = 0
KLAGV = 16.5
BRAKPROP1 = 1
BRAKPROP2 = 1
FXLIMIT = -1000
DAMPCOMF = 0
DAMPEXTF = 0
DAMPCOMR = 0
DAMPEXTR = 0
AIRBRAKES% = 0
BRAKLAG1 = 0.3
BRAKMULTLF = 1
BRAKMULTRF = 1
BRAKMULTLR = 1
BRAKMULTRR = 1

Suspension Parameters

SUSPENSIONF = 1
SUSPENSIONR = 1
HF = 0.1
HR = 0
LF = 1
LR = 1000
KSAF = 1
KSAR = 1
BF = 0
BR = 0
CF = 0
CR = 0
DF = 0
DR = 0
EF = 0
ER = 0
KSLF = 0
KSLR = 0
LSAF = 1000
LSAR = 1000
KSADF = 0
KSADR = 0
KSAD2F = 0
KSAD2R = 0
KACK = 0

Tire Parameters

TWIDTH = 10.00
KA0 = 1.9148e+003
KA1 = 9.1239e+000
KA2 = 2.6632e+004
KA3 = 0.0000e+000
KA4 = 1.0000e+000
KA = 0.0544
KMUy = 0.3454
TPRESS = 125.00
KB1y = -1.4737e-005
KB3y = 6.6176e-001
KB4y = -2.5237e-010
KGAMMA = 0.90
CSFZ = 6.6412
MUNOMy = 0.85
FZTRL = 6175
KK1 = -3.0824e-005
RR = 1.025
TIRE = RADIAL
C1 = 0.4693
C2 = 2.0389
C3 = 1.7886
C4 = 0.7335
G1 = 0.7266
G2 = 1.0000
MUNOMx = 0.85
LONGLAG = 0.25
PLYSTEER = -0.0043
KB1x = -2.9289e-005
KB3x = 9.4338e-001
KB4x = 1.1202e-009
KMUx = 0.3454
C5 = 1.2732
Kx = 0

10. Car And Camper Trailer – PT

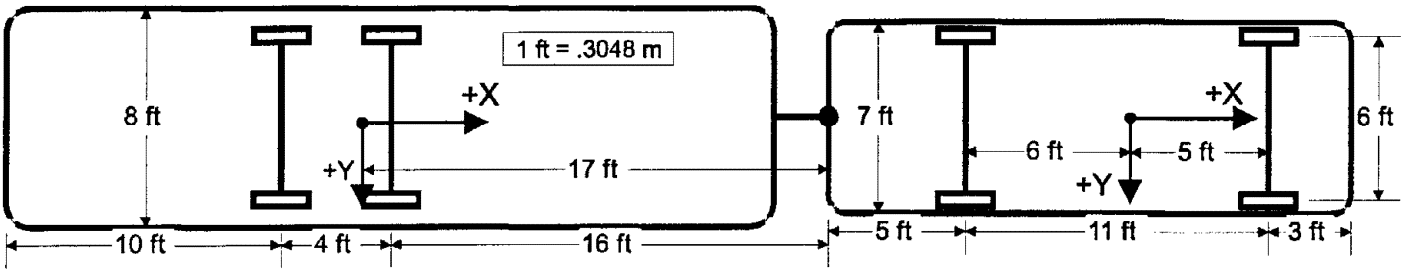

Figure F-10. Dimensions of AASHTO Car and Camper Trailer - PT

Properties of the AASHTO car and camper trailer combination use the passenger car (AASHTO P), and add a camper trailer following the dimensions specified by AASHTO. The passenger car parameter and suspension files are unchanged.

a. Trailer Parameter File "PT.PAR"

The trailer geometry is defined by AASHTO.

MASS Total Vehicle Mass (slugs) - It is assumed that the camper weighs 5000 lb. **MASS = 155 slugs.**

SMASS Vehicle Sprung Mass (slugs) - SMASS = MASS - UMASSF - UMASSR. **SMASS = 142.6 slugs**

UMASSF Front Unsprung Mass (slugs) – The front unsprung mass is assumed to weigh 200 lb. **UMASSF = 6.2 slugs.**

UMASSR Rear Unsprung Mass (slugs) - The rear unsprung mass is assumed to weight 200 lb. **UMASSR = 6.2 slugs.**

LENA Distance from Sprung Mass cg to Front Axle (ft) - AASHTO defines the distance from the hitch to the rear trailer axle as 20 ft. Setting the distance between the axles to 4 ft, and a hitch tongue weight of approximately 300-lb, the cg position can be calculated. **LENA = 1 ft.**

LENB Distance from Sprung Mass cg to Rear Axle (ft) – Based on the distance between the trailer axles being 4 ft. **LENB = 3 ft.**

IXS Sprung Mass Roll Inertia (ft-lb-s^2) – The camper mass moments of inertia are assumed to be equal to the passenger car values. **IXS = 530 ft-lb-s^2**

IYS Sprung Mass Pitch Inertia (ft-lb-s^2) - The camper mass moments of inertia are assumed to be equal to the passenger car values. **IYS = 2942 ft-lb-s^2**

IZZ Total Vehicle Yaw Inertia (ft-lb-s^2) - The camper mass moments of inertia are assumed to be equal to the passenger car values. **IZZ = 3858 ft-lb-s^2**

IXZ Total Vehicle Roll/Yaw Cross Product of Inertia (ft-lb-s^2) - Assumed to be zero.

KTL Tire Lag Constant (ft) - A nominal value of 1 ft is used. **KTL = 1 ft.**

KSF Front Wheel Rate (lb/ft) - The camper suspension stiffness and damping are assumed to be equal to the average passenger car values. **KSF = 1600 lb/ft**

KSR Rear Wheel Rate (lb/ft) - The camper suspension stiffness and damping are assumed to be equal to the average passenger car values. **KSR = 1600 lb/ft**

KSDF Front Wheel Damping Rate (lb/ft/s) - The camper suspension stiffness and damping are assumed to be equal to the average passenger car values. **KSDF = 150 lb/ft/s**

KSDR Rear Wheel Damping Rate (lb/ft/s) - The camper suspension stiffness and damping are assumed to be equal to the average passenger car values. **KSDR = 150 lb/ft/s**

TRWF Front Track Width (ft) - AASHTO defines vehicle width as 8.0 ft. Track width is assumed to be 1 ft less than the vehicle width: **TRWF = 7.0 ft**

TRWR Rear Track Width (ft) - AASHTO defines vehicle width as 8.5 ft. Track width is assumed to be 1 ft less than the vehicle width: **TRWR = 7.0 ft**

HCG Total Vehicle cg Height (ft) - HCG has been assumed to be 3 ft. **HCG = 3.0 ft**

KBS Bump Stop Stiffness (lb/ft) - Bump stop stiffness was set to be approximately five times the average wheel rate: **KBS = 8000 lb/ft**

HBS Bump Stop Position (ft) - HBS was set to a nominal value of: **HBS = 0.2 ft**

KTSF Front Auxiliary Roll Stiffness (ft-lb/rad) – No suspension auxiliary roll stiffness is used for the camper. **KTSF = 0 ft-lb/rad.**

KTSR Rear Auxiliary Roll Stiffness (ft-lb/rad) - No suspension auxiliary roll stiffness is used for the camper. **KTSR = 0 ft-lb/rad.**

HRAF Front Suspension Roll Center Height (ft) - HRAF has been assumed to be at the axle height. **HRAR = 1.0 ft**

HRAR Rear Suspension Roll Center Height (ft) - HRAR has been measured in Ref, F.6. **HRAR = 1.0 ft**

HS Sprung Mass cg Height (ft) – Using the assumed axle height of 1 ft, and the total vehicle cg, the sprung mass cg can be computed. **HS = 3.17 ft**

IXUF Front Unsprung Mass Roll Inertia (ft-lb-s^2) - The camper mass moments of inertia are assumed to be equal to the passenger car values. **IXUF = 40 ft-lb-s^2**

IXUR Rear Unsprung Mass Roll Inertia (ft-lb-s^2) - The camper mass moments of inertia are assumed to be equal to the passenger car values. **IXUR = 40 ft-lb-s^2**

KLT Tire Lateral Compliance (ft/lb) - Tire lateral compliance is estimated to be 76 percent of the tire vertical compliance Ref. F.2: **KLT = 2.3E-5 ft/lb**

SUSPENSIONF Rear Suspension Type (0 or 1) - **SUSPENSIONF = 0**

SUSPENSIONR Rear Suspension Type (0 or 1) - **SUSPENSIONR = 0**

HF & LF Front Axle Roll Steer - Roll steer has been set to zero. **HF = 0 & LF = 1**

HR & LR Rear Axle Roll Steer - Roll steer has been set to zero. **HR = 0 & LR = 1**

TLEND Longitudinal Distance from Tow Vehicle cg to Hitch (ft) - Referring to Figure F-8, the hitch is located at the rear of the passenger vehicle, which is 11 ft behind the cg. **TLEND = 11 ft**

TLENE Longitudinal Distance from Trailer Vehicle cg to Hitch (ft) - Referring to Figure F-8, the hitch is located 17 ft ahead of the trailer cg. **TLENE = 17.0 ft**

THH Initial Height of Hitch Above the Ground (ft) - Initial hitch height is assumed to be 1.5 ft above the ground. **THH = 1.5 ft**

HITCHSP Hitch Translational Spring Stiffness (lb/ft) - Hitch stiffness is assumed to be 5000 lb/in, **HITCHSP = 60000 lb/ft**

HITCHSPD Hitch Translational Damping (lb/ft/s) - Hitch damping is assumed to be 20 lb/in/s, **HITCHSPD = 240 lb/ft/s**

b. Driver Parameter File "DRIVER.PAR"

The VDANL driver parameter file requires the vehicle stability factor for its adaptive control algorithms. This vehicle's understeer gradient is approximately 3.0 deg/g, which gives a stability factor of: **KSTABF = 0.0016 rad/ft/s^2**

c. Other Parameters

The AASHTO specifies that the minimum design turning radius of the outside front tire at 10 mi/h is 24.0 ft, which makes the turning radius of the cg 24.0-T/2 = 21 ft. Running a slowly increasing steer maneuver at 10 mi/h, and knowing that radius of curvature is equal to forward speed divided by yaw rate, a 21 radius turn is achieved at a steering wheel angle of 10.8 radians. In NONLIN.PAR, **DSWMAX = 10.8**

d. Parameter Files

Vehicle Parameters

MASS = 155
SMASS = 132.5
UMASSF = 9.8
UMASSR = 12.7
LENA = 5
LENB = 6
IXS = 530
IYS = 2942
IZZ = 3858
IXZ = 0
KSTR = 20
KSCF = 0.0002
KSCB = 0
DLADV = 0
DYADV = 0
DNADV = 0
DENSITY = 0.00237
REFAREA = 25
CDX = 0.4
AEROVEL = 44
KTL = 1
KSF = 1794
KSDF = 150
KSR = 1468
KSDR = 150
TRWF = 6
TRWB = 6
HCG = 1.833
KBS = 8000
HBS = 0.20
KTSF = 0
KTSR = 0
KRAS = 12000
KRADP = 700
TSPRINGR = 15000
HRAF = 0
HRAR = 0.5
HS = 1.975
IXUF = 40
IXUR = 40
KLT = 1.036E-5
XACC = 0
ZACC = 0
DRAGC = -.015
LENS = 5.4
LM = 1.125
KBTF = -1.525
KVB = 23.5
KMB = 9.4
FBPVL = 55
SWZ = 0.5
SWW = 70
KCF = 0.0
LSO = 0
KLAGV = 16.5
BRAKPROP1 = 0
BRAKPROP2 = 0
FXLIMIT = 0
DAMPCOMF = 0

DAMPEXTF = 0
DAMPCOMR = 0
DAMPEXTR = 0
AIRBRAKES% = 0
BRAKLAG1 = 0
BRAKMULTLF = 1
BRAKMULTRF = 1
BRAKMULTLR = 1
BRAKMULTRR = 1

Suspension Parameters
SUSPENSIONF = 1
SUSPENSIONR = 0
HF = 0
HR = 0
LF = 1
LR = 1000
KSAF = 0
KSAR = 1
BF = 0
BR = 0
CF = 0
CR = 0
DF = 0
DR = 0
EF = 0
ER = 0
KSLF = .1667
KSLR = 0
LSAF = 1000
LSAR = 1000
KSADF = 0
KSADR = 0
KSAD2F = 0
KSAD2R = 0
KACK = 0

Trailer Parameters
MASS = 155
SMASS = 142.6
UMASSF = 6.2
UMASSR = 6.2
LENA = 1
LENB = 3
IXS = 530
IYS = 2942
IZZ = 3858
IXZ = 0
DLADV = 0
DYADV = 0
DNADV = 0
KTL = 1
KSF = 1600
KSDF = 150
KSR = 1600
KSDR = 150
TRWF = 7.0
TRWB = 7.0
HCG = 3.0
KBS = 8000
HBS = 0.20
KTSF = 0
KTSR = 0
KRAS = 12000
KRADP = 700
TSPRINGR = 15000
HRAF = 1.0
HRAR = 1.0
HS = 3.17
IXUF = 40
IXUR = 40
KLT = 2.3E-5
DRAGC = 0
KLAGV = 25
SUSPENSIONF = 0
SUSPENSIONR = 0
HF = 0
HR = 0
LF = 1
LR = 1
KSAF = 1
KSAR = 1
BF = 0
BR = 0
CF = 0
CR = 0
DF = 0
DR = 0
EF = 0
ER = 0
KSLF = 0
KSLR = 0
LSAF = 1000
LSAR = 1000
KSADF = 0
KSADR = 0
KSAD2F = 0
KSAD2R = 0
TLEND = 11.0
TLENE = 17.0
THH = 1.5
THITCHSP = 60000
THITCHSPD = 220
KTFIFTH = 0
BRAKLAG1 = 0
BRAKLAG2 = 0
BRAKLAG3 = 0
KFADE = 0.0005
NDRWHL = 1
NTRWHL = 1

Tire Parameters
TWIDTH = 5.80
KA0 = 2.4381e+003
KA1 = 1.5990e+001
KA2 = 3.7873e+003
KA3 = -4.2042e-001
KA4 = 9.8425e+002
KA = -0.0699
KMUy = 0.6077
TPRESS = 35.00
KB1y = -1.6516e-004
KB3y = 1.1600e+000
KB4y = -2.5069e-008
KGAMMA = 0.90
CSFZ = 16.7535
MUNOMy = 0.85
FZTRL = 1400
KK1 = -1.1534e-004
RR = 1.025
TIRE = RADIAL
C1 = -0.1641
C2 = 1.8594
C3 = 1.9363
C4 = 0.3134
G1 = 0.9789
G2 = -0.3367
MUNOMx = 0.85
LONGLAG = 0.25
PLYSTEER = -0.0048
KB1x = 8.5700e-004
KB3x = 7.0402e-001
KB4x = -5.0229e-007
KMUx = 0.3984
DRAGC = -0.015
C5 = 1.2732
Kx = 0

11. CAR and Boat Trailer – P/B

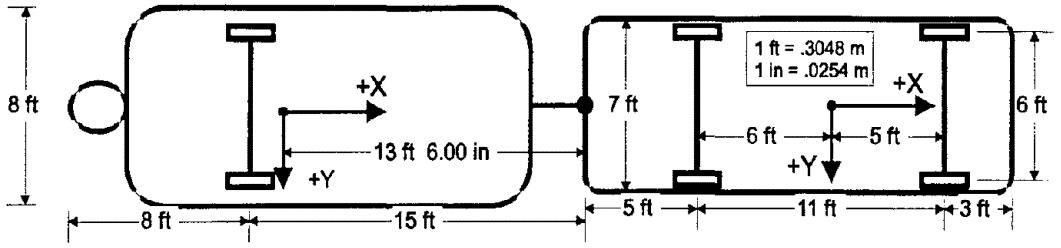

Figure F-11. Dimensions of AASHTO Car and Boat Trailer – P/B

Properties of the AASHTO car and boat trailer combination use the passenger car (AASHTO P), and add a boat trailer following the dimensions specified by AASHTO. The passenger car parameter and suspension files are unchanged.

a. Trailer Parameter File "BT.PAR"

The trailer geometry is defined by AASHTO.

MASS Total Vehicle Mass (slugs) - It is assumed that the camper weighs 3000 lb. **MASS = 93 slugs.**

SMASS Vehicle Sprung Mass (slugs) - SMASS = MASS - UMASSF - UMASSR. **SMASS = 86.8 slugs**

UMASSF Front Unsprung Mass (slugs) – The boat trailer has only one axle, so front axle properties are set to zero. **UMASSF = 0 slugs.**

UMASSR Rear Unsprung Mass (slugs) - The rear unsprung mass is assumed to weigh 200 lb. **UMASSR = 6.2 slugs.**

LENA Distance from Sprung Mass cg to Front Axle (ft) - The boat trailer has only one axle, so front axle properties are set to zero. **LENA = 0 ft.**

LENB Distance from Sprung Mass cg to Rear Axle (ft) – AASHTO defines the hitch to trailer axle distance to be 15 ft. To achieve a hitch tongue weight of approximately 300-lb, the trailer cg must be 1.5 ft ahead of the axle. **LENB = 1.5 ft.**

IXS Sprung Mass Roll Inertia (ft-lb-s^2) – The boat trailer mass moments of inertia are estimated based on small passenger car values. **IXS = 300 ft-lb-s^2**

IYS Sprung Mass Pitch Inertia (ft-lb-s^2) - The boat trailer mass moments of inertia are estimated based on small passenger car values. **IYS = 2000 ft-lb-s^2**

IZZ Total Vehicle Yaw Inertia (ft-lb-s^2) - The boat trailer mass moments of inertia are estimated based on small passenger car values. **IZZ = 2000 ft-lb-s^2**

IXZ Total Vehicle Roll/Yaw Cross Product of Inertia (ft-lb-s^2) - Assumed to be zero.

KTL Tire Lag Constant (ft) - A nominal value of 1 ft is used. **KTL = 1 ft.**

KSF Front Wheel Rate (lb/ft) - The boat trailer has only one axle, so front axle properties are set to zero. **KSF = 0 lb/ft**

KSR Rear Wheel Rate (lb/ft) - The boat trailer suspension stiffness and damping are estimated based on typical passenger car values. **KSR = 2400 lb/ft**

KSDF Front Wheel Damping Rate (lb/ft/s) - The boat trailer has only one axle, so front axle properties are set to zero. **KSDF = 0 lb/ft/s**

KSDR Rear Wheel Damping Rate (lb/ft/s) - The boat trailer suspension stiffness and damping are estimated based on typical passenger car values. **KSDR = 240 lb/ft/s**

TRWF Front Track Width (ft) - The boat trailer has only one axle, so front axle properties are set to zero. **TRWF = 0 ft**

TRWR Rear Track Width (ft) - AASHTO defines vehicle width as 8.0 ft. Track width is assumed to be 1 ft less than the vehicle width: **TRWR = 7.0 ft**

HCG Total Vehicle cg Height (ft) - HCG has been assumed to be 3 ft. **HCG = 3.0 ft**

KBS Bump Stop Stiffness (lb/ft) - Bump stop stiffness was set to be approximately five times the average wheel rate: **KBS = 12000 lb/ft**

HBS Bump Stop Position (ft) - HBS was set to a nominal value of: **HBS = 0.2 ft**

KTSF Front Auxiliary Roll Stiffness (ft-lb/rad) – No suspension auxiliary roll stiffness is used for the camper. **KTSF = 0 ft-lb/rad.**

KTSR Rear Auxiliary Roll Stiffness (ft-lb/rad) - No suspension auxiliary roll stiffness is used for the camper. **KTSR = 0 ft-lb/rad.**

HRAF Front Suspension Roll Center Height (ft) - HRAF has been assumed to be at the axle height. **HRAR = 0 ft**

HRAR Rear Suspension Roll Center Height (ft) - HRAR has been measured in Ref. F.6. **HRAR = 1.0 ft**

HS Sprung Mass cg Height (ft) – Using the assumed axle height of 1 ft, and the total vehicle cg, the sprung mass cg can be computed. **HS = 3.14 ft**

IXUF Front Unsprung Mass Roll Inertia (ft-lb-s^2) - The boat trailer has only one axle, so front axle properties are set to zero. **IXUF = 40 ft-lb-s^2**

IXUR Rear Unsprung Mass Roll Inertia (ft-lb-s^2) - The boat trailer mass moments of inertia are estimated based on small passenger car values. **IXUR = 40 ft-lb-s^2**

KLT Tire Lateral Compliance (ft/lb) - Tire lateral compliance is estimated to be 76 percent of the tire vertical compliance Ref. F.2: **KLT = 2.3E-5 ft/lb**

SUSPENSIONF Rear Suspension Type (0 or 1) - **SUSPENSIONF = 0**

SUSPENSIONR Rear Suspension Type (0 or 1) - **SUSPENSIONR = 0**

HF & LF Front Axle Roll Steer - Roll steer has been set to zero. **HF = 0 & LF = 1**

HR & LR Rear Axle Roll Steer - Roll steer has been set to zero. **HR = 0 & LR = 1**

TLEND Longitudinal Distance from Tow Vehicle cg to Hitch (ft) - Referring to Figure F-11, the hitch is located at the rear of the passenger vehicle, which is 11 ft behind the cg. **TLEND = 11 ft**

TLENE Longitudinal Distance from Trailer Vehicle cg to Hitch (ft) - Referring t o Figure F-11, the hitch is located 13.5 ft ahead of the trailer cg. **TLENE = 13.5 ft**

THH Initial Height of Hitch Above the Ground (ft) - Initial hitch height is assumed to be 1.5 ft above ground. **THH = 1.5 ft**

HITCHSP Hitch Translational Spring Stiffness (lb/ft) - Hitch stiffness is assumed to be 5000 lb/in, **HITCHSP = 60000 lb/ft**

HITCHSPD Hitch Translational Damping (lb/ft/s) - Hitch damping is assumed to be 20 lb/in/s, **HITCHSPD = 240 lb/ft/s**

b. Driver Parameter File "DRIVER.PAR"

The VDANL driver parameter file requires the vehicle stability factor for its adaptive control algorithms. This vehicles understeer gradient is approximately 3.5 deg/g, which gives a stability factor of: **KSTABF = 0.0019 rad/ft/s^2**

c. Other Parameters

The AASHTO specifies that the minimum design turning radius of the outside front tire at 10 mi/h is 24.0 ft, which makes the turning radius of the cg 24.0-T/2 = 21 ft. Running a slowly increasing steer maneuver at 10 mi/h, and knowing that radius of curvature is equal to forward speed divided by yaw rate, a 21 radius turn is achieved at a steering wheel angle of 11.2 radians. In NONLIN.PAR, **DSWMAX = 11.2**

d. Parameter Files

Vehicle Parameters

MASS = 155
SMASS = 132.5
UMASSF = 9.8
UMASSR = 12.7
LENA = 5
LENB = 6
IXS = 530
IYS = 2942
IZZ = 3858
IXZ = 0
KSTR = 20
KSCF = 0.0002
KSCB = 0
DLADV = 0
DYADV = 0
DNADV = 0
DENSITY = 0.00237
REFAREA = 25
CDX = 0.4
AEROVEL = 44
KTL = 1
KSF = 1794
KSDF = 150
KSR = 1468
KSDR = 150
TRWF = 6
TRWB = 6
HCG = 1.833
KBS = 8000
HBS = 0.20
KTSF = 0
KTSR = 0
KRAS = 12000
KRADP = 700
TSPRINGR = 15000
HRAF = 0
HRAR = 0.5
HS = 1.975
IXUF = 40
IXUR = 40
KLT = 1.036E-5
XACC = 0
ZACC = 0
DRAGC = -.015
LENS = 5.4
LM = 1.125
KBTF = -1.525
KVB = 23.5
KMB = 9.4
FBPVL = 55
SWZ = 05
SWW = 70
KCF = 0.0
LSO = 0
KLAGV = 16.5
BRAKPROP1 = 0
BRAKPROP2 = 0
FXLIMIT = 0
DAMPCOMF = 0

DAMPEXTF = 0
DAMPCOMR = 0
DAMPEXTR = 0
AIRBRAKES% = 0
BRAKLAG1 = 0
BRAKMULTLF = 1
BRAKMULTRF = 1
BRAKMULTLR = 1
BRAKMULTRR = 1

Suspension Parameters
SUSPENSIONF = 1
SUSPENSIONR = 0
HF = 0
HR = 0
LF = 1
LR = 1000
KSAF = 0
KSAR = 1
BF = 0
BR = 0
CF = 0
CR = 0
DF = 0
DR = 0
EF = 0
ER = 0
KSLF = .1667
KSLR = 0
LSAF = 1000
LSAR = 1000
KSADF = 0
KSADR = 0
KSAD2F = 0
KSAD2R = 0
KACK = 0

Trailer Parameters
MASS = 94
SMASS = 86.8
UMASSF = 0
UMASSR = 6.2
LENA = 0
LENB = 1.5
IXS = 300
IYS = 2000
IZZ = 2000
IXZ = 0
DLADV = 0
DYADV = 0
DNADV = 0
KTL = 1
KSF = 0
KSDF = 0
KSR = 2400
KSDR = 240
TRWF = 0
TRWB = 7.0
HCG = 3.0
KBS = 12000
HBS = 0.20
KTSF = 0
KTSR = 0
KRAS = 12000
KRADP = 700
TSPRINGR = 15000
HRAF = 1.0
HRAR = 1.0
HS = 3.14
IXUF = 0
IXUR = 40
KLT = 2.3E-5
DRAGC = 0
KLAGV = 25
SUSPENSIONF = 0
SUSPENSIONR = 0
HF = 0
HR = 0
LF = 1
LR = 1
KSAF = 1
KSAR = 1
BF = 0
BR = 0
CF = 0
CR = 0
DF = 0
DR = 0
EF = 0
ER = 0
KSLF = 0
KSLR = 0
LSAF = 1000
LSAR = 1000
KSADF = 0
KSADR = 0
KSAD2F = 0
KSAD2R = 0
TLEND = 11.0
TLENE = 13.5
THH = 1.5
THITCHSP = 60000
THITCHSPD = 240
KTFIFTH = 0
BRAKLAG1 = 0
BRAKLAG2 = 0
BRAKLAG3 = 0
KFADE = 0.0005
NDRWHL = 1
NTRWHL = 1

Tire Parameters
TWIDTH = 5.80
KA0 = 2.4381e+003
KA1 = 1.5990e+001
KA2 = 3.7873e+003
KA3 = -4.2042e-001
KA4 = 9.8425e+002
KA = -0.0699
KMUy = 0.6077
TPRESS = 35.00
KB1y = -1.6516e-004
KB3y = 1.1600e+000
KB4y = -2.5069e-008
KGAMMA = 0.90
CSFZ = 16.7535
MUNOMy = 0.85
FZTRL = 1400
KK1 = -1.1534e-004
RR = 1.025
TIRE = RADIAL
C1 = -0.1641
C2 = 1.8594
C3 = 1.9363
C4 = 0.3134
G1 = 0.9789
G2 = -0.3367
MUNOMx = 0.85
LONGLAG = 0.25
PLYSTEER = -0.0048
KB1x = 8.5700e-004
KB3x = 7.0402e-001
KB4x = -5.0229e-007
KMUx = 0.3984
DRAGC = -0.015
C5 = 1.2732
Kx = 0

12. Motor HomE and Boat Trailer – MH/B

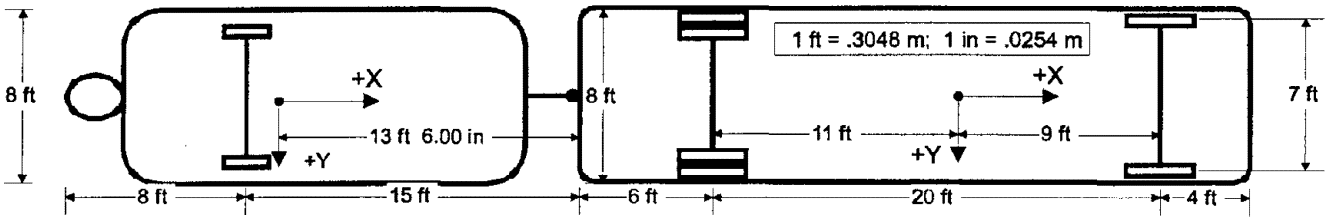

Figure F-12. Dimensions of AASHTO Motor Home and Boat Trailer – MH/B

Properties of the AASHTO motor home and boat trailer combination use the motor home (AASHTO MH), and add the boat trailer (AASHTO P/B). The motor home parameter and suspension files are unchanged.

a. Driver Parameter File "DRIVER.PAR"

The VDANL driver parameter file requires the vehicle stability factor for its adaptive control algorithms. This vehicle's understeer gradient is approximately 3.0 deg/g, which gives a stability factor of: **KSTABF = 0.0016 rad/ft/s^2**

b. Other Parameters

The AASHTO specifies that the minimum design turning radius of the outside front tire at 10 mi/h is 50.0 ft, which makes the turning radius of the cg 50.0-T/2 = 46.5 ft. Running a slowly increasing steer maneuver at 10 mi/h, and knowing that radius of curvature is equal to forward speed divided by yaw rate, a 46.6 ft radius turn is achieved at a steering wheel angle of 12.7 radians. In NONLIN.PAR, **DSWMAX = 12.7**

c. Parameter Files

Vehicle Parameters
MASS = 323
SMASS = 252
UMASSF = 24
UMASSR = 47
LENA = 9
LENB = 11
IXS = 1300
IYS = 13000
IZZ = 13000
IXZ = 0
KSTR = 30
KSCF = 0.00002
KSCB = 0
DLADV = 0
DYADV = 0
DNADV = 0
DENSITY = 0.00237
REFAREA = 50
CDX = 0.4
AEROVEL = 44
KTL = 1
KSF = 10000
KSDF = 1000
KSR = 16000
KSDR = 1600
TRWF = 7.0
TRWB = 7.0
HCG = 3.0
KBS = 660000
HBS = 0.20
KTSF = 215000
KTSR = 256000
KRAS = 120000
KRADP = 7000
TSPRINGR = 55200

HRAF = 1.58
HRAR = 2.17
HS = 3.4
IXUF = 200
IXUR = 400
KLT = 2.3E-5
XACC = 0
ZACC = 0
DRAGC = -.015
LENS = 5.4
LM = 1.125
KBTF = -72.5
KVB = 23.5
KMB = 9.4
FBPVL = 55
SWZ = 0.5
SWW = 0
KCF = -1E-6
LSO = 0
KLAGV = 16.5
BRAKPROP1 = 1
BRAKPROP2 = 1
FXLIMIT = -1000
DAMPCOMF = 0
DAMPEXTF = 0
DAMPCOMR = 0
DAMPEXTR = 0
AIRBRAKES% = 0
BRAKLAG1 = 0.3
BRAKMULTLF = 1
BRAKMULTRF = 1
BRAKMULTLR = 1
BRAKMULTRR = 1

Suspension Parameters
SUSPENSIONF = 1
SUSPENSIONR = 1
HF = 0.2
HR = -0.2
LF = 1
LR = 1
KSAF = 1
KSAR = 1
BF = 0
BR = 0
CF = 0
CR = 0
DF = 0
DR = 0
EF = 0
ER = 0
KSLF = 0
KSLR = 0
LSAF = 1000
LSAR = 1000
KSADF = 0
KSADR = 0
KSAD2F = 0
KSAD2R = 0
KACK = 0

Trailer Parameters
MASS = 94
SMASS = 86.8
UMASSF = 0
UMASSR = 6.2
LENA = 0
LENB = 1.5
IXS = 300
IYS = 2000
IZZ = 2000
IXZ = 0
DLADV = 0
DYADV = 0
DNADV = 0
KTL = 1
KSF = 0
KSDF = 0
KSR = 2400
KSDR = 240
TRWF = 0
TRWB = 7.0
HCG = 3.0
KBS = 12000
HBS = .20
KTSF = 0
KTSR = 0
KRAS = 12000
KRADP = 700
TSPRINGR = 15000
HRAF = 1.0
HRAR = 1.0
HS = 3.14
IXUF = 0
IXUR = 40
KLT = 2.3E-5
DRAGC = 0
KLAGV = 25
SUSPENSIONF = 0
SUSPENSIONR = 0
HF = 0
HR = 0
LF = 1
LR = 1
KSAF = 1
KSAR = 1
BF = 0
BR = 0
CF = 0
CR = 0
DF = 0
DR = 0
EF = 0
ER = 0
KSLF = 0
KSLR = 0
LSAF = 1000
LSAR = 1000
KSADF = 0
KSADR = 0
KSAD2F = 0
KSAD2R = 0
TLEND = 11.0
TLENE = 13.5
THH = 1.5
THITCHSP = 60000
THITCHSPD = 240
KTFIFTH = 0
BRAKLAG1 = 0
BRAKLAG2 = 0
BRAKLAG3 = 0
KFADE = 0.0005
NDRWHL = 1
NTRWHL = 1
KTFIFTH = 0
BRAKLAG1 = 0
BRAKLAG2 = 0
BRAKLAG3 = 0
KFADE = 0.0005
NDRWHL = 1
NTRWHL = 1

MH Tire Parameters
TWIDTH = 10.00
KA0 = 1.9148e+003
KA1 = 9.1239e+000
KA2 = 2.6632e+004

KA3 = 0.0000e+000
KA4 = 1.0000e+000
KA = 0.0544
KMUy = 0.3454
TPRESS = 125.00
KB1y = -1.4737e-005
KB3y = 6.6176e-001
KB4y = -2.5237e-010
KGAMMA = 0.90
CSFZ = 6.6412
MUNOMy = 0.85
FZTRL = 6175
KK1 = -3.0824e-005
RR = 2.0
TIRE = RADIAL
C1 = 0.4693
C2 = 2.0389
C3 = 1.7886
C4 = 0.7335
G1 = 0.7266
G2 = 1.0000
MUNOMx = 0.85
LONGLAG = 0.25
PLYSTEER = -0.0043
KB1x = -2.9289e-005
KB3x = 9.4338e-001
KB4x = 1.1202e-009
KMUx = 0.3454
DRAGC = -0.05
C5 = 1.2732

BT Tire Parameters
TWIDTH = 5.80
KA0 = 2.4381e+003
KA1 = 1.5990e+001
KA2 = 3.7873e+003
KA3 = -4.2042e-001
KA4 = 9.8425e+002
KA = -0.0699
KMUy = 0.6077
TPRESS = 35.00
KB1y = -1.6516e-004
KB3y = 1.1600e+000
KB4y = -2.5069e-008
KGAMMA = 0.90
CSFZ = 16.7535
MUNOMy = 0.85
FZTRL = 1400
KK1 = -1.1534e-004
RR = 1.025
TIRE = RADIAL
C1 = -0.1641
C2 = 1.8594
C3 = 1.9363
C4 = 0.3134
G1 = 0.9789
G2 = -0.3367
MUNOMx = 0.85
LONGLAG = 0.25
PLYSTEER = -0.0048
KB1x = 8.5700e-004
KB3x = 7.0402e-001
KB4x = -5.0229e-007
KMUx = 0.3984
DRAGC = -0.015
C5 = 1.2732

C. APPENDIX F REFERENCES

F.1. Reide, P.M., Leffert, R.L., and Cobb, W.A., "Typical Vehicle Parameters for Dynamic Studies Revised for the 1980's," SAE Paper 840561, 1984.

F.2. Allen, R.W., Szostak, H.T., Klyde, D.H., Rosenthal, T. J., and Owens, K.J., "Vehicle Dynamic Stability and Rollover," NHTSA Final Report DOT-HS-807-956, 1992.

F.3. Chrstos, J.P., *Parameter Measurement and Computation Procedures for 1994 Ford Taurus GL*, NHTSA Final Report (draft), 1996.

F.4. Fancher, P.S., Ervin, R.D., Winkler, C.B., and Gillespie, T.D., *A Factbook of the Mechanical Properties of the Components for Single-Unit and Articulated Heavy Trucks*, University of Michigan Transportation Institute Final Report No. UMTRI-86-12, 1986.

F-5. *Mechanics of Heavy Duty Trucks and Truck Combinations*, The University of Michigan – College of Engineering, Course Notes, July 1998.

F.6. Winkler, C.B., Bogard, S.E., and Karamihas, S.M., *Parameter Measurements of a Highway Tractor and Semitrailer*, University of Michigan Transportation Institute Final Technical Report UMTRI-95-47, December 1995.

APPENDIX G

IHSDM ROADWAY DESIGN DATABASE FORMAT

A. OVERVIEW

The IHSDM database has been constructed such that each record (row) in the file is a "critical point" along a candidate roadway design. A critical point is any location where there is a change in horizontal, vertical, or cross-sectional alignment (i.e., tangent to horizontal curve, tangent to vertical curve, normal crown to superelevation, lane addition, etc.). Currently the end point of a vertical curve (VPT) is not included as critical point, but may be in the future.

The data are tabulated in columns, and each column represents a variable that has currently been identified as a requirement for input into the IHSDM modules. Each record contains all the data pertinent for that station. Currently each row has 37 variables that describe the roadway geometry, including horizontal alignment, vertical profile, pavement width and cross-slope, shoulder width and slope, and side slope information. The convention adopted in this file format is the "look-ahead" convention. This means that all variable values for a particular record are applicable beginning at that station and continuing through to the following critical point station.

The variables are all real numbers. Typically a zero (0.00) represents a measure of 0.00 (i.e., 0.00 m). However, occasionally a 0.0 is used as a flag to indicate a false, or null, condition. When this occurs it will be noted under the description of the variable. IHSDM is being developed entirely in metric. Therefore, all values in the database are in meters unless otherwise noted. A detailed description of the file follows.

B. FILE FORMAT

Header File:

At the top of each database generated by the IHSDM software, there is a header file identifying various key aspects about that file. On the first line is the title of the file "--- IHSDM DATABASE ---". On the third line is the "Job Number:" followed by a three-digit alphanumeric character string, "Chain Name:" followed by an alphanumeric name typically eight characters or less, and "Initial Heading:" of the tangent, which may be the tangent at the point of curvature, from where the job began, in decimal degrees clockwise from North, to five decimal places. On the fourth line is the "Number of Regions:" and a subsequent integer relating how many "sections" are along the chain based on the presence of station equations, and "Starting Station:" and "Ending Station" each to three decimal places.

Column 1: Station

Contains the station number as a real number to three decimal places, e.g., the station 1+234.567 is represented as 1234.567. The following columns, 2 through 37, contain data valid from this station through to the next station (2nd row, 1st column).

Column 2, 3 & 4: X, Y, Z Data

The coordinates of the centerline at the station shown in column 1, in MicroStation world (absolute) coordinates. X and Y are plan view coordinates, and Z represents elevation. These values are also reported to three decimal places, yielding an accuracy of one mm. To obtain relative coordinates, subtract the first row from all the rows, thereby making the first row 0.000, 0.000, 0.000 for X, Y, and Z, respectively.

Column 5: Horizontal Radius of Curvature

Contains the radius of the curve, to two decimal places. A value of "0.00" in this column acts as a flag to indicate no horizontal curvature, or that it is a tangent section through to the next station. Every other critical station reported while in the curve always has the value of the curve radius in this column. Therefore, the first zero value encountered in this column, following a horizontal curve, is the endpoint, or PT, of the curve.

Column 6: Horizontal Curve Central Angle

The central, or entire deflection angle, of the horizontal curve is shown. This value is in decimal degrees, to five decimal places. A nonzero value will be in this column for all critical stations within the horizontal curve. A value of 0.00000 in this column acts as a flag to indicate no horizontal curvature. The value of central angle is signed positive for a horizontal curve to the right, and negative for a curve to the left when traversing the alignment in order of increasing station numbers.

Column 7: Spiral Angle

This column contains the entire spiral deflection angle, in decimal degrees, also to five decimal places. The purpose of this column is twofold. First, it acts as a flag to indicate the presence of a spiral (i.e., a value of "0.00000" indicates that no spiral is present). Second, the value in this column can be used to calculate X and Y coordinates for the centerline of the alignment through the spiral (see accompanying paper on calculation of spiral coordinates). A nonzero value will be in this column at any critical station within the spiral.

The length of the spiral (needed for the spiral coordinate calculations) can be derived from the database by taking the difference in stationing between the first nonzero value in this column (beginning of spiral), and the first zero value in this column (end of spiral). The value of spiral angle is signed positive for a spiral curve to the right, and negative for a curve to the left when traversing the alignment in order of increasing station numbers.

Column 8: Vertical Curve Length

The length of the vertical curve to two decimal places. The vertical curve length is a nonzero value at every critical point within the vertical curve. A value of "0.00" is used as a flag to indicate no vertical curvature. The elevation for any station within the vertical curve is computed using:

$$z = ax^2 + bx + c$$

where:

b = g1, the back grade of the vertical curve (Column 9), divided by 100

a = (g2-g1)/(2L)

g2, the forward grade of the vertical curve (Column 10), divided by 100

L is the total length of the curve measured in the horizontal plane (Column 8)

c = elevation of the station where the vertical curve started

z = elevation of the current station

x = horizontal distance from the beginning of vertical curve to the current station

Column 9: Back Grade

Grade, in percent (m/m), of the vertical tangent, to three decimal places. Two conventions are used when reporting the back grade. If the station is on a vertical tangent (constant grade), the back grade is the tangent grade. Elevations along of the centerline of the roadway can be calculated on the vertical tangent using the following formula:

$$z = mx + b$$

where:

m = back grade

b = known elevation on the vertical tangent

x = horizontal distance from the station of known elevation to the current station

z = elevation at current station

If the station is on a vertical curve (constantly changing grade), the value in this column is the back grade of the vertical curve. Back grade is one of the values needed to calculate positional elevation within a vertical curve as shown in the definition for Column 8.

Column 10: Forward Grade

Grade, in percent (m/m), of the vertical tangent, to three decimal places. Similar to back grade (Column 9), two conventions are used when reporting the forward grade. If the station is on a vertical tangent (constant grade), the forward grade is the tangent grade. Therefore, back grade and forward grade will be equivalent for each station on a vertical tangent. If the station is on a vertical curve (constantly changing grade), the value in this column is the forward grade of the vertical curve. Therefore, the back grade will not equal the forward grade at each critical station on a vertical curve. Forward grade is the final value needed to calculate positional elevation within the vertical curve as shown in the definition for Column 8.

Column 11: Lane 1 Width

Width, to one decimal place, of any auxiliary lane (i.e., climbing lane, right-turn lane, etc.) to the extreme left of the cross-section (opposite direction of travel) on two-lane roadways, when facing in order of increasing station numbering (see Figure G-1 for a graphical representation of all) "Lane" designations). A value of "0.0" is a flag indicating no auxiliary lane on that side of the roadway.

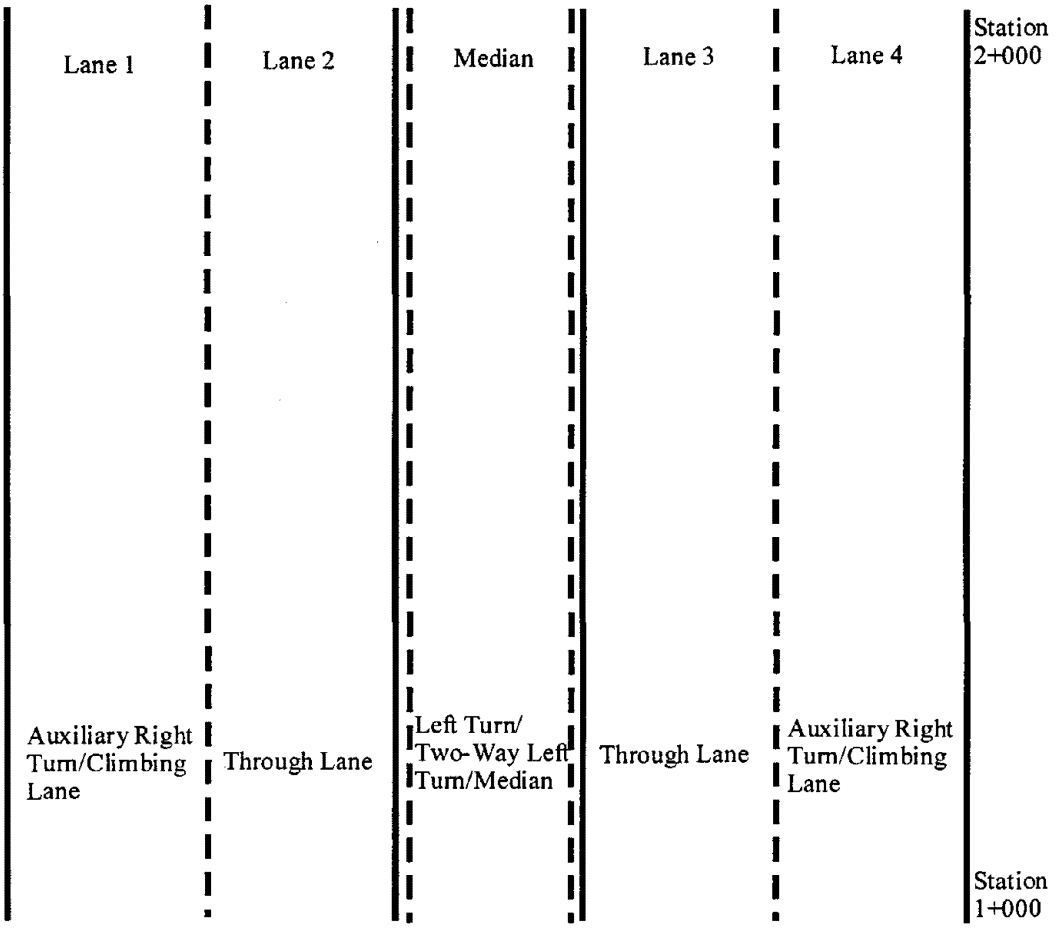

Figure G-1. Lane Designations

Column 12: Lane 1 Type

As defined, Lane 1 can be of several types: a right turn lane, an emergency or scenic turnout, or a truck climbing lane. Currently this information is not being used in the database. However, codes will be constructed at such time when this value is used. This information cannot be automatically extracted from the CAD data files; rather, it will probably be manually input by the user.

Column 13: Lane 1 Cross Slope

The cross slope, in percent (meters of rise/meters of run), of Lane 1 will be contained in this column, to two decimal places. If the cross slope is different at the next critical point station, the cross slope for any interim station is computed using the following formula:

$$\text{Slope@STA}_c = [((SL_f - SL_i)/(STA_f - STA_i))*(STA_c - STA_i)]+SL_i$$

where:

SL_i = cross slope at the station where it started to change

SL_f = cross slope at the station where it stopped changing

STA_i = station where cross slope started to change

STA_f = station where cross slope stopped changing

STA_c = interim station, station where we need to compute the slope

Column 14: Lane 2 Width

Width, to one decimal place, of the through lane to the left of the centerline of the roadway (opposite direction of travel), when facing in order of increasing station numbering (see Figure G-1 for a graphical representation of all "Lane" designations).

Column 15: Lane 2 Cross Slope

The cross slope, in percent (m/m), of Lane 2 will be contained in this column, to two decimal places. If the cross slope is different at the next critical point station, the cross slope for an interim point is computed as shown in Column 13.

Column 16: Median Width

Width, to one decimal place, of the median (i.e., left-turn lane, barrier separation, divided median, etc.). A value of "0.0" indicates that there is no median present on the roadway.

Column 17: Median Type

As defined, median can be of several types: a dedicated left-turn lane, a continuous two-way left-turn lane, or a grassy median separating the through lanes and not meant for vehicular travel. Currently this information is not being used in the database. However, codes will be constructed at such time when this

value is used. This information cannot be automatically extracted from the CAD data files, rather, it will probably be manually input by the user.

Column 18: Median Cross Slope

The cross slope, in percent (m/m), of the median will be contained in this column, to two decimal places. If the cross slope is different at the next critical point station, the cross slope for an interim point is computed as shown in Column 13.

Column 19: Lane 3 Width

Width, to one decimal place, of the through lane to the right of the centerline of the roadway, when facing in order of increasing station numbering (see Figure G-1 for a graphical representation of all "Lane" designations).

Column 20: Lane 3 Cross Slope

The cross slope, in percent (m/m), of Lane 3 will be contained in this column, to two decimal places. If the cross slope is different at the next critical point station, the cross slope for an interim point is computed as shown in Column 13.

Column 21: Lane 4 Width

Width, to one decimal place, of the auxiliary lane to the extreme right of the centerline, when facing in order of increasing station numbering (see Figure G-1 for a graphical representation of all "Lane" designations). A value of "0.0" indicates that there is no auxiliary lane present on that side of the roadway.

Column 22: Lane 4 Type

As defined, Lane 4 can be of several types, similar to Lane 1: a right-turn lane, an emergency or scenic turnout, or a truck climbing lane. Currently this information is not being used in the database. However, codes will be constructed at such time when this value is used. This information cannot be automatically extracted from the CAD data files; rather, it will probably be manually input by the user at a later date.

Column 23: Lane 4 Cross Slope

The cross slope, in percent (m/m), of Lane 4 will be contained in this column, to two decimal places. If the cross slope is different at the next critical point station, the cross slope for an interim point is computed as shown in Column 13.

Column 24: Left Shoulder Width

The width of the shoulder on the left side of the centerline, when viewed from the perspective of increasing station number, to one decimal place. Currently there is no distinction between paved and unpaved shoulder.

Column 25: Left Shoulder Slope

This column contains the left shoulder slope, in percent, to two decimal places. The shoulder slope is computed based on the following criteria:

IF the Lane 1 (or Lane 2 if Lane 1 is not present) cross slope IS LESS THAN -4.0 %

shoulder slope = cross slope

IF the Lane 1 (or Lane 2) cross slope IS GREATER THAN -4.0 % & LESS THAN 4.0 %

shoulder slope = -4.0 %

IF the Lane 1 (or Lane 2) cross slope IS GREATER THAN 4.0 %

shoulder slope = -8.0 % + cross slope

Column 26: Right Shoulder Width

The width of the shoulder on the right side of the centerline, when viewed from the perspective of increasing station number, to one decimal place. Currently there is no distinction between paved and unpaved shoulder.

Column 27: Right Shoulder Slope

This column contains the right shoulder slope, in percent, to two decimal places. The shoulder slope is computed based on the following criteria:

IF the Lane 4 (or Lane 3 if Lane 4 is not present) cross slope IS LESS THAN -4.0 %

shoulder slope = cross slope

IF the Lane 4 (or Lane 3) cross slope IS GREATER THAN -4.0 % & LESS THAN 4.0 %

shoulder slope = -4.0 %

IF the Lane 4 (or Lane 3) cross slope IS GREATER THAN 4.0 %

shoulder slope = -8.0 % + cross slope

Column 28: Left Backslope

This column contains the slope (m/m), in percent, of the backslope to two decimal places. The left backslope is the slope (used in cut sections) to the extreme left of the construction limits when viewing the roadway in order of increasing station numbers (see Figure G-2 for a graphical representation of the cross-section and its accompanying side slopes).

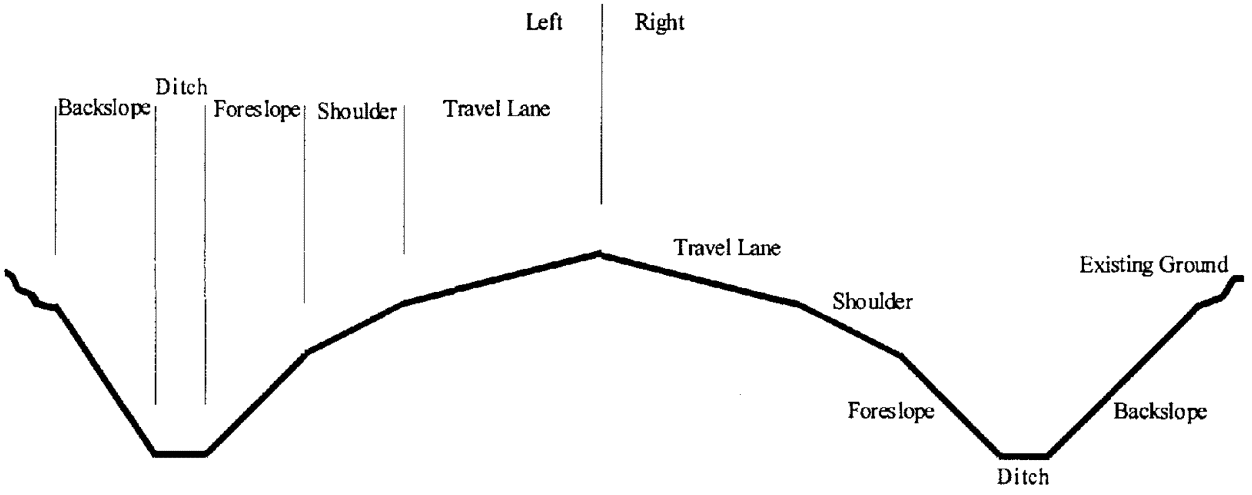

Figure G-2. Roadway Cross-section Including Side Slopes

Column 29: Left Backslope Width

The horizontal width of the left backslope is contained in this column, to two decimal places.

Column 30: Left Ditch Width

If a ditch is present to the left of the roadway, the width will be a nonzero value, to two decimal places.

Column 31: Left Foreslope

This column contains the percent slope of the left foreslope, to two decimal places.

Column 32 : Left Foreslope Width

The horizontal width of the left foreslope is contained in this column, to two decimal places.

Column 33: Right Foreslope

This column contains the percent slope of the right foreslope, to two decimal places.

Column 34: Right Foreslope Width

The horizontal width of the right foreslope is contained in this column, to two decimal places.

Column 35: Right Ditch Width

If a ditch is present to the right of the roadway, the width will be a nonzero value, to two decimal places.

Column 36: Right Backslope

This column contains the slope (m/m), in percent, of the right backslope to two decimal places.

Column 37: Right Backslope Width

The horizontal width of the right backslope is contained in this column, to two decimal places.

C. EXAMPLE OF DESIGN DATA BASE FILES

--- IHSDM DATABASE ---

Job Number: tra Chain Name: ALT3 Initial Heading:

Number Regions: 1 Start Station: 0+000 End Station: 1+950

Station X Y Z Radius DAngle SAngle VClen Bgrade Fgrade
L1Width L1Type L1Slope L2Width L2Slope MWidth
MType MSlope L3Width L3Slope L4Width L 4Type L4Slope
LSWidth LSSlope RSWidth RSSlope LBSlope LBSWdth
LDWidth LFSlope LFWidth RFSlope RFWidth RDWidth
RBSlope RBSWdth

0.000 54156.295 117320.990 47.740 0.00 0.00000 0.00 0.00 -2.650 -2.650 0.000 0
0.000 3.300 -2.000 0.000 0 0.000 3.300 -2.000 0.000 0 0.000 0.000 0.000 0.000
0.000 0.000 0.000 0.000 0.000 0.000 0.000 0.000 0.000 0.000 0.000

253.257 54376.719 117196.281 41.029 0.00 0.00000 0.00 0.00 -2.650 -2.650 0.000 0
0.000 3.300 -2.000 0.000 0 0.000 3.300 -2.000 0.000 0 0.000 0.000 0.000 0.000
0.000 0.000 0.000 0.000 0.000 0.000 0.000 0.000 0.000 0.000 0.000

277.836 54398.111 117184.177 40.377 0.00 0.00000 0.00 0.00 -2.650 -2.650 0.000 0
0.000 3.300 -2.000 0.000 0 0.000 3.300 2.000 0.000 0 0.000 0.000 0.000 0.000
0.000 0.000 0.000 0.000 0.000 0.000 0.000 0.000 0.000 0.000 0.000

283.059 54402.657 117181.605 40.239 155.00 -44.50016 0.00 0.00 -2.650 -2.650 0.000
0 0.000 3.300 -2.850 0.000 0 0.000 3.300 2.850 0.000 0 0.000 0.000 0.000 0.000
0.000 0.000 0.000 0.000 0.000 0.000 0.000 0.000 0.000 0.000 0.000

303.260 54420.596 117172.928 39.704 155.00 -44.50016 0.00 70.00 -2.650 0.800 0.000
0 0.000 3.300 -6.138 0.000 0 0.000 3.300 6.138 0.000 0 0.000 0.000 0.000 0.000
0.000 0.000 0.000 0.000 0.000 0.000 0.000 0.000 0.000 0.000 0.000

312.861 54429.842 117169.506 39.472 155.00 -44.50016 0.00 0.00 -2.650 0.800 0.000
0 0.000 3.300 -7.700 0.000 0 0.000 3.300 7.700 0.000 0 0.000 0.000 0.000 0.000
0.000 0.000 0.000 0.000 0.000 0.000 0.000 0.000 0.000 0.000 0.000

373.641 54489.751 117161.885 39.059 155.00 -44.50016 0.00 0.00 0.800 0.800 0.000
0 0.000 3.300 -7.700 0.000 0 0.000 3.300 7.700 0.000 0 0.000 0.000 0.000 0.000
0.000 0.000 0.000 0.000 0.000 0.000 0.000 0.000 0.000 0.000 0.000

403.443 54519.100 117166.792 39.298 0.00 0.00000 0.00 0.00 0.800 0.800 0.000 0
0.000 3.300 -5.412 0.000 0 0.000 3.300 5.412 0.000 0 0.000 0.000 0.000 0.000
0.000 0.000 0.000 0.000 0.000 0.000 0.000 0.000 0.000 0.000 0.000

473.938 54587.192 117185.038 39.862 0.00 0.00000 0.00 0.00 0.800 0.800 0.000 0
0.000 3.300 0.000 0.000 0 0.000 3.300 0.000 0.000 0 0.000 0.000 0.000 0.000
0.000 0.000 0.000 0.000 0.000 0.000 0.000 0.000 0.000 0.000 0.000

545.427 54656.246 117203.541 40.433 150.00 70.33397 0.00 0.00 0.800 0.800 0.000 0
0.000 3.300 5.488 0.000 0 0.000 3.300 -5.488 0.000 0 0.000 0.000 0.000 0.000
0.000 0.000 0.000 0.000 0.000 0.000 0.000 0.000 0.000 0.000 0.000

575.537 54685.914 117208.373 40.674 150.00 70.33397 0.00 0.00 0.800 0.800 0.000 0
0.000 3.300 7.800 0.000 0 0.000 3.300 -7.800 0.000 0 0.000 0.000 0.000 0.000
0.000 0.000 0.000 0.000 0.000 0.000 0.000 0.000 0.000 0.000 0.000

645.750 54754.679 117196.299 41.236 150.00 70.33397 0.00 50.00 0.800 -1.150 0.000
0 0.000 3.300 7.800 0.000 0 0.000 3.300 -7.800 0.000 0 0.000 0.000 0.000 0.000
0.000 0.000 0.000 0.000 0.000 0.000 0.000 0.000 0.000 0.000 0.000

699.452 54798.953 117166.857 41.106 150.00 70.33397 0.00 0.00 -1.150 -1.150 0.000
0 0.000 3.300 7.800 0.000 0 0.000 3.300 -7.800 0.000 0 0.000 0.000 0.000 0.000
0.000 0.000 0.000 0.000 0.000 0.000 0.000 0.000 0.000 0.000 0.000

729.561 54818.441 117143.972 40.760 0.00 0.00000 0.00 0.00 -1.150 -1.150 0.000 0
0.000 3.300 4.563 0.000 0 0.000 3.300 -4.563 0.000 0 0.000 0.000 0.000 0.000
0.000 0.000 0.000 0.000 0.000 0.000 0.000 0.000 0.000 0.000 0.000

772.013 54842.587 117109.056 40.272 0.00 0.00000 0.00 0.00 -1.150 -1.150 0.000 0
0.000 3.300 0.000 0.000 0 0.000 3.300 0.000 0.000 0 0.000 0.000 0.000 0.000
0.000 0.000 0.000 0.000 0.000 0.000 0.000 0.000 0.000 0.000 0.000

815.710 54867.442 117073.116 39.769 125.00 -79.33341 0.00 0.00 -1.150 -1.150 0.000
0 0.000 3.300 -4.697 0.000 0 0.000 3.300 4.697 0.000 0 0.000 0.000 0.000 0.000
0.000 0.000 0.000 0.000 0.000 0.000 0.000 0.000 0.000 0.000 0.000

846.434 54887.832 117050.237 39.416 125.00 -79.33341 0.00 0.00 -1.150 -1.150 0.000
0 0.000 3.300 -8.000 0.000 0 0.000 3.300 8.000 0.000 0 0.000 0.000 0.000 0.000
0.000 0.000 0.000 0.000 0.000 0.000 0.000 0.000 0.000 0.000 0.000

958.065 54991.780 117021.083 38.132 125.00 -79.33341 0.00 0.00 -1.150 -1.150 0.000
0 0.000 3.300 -8.000 0.000 0 0.000 3.300 8.000 0.000 0 0.000 0.000 0.000 0.000
0.000 0.000 0.000 0.000 0.000 0.000 0.000 0.000 0.000 0.000 0.000

988.789 55021.094 117030.022 37.779 0.00 0.00000 0.00 0.00 -1.150 -1.150 0.000 0
0.000 3.300 -5.063 0.000 0 0.000 3.300 5.063 0.000 0 0.000 0.000 0.000 0.000
0.000 0.000 0.000 0.000 0.000 0.000 0.000 0.000 0.000 0.000 0.000

1041.749 55069.475 117051.562 37.170 0.00 0.00000 0.00 0.00 -1.150 -1.150 0.000 0
0.000 3.300 0.000 0.000 0 0.000 3.300 0.000 0.000 0 0.000 0.000 0.000 0.000
0.000 0.000 0.000 0.000 0.000 0.000 0.000 0.000 0.000 0.000 0.000

1094.709 55117.857 117073.103 36.560 125.00 76.33295 0.00 0.00 -1.150 -1.150 0.000
0 0.000 3.300 5.063 0.000 0 0.000 3.300 -5.063 0.000 0 0.000 0.000 0.000 0.000
0.000 0.000 0.000 0.000 0.000 0.000 0.000 0.000 0.000 0.000 0.000

1125.433 55147.171 117082.042 36.207 125.00 76.33295 0.00 0.00 -1.150 -1.150 0.000
0 0.000 3.300 8.000 0.000 0 0.000 3.300 -8.000 0.000 0 0.000 0.000 0.000 0.000
0.000 0.000 0.000 0.000 0.000 0.000 0.000 0.000 0.000 0.000 0.000

1153.650 55175.626 117083.717 35.883 125.00 76.33295 0.00 90.00 -1.150 2.900 0.000
0 0.000 3.300 8.000 0.000 0 0.000 3.300 -8.000 0.000 0 0.000 0.000 0.000 0.000
0.000 0.000 0.000 0.000 0.000 0.000 0.000 0.000 0.000 0.000 0.000

1230.518 55246.086 117057.074 36.328 125.00 76.33295 0.00 0.00 -1.150 2.900 0.000
0 0.000 3.300 8.000 0.000 0 0.000 3.300 -8.000 0.000 0 0.000 0.000 0.000 0.000
0.000 0.000 0.000 0.000 0.000 0.000 0.000 0.000 0.000 0.000 0.000

1261.242 55267.646 117035.293 37.180 0.00 0.00000 0.00 0.00 2.900 2.900 0.000 0
0.000 3.300 5.532 0.000 0 0.000 3.300 -5.532 0.000 0 0.000 0.000 0.000 0.000
0.000 0.000 0.000 0.000 0.000 0.000 0.000 0.000 0.000 0.000 0.000

1330.094 55309.719 116980.791 39.177 0.00 0.00000 0.00 0.00 2.900 2.900 0.000 0
0.000 3.300 0.000 0.000 0 0.000 3.300 0.000 0.000 0 0.000 0.000 0.000 0.000
0.000 0.000 0.000 0.000 0.000 0.000 0.000 0.000 0.000 0.000 0.000

1398.946 55351.792 116926.290 41.174 125.00 -67.83337 0.00 0.00 2.900 2.900 0.000
0 0.000 3.300 -5.532 0.000 0 0.000 3.300 5.532 0.000 0 0.000 0.000 0.000 0.000
0.000 0.000 0.000 0.000 0.000 0.000 0.000 0.000 0.000 0.000 0.000

1429.670 55373.352 116904.509 42.065 125.00 -67.83337 0.00 0.00 2.900 2.900 0.000
0 0.000 3.300 -8.000 0.000 0 0.000 3.300 8.000 0.000 0 0.000 0.000 0.000 0.000
0.000 0.000 0.000 0.000 0.000 0.000 0.000 0.000 0.000 0.000 0.000

1516.212 55453.831 116877.711 44.574 125.00 -67.83337 0.00 0.00 2.900 2.900 0.000
0 0.000 3.300 -8.000 0.000 0 0.000 3.300 8.000 0.000 0 0.000 0.000 0.000 0.000
0.000 0.000 0.000 0.000 0.000 0.000 0.000 0.000 0.000 0.000 0.000

1546.936 55484.145 116882.219 45.465 0.00 0.00000 0.00 0.00 2.900 2.900 0.000 0
0.000 3.300 -5.152 0.000 0 0.000 3.300 5.152 0.000 0 0.000 0.000 0.000 0.000
0.000 0.000 0.000 0.000 0.000 0.000 0.000 0.000 0.000 0.000 0.000

1602.528 55537.715 116897.076 47.078 0.00 0.00000 0.00 0.00 2.900 2.900 0.000 0
0.000 3.300 0.000 0.000 0 0.000 3.300 0.000 0.000 0 0.000 0.000 0.000 0.000
0.000 0.000 0.000 0.000 0.000 0.000 0.000 0.000 0.000 0.000 0.000

1652.040 55585.388 116910.297 48.513 0.00 0.00000 0.00 120.00 2.900 -3.433 0.000
0 0.000 3.300 4.589 0.000 0 0.000 3.300 -4.589 0.000 0 0.000 0.000 0.000 0.000
0.000 0.000 0.000 0.000 0.000 0.000 0.000 0.000 0.000 0.000 0.000

1658.120 55591.285 116911.932 48.680 125.00 74.33326 0.00 0.00 2.900 -3.433 0.000
0 0.000 3.300 5.152 0.000 0 0.000 3.300 -5.152 0.000 0 0.000 0.000 0.000 0.000
0.000 0.000 0.000 0.000 0.000 0.000 0.000 0.000 0.000 0.000 0.000

1688.844 55621.598 116916.440 49.223 125.00 74.33326 0.00 0.00 2.900 -3.433 0.000
0 0.000 3.300 8.000 0.000 0 0.000 3.300 -8.000 0.000 0 0.000 0.000 0.000 0.000
0.000 0.000 0.000 0.000 0.000 0.000 0.000 0.000 0.000 0.000 0.000

1789.566 55712.693 116880.251 47.592 125.00 74.33326 0.00 0.00 -3.433 -3.433 0.000
0 0.000 3.300 8.000 0.000 0 0.000 3.300 -8.000 0.000 0 0.000 0.000 0.000 0.000
0.000 0.000 0.000 0.000 0.000 0.000 0.000 0.000 0.000 0.000 0.000

1820.290 55731.498 116856.418 46.537 0.00 0.00000 0.00 0.00 -3.433 -3.433 0.000 0
0.000 3.300 3.000 0.000 0 0.000 3.300 -3.000 0.000 0 0.000 0.000 0.000 0.000
0.000 0.000 0.000 0.000 0.000 0.000 0.000 0.000 0.000 0.000 0.000

1826.435 55734.828 116850.912 46.326 0.00 0.00000 0.00 0.00 -3.433 -3.433 0.000 0
0.000 3.300 2.000 0.000 0 0.000 3.300 -2.000 0.000 0 0.000 0.000 0.000 0.000
0.000 0.000 0.000 0.000 0.000 0.000 0.000 0.000 0.000 0.000 0.000

1851.014 55747.549 116829.880 45.482 0.00 0.00000 0.00 0.00 -3.433 -3.433 0.000 0
0.000 3.300 -2.000 0.000 0 0.000 3.300 -2.000 0.000 0 0.000 0.000 0.000 0.000
0.000 0.000 0.000 0.000 0.000 0.000 0.000 0.000 0.000 0.000 0.000

1950.290 55803.714 116754.362 42.074 0.00 0.00000 0.00 0.00 -3.433 -3.433 0.000 0
0.000 3.300 -2.000 0.000 0 0.000 3.300 -2.000 0.000 0 0.000 0.000 0.000 0.000
0.000 0.000 0.000 0.000 0.000 0.000 0.000 0.000 0.000 0.000 0.000

APPRNDIX H

USER'S GUIDE FOR IHSDM/VDANL VEHICLE DYNAMICS MODULE

A. OVERVIEW

STI's IHSDM Vehicle Dynamics Module, VDANLFHA, is used to interactively prepare a simulation run by selecting 1 of 12 AASHTO vehicles, selecting a terrain file, optionally selecting a speed profile or a speed limit and cornering acceleration, selecting a simulation distance, and selecting a vehicle lane position. At the completion of the run, VDANLFHA will display a series of plots of useful vehicle characteristics versus station. After the plots have been examined, VDANLFHA computes and displays a series of safety metrics from the simulation data.

B. INSTALLATION

Installation is performed in two separate steps. VDANLFHA comes on two floppy disks. Disk number 1 contains a file, SETUP.EXE. From the Windows File Manager (Windows 3.x) or Explorer (Windows 95), double click on SETUP.EXE. The setup program will ask for the name of the directory to install the program. While VDANLFHA can be installed anywhere, it is recommended that it be installed in "C:\VDANLFHA\". Once the directory has been selected, click on the install button on the middle of the form. The rest of the installation is automatic except for a prompt to insert disk number two.

The installation of the VDANL data files requires a little more user interaction. The VDANL installation floppy disk contains a single directory below the root named "A:\VDANL\". This directory, along with all of its subdirectories and files, must be copied intact to the "C" drive of the computer. There is no option to rename the directory or to use a different drive. From the Windows File Manager (Windows 3.x) or Explorer (Windows 95), drag the VDANL directory from floppy disk "A" to the root of the "C" drive. If this is not the first time VDANL has been installed on this computer, allow all existing files to be overwritten when prompted.

C. RUNNING A SIMULATION

Before a simulation is run, a terrain file must be available. The terrain files supported by VDANL are in the IHSDM Database Format, based on FHWA document titled *IHSDM Database Format* by G. L. Giering et. al. dated August 21, 1996. Assuming that a terrain database file is available, start VDANLFHA by double clicking on VDANLFHA.EXE in directory "C:\VDANLFHA\" (using the Windows File Manager (Windows 3.x) or Explorer (Windows 95)).

A simulation run is specified by selecting or entering the appropriate information in the seven sections of the VDANLFHA main screen. The seven sections are numbered 1 to 7, and should basically be used in order. Below, each section will be described.

1) - AASHTO Vehicle Selection: Twelve AASHTO vehicles are listed with a radio button to their left. The vehicle to be used in the simulation run is selected by clicking the button next to the vehicle desired. Only one vehicle can be used. Buttons with a white center are available, buttons with a gray center are not currently available. The selected vehicle's button will have a black center.

2) - Select Terrain: Clicking the Select Terrain button opens a Windows "Common Dialog Box" that allows a terrain file to be selected. The default location for the terrain files is "C:\VDANL\TERRAIN\", but terrain files can be located anywhere. The default extension for the terrain files is ".IHM", but any extension can be used. After locating the desired terrain file, select it by either double clicking on its name in the left list box, or single clicking its name in the left list box and clicking the OK button in the upper right corner of the box. The terrain file, along with its path should appear in the text box below the Select Terrain button.

2a) - Select Terrain Speed Profile: Vehicle speed can be controlled in one of two ways. Clicking on the Select Terrain Speed Profile button allows a file to be selected that contains speed (km/h) versus distance (m) information. This file would typically be generated by FHWA using a program from the Texas Transportation Institute, and contains two column of numbers (distance and speed), separated by commas. The default location for the speed files is "C:\VDANL\TERRAIN\", but they can be located anywhere. The default extension for the speed files is ".SPD", but any extension can be used except ".VEL". The vehicle speed files are selected in the same way as the terrain files.

3) - Speed Limit (km/h): If a vehicle speed file is not selected, a vehicle speed limit must be entered in this box (a vehicle speed file, if specified, will override the speed limit entry). This speed limit is used by the driver model in VDANLFHA to control vehicle speed on tangents and on some curves. VDANLFHA will used its throttle and brakes to keep the vehicle speed close to the speed limit, within the limits of the simulated vehicle. While going up and down steep grades, the speed will be controlled (again within the limits of the simulated vehicle).

4) - Cornering Acceleration (g): If a vehicle speed file is not selected, a cornering acceleration must be entered in this box (a vehicle speed file, if specified, will override the cornering acceleration entry). The cornering acceleration is used by the VDANLFHA driver model to control vehicle

speed on spirals and curves. If based on the road curvature, the speed of the vehicle will result in a cornering acceleration that is higher than the cornering acceleration entry, and the vehicle will be slowed down so that it will not corner above the desired lateral acceleration.

5) - **Simulation Distance (m):** The simulation distance is how far along the terrain that the simulation should run. All simulations will start at Station 0.00, but they do not have to run until the last station in the terrain database. If the simulation distance is greater than the last station in the terrain database, the simulation will stop at the end of the database.

6) - **Desired Center Line Offset (m):** Desired center line offset is the lateral distance from the terrain center line that the center of the vehicle should be. Positive entries cause the vehicle to drive on the right side of the road (U.S.), while negative entries cause the vehicle to drive on the left side of the road (England).

7) - **Run Simulation:** After everything above has been set for a simulation run, clicking on Run Simulation will start the VDANLFHA simulation. When the actual simulation starts, a progress bar will appear and show the simulation progress. When the simulation is complete, a DOS box will open, and some menus will be seen flashing on the screen (all automatic). The DOS program PLOTTING.EXE will display detailed plots of a number of simulation variables that can be examined by the user. Hitting the space bar will cause the next plot to be drawn, and this is continued until the end of the plot list is complete (typically four or five plots).

After the last plot has been viewed, the simulation is complete. The DOS screen will disappear, and the system will return to the VDANLFHA main form. A new form will be displayed titled "*Roadway Safety Metrics*". On this form, safety metrics for the tow vehicle and trailer (if present) will be displayed. For each metric, its value will be displayed along with the corresponding station (if relevant). For example, the metric "Maximum Friction Demand (g)" is the absolute value of the maximum roadway friction demand, and the station there the maximum value occurred. The PRINT button on the bottom of the form causes a image of the form to be printed on the computer's default printer.